A method to calculate the probability of dike failure due to wave overtopping, including the infragravity waves and morphological changes

Master of Science thesis

P. Oosterlo

Delft University of Technology

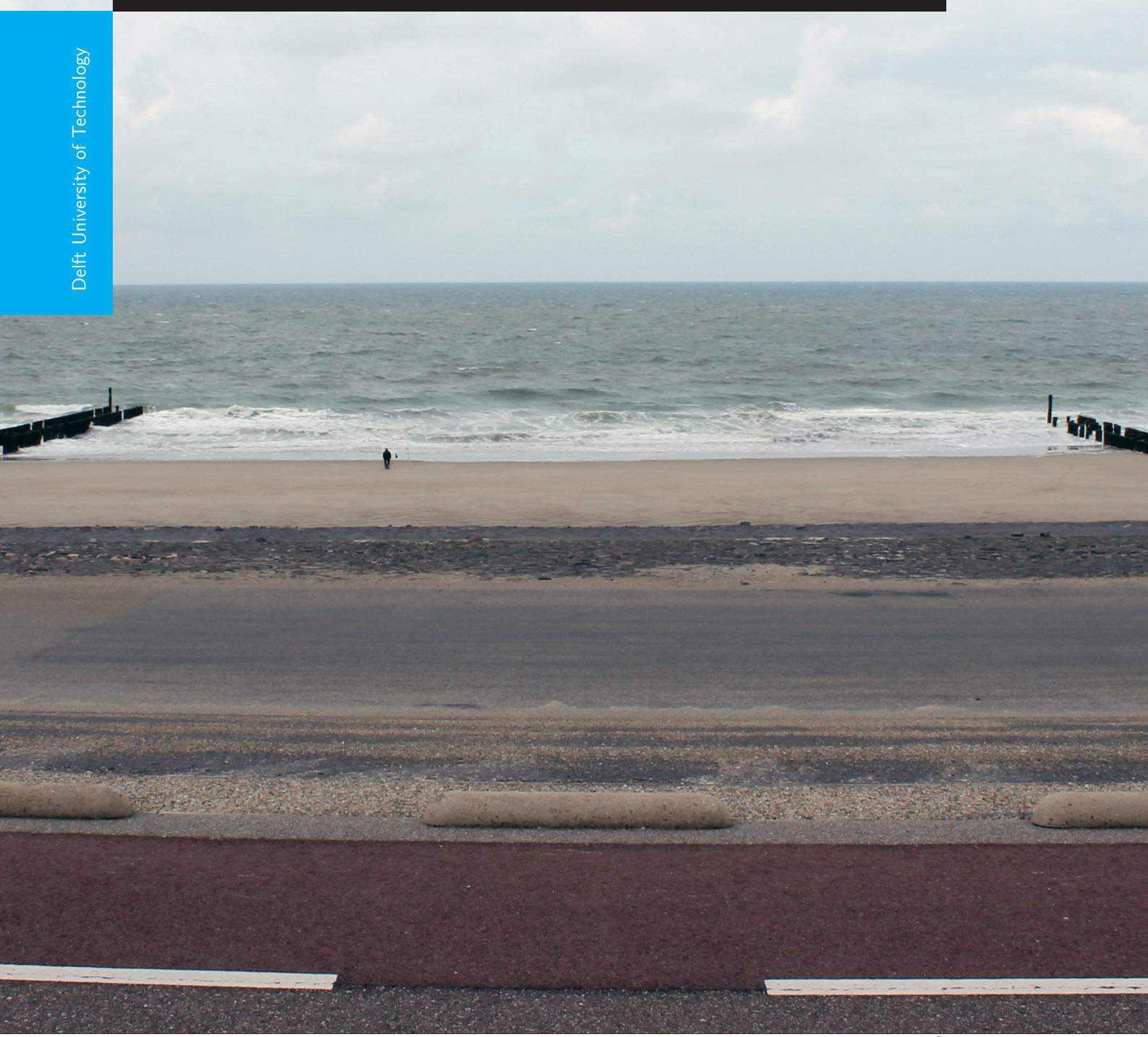

TU Delft Delft University of Technology

Deltares Enabling Delta Life

BE SAFE

Challenge the future | Enabling Delta Life | Bio-Engineering for Safety

A METHOD TO CALCULATE THE PROBABILITY OF DIKE FAILURE DUE TO WAVE OVERTOPPING, INCLUDING THE INFRAGRAVITY WAVES AND MORPHOLOGICAL CHANGES

by

Patrick Oosterlo

in partial fulfillment of the requirements for the degree of

Master of Science
in Civil Engineering

at the Delft University of Technology,
to be defended publicly on Thursday November 19, 2015 at 3:00 PM.

Graduation professor:	Prof. dr. ir. S.N. Jonkman,	TU Delft
Thesis committee:	Prof. dr. ir. J.W. van der Meer,	Van der Meer Consulting, UNESCO-IHE
	Dr. ir. R. McCall,	Deltares
	Ir. V. Vuik,	TU Delft, HKV
	Ir. H.J. Verhagen,	TU Delft

An electronic version of this thesis is available at http://repository.tudelft.nl/.

TU Delft Delft University of Technology

Deltares Enabling Delta Life

BE SAFE

To my parents.

SUMMARY

In this thesis, a method was developed, with which the infragravity waves and morphological changes of a sandy foreshore are included in the calculation of the probability of dike failure due to wave overtopping.

Recently, 'soft solutions' are considered more and more favourable by politicians and dike managers. Traditional solutions do not respond directly to changing boundary conditions. The flexibility to changing boundary conditions is an advantage of soft solutions, which could lead to a reduction in costs, due to less over-dimensioning.

Constructing a natural foreshore in front of the dike can be an attractive and innovative method to decrease the failure probability. However, the uncertainty in the morphological development of these foreshores leads to uncertainty with respect to their contribution in protection against flooding. The morphological stability of a foreshore during extreme conditions is not well known. The current Dutch safety assessment tools do not yet include the infragravity waves and morphological changes of a foreshore during a storm. Hence, it is not yet possible to guarantee the robustness and safety of dike-foreshore system. Amongst others, these causes have led to the fact that foreshores are often not considered as an alternative during the design of protection measures.

This thesis considered hybrid defences (dike-foreshore systems), where the dike is still of importance in the protection of the hinterland. The considered hybrid defence was a schematized version of the Westkapelle sea defence, located at the coast of Walcheren in the Netherlands. The morphological changes of the foreshore calculated in this thesis, were the changes during (severe) storms. The main research question of this thesis is:

How can infragravity waves and morphological changes of a sandy foreshore be included in the calculation of the probability of dike failure due to wave overtopping?

This thesis aims to contribute to assessing dike-foreshore systems in the light of the new Dutch assessment tools based on flood risk. The research increases knowledge on dike-foreshore systems and paves the way for an increase in the implementation of innovative Building with Nature solutions. The results of this thesis contribute to the BE-SAFE project on safety of flood defences with (vegetated) foreshores.

Because a single model that includes all the different relevant processes does not exist, a model framework or 'model train' was developed, in which different models were combined. The modelling framework best fit to solve the research questions was determined as a combination of XBeach hydrostatic, the EurOtop formulae and the probabilistic method Adaptive Directional Importance Sampling (ADIS), see figure 1.

XBeach hydrostatic was chosen to model the hydrodynamics and morphological changes. It was chosen for its inclusion of the infragravity waves and morphological changes, and its limited calculation duration. The EurOtop formulae were chosen to model the wave overtopping discharge, because they are the most commonly used formulae and form a set of equations that can be used for all types of wave breaking conditions and slopes. Furthermore, the EurOtop formulae are the only formulae that include the infragravity waves in any way, by using the $T_{m-1,0}$ wave period. ADIS, a probabilistic method, was chosen to determine the probability of failure, because ADIS can be used for small probabilities of failure, medium amounts of random variables, non-normal distributed variables, non-linear reliability functions, dependent stochastic variables and multiple reliability functions.

17 stochastic variables were chosen according to expert judgement. The parameters with the largest influence on the wave overtopping discharge were determined by a sensitivity analysis. This resulted in five sets of parameters, where the (uncertainty in the) offshore conditions (water level, wave height and wave period) had the largest influence on the wave overtopping discharge, and the (uncertainty in the) dike slope and crest level the smallest influence.

Including infragravity waves (and wave set-up) lead to much larger failure probabilities for the hybrid defence considered in this thesis (factor 50-10^4). This difference is mainly caused by the difference in wave period at the toe of the dike, between calculations with and without infragravity waves.

The inclusion of the morphological changes leads to a somewhat larger failure probability (factor 4). The fact that this difference is not that large, was mainly caused by less dissipation (higher waves) due to erosion

of the foreshore, but at the same time less transfer of energy to the low frequencies, thus a smaller wave period.

The offshore conditions and breaker index had the largest influence on the probability of failure. The wave directional spreading (only in a 1D model) and the phase of the tide had the smallest influence.

The calculation duration of some of the probabilistic calculations was rather large. Using a morphological acceleration factor, stopping the XBeach calculation when the maximum wave overtopping discharge during a storm has been reached, and/or modifying ADIS such that multiple random directions are examined at the same time can help solve this problem.

The combination of a (very) shallow foreshore and dike slope of 1:8 make that the case considered here is (largely) outside the previously studied wave overtopping area. It is possible, that when the wave period becomes very large, the wave overtopping is not dependent anymore on the dike slope, but on the wave parameters only. It is therefore questionable if the EurOtop formulae calculate the right amount of wave overtopping for these types of situations, because in the formulae, the wave overtopping is dependent on the dike slope. This could possibly lead to a lower estimation of the wave overtopping when using the EurOtop formulae in these kinds of situations. Further research is necessary to determine if this is actually the case.

Furthermore, the EurOtop formulae use the $T_{m-1,0}$ wave period. This wave period is very sensitive to the low frequencies. Clear guidelines should be determined on which frequency resolution and, if necessary, cut-off frequencies should be used when determining wave spectra. More research is required to determine the influence of the infragravity waves on wave overtopping and to be able to determine if the $T_{m-1,0}$ wave period is a good predictor or not. Also, the EurOtop equations currently use the still water level, the SWL. Large infragravity waves can give large wave set-up values, which give larger wave overtopping discharges. Further research should also include the influence of the wave set-up on the wave overtopping.

All these problems should preferably be studied by doing field experiments. Physical model tests could be done as well. These physical model tests should preferably be done in a wave basin instead of a wave flume, because of the overestimation of the infragravity wave height in a wave flume by ignoring the wave directional spreading.

The infragravity waves that were found in this study were rather large, and showed to have a large influence on the probability of failure, especially with a 1D model. To further validate the calculated infragravity waves, a validation of XBeach could be performed by comparing with actual offshore and near-shore heights and periods of infragravity waves. The offshore infragravity wave data could be determined from a wave buoy, for the near-shore infragravity waves, the (old situation at the) Petten sea defence could be used, because large amounts of data are available for that location.

Hence, this thesis presented a method with which infragravity waves and morphological changes of a sandy foreshore can be included in the calculation of the probability of dike failure due to wave overtopping. Before this thesis, this was not yet possible. As shown in this thesis, it is important that the infragravity waves are included in the calculation of the dike failure probability due to wave overtopping at this dike-foreshore system, because they had a large influence on the probability of failure. The method developed in this thesis can be used at other locations without many problems, however the influence of the infragravity waves and morphological change as determined in this thesis, could be different at another location.

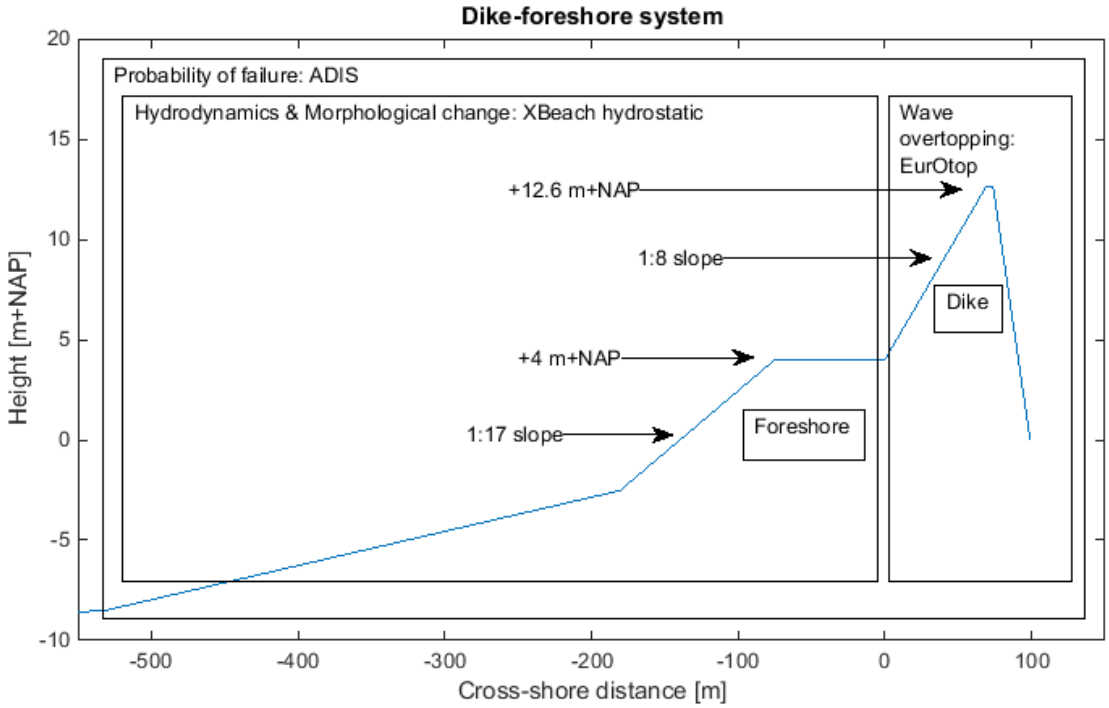

Figure 1: Schematized version of the Westkapelle dike-foreshore system, with the models that were used in the model framework and the processes that they model.

SAMENVATTING

In deze thesis is een methode ontwikkeld, waarmee de lange golven en morfologische veranderingen van een zandig voorland worden meegenomen in de berekening van de faalkans van een dijk door golfoverslag.

Er ontstaat steeds meer een voorkeur van de politiek en dijkmanagers voor de zachte oplossingen. De traditionele oplossingen reageren niet op veranderende randvoorwaarden, de zachte oplossingen doen dit wel. Deze flexibiliteit is een van de voordelen van de zachte oplossingen, wat tot een reductie in kosten kan leiden, doordat er minder over-dimensionering nodig is.

Het aanleggen van een voorland voor een dijk kan een aantrekkelijke en innovatieve methode zijn om de faalkans van de dijk te verlagen. Echter, te onzekerheid in de morfologische veranderingen van dit soort voorlanden leidt tot onzekerheid in de mate waarin deze voorlanden bijdragen aan de bescherming tegen overstromingen. Over de morfologische stabiliteit van een voorland tijdens extreme condities is niet veel bekend. De huidige Nederlandse toetsingsmethoden kunnen nog niet omgaan met infragravity golven en morfologische veranderingen van een voorland tijdens een storm. De veiligheid en robuustheid van dijk-voorlandsystemen kan dus nog niet worden gegarandeerd met de huidige Nederlandse veiligheidsstandaarden.

Dit onderzoek heeft zich gericht op de hybride keringen, waar de dijk nog van belang is voor de bescherming van het achterland. De hier beschouwde hybride kering was de Westkapelse zeedijk, gelegen aan de kust van Walcheren. De morfologische veranderingen van het voorland, welke in deze thesis berekend zijn, waren de veranderingen tijdens een (extreme) storm, niet de veranderingen op de lange duur. De hoofdvraag van dit onderzoek is:

Hoe kunnen lange golven en morfologische veranderingen van een zandig voorland worden meegenomen in de berekening van de faalkans van een dijk door golfoverslag?

Deze thesis heeft tot doel bij te dragen aan het toetsen van dijk-voorlandsystemen met de nieuwe Nederlandse normen gebaseerd op overstromingsrisico's. Dit onderzoek vergroot de kennis van dijk-voorlandsystemen en kan hierdoor zorgen voor een toename in de mate waarin Building with Nature oplossingen worden toegepast. De resultaten van deze thesis dragen bij aan het BE-SAFE project naar de veiligheid van waterkeringen met voorlanden (inclusief vegetatie).

Een modelraamwerk of 'modeltrein' waarin verschillende modellen worden gecombineerd, is ontwikkeld, omdat een enkel model, waarin alle relevante processen kunnen mee worden genomen, niet bestaat. Het modelraamwerk dat is gekozen als het meest gepast om de onderzoeksvragen te kunnen beantwoorden, bestaat uit XBeach hydrostatisch, de EurOtop formules en de probabilistische methode Adaptive Directional Importance Sampling (ADIS), zie figuur 2.

XBeach hydrostatisch is gekozen als het model dat de hydrodynamica en morfologie modelleert, omdat de lange golven en morfologische veranderingen kunnen worden meegenomen, en omdat de rekentijden beperkt zijn. De EurOtop formules zijn gekozen om de golfoverslag te modelleren, omdat ze de meest gebruikte formules zijn, die een set van vergelijkingen vormen die gebruikt kunnen worden voor alle typen golfbreking. De EurOtop vergelijkingen zijn de enige vergelijkingen waarin de infragravity golven op enige manier worden meegenomen, door het gebruik van de $T_{m-1,0}$ golfperiode. ADIS, een probabilistische methode, is gekozen voor het bepalen van de faalkans. ADIS kan gebruikt worden voor kleine faalkansen, gemiddeld tot grote aantallen stochastische variabelen, niet-normaal verdeelde variabelen, non-lineaire betrouwbaarheidsfuncties, afhankelijke stochastische variabelen en meerdere betrouwbaarheidsfuncties.

17 stochastische variabelen zijn gekozen op basis van 'expert judgement'. De parameters met de grootste invloed op de golfoverslag zijn gekozen door middel van een gevoeligheidsanalyse. Dit resulteerde in vijf sets van parameters, waar de (onzekerheid in de) offshore condities (waterstand, golfhoogte en golfperiode) de grootste invloed hadden op de golfoverslag, en (de onzekerheid in) het dijktalud en de kruinhoogte de minste invloed.

Het meenemen van de infragravity golven (en golfopzet) leidde tot veel grotere faalkansen voor de hier beschouwde hybride kering (factor 50-10^4). Dit verschil werd vooral veroorzaakt door het verschil in golfperiode bij de teen van de dijk, bij berekeningen met en zonder infragravity golven.

Het meenemen van de morfologische veranderingen leidt tot een grotere faalkans (factor vier). Dit niet zo heel grote verschil in de faalkans werd vooral veroorzaakt door minder golfdissipatie (grotere golfhoogte),

door erosie van het voorland, met aan de andere kant minder overdracht van energie naar de lage frequenties, wat een kleinere golfperiode veroorzaakte.

De offshore condities and brekerindex hadden de grootste invloed op de faalkans. De golfrichtingsspreiding (alleen in een 1D-model) en de fase van het getij hadden de minste invloed.

De combinatie van een (zeer) ondiep voorland en een dijktalud van 1:8 zorgen ervoor dat de casus die hier is onderzocht (ver) buiten het onderzochte overslaggebied ligt. Het is mogelijk dat de golfoverslag niet meer afhankelijk is van het dijktalud, wanneer de golfperiode zeer groot wordt. Het is daarom onzeker of de EurOtop formules wel de juiste hoeveelheid overslag geven in dit soort situaties, omdat de golfoverslag afhankelijk is van het dijktalud in de formules. Dit zou mogelijk tot een lagere schatting van de golfoverslag kunnen leiden, wanneer de EurOtop formules in dit soort situaties gebruikt worden. Verder onderzoek is nodig om te bepalen of dit inderdaad het geval is.

De EurOtop formules gebruiken de $T_{m-1,0}$ golfperiode, welke zeer gevoelig is voor de lage frequenties. Duidelijke richtlijnen voor de frequentieresolutie en cutoff frequenties bij de bepaling van een golfspectrum moeten worden bepaald. Meer onderzoek is nodig om de invloed van infragravity golven op golfoverslag te kunnen bepalen en om te bepalen of de $T_{m-1,0}$ een goede predictor is of niet. Verder gebruiken de EurOtop formules de gemiddelde waterstand. Grote infragravity golven kunnen een grote golfopzet geven, wat leidt tot grotere golfoverslagdebieten. Verder onderzoek zou ook de invloed van de golfopzet op de golfoverslag moeten beschouwen.

Al deze problemen kunnen het best onderzocht worden door middel van veldmetingen. Modelproeven zijn ook een optie. Deze proeven moeten bij voorkeur gedaan worden in een basin, in plaats van een goot, omdat de infragravity golven worden overschat in een goot, doordat de richtingsspreiding niet gemodelleerd kan worden in een goot.

De infragravity golven, welke werden gevonden in deze thesis, waren vrij groot en hadden een grote invloed op de faalkans, helemaal met een 1D model. Een validatie van XBeach zou kunnen worden gedaan door middel van het vergelijken met data van offshore en near-shore infragravity golfhoogten en -perioden, om zo de grootte van de infragravity golven verder te kunnen valideren. De offshore infragravity golfdata kan bepaald worden uit golfboeidata, voor de near-shore golven zou de (oude situatie bij de) Pettemer zeewering gebruikt kunnen worden, omdat daarvan grote hoeveelheden data beschikbaar zijn.

In deze thesis is een methode bepaald, waarmee de infragravity golven en morfologische veranderingen van een zandig voorland kunnen worden meegenomen in de bepaling van de faalkans door golfoverslag. Dit was nog niet mogelijk voor deze thesis. Het is, voor het hier beschouwde dijk-voorlandsysteem, belangrijk dat de infragravity golven worden meegenomen in de bepaling van de faalkans, omdat ze een grote invloed hadden op de faalkans. De hier ontwikkelde methode kan zonder problemen gebruikt worden op andere locaties, echter kan de invloed van de infragravity golven en morfologische veranderingen anders zijn op een andere locatie.

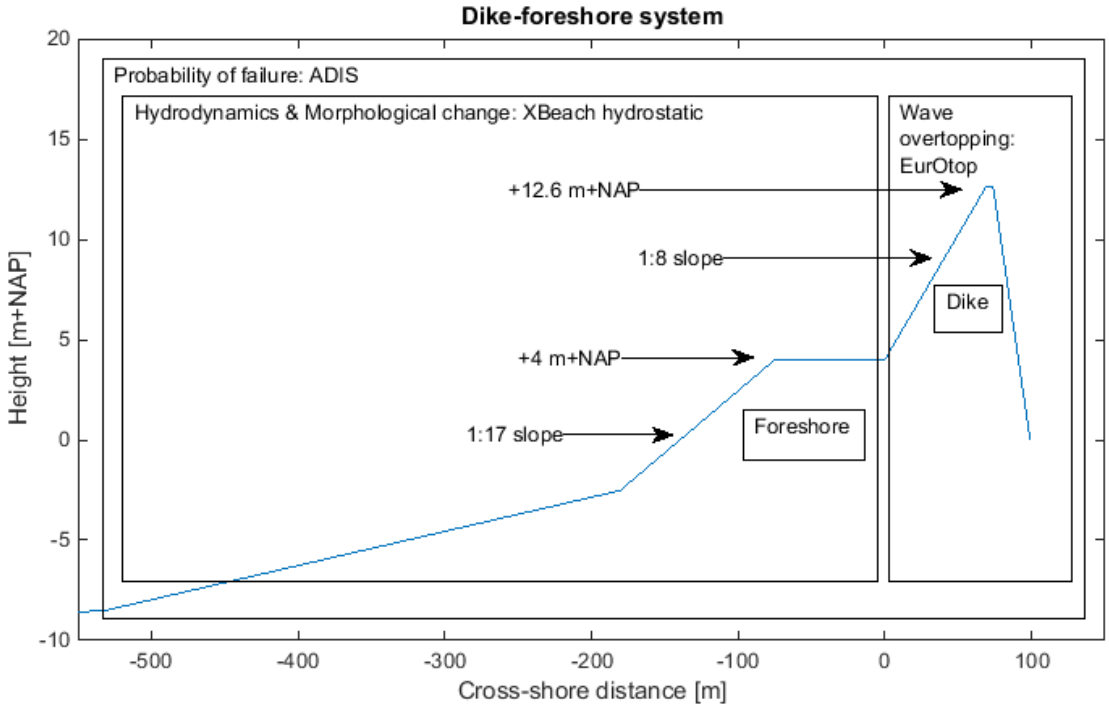

Figure 2: Geschematiseerde versie van de Westkapelse zeedijk, met de modellen welke gebruikt zijn in het modelraamwerk, en de processen die ze beschrijven.

ACKNOWLEDGEMENTS

First of all, I would like to thank my supervisors at Deltares and Delft University of Technology, Robert McCall and Vincent Vuik, for supporting me with their expertise, for always coming up with thought provoking ideas and for stimulating me to make the most out of my research. Furthermore, I would like to thank Joost den Bieman. Even though he was not a member of the committee, he helped a great deal with the probabilistic aspects of my thesis. I would like to thank Jentsje van der Meer, whose enthusiasm and expertise helped me make the decision to begin to study civil engineering and for the opportunities that he has given me over the past years. Furthermore, I would like to acknowledge Bas Jonkman, who sparked my interest in probabilistic design and flood defences, for example by letting me work as his student assistant. I would also like to thank my parents, for always supporting me in every way possible and for never stopping to believe in me. Last but not least, I would like to thank my grandmother, for always motivating me to study hard and have a critical attitude, already from a very young age.

CONTENTS

List of Figures

List of Tables

List of Symbols

Roman letters

A_{sb}	Bed load coefficient	-
A_{ss}	Suspended load coefficient	-
A	Dimensional constant in cross-shore profile equations, amplitude in FFT, wave action density	$m^{1/3}$, m, Jm^{-2}
a	Location dependent parameter in function for determining significant wave height from storm surge level, wave amplitude, lower limit Uniform distribution	m, -
B	Amplitude in FFT, length of berm	m
b	Location dependent parameter in function for determining significant wave height from storm surge level, point of breaking, upper limit Uniform distribution	-
$C1$	EurOtop coefficient for breaking waves and ξ<5	-
$C2$	EurOtop coefficient for non-breaking waves and ξ<5	-
$C3$	EurOtop coefficient ξ>7	-
$C4$	EurOtop coefficient zero freeboard	-
C_d	Drag coefficient	-
C_{eq}	Equilibrium sediment concentration	kgm^{-3}
c_f	Dimensionless friction factor	-
c_g	Wave group velocity	ms^{-1}
c	Location dependent parameter in function for determining significant wave height from storm surge level, wave propagation velocity	-, ms^{-1}
D_{50}	Median grain size	m
D_{90}	90th percentile grain size	m
D_w	White-capping term	-
D	Duration of part of a wave record	s
d_b	Distance between SWL and berm level	m
d	Water depth, location dependent parameter in function for determining significant wave height from storm surge level	m
E	Wave energy	Jm^{-2}
e	Location dependent parameter in function for determining significant wave height from storm surge level	-
F_e	Frequency of exceedance	$year^{-1}$
F	Forcing terms (shear stresses or wave forces) in shallow water equations, cumulative distribution function	-
f_0	Inverse of the zero-crossing wave period	s^{-1}

f_{SUSW}	User defined tuning parameter in suspended load transport calculation	-
f_{max}	Upper frequency limit used for the integration of a spectrum	s^{-1}
f_{min}	Lower frequency limit used for the integration of a spectrum	s^{-1}
f_{peak}	Peak frequency	s^{-1}
f	Frequency	s^{-1}
g	Gravitational acceleration	ms^{-2}
H_0	Deep water wave height	m
H_b	Wave height at the point of breaking	m
H_{m0}	Significant wave height based on spectral analysis	m
H_{mean}	Mean wave height	m
H_{rms}	Root-mean-square wave height	m
H_s	Significant wave height	m
H	Root-mean-square wave height based on the instantaneous wave energy	m
$\hat{h}_a$	Amplitude of tide	m
h_b	Water depth at wave breaking	m
$\hat{h}_s$	Amplitude of surge	m
h	Water depth, highest storm surge level	m
K_r	Refraction factor	-
K_{sh}	Shoaling factor	-
$k_{R,S}$	Parameter to determine representative strength/-load value	-
k	Wave number	$radm^{-1}$
L_T	Suspended sediment load	kgm^{-2}
L_{berm}	Length of intersection between slope and horizontal center plane of berm	m
L	Lognormal distribution, deep-water wavelength	-, m
M	Sediment mobility number due to waves and currents	-
m	Spectral moment, bed slope, exponent in Bruun equation	°
N	Normal distribution	-
n	Manning friction factor, ratio wave group velocity to wave celerity, integers parameter in Hann window, amount of variables, number of observations	$sm^{-1/3}$, -
P_f	Probability of failure	-
P	Reliability threshold	-
p	Pressure	Nm^{-2}
Q_b	Fraction of breaking waves	-
Q	Discharge	m^2s^{-1}
q_{crit}	Critical wave overtopping discharge	$ls^{-1}m^{-1}$
q	Mean wave overtopping discharge	$ls^{-1}m^{-1}$
R_c	Crest freeboard	m

$R_{u2\%}$	Run-up height exceeded by 2% of number of incoming waves	m
R	Strength parameters in Limit State Function (Résistance)	-
S_{tot}	Generation and dissipation term in wave action balance	-
S	Sediment transport per unit width, load parameters in Limit State Function (Sollicitation), wave steepness, energy density, radiation stress	$m^3s^{-1}m^{-1}$, -, -, m^2s, Nm^{-1}
s	JONSWAP wave directional spreading parameter	-
$T_{1/3}$	Significant wave period (based on average of highest $1/3^{th}$ of the waves	s
$T_{m-1,0}$	Spectral wave period defined by m_{-1}/m_0	s
T_m	Average wave period	s
T_{peak}	Time at which tide and/or surge are maximum	s
T_p	Wave peak period	s
T_{surge}	Surge duration	s
T_{tide}	Duration of a tidal cycle	s
t	Time	s
U_A	Velocity asymmetry value in suspended load transport calculation	ms^{-1}
U_n	Current velocity	ms^{-1}
U	Uniform distribution, energy flux per unit wave crest width	-, $Jm^{-1}s^{-1}$
u_b	Particle velocity at the bed	ms^{-1}
u_{cr}	Critical velocity	ms^{-1}
$u_{rms,b}$	Root-mean-squared orbital velocity at the bed	ms^{-1}
uu	GLM velocity in x-direction	ms^{-1}
u	(Horizontal) flow velocity, standard normal value	ms^{-1}, -
V	Coefficient of variation	-
v	Horizontal flow velocity	ms^{-1}
W	(Conditional) Weibull distribution	-
w_s	Particle fall velocity	ms^{-1}
w	Vertical current velocity	ms^{-1}
X	Observation from statistical data	-
x'	Offshore distance measured from mean water line	m
x	Offshore distance measured from storm surge level line	m
y	Test quantity in Kolmogorov-Smirnov test	-
Z	Reliability function	-
zb	Bed level	m
zs	Water level	m

GREEK LETTERS

Γ	Steepness coefficient	-
α_b	Calibration factor in Soulsby-Van Rijn sediment transport equation	-

α_{BJ}	Battjes-Janssen tunable wave breaking coefficient	-
α_{wall}	Slope of wall on top of structure	°
α	Shape parameter Weibull distribution, location dependent parameter in function for determining wave peak period from significant wave height, phase, influence coefficient, dike slope, energy scale parameter, coefficient depending on the reliability threshold	-, s, rad, -, °, -
β_b	Indication of the shoaling of bound long waves	-
β	Location dependent parameter in function for determining wave peak period from significant wave height, reliability index, angle of wave incidence	sm^{-1}, -, °
η	Surface elevation	m
γ_β	Influence factor for angle of wave incidence	-
γ_b	Influence factor for a berm	-
γ_f	Influence factor for roughness and permeability	-
γ_v	Influence factor for a vertical wall on top of the crest	-
γ	Breaker index, phase lag coefficient, peak enhancement factor	-
λ	Location parameter Lognormal distribution	-
μ	Mean value Normal distribution	-
ω	Threshold in conditional Weibull distribution, wave frequency	m, $rads^{-1}$
ϕ	Time shift in the occurrence of the maximum tidal water level opposed to the maximum surge level, wave angle relative to shore normal, porosity	-, °, -
ρ	Frequency of exceedance of the threshold level in the conditional Weibull distribution, density of water	$year^{-1}$, kgm^{-3}
σ	Scale parameter Weibull distribution, wave directional spreading, standard deviation, peak width parameter, relative radian frequency	m, rad, -
τ_b	Time-varying shear stress	Nm^{-2}
θ	Wave direction	°
ξ_{mean}	Irirbarren number based on the mean wave height and wave period	-
ξ	Iribarren number, breaker parameter, surf similarity	-
ζ	Scale parameter Lognormal distribution	-

PROBABILITY DISTRIBUTIONS

The following notations are used for the Normal, Lognormal, Uniform and (conditional) Weibull distributions:

$$N(\mu_N;\sigma_N)$$
$$L(\lambda;\zeta)$$
$$U(a;b)$$
$$W(\omega;\rho;\alpha;\sigma)$$

where μ_N is the mean, σ_N the standard deviation, λ a location parameter, ζ a scale parameter, a a lower limit, b an upper limit, ω a threshold value, σ a scale parameter, ρ the frequency of exceedance of the threshold level and α a shape parameter.

ABBREVIATIONS

ADIS	Adaptive Directional Importance Sampling
ARS	Adaptive Response Surface
BE-SAFE	Bio-Engineering for Safety
CFL	Courant-Friedrichs-Lewy condition
DUROS	DUne eROSion
ENDEC	ENergy DECay
EurOtop	European Overtopping (Manual)
FFT	Fast Fourier Transform
FORM	First Order Reliability Method
GLM	Generalized Lagrangian Mean
HR	Hydraulische Randvoorwaarden (Hydraulic boundary conditions)
Hydra	HYDraulische RAndvoorwaarden (Hydraulic boundary conditions)
JARKUS	JaARlijkse KUStmeting (Yearly coastal measurement)
JONSWAP	JOint North Sea WAve Project
LSF	Limit State Function
M2	Principal lunar semi-diurnal tidal constituent
MATLAB	MATrix LABoratory
MCS	Monte Carlo Simulation
morfac	MORphological acceleration FACtor
MPI	Message Passing Interface
MSL	Mean Sea Level
MWL	Mean Water Level
NAP	Normaal Amsterdams Peil (Dutch ordnance level)
NLSW	Non-Linear Shallow Water equations
SORM	Second Order Reliability Method
SWAN	Simulating WAves Nearshore
SWASH	Simulating WAves till SHore
SWL	Still Water Level
VLF	Very Low Frequency
VNK	Veiligheid Nederland in Kaart (The safety of The Netherlands mapped)
WTI	Wettelijk ToetsInstrumentarium (Safety assessment tools)

1

INTRODUCTION

In recent years, Building with Nature solutions ('soft solutions') are more and more considered as a supplement to flood protection. In this thesis, sandy foreshores are considered, one type of soft solution. The uncertainty in the morphological development of these solutions leads to uncertainty with respect to their contribution in protection against flooding. Furthermore, the influence of the infragravity waves that occur at these types of solutions is unknown and not yet included in safety assessments. This chapter describes the motivation for and aim of this thesis. An introduction to the subject is given, as well as background information to the subject. Furthermore, the relevance of this thesis is presented, as well as the problem, research questions and hypotheses. The methodology, limitations and knowledge gaps are given as well. Finally, the outline shows an overview of the chapters and their relations.

1.1. MOTIVATION AND RELEVANCE

Recently, 'soft solutions' are considered more and more favourable by politicians and dike managers, as a supplement to the usual 'hard' measures that were mostly used as flood protection in the past. Building with Nature can be described as the actual building with nature, instead of building in nature, thus limiting the consequences for the environment. Subjects as safety, naturalness, economic potential, quality of life and durability and sustainability are considered. Building with Nature is supported by the Dutch water sector and by a number of government institutions in The Netherlands. According to EcoShape (2011), the solutions that are found by using Building with Nature aim to be flexible, make use of natural processes and boost ecology and economy. Furthermore, they aim to be cost effective and sustainable. However, the cost effectiveness and sustainability should be thoroughly checked for each project.

Traditional solutions do not respond directly to changing boundary conditions. In general, hard solutions need to be improved (e.g. every 50 years) and soft solutions need to be maintained. Cases could be imagined, in which no soft solution is possible or in which a soft solution would be too expensive. However, the flexibility to changing boundary conditions is an advantage of soft solutions. Due to this flexibility of soft solutions, it is e.g. possible that not all sea level rise scenarios have to be considered when assessing a soft solution, which could lead to a reduction in costs. Hence, in certain situations, when using adaptive Building with Nature solutions, costs can be reduced, because of less over-dimensioning.

Three types of natural defences can be distinguished (EcoShape, 2011):

- Completely 'soft solutions': The dike loses its function as flood defence. The dike gets replaced by a dune or independent sand or clay dike in front of the current dike (e.g. Petten sea defence).
- Hybrid defences: a combination of a traditional dike and a natural foreshore, consisting of a body of sand or clay, possibly covered with vegetation. The foreshore reduces the loads on the dike. The dike remains part of the defence.
- Enhanced 'hard solutions': dikes that are enhanced with ecological features, which enables nature to develop more. These structures and roughness decrease wave run-up and wave overtopping.

A foreshore leads to a reduction of wave loads on the dike, but will also deform during severe storms. In a case where the current dike does not comply with the safety criteria, the construction of a foreshore

can reduce the loads on the dike to a value for which the dike does comply with the safety criteria, without increasing, for example, the crest height. With the current calculation methods described by the Dutch safety standards, the deformation of the foreshore and the influence of infragravity waves on the failure probability cannot yet be calculated.

Figure 1.1 shows a dike-foreshore system, divided into two main zones: the foreshore deformation and wave transformation zone, and the wave run-up and wave overtopping zone.

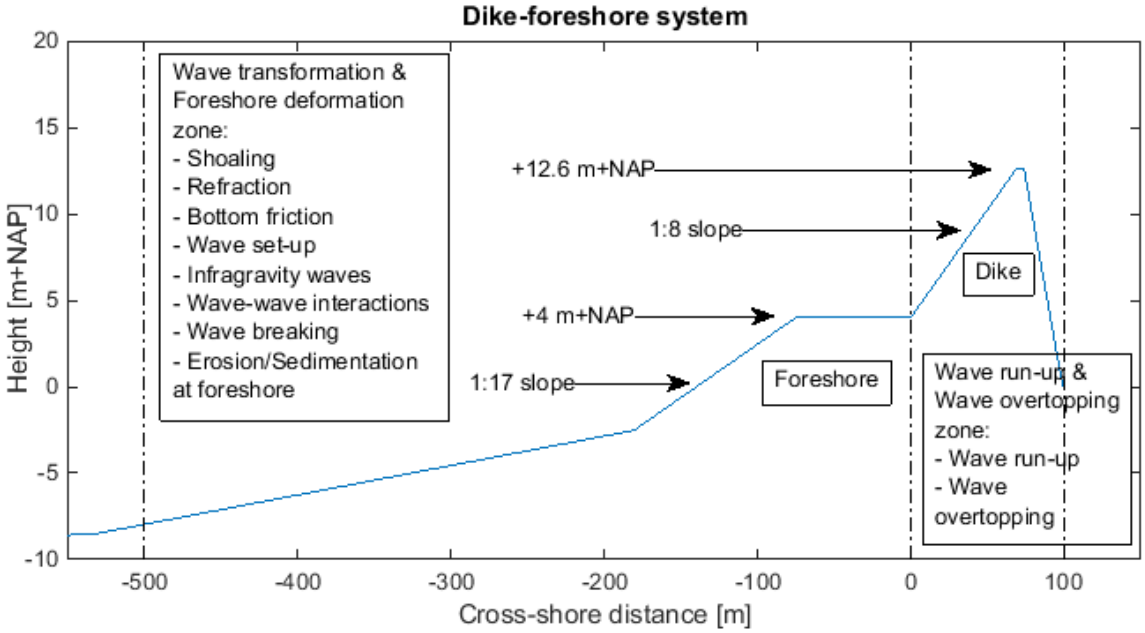

Figure 1.1: Schematized version of the Westkapelle dike-foreshore system, with indicated two zones, the foreshore deformation & wave transformation zone, and the wave run-up & wave overtopping zone. The in each zone occurring processes are indicated as well.

This thesis focuses on developing a method to calculate the probability of dike failure due to wave overtopping, including the infragravity waves and morphological changes of the foreshore. More specifically, hybrid defences (dike-foreshore systems) are considered, where the dike is still of importance in the protection of the hinterland. Hybrid defences were chosen because, as the name suggests, they are a combination of hard and soft parts. The dike, a classic hard solution, and the foreshore, a soft solution. Where the completely soft solutions could be considered as a dune, and the enhanced hard solutions could still be considered as a dike, is a hybrid defence really a combination in which both parts are of importance in the flood protection. Only the failure mode wave overtopping is considered in this thesis. Wave overtopping was chosen because this is one of the failure modes that is influenced by the construction of the foreshore. As described before, the influence on the failure probability of the morphological change during severe storms and of infragravity waves is not yet known. The considered hybrid defence is a schematized version of the Westkapelle sea defence. This location was chosen because it is a perfect example of a hybrid defence.

1.1.1. FAILURE MODES

When a system or part of it no longer fulfils one or more desired functions failure occurs. The state of failure can be reached through various ways. A way that leads to failure is known as a failure mode. The state on the border of failure and non-failure is called a limit state. The reliability is the probability that this limit state is not exceeded. Using limit states it is possible to define a reliability functions. The general form of a reliability function is:

$$Z = R - S \tag{1.1}$$

In which R indicates the strength parameters and S the load parameters. In the limit state, the limit state function is equal to 0 (Vrijling et al., 2014). Several failure modes for dikes are shown in figure 1.2.

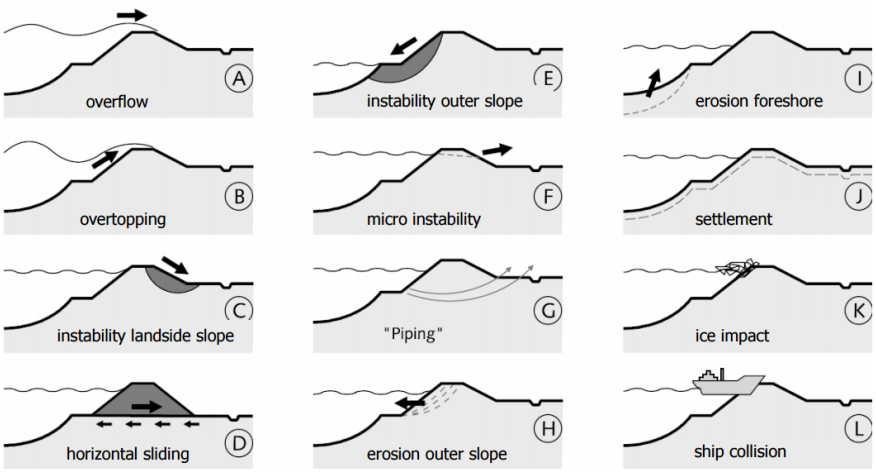

Figure 1.2: Dike failure modes (TAW, 1998).

1.1.2. WAVE OVERTOPPING

Wave overtopping is a dike failure mode. Wave overtopping occurs because of waves running up the face of a flood defence. If the run-up levels are large enough, water will pass over the crest of the defence. This is called overtopping. Wave overtopping is characterized by the overtopping discharge q per meter width of the defence, averaged over time. The overtopping discharge depends on the wave run-up and the existing freeboard (EurOtop, 2007). The process of wave overtopping is further described in chapter 2 and Appendix D (q.v.).

1.1.3. INFRAGRAVITY WAVES

Infragravity waves are generated by groups of wind induced waves, and are sometimes called long waves or surf beat (in the surf zone). The surf zone is the area between the outermost breaker and the limit of wave up-rush. A bound long wave is forced and travels at the wave group speed. The correlation between short and long waves changes in the surf zone, where the long wave is released from the group (Bosboom and Stive, 2012). Typical infragravity wave periods range from 25-30 s until 250-300 s (Munk, 1950), see also figure 1.3. Infragravity waves are described in more detail in chapter 2 (q.v.).

1.1.4. WESTKAPELLE SEA DEFENCE

The Westkapelle sea defence is located at the coast of Walcheren in the Netherlands. The dike is located near the city of Westkapelle. The dike is meant to protect the land from wave attack and erosion due to the tidal currents in the Oostgat, a deep tidal channel close to the coastline. The revetment of the outer slope consists of asphalt above the berm and rubble stone penetrated with mastic asphalt below the berm. The average crest height is 12.6 m+NAP.

In 2002, research indicated that the wave attack on the coast during severe storms can be higher than what was expected before (DWW, 2002). The expected wave overtopping discharge during design conditions exceeded the acceptable 0.1 $ls^{-1}m^{-1}$. Because the inner slope of the dike consists of bare sand, a larger discharge than 0.1 $ls^{-1}m^{-1}$ could not be accepted. Therefore, in 2008, a foreshore with a volume of 2.5 million cubic meter of sand was created in front of the dike. The width of the nourishment increases over a distance of 500 m to 100% and decreases over a distance of 1,000 m to 0%. In between, the maximum length is present over a length of 1,000 m, see figure 1.5. Figure 1.6 shows the transect 1832 of the JARKUS yearly bathymetric survey of 2008 and 2009, hence before and after the construction of the foreshore. The figure shows the initial height and width of the foreshore, being approximately 4 m+NAP and 75 m, with an average foreshore slope of approximately 1:17. Figure 1.7 shows the inner and outer slope of the Westkapelle sea defence.

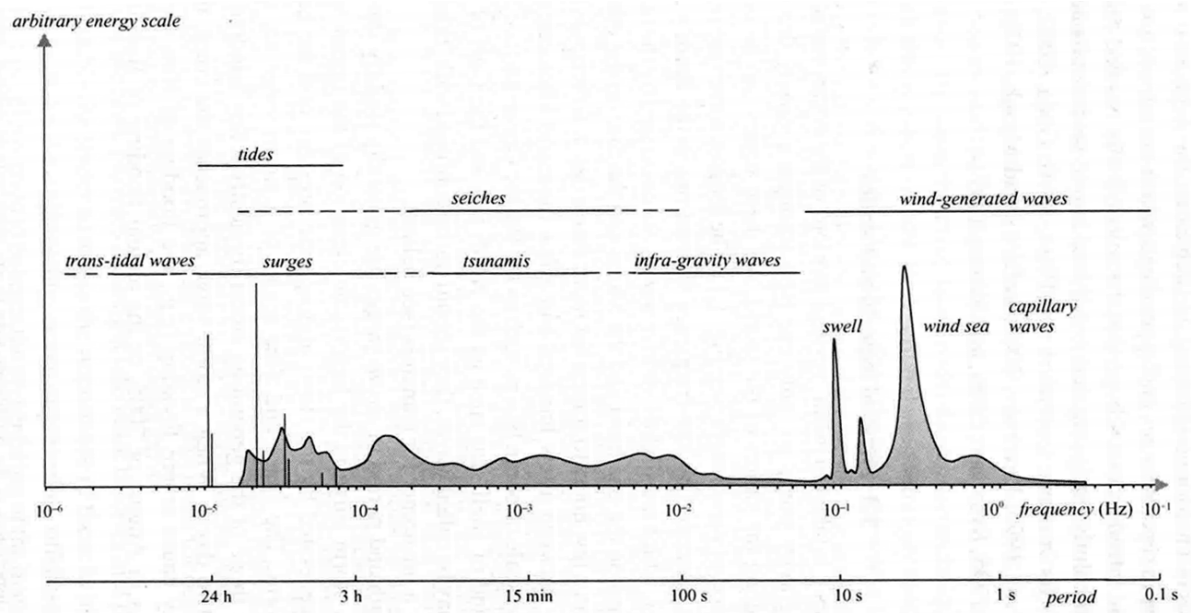

Figure 1.3: Frequencies and periods of the vertical motions of the ocean surface (Holthuijsen, 2007), after Munk (1950).

Figure 1.4: The Netherlands, the western part of Walcheren and the Westkapelle sea defence, running from the beach in the Northeast until the beach in the South. In this figure North is upward.

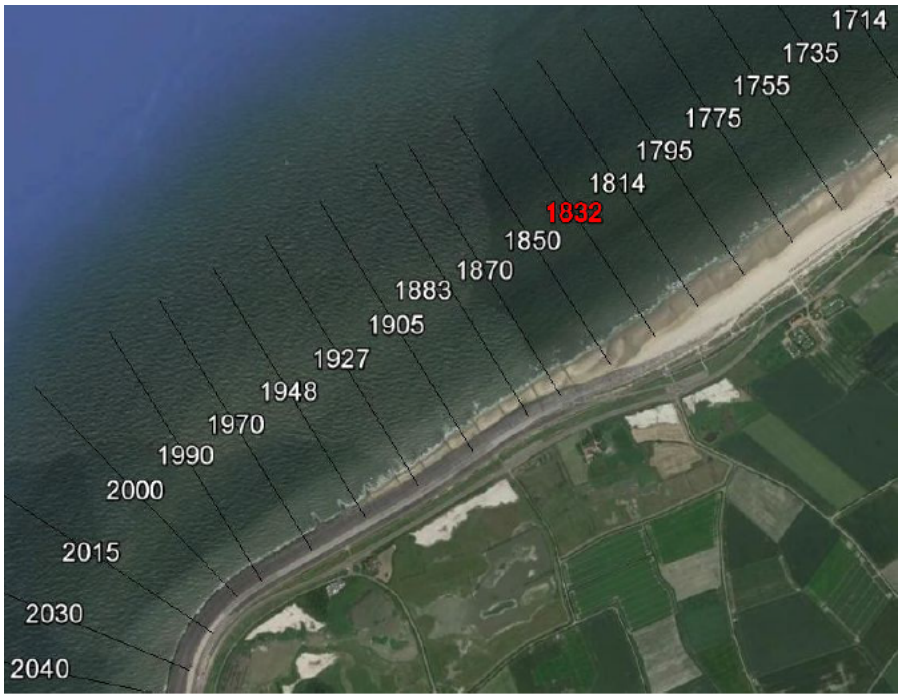

Figure 1.5: JARKUS transects at the Westkapelle sea defence, with transect 1832 shown in red. In this figure North is upward.

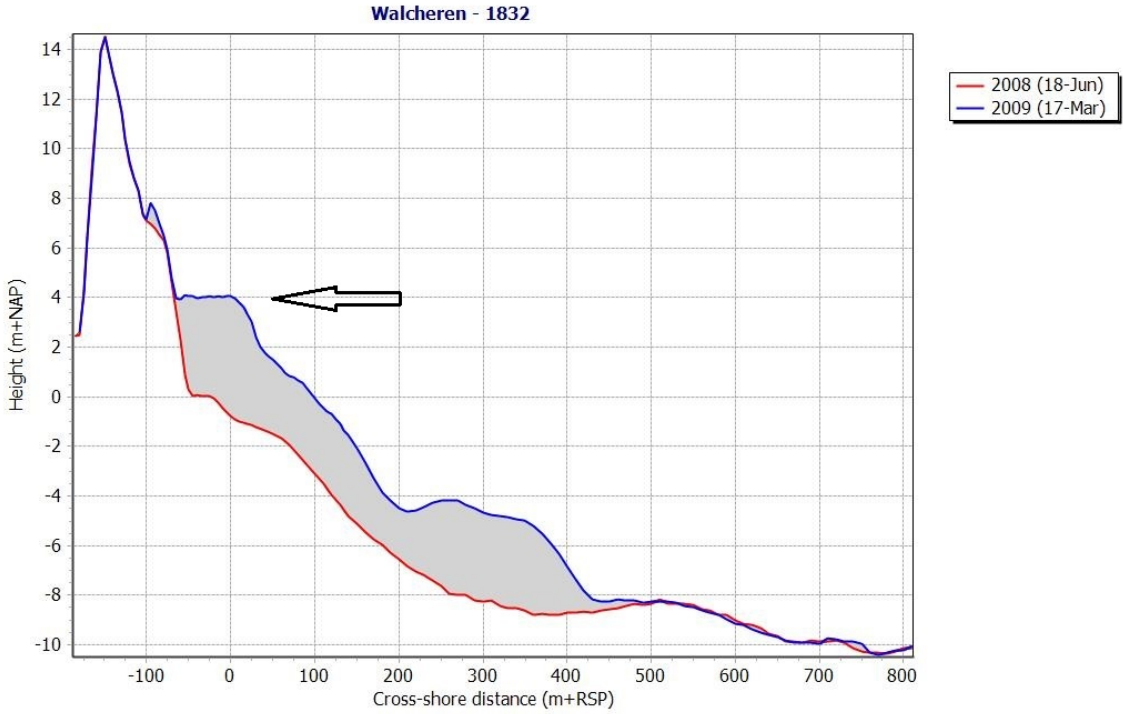

Figure 1.6: 2008 and 2009 JARKUS measurements at the Westkapelle sea defence, transect 1832. Visible in the 2009 profile are the foreshore with a horizontal section with a width of 75 m and a height of 4 m+NAP, and the sloping section with an average slope of 1:17. The arrow indicates the horizontal part of the foreshore. In the figure, to the right is in the offshore direction, to the left in the landward direction.

1.2. PROBLEM DESCRIPTION

Constructing a natural foreshore in front of the dike can be an attractive and innovative method to decrease the failure probability. However, the uncertainty in the morphological development of these foreshores leads to uncertainty with respect to their contribution in protection against flooding. The morphological stability of a foreshore during extreme conditions is not well known. Amongst others, this uncertainty has led to the fact that foreshores are often not considered as an alternative during the design of protection measures (Jonkman, 2013). Herein, issues like the designation of the owner and maintainer of the foreshore also play a role. Furthermore, the influence of the infragravity waves on the probability of dike failure due to wave overtopping is unknown and not yet included in the Dutch safety standards.

A first investigation on the influence of the foreshore at Westkapelle on the failure probability of the dike was conducted by HKV (2014), where the development of the wave loads due to the construction of the foreshore was determined by calculating the failure probabilities of the sea dike with the software package PC-Ring and the model ENDEC. However, this research did not consider the morphological change of the foreshore during design conditions, nor the influence of infragravity waves.

The safety of hybrid defences is difficult to assess, in part due to the uncertainties in the natural elements, such as foreshores. The new Dutch safety assessment protocols aim to use flood risks instead of exceedance probabilities of hydraulic loads. However, with the current safety assessment protocols in The Netherlands, only morphostatic dike-foreshore systems can be assessed. Furthermore, the infragravity waves are not included in the dike-foreshore system calculations and wave overtopping formulae yet. Quantifying the uncertainties in the system and the integration in a failure probability analysis is also not yet done within these safety assessment tools. In other words, within the current Dutch safety standards it is not possible yet to guarantee the robustness and safety of dike-foreshore systems. Increasing interest in soft solutions by politicians and dike managers, as well as a possible increase in durability and sustainability and reductions in costs make it interesting to investigate the contribution of foreshores to flood protection further.

Figure 1.7: Inner slope Westkapelle sea defence.

Figure 1.8: Outer slope Westkapelle sea defence.

1.3. RESEARCH AIMS & CONSTRAINTS

The main goal of this thesis is to develop a method to calculate the probability of dike failure due to wave overtopping, which accounts for morphological changes of the foreshore and infragravity waves. Probabilistic, thus indicating it can include stochastic variables. The focus will be on the Westkapelle sea defence, a hybrid defence where the dike is still of importance in the determination of the failure probability. The morphological changes of the foreshore calculated in this thesis, will be the changes during (severe) storms, not the changes on the long term. The cross-shore profile of the Westkapelle sea defence will be schematized, to be able to clearly determine the influence of the foreshore.

Hence, the goals are to determine the influence of morphological changes of the foreshore and infragravity waves on the dike failure probability due to wave overtopping. Furthermore, the parameters that dominate the failure probability and wave overtopping process will be determined, i.e. the parameters that need to be taken into account in the probabilistic calculations. The aim is to gain more insight in the contribution of foreshores to flood protection and possibly increase the use of foreshores as a supplement to flood management.

1.3.1. MAIN QUESTION AND SUB-QUESTIONS

The main question of this thesis is:

How can infragravity waves and morphological changes of a sandy foreshore be included in the calculation of the probability of dike failure due to wave overtopping?

The main question can be split up into several sub-questions:

- Sub-question 1: What method is appropriate to calculate the morphological changes of the foreshore, the infragravity waves and wave overtopping during a storm?
- Sub-question 2: With what kind of probabilistic framework can the probability of dike failure due to wave overtopping, influenced by a sandy, erodible foreshore be calculated?
- Sub-question 3: With which probability distribution can the important parameters be described, and which parameters have the largest influence on morphological change, wave height and wave overtopping?
- Sub-question 4: What is the influence of infragravity waves on the probability of dike failure due to wave overtopping?
- Sub-question 5: How does morphological change during severe storms influence the probability of dike failure due to wave overtopping?
- Sub-question 6: Which parameters dominate the failure probability and overtopping process, i.e. which parameters need to be taken into account in the probabilistic calculations?

1.3.2. KNOWLEDGE GAPS

The knowledge gaps that this study addresses consist of:

- The most appropriate methods to determine morphological change, wave overtopping and their effect on the probability of failure.
- The importance of the different variables that influence morphological change and wave overtopping and their probability distributions.
- The influence of morphological changes of a foreshore during storms on the dike failure probability due to wave overtopping.
- The influence of infragravity waves on the failure probability due to wave overtopping of a dike failure with a foreshore in front of it.
- The relative importance of the different parameters in the probabilistic framework and ways to simplify the framework.

1.4. CONTRIBUTION OF THIS THESIS

This thesis aims to contribute to assessing dike-foreshore systems in the light of the new Dutch assessment tools based on flood risk instead of exceedance probabilities of hydraulic loads. The research will increase knowledge on dike-foreshore systems and contribute to an increase in the implementation of innovative Building with Nature solutions. Innovative aspects of the thesis are:

- The influence of infragravity waves on the probability of dike failure due to wave overtopping.
- The influence of morphological changes of a foreshore during severe storms on the probability of dike failure due to wave overtopping.
- The use of a probabilistic framework to calculate the probability of dike failure due to wave overtopping, influenced by a sandy, erodible foreshore.

To increase the applicability of the results of this thesis, it is important that an assessment is made to determine when which type of calculation is sufficient, e.g. when a morphostatic foreshore calculation combined with a probabilistic overtopping calculation is more suitable, or when a fully probabilistic calculation is required. It is therefore necessary to determine the importance of the different parameters.

The results of this thesis contribute to the BE-SAFE project on safety of flood defences with vegetated foreshores. The BE-SAFE project aims to develop new methods to assess how, and how much vegetated foreshores can contribute to flood risk reduction.

1.5. OUTLINE

The outline of the research is depicted in figure 1.9 and shows how the different chapters are connected to one another and to the research questions.

First, the literature study determines the physical processes involved in a dike-foreshore system, the state of the art of empirical and numerical models on wave transformation and morphological change, the available wave overtopping equations and the available probabilistic calculation methods. Furthermore it presents an inventarisation of the previous research which has been done on the subject (chapter 2).

Next, the models best fit for the purpose of this thesis need to be chosen. The best fit hydrodynamic and morphological model, the wave overtopping model and the probabilistic method need to be chosen (chapter 3).

After that, an assessment has to be made of the, for this dike-foreshore system, most relevant parameters and their probability distributions (chapter 4).

Following the choice of the best fit models and methods, the ways in which these models and methods need to be applied for this research need to be determined. Furthermore, a validation of the methods is necessary (chapter 5).

After the determination of the most relevant parameters, determination of the influence of each of these parameters on wave heights, wave periods, bed level changes and wave overtopping discharge is necessary. Hence, performing a sensitivity analysis, such that choices can be made to neglect certain parameters and include others in the determination of the failure probability (chapter 6).

The next step is to determine the probability of dike failure for the dike-foreshore system with the previously developed method. This will be done by starting with only the most important stochastic variables (as determined by the sensitivity analysis) and neglecting morphological change of the foreshore. After that, step by step more and more parameters are included, as well as the morphological changes. With the results of the different calculations, the influence of the foreshore, the morphological changes, the infragravity waves and the most important stochastic variables are determined. With these results, it can be determined if, in certain situations, parameters or processes can be neglected (chapter 7).

The outcomes of the different chapters come together in the final two chapters, in which a discussion is presented (chapter 8), as well as the conclusions and recommendations (chapter 9).

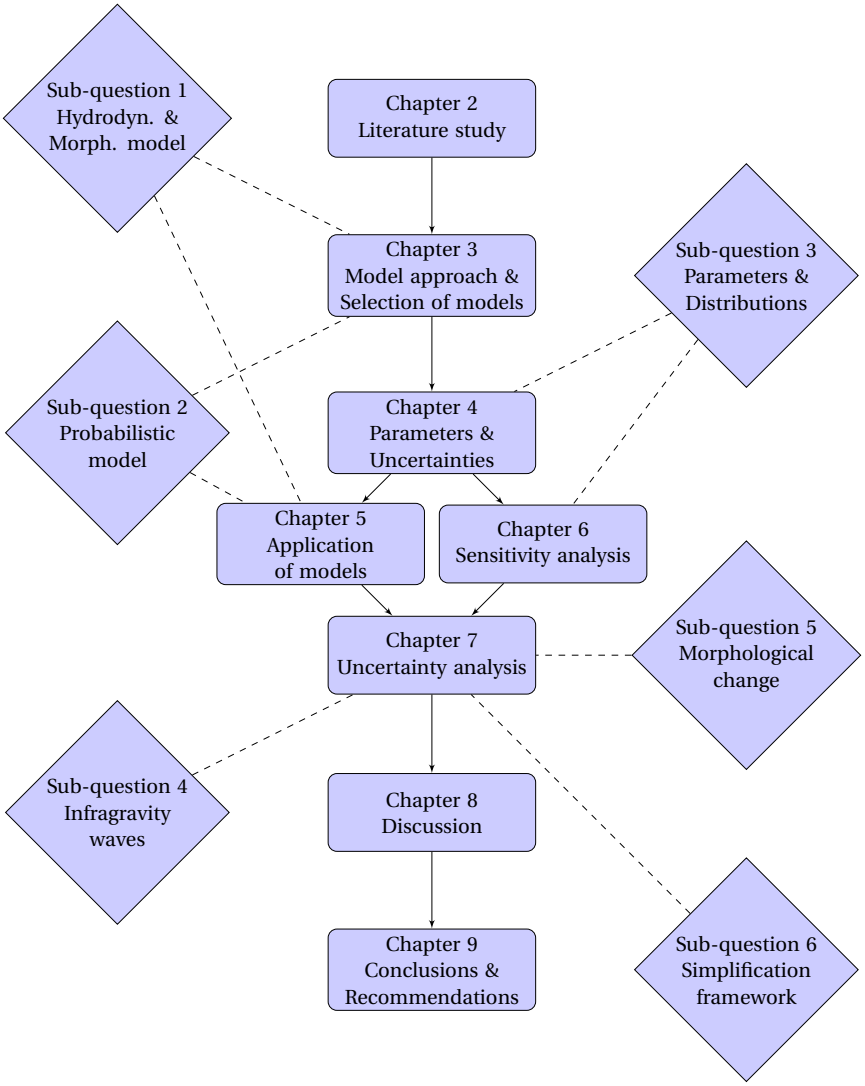

Figure 1.9: Outline of this report.

2

LITERATURE STUDY

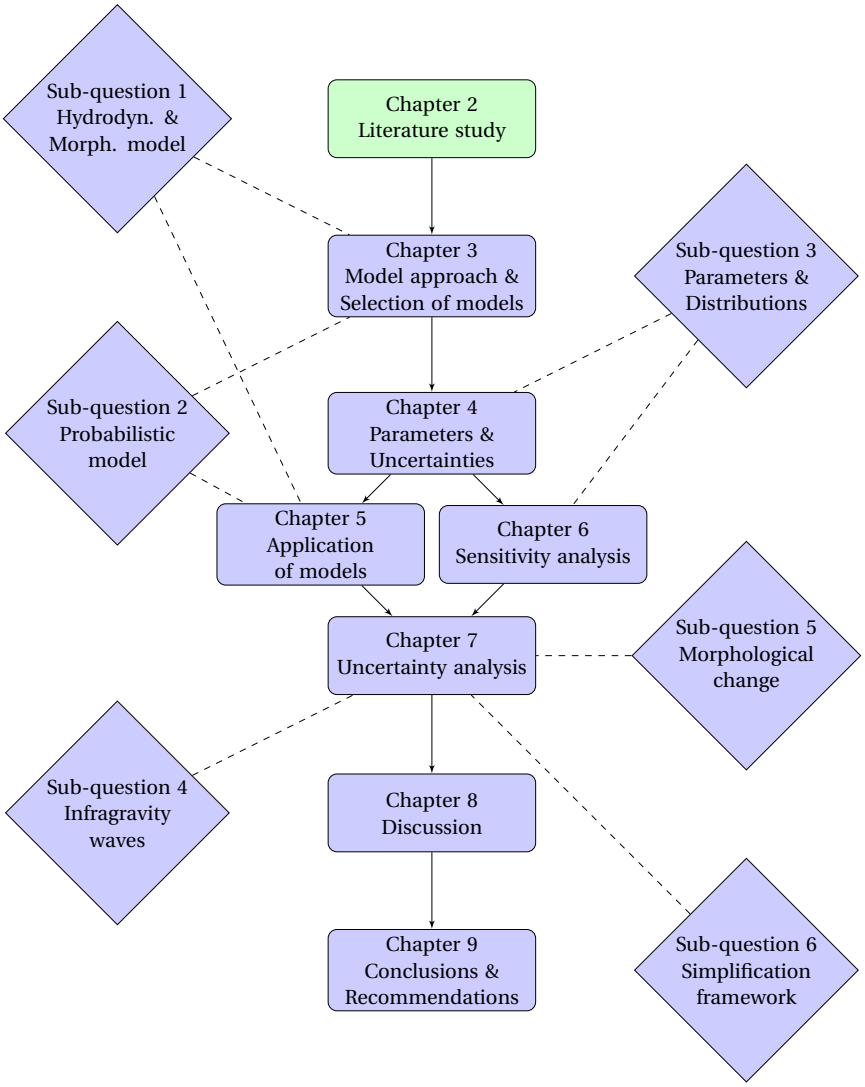

Figure 2.1: Outline of this report.

The literature study is described in this chapter. In the literature study, the physical processes involved in the dike-foreshore system are described and the state of the art of empirical and numerical models and the available probabilistic calculation methods are inventarised.

In section 2.1 an introduction to the in the near-shore occurring processes is presented and the near-shore models h/2-model and XBeach are described. Next, a short description of wave spectra is given, followed by an overview of the state of the art on wave overtopping in sections 2.2 and 2.3. After that, in section 2.4, an overview of probabilistic calculation models and an introduction into the adaptive directional importance sampling (ADIS) method is described. This is followed by a description of relevant previous research in section 2.5. Finally, in section 2.6 a summary and conclusions to the chapter are presented.

2.1. NEAR-SHORE PROCESSES & MODELLING

Many different near-shore processes can be resolved by using near-shore models, in the next sections some of the processes that occur in the near-shore and the models that resolve them are described.

2.1.1. WAVE TRANSFORMATION

When travelling from deep to intermediate to shallow water, wave height, length and direction change until they break and lose their energy. Several processes can be distinguished, the accompanying empirical and numerical models which describe these processes are further elaborated in Appendix B:

- Wind input: the generation of waves by wind blowing over the water surface. The wave height, period and direction are dependent on the wind field, fetch length and water depth. The air pressure at the water surface is maximum on the windward side of the wave crest and minimum on the leeward side of the wave crest, which means that the wind pushes the water surface down at the windward side and up at the leeward side. This process is a positive feedback mechanism: as the wave grows by this mechanism, the mechanism becomes more effective (Miles, 1957). The most important parameters are the ratio of wind speed over wave phase speed.
- Shoaling: when waves enter shallow water, the waves start to deform. The wave height increases, waves steepen and the propagation velocity decreases for waves entering shallow water (the shoaling zone), due to variations in the group velocity, see figure 2.2.

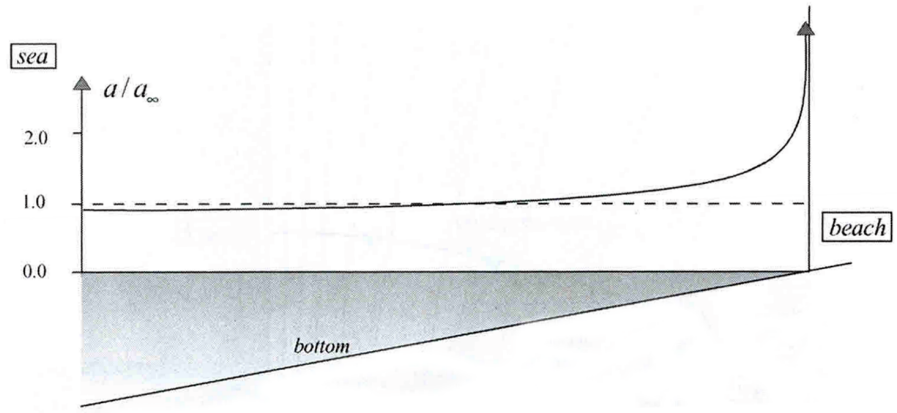

Figure 2.2: The amplitude evolution due to shoaling, as a harmonic wave approaches the coast normally over a flat, gently sloping bottom (a is the amplitude and a_∞ is the amplitude in deep water). In reality, the amplitude growth is bounded by wave breaking (Holthuijsen, 2007).

- Refraction: the phenomenon where wave crests turn towards the depth contour. Sections of the crest in deeper water travel faster than those in shallower parts of the water, see figure 2.3.
- Bottom friction: as the water depth becomes less, waves 'feel' the bottom more. The friction between bed and water causes dissipation and wave height reduction. This process can be indicated as located in the thin turbulent boundary layer near the bed, which is created by the wave-induced motion of the water particle. Bottom friction causes dissipation over the complete range of frequencies of the wave spectrum.
- Wave set-up: variations in wave amplitudes affect the transport of momentum of the waves, which affect the wave forces. The transport of wave-induced momentum is equivalent to a stress, the radiation stress. Gradients in this stress are equivalent to forces. The wave forces can induce variations in mean water level. The reduction in wave height in the surf zone causes an elevation in the mean water level, see also figure 2.5.
- Infragravity waves: due to wave height variation in wave groups, the radiation stresses (see Appendix A) vary and lead to a time-dependent set-down. The largest set-down occurs under the highest waves. This leads to a long wave motion on the wave group scale in the shoaling zone. This bound long wave travels at the wave group speed. The correlation between short and long waves changes into a positive

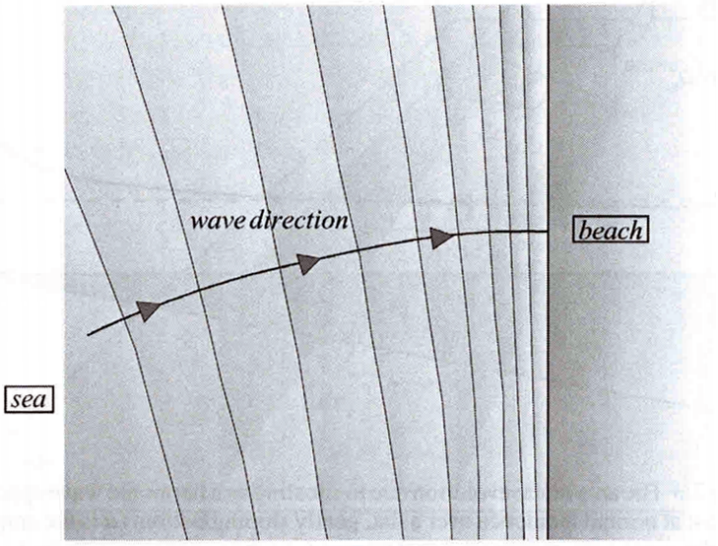

Figure 2.3: A wave always turns to the region with lower propagation speed, i.e. a wave generally turns towards the coast (Holthuijsen, 2007).

one in the surf zone, where the short waves start breaking and the long wave is released from the group. Typical infragravity wave periods range from 25-30 s until 250-300 s (Munk, 1950), see also figure 1.3.

- Wave-wave interactions: the interactions between waves, whereby energy is transferred amongst the waves by resonance. In deep water, it is possible for two pairs of wave components to interact with each other, which is called quadruplet wave-wave interactions. The quadruplet interactions redistribute energy over the spectrum. Most of the energy is transferred from the midrange frequencies to lower frequencies, a small fraction is transferred from the midrange frequencies to the high frequencies. In shallow water, three wave components can interact with each other: triad wave-wave interactions. The triad interactions shift energy from the peak frequency to higher frequencies.

- Wave breaking: a physical limit on wave steepness exists. A wave crest becomes unstable when the particle velocity exceeds the crest velocity, which, in practice, means that the wave height becomes larger than a certain fraction of the water depth. Several types of wave breaking can be defined, see also section 2.3. Wave breaking in deep water is called white-capping, also induced by the steepness, where the wave height becomes to large compared to the wave length.

2.1.2. FORESHORE DEFORMATION

Changes in coastal morphology are the consequence of spatial gradients in net sediment transport rates. Sediment transport is defined as the movement of sediment particles through a certain plane over a certain period of time. The movement of the particles depends on the characteristics of the material. Generally two transport modes are considered: bed load and suspended load transport. During bed load transport, the particles stay close to the bed and can roll, shift or make jumps over the bed. During suspended load transport, the grains are in suspension in the water column and transported by the water (Bosboom and Stive, 2012). Sediment transport can be induced by currents and/or waves. Near the coast, distinction can be made between long-shore transport and cross-shore transport. In a coastal stretch where no alongshore transport gradients occur, an assumption can be made, that the amount of sediment in the upper shoreface remains constant. In general, the profile variations remain in an envelope. Inside this envelope, the profile oscillates, by varying forcing, around a dynamic equilibrium profile. The dynamic equilibrium profile is defined as the mean of the envelope. The erosion profile describes the post-storm profile (Vellinga, 1986). The erosion profile describes the profile after a specific 'normative' storm condition and for a 'typical' dune profile.

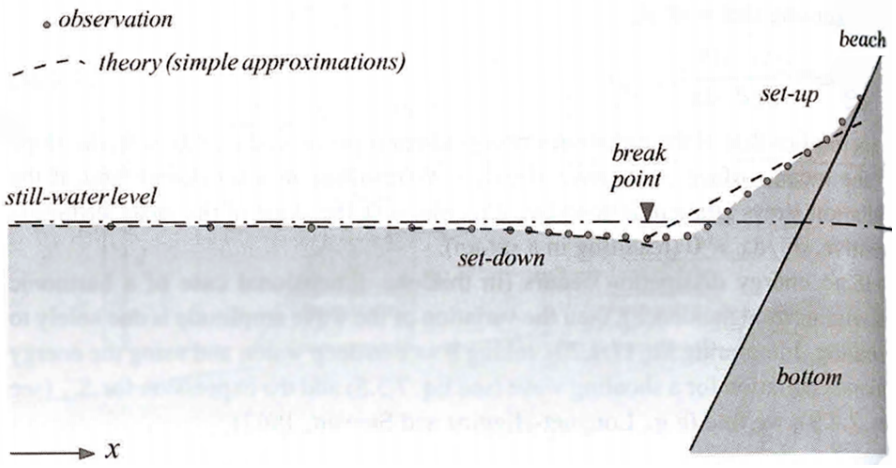

Figure 2.4: Simple approximations of set-down and set-up. Waves approaching a very steep beach in a one-dimensional laboratory situation with a harmonic wave at normal incidence, compared with observations of Bowen et al. (1968) (Holthuijsen, 2007).

2.1.3. EMPIRICAL AND NUMERICAL MODELS

Many different empirical and numerical models exist. Numerical models include for example ENDEC, SWAN, XBeach and SWASH. Here two models are described that are applied later in this thesis. A description of the other models is given in Appendix B.

A commonly used empirical formula by e.g. Dutch water boards to calculate the wave height at the toe of a structure is the $h/2$-model, in which the maximum significant wave height that can occur at a given location (H_s) is half the water depth at that location ($h/2$). However, to calculate the wave height at the toe of a structure like a dike with this method, not the water depth at the toe needs to be taken, but the water depth at half a deep water wavelength ($L_0 = 1.56 T_p{}^2$ [m]) from the toe. This rule of thumb only calculates the change in wave height, not the change in wave period or any morphological changes.

According to Sheremet et al. (2011), numerical wave models can be divided into two categories: stochastic (phase averaged) and deterministic (phase-resolving). The stochastic models simulate the wave processes in a probabilistic way, often based on empirical formulations. Deterministic models simulate wave processes based on the conservation laws. The deterministic models resolve the individual waveforms. For an overview and comparison of the different models, see Appendix B.

A commonly used numerical model is XBeach. Roelvink et al. (2009) gives a description of XBeach, a near-shore numerical model to assess the natural coastal response during storm and hurricane conditions, e.g. on beaches dunes and barrier islands. XBeach is a coupled phase-averaged spectral wave model for sea-swell and non-linear shallow water model for infragravity waves. It combines stochastic and deterministic approaches. XBeach solves the phase-averaged wave action equation. For more information on the wave action balance, refer to Appendix A. The difference compared to SWAN is that XBeach only solves the wave action for a single representative frequency, however XBeach solves the non-linear shallow water equations and wave action balance at the wave group time scale, which gives the infragravity wave motions and mean flows in deterministic way. XBeach uses a form of the dissipation formula for wave breaking according to Roelvink (1993). XBeach uses a roller energy balance, which is coupled to the wave action balance. The formulation which is used for the total roller energy dissipation is the one given by Reniers et al. (2004). For the low frequency and mean flows the shallow water equations are used. XBeach is also capable of calculating sediment transport, which is modelled by a depth-averaged advection diffusion equation by Galappatti and Vreugdenhil (1985). The equilibrium sediment concentration is calculated by the sediment transport formula of Soulsby - Van Rijn Soulsby (1997). XBeach uses a dune erosion avalanching formulation to account for the slumping of sandy material during storms, when a critical bed slope is exceeded. The approach that is used in consistent with Vellinga (1986). Roelvink et al. (2010) gives more background information on the numerical near-shore process model XBeach. It presents the processes, formulations and numerical schemes embedded in the model.

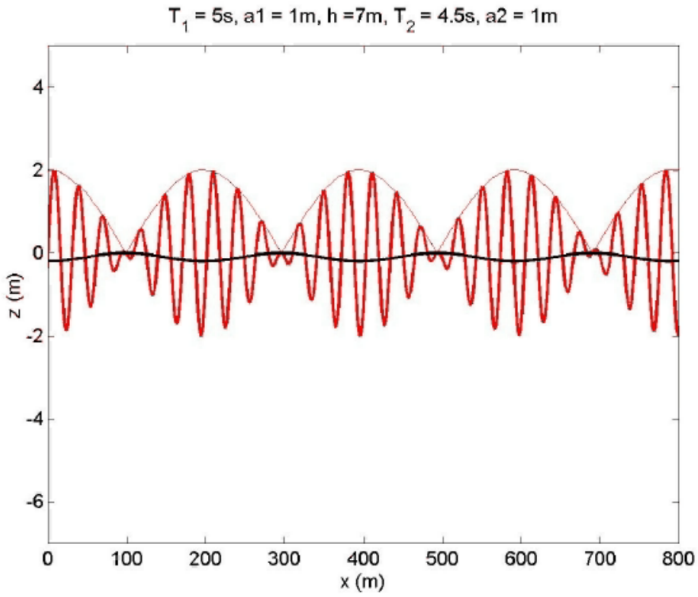

Figure 2.5: Wave groups resulting from two waves with the same amplitudes, but slightly different wave periods. The bound long wave is indicated with black. Hence, the bound long wave has a trough under the largest short waves, a crest under the smallest short waves (Bosboom and Stive, 2012).

2.2. WAVE SPECTRA

The wave spectrum can be estimated from data measured by e.g. a wave buoy. To determine the spectrum from data, usually the Fast Fourier Transform (FFT) is used. For a description of the Fast Fourier Transform, refer to Appendix C. The most simple shape of a wave spectrum would be a delta function, where the wave energy is zero at all frequencies except one, where all the energy is concentrated.

A commonly used shape of the spectrum is the JONSWAP spectrum (JOint North Sea WAve Project, (Hasselmann et al., 1973)), which can be used for arbitrary wind conditions in deep water. The JONSWAP spectrum is given by:

$$E_{JONSWAP}(f) = \alpha g^2 (2\pi)^{-4} f^{-5} \exp\left[-\frac{5}{4}\left(\frac{f}{f_peak}\right)^{-4}\right] \gamma^{\exp\left[-\frac{1}{2}\left(\frac{f/f_{peak}-1}{\sigma}\right)^2\right]} \tag{2.1}$$

where α is the energy scale parameter [-], commonly taken as 0.0081, g is the gravitational acceleration [ms^{-2}], f is the frequency [s^{-1}], f_{peak} is the frequency scale parameter [s^{-1}], γ is a peak enhancement parameter [-], commonly taken as 3.3, and σ is a peak width parameter, with σ= 0.07 for $f \leq f_{peak}$ and 0.09 for $f \geq f_{peak}$. Figure2.7 shows a delta function spectrum, figure 2.6 shows a JONSWAP spectrum.

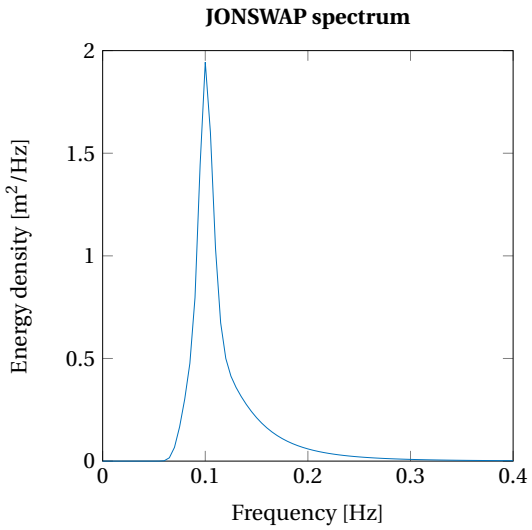

Figure 2.6: JONSWAP spectrum, Hs=1 m, Tp=10 s.

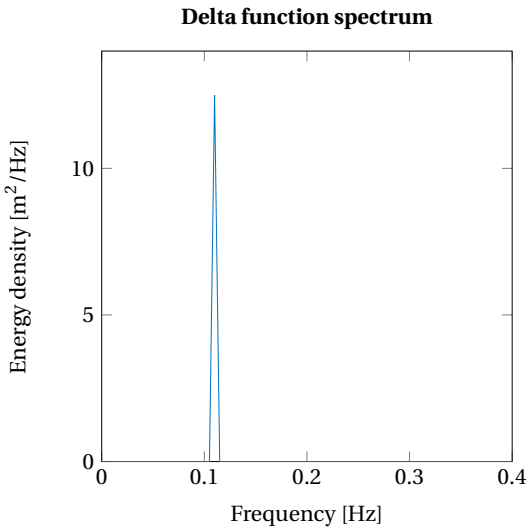

Figure 2.7: Delta function spectrum, Hs=1 m, Tp=10 s.

2.3. WAVE OVERTOPPING

Wave overtopping occurs because of waves running up the face of a flood defence. If the run-up levels are large enough, water will pass over the crest of the defence. This is called 'green water' overtopping, where a continuous sheet of water passes over the crest. Waves can also break on the face of the defence and produce splash which is carried over the crest by its own momentum or by the wind. Small volumes of water may be carried over the crest in the form of spray, by wind acting on the wave crests directly in front of the defence ('white water'). Wave overtopping is characterized by the overtopping discharge q per meter width of the defence, averaged over time. The overtopping discharge depends on (EurOtop, 2007):

- the wave run-up;
- the existing freeboard.

2.3.1. IRIBARREN NUMBER

The breaker parameter, also referred to as surf similarity or Iribarren number $\xi_{m-1,0}$ is commonly used in defining types of wave breaking and is defined, viz.

$$\xi_{m-1,0} = \frac{\tan\alpha}{\sqrt{H_{m0}/L_{m-1,0}}} \tag{2.2}$$

where $L_{m-1,0}$ is the deep-water wave length [m]

$$L_{m-1,0} = \frac{g T_{m-1,0}^2}{2\pi} \tag{2.3}$$

where $T_{m-1,0}$ is the spectral wave period (defined by the moments m_{-1}/m_0) [s].

The breaker parameter can be used as an indication of the type of breaking waves, see figure 2.8. Spilling waves can be indicated by a gentle foreshore, e.g. a beach. More than one breaker line can be found. Plunging waves are indicated by steep, overhanging fronts. The transition between plunging and surging waves is collapsing, which is characterized by an almost vertical wave front and the excursion (wave run-up and run-down) is largest for this type of breaking. Surging waves are actually non-breaking waves, although there may be some breaking (EurOtop, 2007).

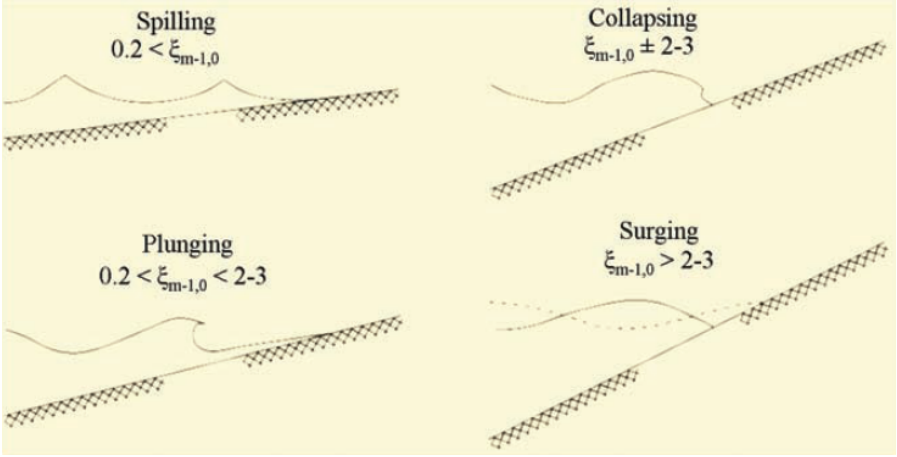

Figure 2.8: Breaker types, (Battjes, 1974); (EurOtop, 2007).

2.3.2. EUROTOP FORMULAE

The formulae described in Van der Meer (2002) and EurOtop (2007) are the most commonly used to describe wave overtopping. For an overview of different wave run-up and wave overtopping formulae, see Appendix D. The following formulae give the average overtopping discharge for gentle slopes (breaking waves), described by:

$$\frac{q}{\sqrt{g H_{m0}{}^3}} = \frac{0.067}{\sqrt{\tan\alpha}} \gamma_b \xi_{m-1,0} \exp\left(-C1 \frac{R_c}{\xi_{m-1,0} H_{m0} \gamma_b \gamma_f \gamma_\beta \gamma_v}\right) \tag{2.4a}$$

with a maximum of:

$$\frac{q}{\sqrt{g H_{m0}{}^3}} = 0.2 \exp\left(-C2 \frac{R_c}{H_{m0} \gamma_f \gamma_\beta}\right) \tag{2.4b}$$

where q is the average overtopping discharge [$m^3 s^{-1} m^{-1}$], g the gravitational acceleration (=9.81) [ms^{-2}], R_c the crest freeboard [m], γ_f a correction factor for roughness and permeability [-], γ_b a correction factor for a berm [-], γ_β a correction factor for oblique wave attack [-], γ_v a correction factor for a vertical wall on top of the crest [-]. In these formulae, the H_{m0} and $T_{m-1,0}$ values at the toe of the structure are used. The reliability is described by assuming the coefficients $C1-4.75$ and $C2=2.6$ to be normal distributed with $\sigma(C1) = 0.5$ and $\sigma(C2) = 0.35$. These formulae are valid for $\xi_{m-1,0} < 5$. The different influence factors are described in more detail in Appendix D.

For breaker parameters $5 < \xi_{m-1,0} < 7$ a linear interpolation is recommended. For $\xi_{m-1,0} > 7$ (non-breaking waves, surging waves) and probabilistic design holds:

$$\frac{q}{\sqrt{g H_{m0}{}^3}} = 10^{C3} \exp\left(-\frac{R_c}{\gamma_f \gamma_\beta H_{m0} (0.33 + 0.022 \xi_{m-1,0})}\right) \tag{2.5}$$

which was derived from measurements, in which $C3$ is normal distributed with a mean of -0.92 and standard deviation of 0.24.

For zero freeboard, the following set of formulae can be used:

$$\frac{q}{\sqrt{g H_{m0}{}^3}} = 0.0537 C4 \xi_{m-1,0} \text{ for } \xi_{m-1,0} < 2 \tag{2.6a}$$

$$\frac{q}{\sqrt{g H_{m0}{}^3}} = C4 \left(0.136 - \frac{0.226}{\xi^3_{m-1,0}}\right) \text{ for } \xi_{m-1,0} \geq 2 \tag{2.6b}$$

where, for probabilistic design, $C4$ is normal distributed with a mean value of 1 and standard deviation of 0.14.

For negative freeboard, the total quantity which will overflow/overtop the structure is composed of a part due to overflow and a part due to overtopping. The following formula was derived:

$$q = q_{overflow} + q_{overtop} = 0.6\sqrt{g\left|-R_c^3\right|} + 0.0537\xi_{m-1,0}\sqrt{gH_{m0}^3} \tag{2.7}$$

This formula is valid for $\xi_{m-1,0} < 2$.

2.3.3. CRITICAL WAVE OVERTOPPING DISCHARGE

The European Overtopping manual (EurOtop, 2007) gives several tables with tolerable wave overtopping discharges, see table 2.1 and also Appendix D. These limits are commonly used as critical wave overtopping discharges in dike safety assessments, in which case they represent a maximum allowable wave overtopping discharge.

Table 2.1: Overtopping limits for damage to the defence crest or rear slope (EurOtop, 2007).

Hazard type and reason	Mean discharge, q [ls^{-1}m^{-1}]
Embankment seawalls/sea dikes	
No damage if crest and rear slope are well protected	50-200
No damage to crest and rear face of grass covered embankment of clay	1-10
No damage to crest and rear face of embankment if not protected	0.1
Promenade or revetment seawalls	
Damage to paved or armored promenade behind seawall	200
Damage to grassed or lightly protected promenade or reclamation cover	50

2.3.4. SPECTRAL WAVE PERIOD

Several wave periods can be defined for a wave spectrum or wave record. Commonly used wave periods are the peak period T_p, which gives the peak of the spectrum, the average period T_m and the significant period $T_{1/3}$, which is based on the average of the highest $1/3^{\text{th}}$ of the waves.The EurOtop formulae use the spectral period $T_{m-1,0}$, which is based on the first negative moment of the wave spectrum (m_{-1}/m_0):

$$m_k = \int_{f=0}^{\infty} f^k S(f)\,df \tag{2.8}$$

and

$$T_{m-1,0} = \frac{m_{-1}}{m_0} \tag{2.9}$$

where m_k is the k^{th} moment of the wave spectrum, f is the wave frequency [s^{-1}] and S the energy density [m^{2}s]. Figures 2.9 and 2.10 compares the T_p and $T_{m-1,0}$ wave periods for two types of spectra. Visible is that when the low frequency energy increases, the $T_{m-1,0}$ is heavily influenced and largely different from the peak period.

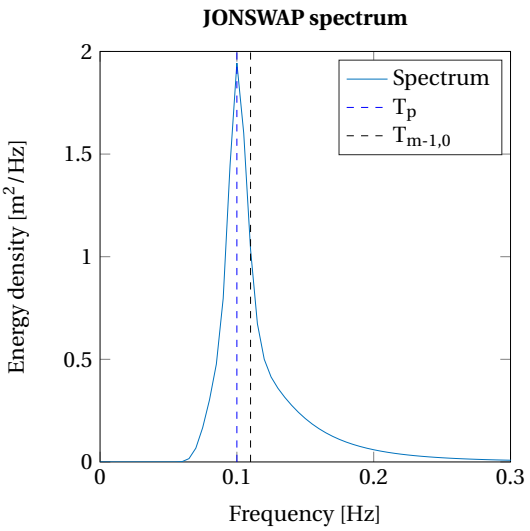

Figure 2.9: JONSWAP spectrum with peak period and spectral period indicated.

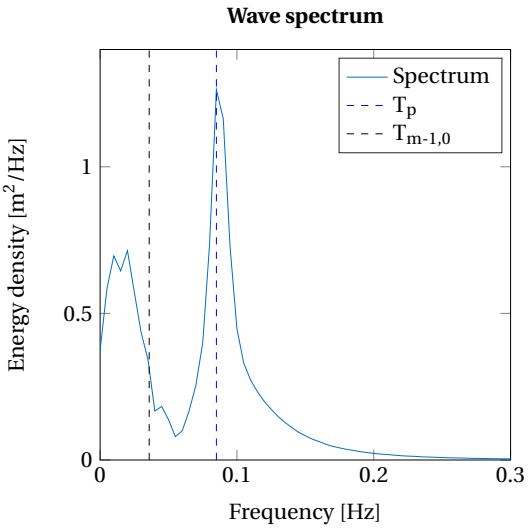

Figure 2.10: Typical wave spectrum at dike toe in dike-foreshore system, with peak period and spectral period indicated.

2.4. PROBABILISTIC CALCULATION METHODS

Many probabilistic calculation methods are available. One model will be highlighted here, for an overview refer to Appendix F. A common subdivision of the methods is presented below.

2.4.1. CLASSIFICATION OF METHODS

Vrouwenvelder and Steenbergen (2003) and Vrijling et al. (2014) give extensive descriptions of the different probabilistic calculation methods. The Joint committee on structural safety proposed a level-classification of probabilistic calculation methods for the reliability of an element:

- Level I: Does not calculate the failure probabilities. A design method according to the standards, by using partial safety factors. The element is deemed sufficiently reliable if a certain margin is present between the representative values of the strengths and loads.
- Level II: Linearise the reliability function in the design point and approximate the probability distribution of each variable by a standard normal distribution.
- Level III: Calculate the probability of failure, by considering the probability density functions of all strength and load variables. The reliability of an element is linked directly to the probability of failure.

Den Heijer et al. (2012) describes and compares a fully probabilistic approach to dune resilience assessment to the traditional deterministic approach, using the DUROS+ model and the Monte Carlo method. In Den Bieman et al. (2014), an advanced probabilistic method, Adaptive Directional Importance Sampling (ADIS), is used in combination with the process-based dune erosion model XBeach, to perform a dune safety assessment.

2.4.2. ADAPTIVE DIRECTIONAL IMPORTANCE SAMPLING

Adaptive directional importance sampling is an example of a level III method. The adaptive directional importance sampling method is described in Grooteman (2011) (q.v.). It is based on directional sampling, where directions are randomly sampled from standard normal space. With a chosen random direction, a line search algorithm is used, which searches the limit state $Z = 0$ in that direction, see figure 2.11. When the limit state is reached or when the limit state cannot be found, a next random direction is chosen. A(n) (adaptive) response surface (ARS) is a (simpler) function which replaces the limit state function, which reduces the computational effort required. The response surface is useful, because it has a simple analytical solution, opposed to the computationally demanding XBeach computation. ADIS uses a second order polynomial as response surface, as shown in figure 2.12. If the root-mean-squared error between the ARS and the limit state func-

tion (LSF) is small enough, the ARS is accepted and used instead of the LSF, which reduces the computation time. The ARS is updated with information that comes available from the exact evaluations, which also makes the scheme adaptive. The importance sampling part of ADIS is expressed in the use of the β-sphere. The β-sphere is used when an ARS with a good fit has been found. In that case, the ARS is used instead of the LSF, but still a small amount of exact (LSF) evaluations will be made to maintain precision. These exact evaluations are performed for the most important points, i.e. the points that are near $Z = 0$.These most important points are determined by the β-sphere, which encloses the most important parts of the limit state. The β-sphere defines the area that is excluded from the sampling domain, which reduces the amount of exact LSF-simulations needed. The response surface is applied in the areas outside of the β-sphere, inside the sphere, the real limit state function is used. The ADIS method is useful for small probabilities of failure and medium amounts of random variables (Grooteman, 2011) and (Den Bieman et al., 2014).

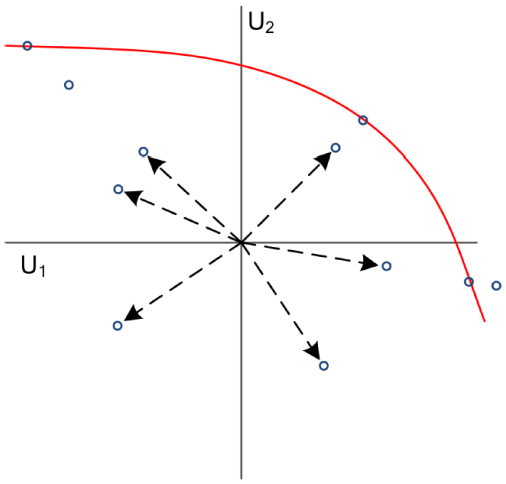

Figure 2.11: ADIS method, with two stochastic variables (U1 and U2). Standard normal space with limit state (red line), random directions (arrows) and evaluations (circles), (Den Bieman et al., 2014).

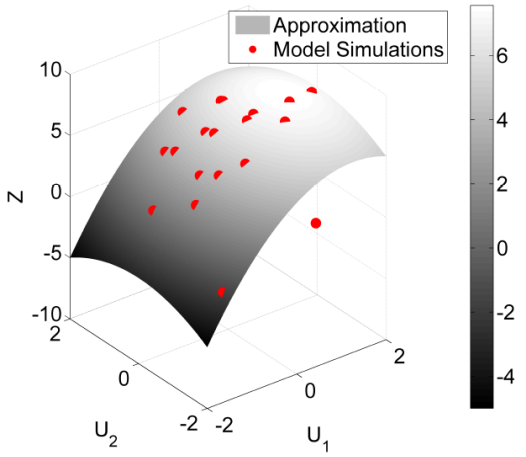

Figure 2.12: LSF evaluations (dots) and ARS (gray plane), (Den Bieman et al., 2014).

2.5. RESEARCH ON DIKE-FORESHORE SYSTEMS

A significant amount of research has already been done on dike-foreshore systems. An overview is presented below.

Van der Most (1979) investigated the wave transformation on a (shallow) foreshore. It was concluded that the water depth is the determining factor in the magnitude of the wave height on the foreshore, the wave steepness was only of minor importance. The influence of a foreshore on the wave run-up is dependent on the relation between width of the foreshore and width of the breaker zone. An increase in width of the foreshore is not beneficent anymore if this ratio is larger than one.

Van der Meer (1997) showed that wave energy is dissipated on foreshores by wave breaking, which leads to a reduction in wave height compared to the case in which no foreshore is present. When a foreshore is present, the wave height distribution at the toe does not satisfy the Rayleigh distribution anymore. A distinction between shallow and deep foreshore was made, where $h_{toe}/H_{s,toe} < 4$ indicates a shallow foreshore. Very shallow foreshores were defined as well, by $H_{s,toe}/H_{s,offshore} < 0.5$. Because of the change in the energy density spectrum by waves breaking on the foreshore, the peak period T_p is not a useful measure anymore to calculate the run-up. On foreshores where intense breaking occurs, the wave set-up becomes of large importance on the run-up.

Holterman (1998) showed that because of wave transformation on a foreshore, there is not one clear peak frequency visible anymore in the energy density spectrum. Also, the Rayleigh distribution cannot be applied anymore to calculate the wave run-up. A formulation was derived, based on the negative spectral moments ($T_{m-1,0}$), which showed good results in predicting the run-up.

In Van Gent (1999) prototype measurements, physical model tests and numerical model computations

were compared to study wave run-up on dikes with shallow foreshores. A shallow foreshore considerably changes the wave height distributions and wave energy spectra between deep water and the toe of the structure. Here, also the use of the wave period parameter $T_{m-1,0}$ was proposed, to account for the effects of wave energy spectra with multiple peaks on wave run-up. A formula was derived for wave run-up, for situations with deep water at the toe up until shallow foreshores.

Mai and Lieberman (2001) studied the importance of foreshores in coastal protection on the German coast. The efficiency of a foreshore was tested for the coast at Schleswick-Holstein in Germany. Field measurements, physical model tests and numerical modelling with SWAN were performed. It was shown that wave breaking increases over shallow foreshores. They found that the optimal width of the foreshore was in the range of 300 m, for which maximum reduction in wave load on the dike was found. The effectiveness of the foreshore was found to be restricted to a maximum ratio of water depth and significant wave height of 2.5, above which the wave parameters were much less affected by the foreshore.

Van Gent and Giarrusso (2005) did calculations with the Boussinesq-type model Triton, on foreshores characterized by a bar, trough and low-tide terrace in front of a dike. The wave conditions were hardly affected by the level of the bar and trough, but strongly by the terrace. The decrease in wave height between deep water and the toe was 50%, the increase in mean period was 50% and the contribution of low frequency energy to the total energy reached 30%. A method to deduce the amount of low frequency energy was derived. By using deep water wave parameters and foreshore characteristics, the contribution of low frequency energy could be estimated. However, the effect of directional spreading was not included.

Verheij (2006) investigated the influence of islands, flats and foreshores on the wave heights and required crest heights of the dikes around the IJsselmeer and Markermeer in The Netherlands. It was concluded that foreshores can be very effective in reducing wave heights, but that the reducing effect strongly depends on the height of the foreshore. This study used the 2D SWAN model to calculate the wave heights at the toe. Several options were tested for several locations: different breakwater heights and widths, different wetland widths behind the breakwater and different foreshore widths, heights and slopes. The influence of the foreshores was determined by using the 2% run-up level, using the Van der Meer (2002) formulation. It was shown that the cases with only a breakwater showed limited reduction in run-up height, whereas the cases with a breakwater and foreshore showed significant reduction. The cases with a breakwater and sloping foreshore showed larger reductions in wave height, caused by dissipation on the sloping foreshore. The largest reduction was achieved for the swamp foreshores which were very effective in dissipating wave energy after transmission by the breakwater. In general, more reduction was achieved for wider and higher foreshores. Hydra-M was used for probabilistic calculations, which showed that for the dikes around the IJsselmeer, a beach shaped foreshore was much more effective than a berm shaped foreshore.

In Suzuki et al. (2012), research was done on the effect of beach nourishments at shallow foreshores on wave overtopping by using the SWASH model. The impact of the 1/17,000 years super storm was tested for the coast at Wenduine, Belgium. It was concluded that infragravity waves are generated on the foreshore. Also, they concluded that beach nourishments do not always give positive effects for the reduction of wave overtopping discharge. Furthermore, it was concluded that to reduce the overtopping discharge, the horizontal momentum of the bores have to be reduced. In this study, it was stated that long waves and wave-wave interactions on the foreshore play a significant role in the wave transformation and therefore on the wave height at the toe, which is commonly used as input for overtopping calculations. The calculations were compared to physical model results from the large wave flume at Flanders Hydraulics Research. Different foreshore slopes and heights were tested, as well as several storm wall heights. The results between physical and numerical model showed good agreement. An increase of the storm wall height showed a reduction in the wave overtopping discharge. An increase of the toe level (beach nourishment) showed a reduction in overtopping discharge. In the wave energy spectra, it was visible that the energy shifted from higher to lower frequencies, which indicates infragravity wave formation. The effect of directional spreading was not included in the study.

The influence of a foreshore on the probability of dike failure due to wave overtopping has been studied in HKV (2014) which, however, did not include the influence of the morphological changes on the failure probability directly, nor the influence of infragravity waves. HKV (2014) states that the influence of a foreshore on the dike failure probability due to overtopping can be considerable (order 10^5 decrease in failure probability at Westkapelle, The Netherlands). The failure probability was calculated for each year with the shape of the foreshore as measured in that year. The increase in failure probability due to the morphological changes of the foreshore between 2009 and 2014 was approximately a factor 10.

Roeber and Bricker (2015) show that during Typhoon Haiyan, at the town of Hernani, the Philippines,

an infragravity wave steepened into a tsunami-like wave that caused excessive damage and casualties. The fringing reef present near the town protected the community from moderate storms, but increased flooding during this extreme event. Typical for these reef environments is a very short wave-breaking zone over a steep reef face, which releases the bound infragravity waves with little energy loss. Furthermore, it was shown that had the wave been in resonance with the reef flat, the wave would have been even larger. Coastal flood planning relies largely on phase-averaged wave modelling, which does not account for infragravity waves. A policy change with the adoption of phase-resolving models was proposed for regions with fringing reefs or other types of bathymetry that favour the abrupt release of infragravity waves.

The overview of previous research shows that research has been done on different aspects that are considered in this thesis, such as wave run-up and wave overtopping and morphological change of and infragravity waves on (sandy) foreshores, but that a method which includes the influence of infragravity waves and (short-term) morphological changes of a sandy foreshore on the probability of dike failure due to wave overtopping does not yet exist.

2.6. SUMMARY & CONCLUSIONS

This chapter aimed to inventarise the physical processes involved in the dike-foreshore system, the state of the art of empirical and numerical models and the available probabilistic calculation methods, as well as the previous research on the subject.

2.6.1. NEAR-SHORE PROCESSES & MODELS

Some important hydrodynamic processes that occur in the near-shore at a dike-foreshore system are, amongst others, shoaling, bottom friction, wave set-up, infragravity waves, wave-wave interactions and wave breaking. An overview of different near-shore models was given in Appendix B. Two commonly used near-shore models are the $h/2$-model and XBeach. XBeach seems well fit to model a dike-foreshore system. These models will be looked at in more depth, as well as compared to each other in the following chapters.

2.6.2. WAVE OVERTOPPING

Wave overtopping occurs because of waves running up the face of a flood defence. If the run-up levels are large enough, water will pass over the crest of the defence. An overview of different wave run-up and wave overtopping models was given in Appendix D. Commonly used equations are the EurOtop formulae, which form a set of formulae, applicable for all types of slopes and wave conditions. The EurOtop formulae use the $T_{m-1,0}$ wave period. For dike safety assessments, a critical wave overtopping discharge is used. This critical discharge was set to 0.1 $ls^{-1}m^{-1}$ for the Westkapelle sea defence.

2.6.3. PROBABILISTIC CALCULATION METHODS

A common subdivision of probabilistic methods is the one according to three different levels. Level I methods do not calculate failure probabilities, but uses partial safety factors. Level II methods linearise the reliability function in the design point and approximate the probability distribution of each variable by a standard normal distribution. An example of a level II method is FORM. Level III methods calculate the probability of failure by considering the probability density functions of all variables. An overview of different probabilistic models was given in Appendix F.

ADIS is an example of a level III method. The method is based on directional sampling, where random directions are sampled from standard normal space. ADIS uses an ARS to replace the limit state function, which reduces the amount of computations required. The ADIS-method is useful for small probabilities of failure and medium amounts of random variables. In chapter 3, different probabilistic models will be compared.

2.6.4. PREVIOUS RESEARCH

Results of the studies indicate that wave energy is dissipated on foreshores by wave breaking and that in the wave spectrum a shift from the peak frequency to the lower frequencies occurs, due to infragravity waves. Therefore, instead of the wave peak period, the $T_{m-1,0}$ wave period was recommended as a measure in these situations to calculate the wave run-up or wave overtopping. Furthermore, on foreshores where intense breaking occurs, the wave set-up becomes important for the wave run-up. It was concluded that beach nourishments do not always reduce the wave overtopping discharge. Most of these studies did not include the wave directional spreading, which is a result of physical flume model tests, which cannot include the directional spreading.

The determination of the influence of a foreshore on the probability of dike failure due to wave overtopping in the research of HKV (2014), is closest related to the goal of this research. However, as explained above, this study did not include the influence of infragravity waves, nor the influence of the morphological changes of the foreshore.

The overview of previous research shows that a lot of research has already been done, but that a method which includes the influence of infragravity waves and morphological changes of a sandy foreshore on the probability of dike failure due to wave overtopping does not yet exist.

3

DEFINITION OF MODEL APPROACH & SELECTION OF MODELS

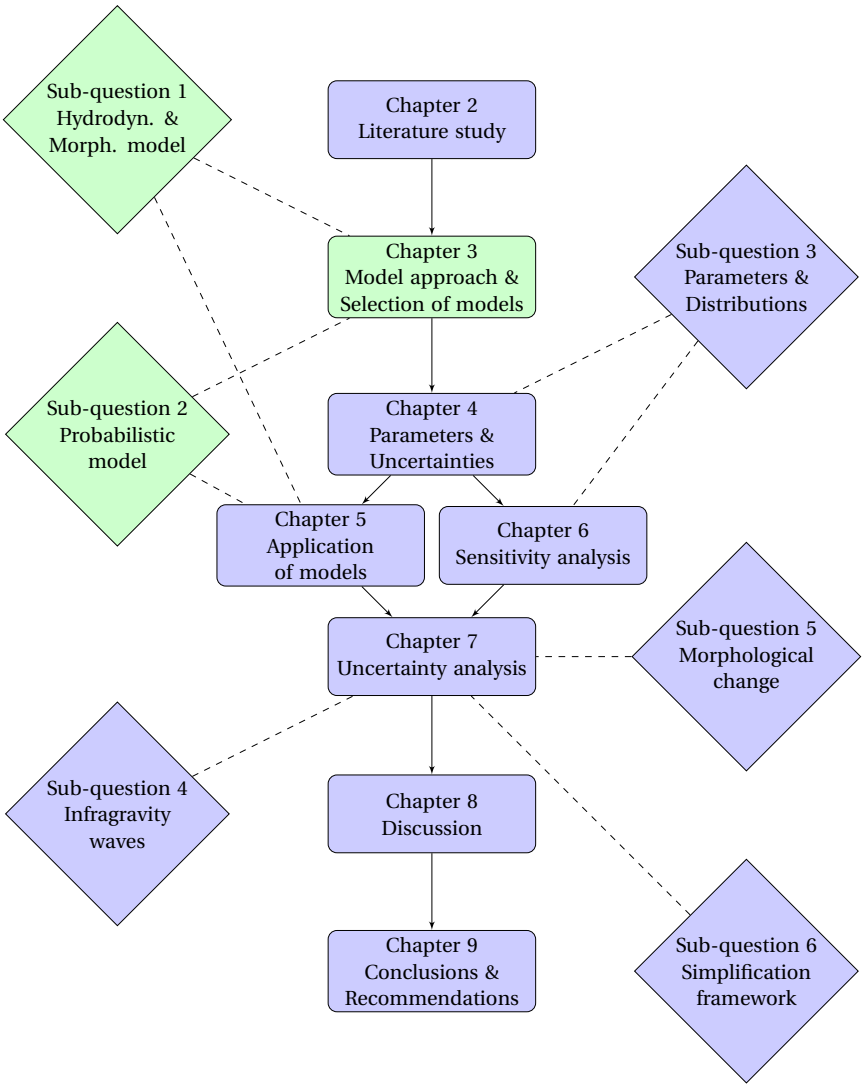

Figure 3.1: Outline of this report.

In this chapter it is determined which model(s) can best be used to reach the goal of this thesis. A model is sought which describes the wave transformation, morphological changes, wave overtopping and failure probability. Hence, this chapter aims to provide an answer to the first and second sub-question. The first sub-question was: What method is appropriate to calculate the morphological changes of the foreshore, the infragravity waves and wave overtopping during a storm? The second sub-question was: With what kind of probabilistic framework can the probability of dike failure due to wave overtopping, influenced by a sandy, erodible foreshore be calculated? Chapter 5 will deal with the application of the model(s) and method.

In section 3.1, the definition of the model approach is presented. Next, in section 3.2 the hydrodynamic and morphological model best fit for the purpose of this research will be chosen. After that, the best method to model wave overtopping is chosen in section 3.3. Next, the best fit probabilistic calculation method is chosen in section 3.4. After that, the chosen 'model train' is presented in section 3.5. Finally, in section 3.6 a summary and conclusions to the chapter are presented.

3.1. INTRODUCTION

The current Dutch safety assessments do not yet include the infragravity waves or morphological changes of the foreshore. Currently, when a shallow foreshore is present, the $h/2$-model or the 'foreshore module' (ENDEC) are used. These models do not include infragravity waves or morphological changes. The $h/2$-model does also not include the wave set-up. Both these models do not calculate the change in wave period.

The goal of this thesis is to determine how infragravity waves and morphological changes of a sandy foreshore be included in the calculation of the probability of dike failure due to wave overtopping. However, a model that includes all these different processes and which can also calculate the probability of failure does not exist. Therefore, a combination of different models needs to be used. These models will be combined in order to calculate the probability of dike failure. Combining these models leads to a calculation framework. The search for models for the framework will be split up into different model types, viz. the hydrodynamic and morphological model, the wave overtopping model, and the probabilistic model. Using this method leads to a core of the framework in which the wave transformation, morphological changes of the foreshore and the wave overtopping are calculated, and a probabilistic shell around these models, which calculates the probability of dike failure due to wave overtopping. Table 3.1 gives several options to model the dike-foreshore system. The models are described in more detail in the previous chapter and in Appendix B. In each of the next sections, the models from a row will be compared and the one best fit for this research will be chosen.

Table 3.1: Different options to model the dike-foreshore system.

Processes	Models					
Wave transformation	$h/2$-model	ENDEC	SWAN	XBeach	XBeach non-h	SWASH
Foreshore deformation	None	DUROS	XBeach			
Wave overtopping	EurOtop	XBeach nonh	SWASH			
Probability of failure	FORM	MCS	ADIS			

3.2. CHOICE OF HYDRODYNAMIC AND MORPHOLOGICAL MODELS

In this section the hydrodynamic and morphological models best fit for the thesis are chosen.

Brandenburg (2010) compared the cross-shore dune erosion model DUROS with the more generic model XBeach. Both models performed well for large scale experiments. For small scale experiments, the performance was less for both models. In Buckley and Lowe (2013) three models, SWAN, SWASH and XBeach, were compared for their performance in predicting bulks sea-swell wave height, infragravity wave height, wave spectra and wave set-up for a fringing reef profile. All models were able to predict sea-swell wave height variation across a steep fringing reef profile. SWASH and XBeach were also able to predict infragravity wave height and spectral transformation, which SWAN could not.

XBeach was used to determine the foreshore deformation and wave transformation in this thesis. A comparison of the different models is presented in table 3.2.Because of the fact that many processes are included in numerical models, which can calculate these processes by using the wave action balance or shallow water equations directly, a numerical model seems more suited for this research than an empirical model. The wave set-up is not included in the h/2-model and DUROS. XBeach includes the long waves, which the h/2-model, DUROS, SWAN and ENDEC do not. XBeach can calculate the morphological changes, which the h/2-model, ENDEC and SWASH cannot. Because the infragravity waves and morphology are important parts of the research, this makes XBeach a good candidate. Furthermore, the calculation time for the whole system would become very large when using SWASH, which is inconvenient for the probabilistic calculations. The standard version of XBeach is the hydrostatic version, which calculates the transformation of long wave heights and periods and of short wave heights, but not of periods. Also, the non-hydrostatic version of XBeach could be used, which also calculates the short wave period transformation, and could calculate the wave overtopping discharge directly. The non-hydrostatic XBeach version is quite similar to SWASH. However, XBeach non-hydrostatic can only calculate large wave overtopping discharges accurately, while the focus is on the small discharges ($0.1\ \mathrm{ls^{-1}m^{-1}}$). Furthermore, the calculation times would increase significantly. Another advantage of XBeach is, that XBeach will probably become the new Dutch safety assessment tool for dunes starting in 2023.

Because the simple $h/2$-model is a commonly used empirical formula by e.g. Dutch water boards, a comparison between XBeach and the simple $h/2$-model was made and is presented in Appendix E. The $h/2$-

model can, however, only calculate changes in wave heights. It does not calculate changes in wave periods, infragravity waves, or morphological changes. However, when a certain morphological change is given, the $h/2$-model can then be used to calculate the wave transformation.

Table 3.2: Overview of hydrodynamic and morphological models and the processes included in these models. x indicates that the model includes the process.

Model	Short wave height trans-formation	Short wave period trans-formation	Wave set-up	Infragravity wave trans-formation	Changes in mor-phology	Calculation duration
h/2-model	x					very short
DUROS					x	short
ENDEC	x	x	x			short
SWAN	x	x	x			short
XBeach	x		x	x	x	short
XBeach non-h	x	x	x	x	x	long
SWASH	x	x	x	x		long

3.3. CHOICE OF WAVE OVERTOPPING MODEL

Table 3.3 shows the characteristics of some different formulae and models that capture the wave overtopping. The EurOtop formulae are the most commonly used formulations to calculate the wave overtopping discharge. Using linear interpolation between $5 < \xi_{m-1,0} < 7$, leads to a set of formulae that is applicable for all types of slopes and wave breaking conditions, which is most useful for the research in this thesis. Furthermore, the EurOtop formulae are the only formulae that capture the long waves in any way, by using the $T_{m-1,0}$ and $\xi_{m-1,0}$. Using XBeach for the calculation of the wave overtopping would mean using the non-hydrostatic version of XBeach, thus calculating the individual waves. This would increase the calculation times significantly, which is unwanted because of the large amount of calculations necessary to be able to calculate the probability of failure. The same holds for SWASH. Therefore, the EurOtop formulae were used to determine the wave overtopping.

Table 3.3: Overview of wave overtopping formulae and models, with their pros and cons. x indicates that the model includes the process.

Model	Type	Infragravity waves	Calculation duration
EurOtop	Analytical	x	very short
XBeach non-h	Numerical	x	long
SWASH	Numerical	x	long

3.3.1. COMPARISON OF HYDRODYNAMIC, MORPHOLOGICAL AND WAVE OVERTOPPING MODELS AT THE WESTKAPELLE SEA DEFENCE

The performance of XBeach, the $h/2$-model and wave height graphs from the Rock Manual (CIRIA, 2007) in combination with EurOtop were compared for storms with return periods of 100, 1,000 and 10,000 years at the Westkapelle sea defence. The conditions belonging to these return periods were determined with the distributions as described in chapter 4 (q.v.). All the results can be found in Appendix E, some conclusions are given below.

For a larger water depth at the toe of the dike, the h/2-model and Rock Manual rule of thumb perform somewhat better than for a smaller water depth. This can be explained by the fact that these models were not designed for use in 'special' cases as dike-foreshore systems, but for more general situations without foreshore and thus with a larger water depth at the toe. Using the h/2-model or the Rock Manual graphs could lead to underestimation of the wave height caused by the exclusion of the wave set-up in these models, and certainly leads to an underestimation of the wave period, which is not calculated with these models. This also causes an underestimation of the wave overtopping discharge, hence an overestimation of the safety of

the dike. It is therefore inadvisable to use these methods for dike-foreshore systems as the Westkapelle sea defence.

The XBeach calculations, which do calculate the change in wave period, show much larger wave periods at the toe and thus much larger wave overtopping discharges. The differences between the 1D and 2D XBeach models are mainly caused by the exclusion of the wave directional spreading in the 1D-model, which leads to an overestimation of the infragravity wave height in XBeach 1D. The results of the 2D-model are therefore more realistic. However, the 1D-model is still useful, because of its improved performance compared to the $h/2$-model and the graphs from the Rock Manual, as well as the limited calculation durations when using the 1D-model, compared to the 2D-model. Therefore, both 1D- and 2D-models were used in this thesis.

3.4. CHOICE OF PROBABILISTIC CALCULATION METHOD

Some commonly used probabilistic calculation methods with their properties are shown in table 3.4. Of the probabilistic calculation methods mentioned in chapter 2 and Appendix F, adaptive directional importance sampling seems the most useful for this thesis: small probabilities of failure, medium amounts of random variables and the least amount of simulations needed to calculate the probability of failure. Furthermore, the ADIS-method was successfully used for a fully probabilistic dune safety assessment in combination with XBeach in Den Bieman et al. (2014). Grooteman (2011) compared the performance of ADIS against inter alia, FORM and Monte Carlo Simulation (MCS), for a set of sample problems, with different limit state functions and stochastic variables. For the implementation of ADIS in MATLAB in Den Bieman et al. (2014), these sample problems were repeated to test the performance of the MATLAB version of ADIS. For less than 10 stochastic variables, ADIS and FORM performed approximately equally in terms of the amount of evaluations necessary to reach a converged probability of failure. For larger amounts of variables, ADIS always performed better. Monte Carlo Simulation always required many more simulations. An additional problem with FORM can be the complex shape of the LSF and the consistent derivatives necessary to reach the design point. For this thesis, the performance of ADIS, FORM and MCS was compared for the failure mechanism wave overtopping at Westkapelle, see the subsection below.

Table 3.4: Commonly used probabilistic calculation methods and their properties. x indicates that the model can cope well with the indicated situation. * Only with Rosenblatt transformations.

Model	Large number of variables	Accuracy with non-linearity	Shape failure space discontinuous	Statistical dependence base variables	Statistical dependence limit state functions	Calculation duration
FORM	x			x*		short
MCS	x	x	x	x	x	long
ADIS	x	x	x	x	x	short

3.4.1. COMPARISON OF PROBABILISTIC METHODS AT THE WESTKAPELLE SEA DEFENCE

Vrijling et al. (2014) gives several methods to be able to compare different probabilistic methods:

- The influence of the number of variables: for level II methods the calculation time increases linearly with the increase of the number of variables. For Monte Carlo simulation, the amount of variables has hardly any influence on the calculation time.
- The desired accuracy of the failure probability: in the case of only normal distributed variables and a linear limit state function, the probability of failure calculated with a level II method is exact. With non-normal distributed variables or non-linearity, the accuracy will decrease. For numerical level III methods, the accuracy is increased with decreasing step size and increasing number of simulations. Importance and Adaptive sampling can lead to high accuracies.
- The shape of the failure space: in theory, discontinuities in the failure space do not pose problems for level III methods. For level II methods, discontinuities in the LSF can lead to large inaccuracies in the calculation of the failure probability.

- The statistical dependence of the base variables: for level II methods, the Rosenblatt transformation needs to be used with dependent variables, which can lead to difficulties and increases calculation times. For level III methods, calculations with dependent variables are the same as calculations with only independent variables.
- The statistical dependence of the limit state functions: when a failure space is defined by different reliability functions, the level III methods can directly be used. The level II methods need to consider the different reliability functions as a serial system. The resulting probability of failure from the level II method can only approximate lower or upper boundaries.

For this thesis, the performance of ADIS, FORM and MCS was compared for the failure mode wave overtopping at the Westkapelle sea defence. However, for the comparison of the probabilistic models, the crest height was kept at a low value (6 m), which increases the failure probability and thus reduces the amount of MCS calculations necessary. If the real mean crest height of 12.6 m+NAP would have been used, the amount of MCS simulations would have become very large. Three stochastic variables were used, the water level zs, the wave height H_{m0} and the wave period T_p, with the accompanying probability distributions as described in chapter 4 (q.v.). The LSF used was $\log(q_{crit}) - \log(q)$, with $q_{crit} = 0.1$ ls^{-1}m^{-1}. Because of the large amount of calculations necessary for MCS, the $h/2$-model was used for this comparison, instead of XBeach. In the simple $h/2$-model, the maximum wave height H_s is half the water depth h. The change in wave period is not calculated by this model. This model is commonly used by water boards and also in some situations in the VNK project (VNK2, 2015). For the calculation of the wave overtopping discharge, the EurOtop formulae were used. For all probabilistic methods an accuracy of 95% was used, with a confidence level of 20%. The calculated probabilities of failure P_f, the amount of calculations necessary and the differences between ADIS and MCS and FORM and MCS are presented in table 3.5. The results show the same pattern as the comparison in Grooteman (2011) that was mentioned above, MCS requires a very large number of calculations, the amount of calculations needed for FORM and ADIS are of the same order of magnitude, with FORM requiring somewhat more calculations. The resulting P_f of both ADIS and FORM lie within the confidence level of 20%, with FORM performing better in this case. As mentioned before, FORM performs worse compared to ADIS with increasing amounts of random variables and more complex limit state functions, which is, amongst the reasons mentioned before, the reason that ADIS was chosen for this thesis.

Table 3.5: Comparison MCS, FORM & ADIS for the Westkapelle sea defence, with a lowered crest level.

Model	P_f [-]	Calculations [-]	Difference in P_f [%]
MCS	0.0394	10,000	0
ADIS	0.0326	70	-17
FORM	0.0418	85	+6.1

3.5. RESULTING 'MODEL TRAIN'

XBeach hydrostatic, EurOtop and ADIS were chosen for this thesis. Figure 3.2 and table 3.6 show which part of the dike-foreshore system is modelled with each of these models, as well as the input and output of the models.

Table 3.6: Input and output of each of the models used in the calculation framework.

Input	Model	Output
Stochastic variables	ADIS	Random direction & samples
Samples of stochastic variables	XBeach	Parameters at dike toe
Parameters at dike toe	Fourier analysis	H_{m0} & $T_{m-1,0}$ at dike toe
H_{m0} & $T_{m-1,0}$ at dike toe	EurOtop	Wave overtopping discharge
Wave overtopping discharge	ADIS	LSF-value & estimate of P_f

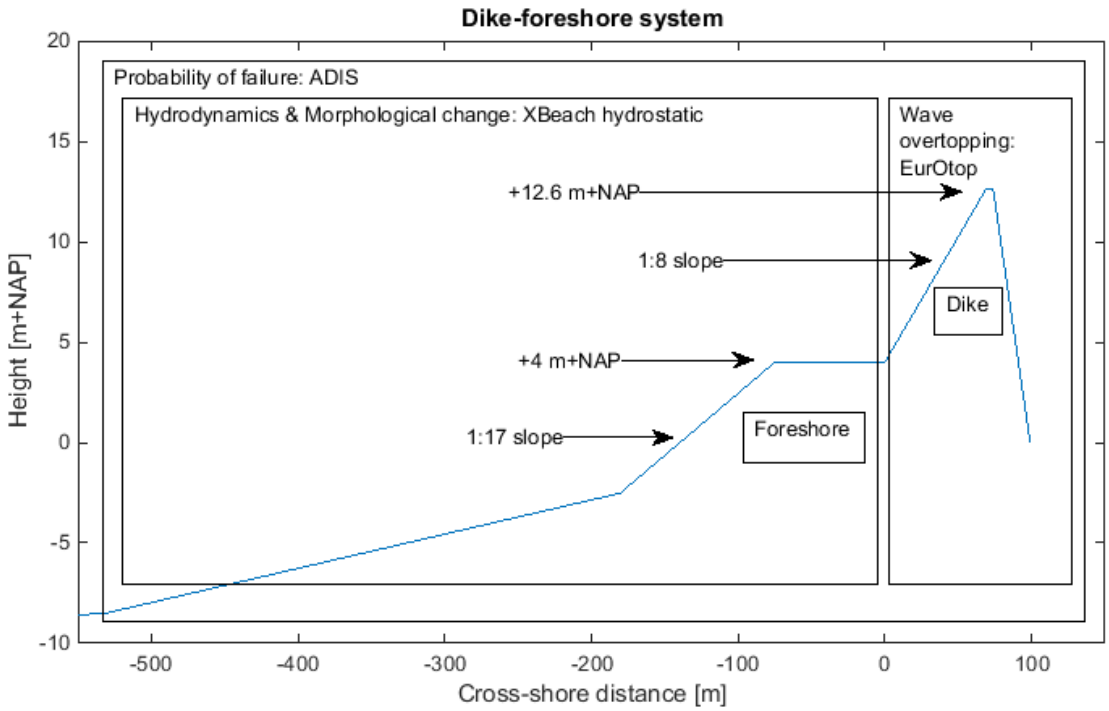

Figure 3.2: Schematized version of the Westkapelle dike-foreshore system, with the models that are used in the model framework and the processes that they model.

3.6. SUMMARY & CONCLUSIONS

This chapter aimed to provide an answer to the sub-questions 1 and 2: the most appropriate models and methods to determine morphological change, wave overtopping and the probability of failure for this thesis. The ways in which these models were applied is described in chapter 5.

3.6.1. CHOICE OF HYDRODYNAMIC AND MORPHOLOGICAL MODEL

XBeach hydrostatic was chosen as method to model the hydrodynamics and morphological changes of the foreshore for this thesis. XBeach is able to calculate the morphological changes during a storm as well as infragravity waves. The hydrostatic version of XBeach was chosen for its limited calculation duration. Furthermore, XBeach will probably become the new Dutch safety assessment tool for dunes starting in 2023.

3.6.2. CHOICE OF WAVE OVERTOPPING MODEL

The EurOtop formulae were chosen to model the wave overtopping for this thesis. These formulae are the most commonly used formulations to calculate the wave overtopping discharge and form a set of formulae that is applicable for all types of slopes and wave breaking conditions. Furthermore, the EurOtop formulae are the only formulae that include the infragravity waves in any way, by using the $T_{m-1,0}$ wave period.

A comparison between XBeach, the $h/2$-model and wave height graphs from the Rock Manual (CIRIA, 2007) was made, in combination with EurOtop. Using the h/2-model or the Rock Manual graphs could lead to underestimation of the wave height caused by the exclusion of the wave set-up in these models, and certainly leads to an lower estimation of the wave period, which is not calculated with these models. This also causes an lower estimation of the wave overtopping discharge, hence an higher estimation of the safety of the dike. It is therefore uncertain if these methods can be used for dike-foreshore systems as the Westkapelle sea defence. The XBeach calculations, which do calculate the change in wave period, show much larger wave periods at the toe and thus much larger wave overtopping discharges. The differences between the 1D and 2D XBeach models are mainly caused by the exclusion of the wave directional spreading in the 1D-model, which leads to an overestimation of the infragravity wave height in XBeach 1D. The results of the 2D-model are therefore more realistic. However, the 1D-model is still useful, because of its improved performance compared to the

$h/2$-model and the graphs from the Rock Manual, as well as the limited calculation durations when using the 1D-model, compared to the 2D-model. Therefore, both 1D- and 2D-models were used in this thesis.

3.6.3. CHOICE OF PROBABILISTIC METHOD

ADIS was chosen as the probabilistic method for this thesis. ADIS can be used for small probabilities of failure and medium amounts of random variables. Furthermore, as was shown in a comparison of different probabilistic methods, ADIS was the method with the least amount of simulations needed to calculate the probability of failure. Furthermore, the ADIS-method was successfully used for a fully probabilistic dune safety assessment in combination with XBeach in Den Bieman et al. (2014). Also, ADIS can cope with complex limit state functions.

4

PARAMETERS & UNCERTAINTIES

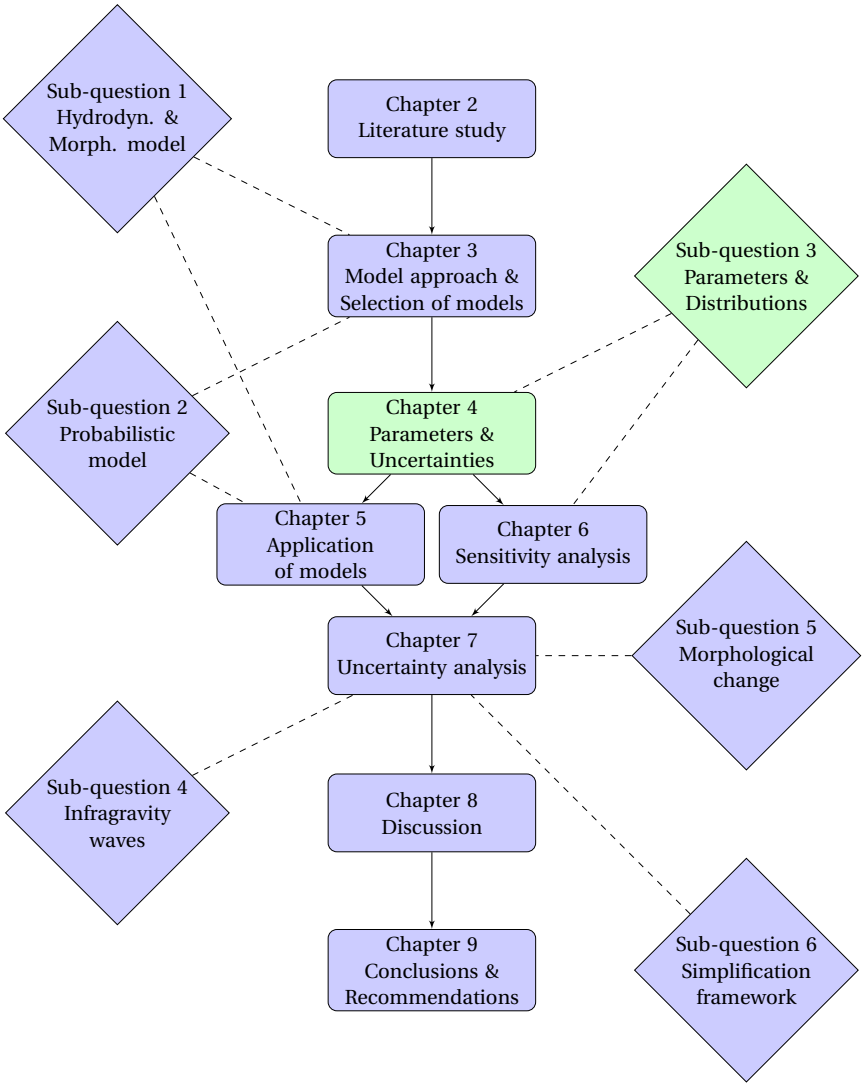

Figure 4.1: Outline of this report.

In this chapter the most relevant parameters and their probability distributions are determined. Hence, this chapter aims to provide an answer to the third sub-question. The third sub-question was: With which probability distribution can the important parameters be described, and which parameters have the largest influence on morphological change, wave height and wave overtopping? More specifically, this chapter deals with the identification of the probability distributions of the parameters. The determination of the most important parameters as identified in this chapter, with respect to hydrodynamics, morphological changes and wave overtopping will be performed in the model sensitivity analysis, in chapter 6.

An introduction into different types of uncertainty and an overview of the different types of parameters is shown in section 4.1. In the next sections, the different parameters adhering to the different types of uncertainties are described in more detail. In succession, parameters that describe statistical uncertainty (section 4.2), model uncertainty (section 4.3), inherent uncertainty in time (section 4.4) and inherent uncertainty in space (section 4.5) are treated. Next, the limit state function which was used in this thesis is presented in section 4.6. Finally, in section 4.7 a summary and conclusions to the chapter are presented.

4.1. INTRODUCTION

According to Van Gelder (2000), there are two types of uncertainty: uncertainty that stems from variability in known populations and represents randomness in samples (inherent uncertainty) and uncertainty that comes from basic lack of knowledge of fundamental phenomena (epistemic uncertainty). Inherent uncertainties represent randomness of the variations in nature. It is not possible to reduce inherent uncertainties. When not all causes and effects in physical systems are known, or not enough data is available, one speaks of epistemic uncertainty. Epistemic uncertainties may change as knowledge increases. Van Gelder (2000) proposes a division of inherent and epistemic uncertainty into five types of uncertainty, see figure 4.2.

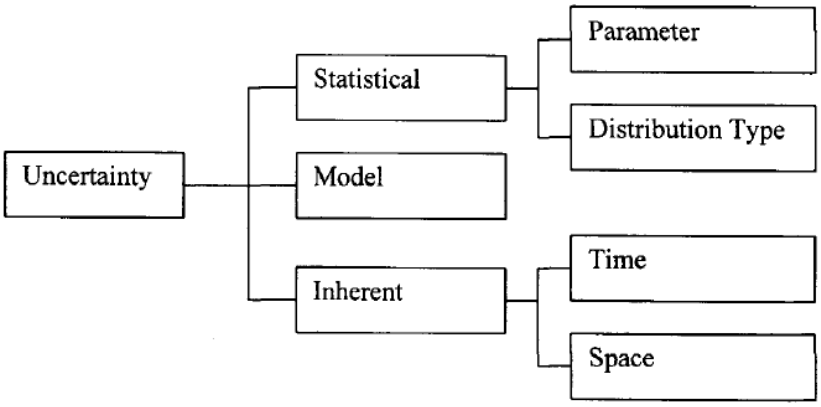

Figure 4.2: Types of uncertainty, (Van Gelder, 2000).

In this chapter 17 parameters are identified as potentially relevant stochastic parameters, based on expert judgement. The importance of each of these parameters is determined through sensitivity analysis in chapter 6. A division of the 17 parameters was made according to figure 4.2 and is presented in table 4.1. The parameters are also tagged with a capital letter, thereby grouping them together according to the location in the dike-foreshore system where the parameters act on (see figure 4.3).

Table 4.1: Stochastic variables and accompanying probability distributions.

Description	Parameter	Distribution	Reference	Tag
Statistical uncertainty: Parameter				
Not considered				
Statistical uncertainty: Distribution type				
Not considered				
Model uncertainty				
Breaker index [-]	*gamma*	N(0.541;0.0541)	(Roelvink, 1993)	A
Calibration factor wave skewness in sediment transport [-]	*facSk*	L(-1.0239;0.2936)	(Van Thiel de Vries, 2009)	A
Calibration factor wave asymmetry in sediment transport [-]	*facAs*	L(-2.1387;0.2936)	(Van Thiel de Vries, 2009)	A
EurOtop coefficient $\xi < 5$ [-]	$C1$	N(4.75;0.5)	(EurOtop, 2007)	B
EurOtop coefficient $\xi < 5$ [-]	$C2$	N(2.6;0.35)	(EurOtop, 2007)	B
EurOtop coefficient $\xi > 7$ [-]	$C3$	N(-0.92;0.24)	(EurOtop, 2007)	B
EurOtop coefficient zero freeboard [-]	$C4$	N(1;0.14)	(EurOtop, 2007)	B
Inherent uncertainty: Time				
Storm duration [hrs]	*tstop*	L(3.9379;0.3365)	(RIKZ, 2006)	C
Water level [m]	*zs, zs0file*	$W(\omega; \rho; \alpha; \sigma)$	(Deltares, 2007)	C
Wave height [m]	H_{m0}	N(0;0.6)	(Deltares, 2007)	C
Wave period [s]	T_p	N(0;1)	(Deltares, 2007)	C
Wave directional spreading [-]	s	U(1.5;10)	Buoy data Rijkswaterstaat	C
Location tidal peak relative to surge peak [-]	*loc_peak*	U(-6.21;6.21)		C
Inherent uncertainty: Space				
Dike slope [-]	*alpha*	N(0.125;0.00625)	(TNO, 1999)	D
Crest height [m]	*crest*	N(12.6;0.1)	(TNO, 1999)	D
Sediment size [m]	D_{50}	L(-8.1229;0.1492)	(TNO, 1999)	E
Manning friction factor [$sm^{-1/3}$]	n	U(0.01;0.03)	(Deltares, 2015b)	E

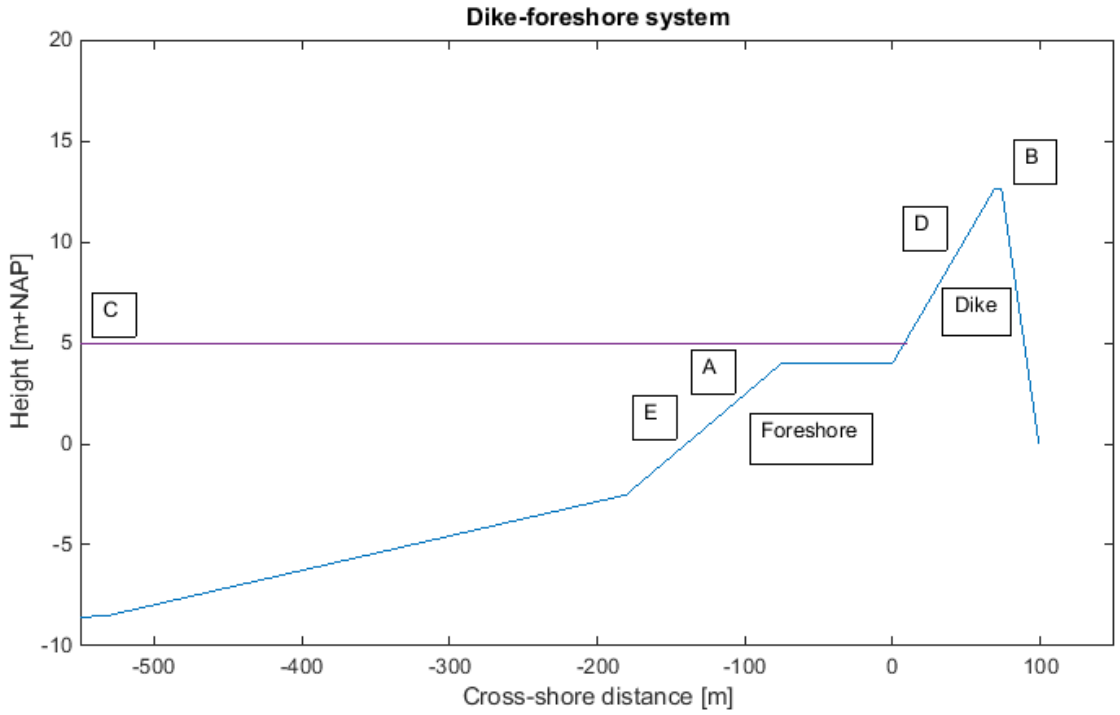

Figure 4.3: Schematized version of the Westkapelle dike-foreshore system, with the stochastic variables indicated by their tags.

4.2. STATISTICAL UNCERTAINTY

According to Van Gelder (2000), statistical uncertainty occurs when the parameters of a distribution are determined with a limited number of data, The smaller the number of data, the larger the parameter and distribution type uncertainty.

Because the influence of the statistical uncertainties was considered small, they were not included in this study, as well as to keep the total amount of stochastic variables and thus calculation times reasonably small.

4.3. MODEL UNCERTAINTY

According to Van Gelder (2000), many of the models describing for instance wind and waves are imperfect, caused by omitting variables of lesser importance for reasons of efficiency or because the physical phenomena are not known. The parameters indicating model uncertainty are given below.

4.3.1. BREAKER INDEX

The wave breaker index (γ), which affects high frequency waves and low frequency generation, was taken as normal distributed. The mean value stems from the preferred WTI 2017 settings for XBeach (see table 5.1), the standard deviation was taken from Roelvink (1993), in which a calibrated formulation for the dissipation of short-wave energy was derived. It has to be noted that the parameter described here concerns the XBeach breaker index parameter (see e.g. Deltares (2015b)), which has a different definition than the breaker index in Battjes and Janssen (1978). The XBeach parameter is based on Roelvink (1993), with one difference with the original formulation being that the wave dissipation is considered proportional to H^3/h instead of H^2.

4.3.2. WAVE SKEWNESS & ASYMMETRY

A discretization of the wave skewness (*FacSk*) and asymmetry (*FacAs*) was introduced by Van Thiel de Vries (2009), to affect the sediment advection velocity and foreshore morphodynamics. This formulation is also included in XBeach. The mean values of the calibration factors for wave skewness and asymmetry were taken from the WTI 2017 settings for XBeach. Not much information is available on these factors, so some variation (a standard deviation of 0.10) was taken around the mean values. Because negative values of these factors are not possible, the normal distributions were changed into lognormal distributions, using the method de-

scribed in Appendix F.

4.3.3. EUROTOP COEFFICIENTS

The values of the normal distributions of the EurOtop coefficients $C1$ and $C2$ for $\xi < 5$, $C3$ for $\xi > 7$ and $C4$ for zero freeboard, which all affect the wave overtopping discharge, are presented in EurOtop (2007).

4.4. INHERENT UNCERTAINTY: TIME

According to Van Gelder (2000), when determining the probability distribution of a random variable that represents the variation in time of a process, there is essentially a problem of information scarcity.

4.4.1. STORM DURATION

The distribution of the storm duration was taken from the Hydra-K project and software package (RIKZ, 2006), which recommends a normal distribution with a mean of 54.3 hours and a standard deviation of 18.8 hours, which is then converted into a lognormal distribution, using the method as presented in Appendix F. A maximum storm duration was set at 200 hours, to save computational time.

4.4.2. WATER LEVEL

The distributions for the hydraulic boundary conditions were taken from Deltares (2007), in which a probabilistic dune erosion method was developed. Deltares (2007) in turn, used the statistics in the so-called stations or 'steunpunten' from the Dutch hydraulic boundary conditions framework (Hydraulische Randvoorwaarden) HR 2006, which provided a list of boundary conditions for each dune profile along the Dutch coast, e.g. (Deltares, 2004). The omni-directional statistics in the stations are valid for the -20 m+NAP depth contour to the North of the Maasvlakte, and valid for a location past the most offshore breaker zone to the South of the Maasvlakte. In these statistics, the water level, significant wave height and wave peak period are correlated, as is further explained below.

A conditional Weibull distribution is recommended for the maximum water level reached during a storm (RWS/RIKZ, 2000). This conditional Weibull distribution is described by:

$$F_e(H > h) = \rho \exp\left[-(h/\sigma)^{\alpha} + (\omega/\sigma)^{\alpha}\right] \tag{4.1}$$

where h is the highest water level during a storm [m], F_e is the frequency of exceedance of the highest level h [year^{-1}], α is a shape parameter that depends on the location along the coast, ω is a threshold above which the function is valid, σ is a scale parameter that depends on the location along the coast and ρ is the frequency of exceedance of the threshold level ω. This equation gives the frequency of exceedance, to convert this into the probability of exceedance, the following equation is used:

$$P_e(H > h) = 1 - \exp\left[-F_e(H > h)\right] \tag{4.2}$$

The parameters of the conditional Weibull distribution are given for different for locations along the North Sea Coast in the stations or 'steunpunten'. The parameters for the different stations are presented in table 4.2.

Table 4.2: Conditional Weibull parameters for Dutch Coast stations (Deltares, 2007).

Location (station)	ω [m]	ρ [year^{-1}]	α [-]	σ [m]
Vlissingen	2.97	3.907	1.04	0.2796
Hoek van Holland	1.95	7.237	0.57	0.0158
IJmuiden	1.85	5.341	0.63	0.0358
Den Helder	1.6	3.254	1.6	0.9001
Eierland	2.25	0.5	1.86	1.0995
Borkum	1.85	5.781	1.27	0.535

4.4.3. WAVE HEIGHT

For a given surge level according to the distribution described above, different wave heights can occur, due to the effects of wind speed, wind direction and wind duration. It was found that this correlation could be approximated by a normal distribution with a mean of 0 and a standard deviation of 0.6 m (Deltares, 2004).

In the HR 2006 framework (Deltares, 2004), the relation between surge and wave height has been determined as:

$$H_s = a + bh - c(d-h)^e \tag{4.3a}$$

which is valid for the interval NAP+3 m< h< d. For h> d, the following equation can be used:

$$H_s = a + bh \tag{4.3b}$$

where a, b, c, d and e are statistical parameters, again given for the different stations. They can be found in table 4.3. To prevent negative wave height values from occurring, a minimum wave height value was set at 0.5 m.

Table 4.3: Parameters relation mean wave height and maximum water level (Deltares, 2007).

Location (station)	a [m]	b [-]	c [-]	d [m]	e [-]
Vlissingen	2.4	0.35	0.0008	7	4.67
Hoek van Holland	4.35	0.6	0.0008	7	4.67
Ijmuiden	5.88	0.6	0.0254	7	2.77
Den Helder	9.43	0.6	0.68	7	1.26
Eierland	12.19	0.6	1.23	7	1.14
Borkum	10.13	0.6	0.57	7	1.58

4.4.4. WAVE PERIOD

The relation between the wave peak period and the wave height was studied in HKV (2005). A normal distribution with a mean of 0 and a standard deviation of 1.0 s was used for the correlation between wave peak period and wave height. The relation is given as:

$$T_p = \alpha + \beta H_s \tag{4.4}$$

where α [s] and β [sm^{-1}] are parameters that depend on the location along the coast, which are given below in table 4.4. To prevent negative wave period values from occurring, a minimum wave period value was set at 2.5 s. Figure 4.4 shows the probability of exceedance curves for the water level, wave height and wave period.

Table 4.4: Parameters relation wave height and wave peak period (Deltares, 2007).

Location (station)	α [s]	β [sm^{-1}]
Vlissingen	3.86	1.09
Hoek van Holland	3.86	1.09
Ijmuiden	4.67	1.12
Den Helder	4.67	1.12
Eierland	4.67	1.12
Borkum	4.67	1.12

4.4.5. WAVE DIRECTIONAL SPREADING

Not much information is available on the probability distribution of the wave directional spreading during storms on the North Sea. To gain a first insight, the data of several storms were analysed, amongst which the storm on 28 October 2013 and the storm on 5 December 2013 (also called 'Sinterklaasstorm'). The data on the wave directional spreading were received from the Rijkswaterstaat Service Desk for the measurement location Europlatform. Because of the shape of the histograms, a normal distribution seemed the most probable, hence a normal distribution was fitted to the data. A Kolmogorov-Smirnov test was used to test the hypothesis that data could be described by this normal distribution, but the distribution had to be dismissed. For a description of the Kolmogorov-Smirnov test, refer to Appendix F. Therefore, the minimum and maximum directional spreading values were taken and a uniform distribution was applied. The data from the Europlatform are given in degrees, to calculate the XBeach JONSWAP directional spreading parameter s, the following formula can be applied:

$$s = \frac{2}{\sigma^2} - 1 \tag{4.5}$$

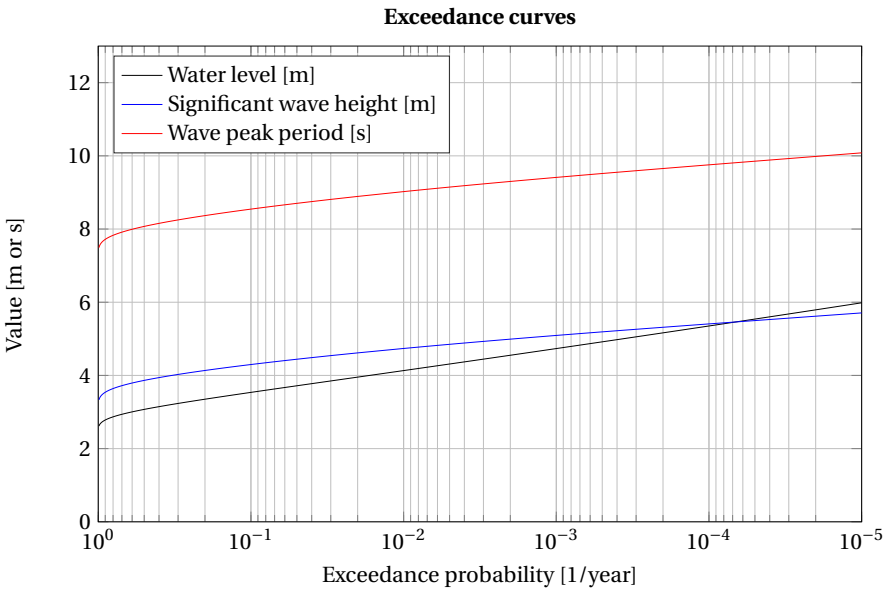

Figure 4.4: Probability of exceedance curves for the hydraulic boundary conditions water level, wave height and wave period at Westkapelle. Based on the HR 2006 for dunes (e.g. Deltares (2007)).

where σ is the directional spreading in radians. More data analysis is required to improve the estimation of the probability distribution of the wave directional spreading during storms.

4.4.6. LOCATION TIDAL PEAK RELATIVE TO SURGE PEAK

The from the above resulting maximum surge level, wave height and wave period were used with an updated version of the formulae from, cf. Steetzel (1993), to create a storm profile. The surge profile is composed of a tidal effect and a surge effect. For this thesis, an adjusted version of the formula from, cf. Steetzel (1993) was made, to be able to include a random phase of the tide at the moment of the maximum water level:

$$zs(t) = h_0 + \hat{h}_a \cos\left(\frac{2\pi\left(t - T_{peak}\right)}{T_{tide}} + \phi\right) + \hat{h}_s \cos\left(\frac{\pi\left(t - T_{peak}\right)}{T_{surge}}\right)^2 \tag{4.6}$$

where h_0 is the mean water level [m] (here set to zero), $\hat{h}_a$ is the tidal amplitude [m], t the time [s], T_{peak} the time at which the surge is maximum [s], T_{tide} the duration of the tide [s], ϕ the time shift in the occurrence of the maximum tidal water level opposed to the maximum surge level [-], $\hat{h}_s$ is the surge amplitude [m] and T_{surge} is the surge duration [s].

The tidal signal at Westkapelle was schematized as a simple M2-tide, with the same amplitude as the in reality occurring maximum spring tide water level, 2.15 m+NAP and a cycle duration of 12.42 hours. No spring-neap tidal cycle was included in the calculations. The storm duration and maximum water level follow from the above described probability distributions.

The time difference between the occurrence of the peak of the tide and peak of the surge was schematized as an uniform distribution with values $[-2\pi; 2\pi]$. T_{peak} was set to half the storm duration T_{surge}. Because of this and the shape of the surge profile, the maximum surge level occurs at the middle of the storm. This maximum surge level coincides with a random phase of the tide level, because of the uniform distribution of ϕ. The maximum water level resulting from the conditional Weibull distribution of the North Sea stations is the maximum water level measured in a certain storm with a certain return period at the -20 m+NAP depth contour. This maximum water level is thus the combination of a certain surge and a certain tidal water level, not necessarily the maximum tidal water level.

The maximum tidal water level $\hat{h}_a$ and maximum surge level $\hat{h}_s$ need to be entered in formula 4.6. However, only the maximum water level from the conditional Weibull distribution and the maximum tidal level are known. To cope with this, the maximum surge level is first calculated with $h_{Weibull} - \hat{h}_a$ and entered into the formula. After that, the tidal level and surge level in time are calculated and the total water level in time is determined. However, due to the fact that, by definition, the maximum water level from the conditional

Weibull distribution occurs at an arbitrary tidal level, the calculated maximum water level during the storm $h_{max} = \hat{h}_a + \hat{h}_s$ is not equal anymore to the conditional Weibull water level. Therefore, the surge level is scaled, by using $scale = (h_{Weibull} - \hat{h}_a)/\hat{h}_s$ and $\hat{h}_{sscaled} = \hat{h}_s * scale$. Then, the surge level, tidal level and total water level in time are again calculated. Now, the maximum water level during the storm agrees with the level from the conditional Weibull distribution and consists of a certain surge and a certain tidal level, which is not necessarily the maximum tidal level.

The variation of the significant wave height during the storm was modelled by

$$H_s(t) = \hat{H}_s \cos^2\left(\frac{\pi\left(t - T_{peak}\right)}{3T_{surge}}\right) \tag{4.7}$$

in which H_s is the significant wave height [m] at time t [s] and $\hat{H}_s$ is the maximum significant wave height (from equation 4.3) [m].

The wave peak period was then modelled, viz.

$$T_p(t) = \hat{T}_p \cos\left(\frac{\pi\left(t - T_{peak}\right)}{3T_{surge}}\right) \tag{4.8}$$

where T_p is the wave peak period [s] at time t [s] and $\hat{T}_p$ is the maximum wave peak period (from equation 4.4) [s]. An overview of the resulting hydraulic boundary conditions for an arbitrary situation is presented in figure 4.5.

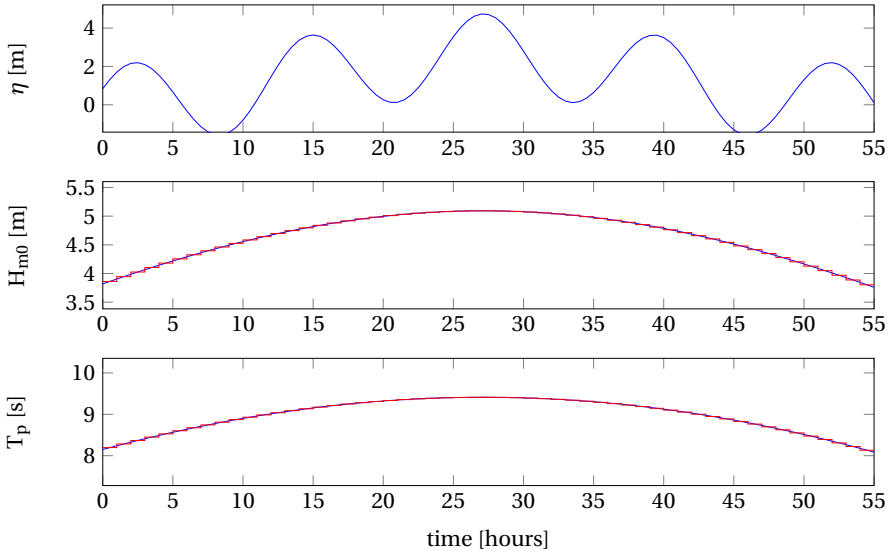

Figure 4.5: Hydraulic boundary conditions during a storm. Water level, significant wave height and wave peak period. Tidal peak coinciding with surge peak. Divided into one hour sections. Storm shape based on Steetzel (1993).

4.5. INHERENT UNCERTAINTY: SPACE

According to Van Gelder (2000), when determining the probability distribution of a random variable that represents the variation in space of a process, there is essentially a problem of shortage of measurements.

4.5.1. DIKE PARAMETERS

As mentioned earlier, the dike at Westkapelle was schematized for this thesis. The berm is not included and the average slope is considered, which is $\tan\alpha = 0.125$ or 7.13°. According to TNO (1999), the dike slope is normal distributed, with a coefficient of variation of $V = 0.05$. According to the same source, the crest height is normal distributed, with a standard deviation of 0.1. As mentioned before, the mean crest height of the Westkapelle sea defence was taken as the crest height in the schematization for this thesis, being 12.6 m+NAP.

4.5.2. SEDIMENT SIZE AND BED FRICTION

The sediment size D_{50} was determined from Van de Graaff et al. (2007) as being approximately 300 μm and is lognormal distributed with a coefficient of variation of 0.15, according to TNO (1999). The D_{90} was then calculated by taking 1.5 times the D_{50}. Not much information about the Manning friction factor is available for this location. Therefore, the preferred value of 0.02 was taken from Deltares (2015b) with some spreading around it, which results in the uniform distribution with lower and upper limits of 0.01 and 0.03.

4.6. LSF

In general, the limit state function (LSF) that is used for wave overtopping is defined as $Z = q_{crit} - q$, with q_{crit} a critical wave overtopping discharge depending on the type of layer and quality of the layer on the inner slope of the dike. For Westkapelle, this limit is 0.1 $ls^{-1}m^{-1}$.

Sometimes, the deterministic value of the critical wave overtopping discharge is assumed to also contain uncertainty. This was not used here, because of efficiency reasons. A changing critical wave overtopping discharge increases the difficulty of finding a good ARS fit with ADIS.

The shape of the standard wave overtopping LSF is shown in figure 4.6. This function shows a constant value of $Z = q_{crit}$ for a large part of the wave heights and then suddenly drops very fast below zero. It was determined that ADIS has difficulties with finding a ARS which fits this function. Therefore, the LSF that was used for this thesis, was changed into $Z = \log(q_{crit}) - \log(q)$, which has a much smoother shape, see figures 4.6 and 4.7. For the situation as described in section 3.4.1, the amount of calculations necessary for these two limit state functions was 342 exact evaluations for the standard wave overtopping LSF versus 70 exact evaluations for the LSF with the logarithm. However, a disadvantage of this LSF is that it becomes infinity if q becomes 0. Therefore, a minimum value of q= 10^{-99} $ls^{-1}m^{-1}$ was set. Such discontinuities cause problems when using FORM, which was also one of the reasons that ADIS was chosen.

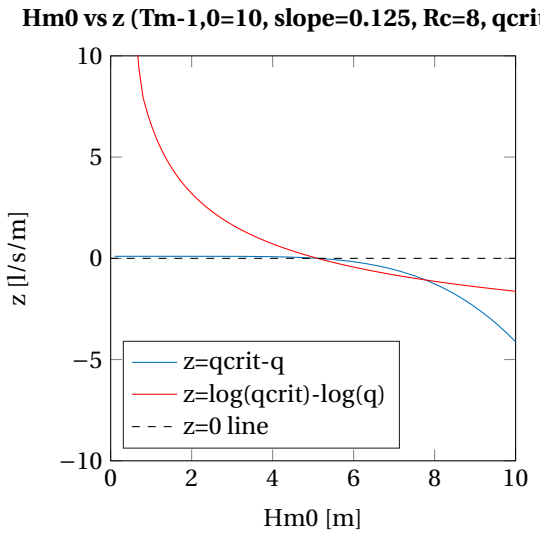

Figure 4.6: Wave overtopping limit state functions.

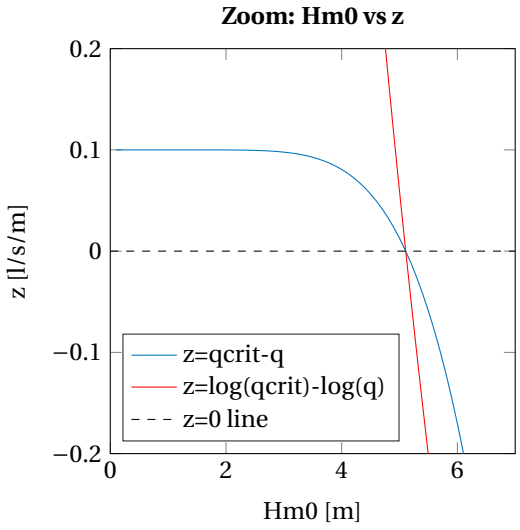

Figure 4.7: Zoom of wave overtopping limit state functions.

4.7. SUMMARY & CONCLUSIONS

This chapter aimed to provide an answer to sub-question 3: the probability distributions that describe the important parameters, and the parameters with the largest influence on morphological change, wave height, wave period and wave overtopping. The first part was answered in this chapter, the second part will be answered in chapter 6.

4.7.1. CHOICE OF PARAMETERS

17 parameters were chosen according to expert judgement and categorized according to Van Gelder (2000), as shown in table 4.1. Statistical uncertainties were not considered, in order to keep the total amount of vari-

ables small and because the influence was deemed small. Under model uncertainty, the breaker index, the calibration factors for wave skewness and wave asymmetry and four EurOtop coefficients were chosen. In the category inherent uncertainty in time, the storm duration, water level, wave height, wave period, wave directional spreading and the moment in time of the tidal peak relative to the surge peak were chosen. The distributions of water level, wave height and wave period were chosen according to the HR 2006 for dunes, which relates these parameters to one another. The storm profile in time was schematized according to Steetzel (1993). Parameters that represent inherent uncertainty in space were the dike parameters crest height and outer slope, and the sediment size and Manning bed friction factor.

4.7.2. LIMIT STATE FUNCTION

Due to the shape of the standard wave overtopping LSF, the function was changed to $Z = \log(q_{crit}) - \log(q)$, which has a much smoother shape. Sometimes, the critical wave overtopping discharge q_{crit} is also chosen as a stochastic variable. This was not done here, for the same reason as the change in LSF, because of the increased difficulty for ADIS to fit a good adaptive response surface.

5

APPLICATION OF MODELS

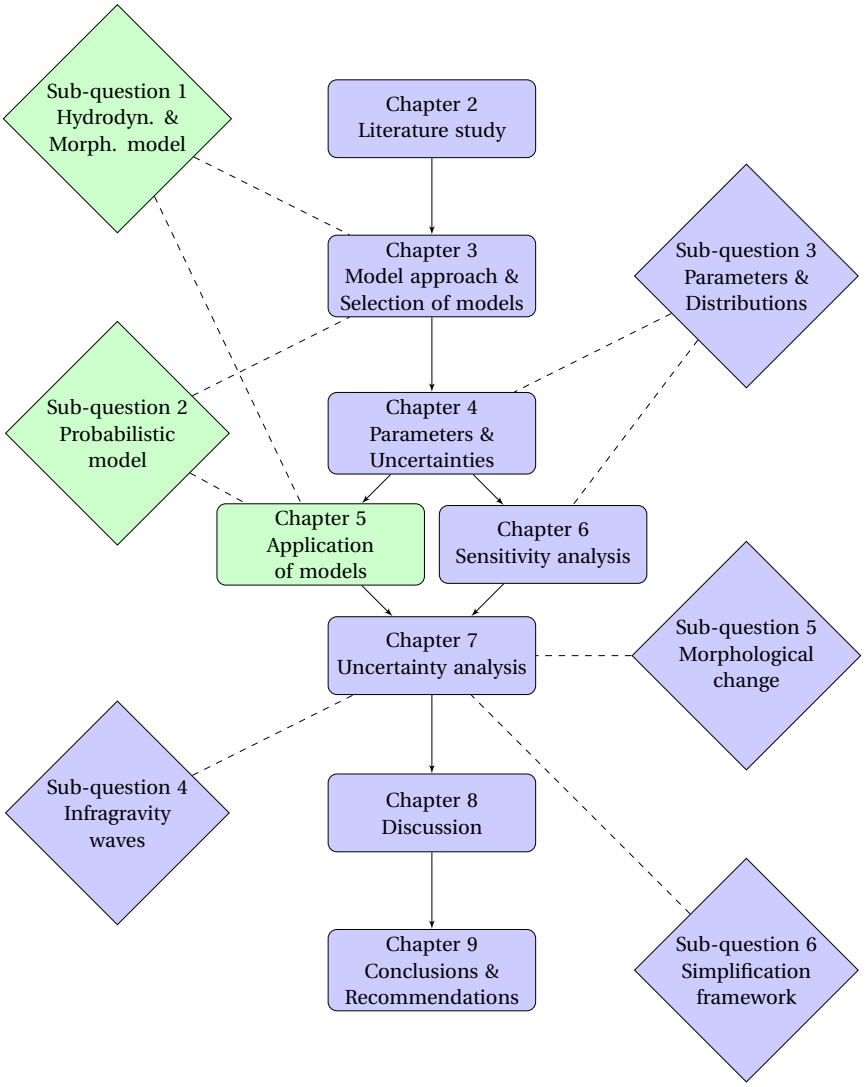

Figure 5.1: Outline of this report.

In this chapter, it is described how the models that were chosen in chapter 3 are applied in the probabilistic framework of ADIS, XBeach and EurOtop. Thus, this chapter aims to provide an answer to parts of the first and second sub-question. The first sub-question was: What method is appropriate to calculate the morphological changes of the foreshore, the infragravity waves and wave overtopping during a storm? The second sub-question was: With what kind of probabilistic framework can the probability of dike failure due to wave overtopping, influenced by a sandy, erodible foreshore be calculated? This chapter describes the settings that were used for the different models, and also presents a validation of XBeach.

Section 5.1 gives an introduction to the chapter and set-up of the framework. In section 5.2, the XBeach models that were used for the calculations are described. Section 5.3 describes the determination of the wave spectra at the toe of the dike. Next, section 5.4 shows the calculation of the wave overtopping discharge and 5.5 presents the ADIS settings that were used. After that, in section 5.6 a validation of XBeach was performed by comparison to experiments of Van Gent (1999). Finally, in section 5.7 a summary and conclusions to the chapter are presented.

5.1. INTRODUCTION

The models that were chosen in chapter 3 need to be combined to be able to calculate the probability of dike failure due to wave overtopping. The combination and application of the models is described in this chapter. The combination of models leads to a framework or 'model train', as shown in figure 5.2.

In the framework, ADIS determines the random variables. The calculation is started and a random direction and samples are determined. After that, using the samples from the random variables, XBeach calculates the wave transformation (and when enabled the morphological changes) in the dike-foreshore system and gives several parameters at the toe of the dike. Next, for each hour of the storm, the wave spectra at the dike toe are calculated and from that the spectral wave period ($T_{m-1,0}$) and wave height (H_{m0}) at the dike toe are determined. This wave heights and wave periods are entered into the EurOtop formulae, which calculates the wave overtopping discharge for each hour of the storm. The wave overtopping discharges during the storm are compared and the largest one is chosen. ADIS then calculates the Z-value, hence the result of the limit state function. When the converged probability of failure is found, the calculation is stopped. Otherwise, the process is repeated with a new random direction and new samples from the random variables. When a good fit for the ARS is found, analytical calculations using the ARS are used instead of XBeach calculations, which reduces the computation duration. However, still a small amount of 'exact' XBeach calculations will be needed to maintain precision.

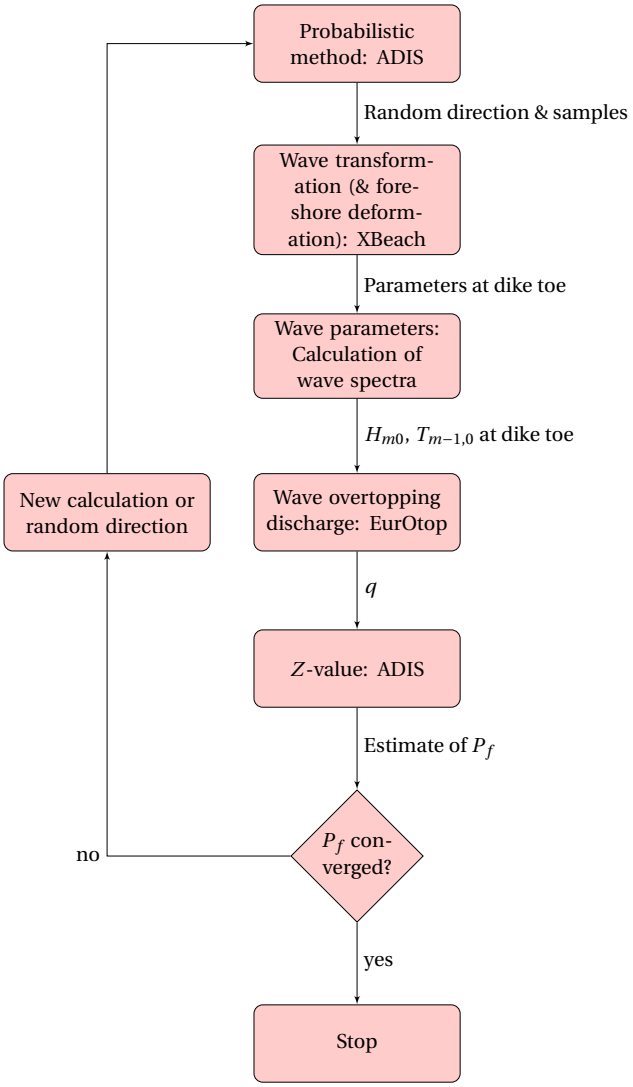

Figure 5.2: Modelling framework or 'model train', using ADIS, XBeach and EurOtop to calculate the probability of dike failure due to wave overtopping.

5.2. XBEACH CALCULATIONS

For the XBeach calculations, the surf-beat version of XBeach was used. The models that were used, included the long waves, the short waves on the wave group scale, flow, sediment transport and morphology. Two different types of models were used, a 1D model and a 'semi-2D'model, in which no alongshore variations in the profile were included. For the calculations in this thesis, the Westkapelle sea defence was schematized based on the 2009 JARKUS transect 1832, see figures 1.5 and 1.6. Instead of the local crest height at transect 1832, the mean crest height of the Westkapelle sea defence was used, being 12.6 m+NAP. Furthermore, the dike was shchematized without the berm and the bathymetry was simplified to two line sections, to be able to easily include different foreshore shapes and sizes, and to be able to easily compare a situation without and with a foreshore in future studies. See figure 5.3. The JARKUS profile runs to approximately -10 m+NAP. According to common XBeach practice, the profiles were extended to a depth of -20 m+NAP with a slope of 1:50, to remove boundary effects. As mentioned in the previous chapter, to the South of the Maasvlakte, the hydraulic boundary conditions from the stations ('steunpunten') are valid for a point past the most offshore breaker zone. Hence, this is not necessarily -20m+NAP, but the calculations showed that virtually no change in wave height occurs between -20 m+NAP and the most offshore breaker zone. The dike itself was implemented as a hard structure, which means that no erosion of the dike slope was possible. For the 1D- and 2D-models, the cross-shore grid sizes were automatically calculated with the XBeach MATLAB toolbox, which determines these sizes by using the CFL condition. For the 2D-model, in the alongshore direction, a section of 1 km was modelled with grid cell sizes of 50 m. which was created by applying the cross-shore profile everywhere in the alongshore direction, which means that no alongshore variations in the profile were included. An example of a computational grid and bathymetry file for the 2D-model is given in figure 5.4.

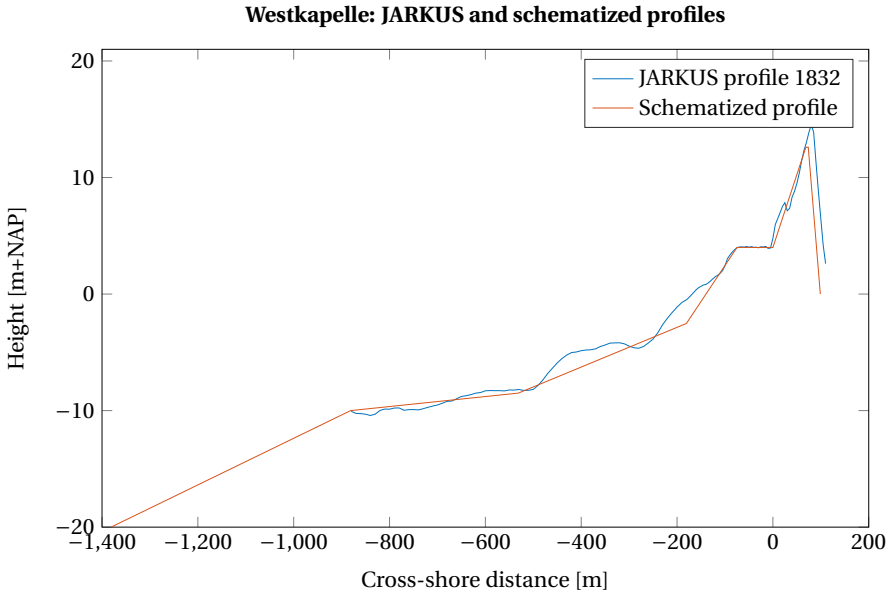

Figure 5.3: Comparison of JARKUS transect 1832 (2009) and the schematized cross-shore profile.

XBeach uses a coordinate system where the x-axis is always oriented towards the coast and the y-axis is oriented in the alongshore direction. The models used a rectilinear grid with variable grid cell sizes. Furthermore, the MPI version of XBeach was used with the 2D-model, which makes it possible to run XBeach on multiple processor cores, by splitting the computational grid in several sections. This was done in order to save computational time. A comparison between the standard XBeach version and the MPI version showed negligible differences in the results.

The 1D model was used for its short calculation duration. The semi-2D approach was chosen because it allows for the inclusion of waves approaching from different directions, good representation of the wave directional spreading, as well as a better representation of the infragravity waves in a 2D model. As is further discussed in Appendix E, with the 1D model, the infragravity waves are not represented as well as with the 2D model, because of the exclusion of the wave directional spreading, which influences the infragravity wave height. However, due to the reasonable results and especially the short calculation durations, the 1D model

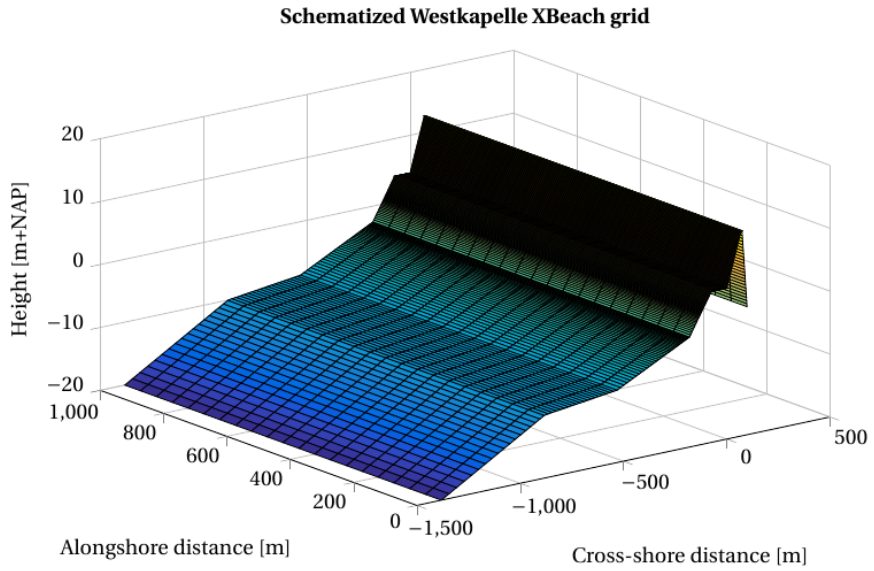

Figure 5.4: XBeach computational grid and bathymetry for the 2D-model of the schematized Westkapelle sea defence. The 1D-model uses the same cross-shore transect.

was used as well.

Where possible, default XBeach settings were used, with the exception of the stochastic model parameters identified in chapters 3 and 6. The settings which differed from the standard XBeach settings, are explained in more detail below. An example of the input files for XBeach, as used for the calculations, is presented in Appendix G.

To reduce the computational time with the 2D models, the wave direction was solved at regular intervals using the stationary solver ($single\_dir = 1$), which then propagates the wave energy along the mean wave direction. In the stationary solver, the wave energy and roller energy balances are solved line by line, from the seaward boundary in the landward direction. For the in-stationary mode ($dtheta$) a single directional bin of 120 degrees was used and for the stationary solver ($dtheta\_s$) a smaller bin size of 10 degrees was used. As the solving interval, 60 seconds was chosen. The same settings were used for the 1D XBeach calculations. However, XBeach 1D does not include refraction or wave directional spreading. For the spin-up time of the wave boundary conditions ($taper$), 1200 seconds was chosen.

For the offshore and onshore boundaries, absorbing-generating (weakly-reflective) 2D-boundary conditions were included, to reduce boundary effects (abs_2d), abs_1d in the case of the 1D-model. For the lateral boundaries, cyclic boundary conditions were chosen ($cyclic = 1$), to remove shadow zones with obliquely incoming waves. With the cyclic boundary conditions, the wave energy leaving the lateral boundary on one side can be inserted at the other boundary again. The cyclic boundary conditions can only be used with the MPI version of XBeach, which meant that for the 1D-model, Neumann boundary conditions were used instead. The wind was not used in the models. The wind speed was already incorporated into the boundary conditions of the model (water level, wave height, wave period). Furthermore, a wind stress acting on the water surface inside the model was not used, because the influence was negligible. The keyword $random = 0$ was used, which means that the same set of random numbers was used for each XBeach calculation.

According to the new Dutch assessment guidelines (WTI 2017, (Deltares, 2015a)), it is recommended to change a number of default XBeach settings, as shown below in table 5.1. These settings were also used in the XBeach models.

The intervals for the output of the global and point variables were set to 1800 and 1 s. No mean output was generated. Global model output was given for 1 variable, the bed level. Point output was given at one point, in the (alongshore) centre of the model, at the toe of the dike. At the toe, the time series output of 4 variables was given; the root-mean-square wave height based on the instantaneous wave energy (H) (short wave energy), the water level (zs) (this also includes the infragravity waves, the bed level (zb), and the GLM velocity in x-direction (uu).

The parameters that were considered as stochastic variables were presented previously in chapter 4.

Table 5.1: WTI 2017 preferred XBeach settings (Deltares, 2015a). Note that $facSk$, $facAs$ and $gamma$ were used as stochastic parameters. The values from the table were used as mean values in the probability distributions.

Parameter	Default	WTI settings	Description
fw	0	0	Short wave friction coefficient (bed friction)
$gammax$	2	2.364	Maximum ratio wave height to water depth (breaking waves)
$beta$	0.1	0.138	Breaker slope coefficient (wave roller model)
$wetslp$	0.3	0.26	Critical bed slope for wet area (avalanching)
$alpha$	1	1.262	Wave dissipation coefficient (breaking waves)
$facSk$	0.1	0.375	Effect of wave skewness on sediment transport
$facAs$	0.1	0.123	Effect of wave asymmetry on sediment transport
$gamma$	0.55	0.541	Breaker index (breaking waves)

5.2.1. COMPARISON JARKUS & SCHEMATIZED BATHYMETRY

2D XBeach calculations without sediment transport or morphological changes were performed with the real JARKUS bathymetry as well as with the schematized profile, the results were compared and agreed reasonably well. The boundary conditions that were used for this comparison were the conditions of the 1/1,000 years storm, deduced from the probability distributions as described in the previous chapter (q.v.). For the 2D-model, the wave heights and wave periods at seven locations along the profile were compared and showed similar results (see figure 5.5 and figure 5.6), with the largest difference in wave height occurring along the foreshore slope, being 0.35 m, and the largest difference in wave period occurring at the dike toe and being 1.2 s. The differences were much smaller along the rest of the profiles, due to which the representation of the schematized profile was deemed sufficient.

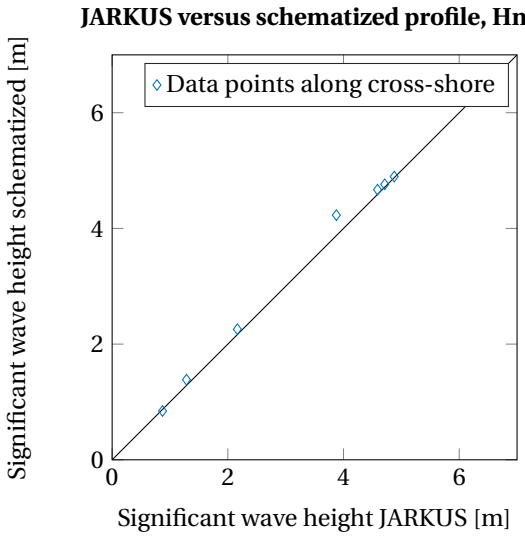

Figure 5.5: Comparison between wave heights for XBeach calculations with JARKUS transect 1832 bathymetry and schematized bathymetry.

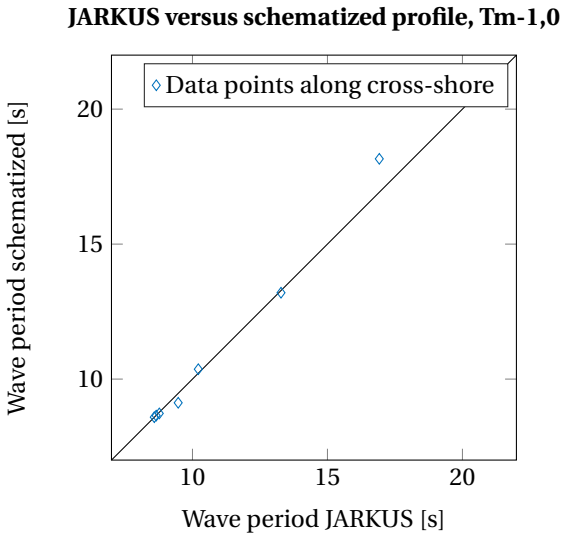

Figure 5.6: Comparison between wave periods for XBeach calculations with JARKUS transect 1832 bathymetry and schematized bathymetry.

5.3. CALCULATION OF THE WAVE SPECTRA AT THE TOE

The time series of model data at the toe of the dike were loaded into MATLAB. The de-trended water depth data can be used to calculate the low frequency (infragravity) wave height and period. The GLM velocity in x-direction and water depth were used to separate the incoming from the reflected waves. The water depth is calculated by subtracting the bed level from the water level. The spectra can be calculated on the basis of the incoming waves only or the incoming and reflected waves. For this thesis, only the incoming waves were used, because the physical model tests on which the EurOtop formulae are based also only included the incoming waves. To separate the incoming and reflected waves, a method based on Van Thiel de Vries (2009)

was used, which was in turn based on Guza et al. (1984):

$$\eta_{in} = \frac{\eta c_{out} + Q}{c_{in} + c_{out}} \tag{5.1}$$

$$\eta_{out} = \frac{\eta c_{out} - Q}{c_{in} + c_{out}} \tag{5.2}$$

where η_{in} and η_{out} [m] are the surface elevations associated with the incoming and reflected waves and $Q = uh$, with u the velocity [m/s] and h the water depth [m]. Because of the limited water depth at the toe, it is assumed that the outgoing waves travel with $c_{out} = \sqrt{gh}$. For the velocity of the incoming waves, the actual wave group velocity is used: c_{in}=c_g (based on the $T_{m-1,0}$ wave period).

Next, the data was split into sections during which the boundary conditions were approximately constant (set to 1 hour). For each section, the low frequency spectrum was calculated by taking the resulting data of the incoming waves only. A linear de-trending method was used for the data. The measurement interval was the same as the resolution of the data, thus 1 s. The frequency resolution was set to 0.005 Hz. The time series was split into smaller overlapping sections, using the Welch method with a maximum overlap of 50%. The Welch method reduces the noise in the estimated spectrum in exchange for reducing the frequency resolution. After the division into segments, the segments were windowed, using a Hann window. The Hann or Von Hann window is given by a cosine function which goes to zero at both ends. For a further description of the Welch method and the Hann window function, refer to Appendix C. In the small scale tests of Van Gent (1999), on which the wave overtopping formula for $\xi > 7$ was based, the limits of the spectra were set to f_{min}= 0.02 and f_{max}= 1.2 Hz. For prototype scale used in this thesis, these limits were scaled with the peak period, which was 1.6 s in the small scale tests and is approximately 10 s in prototype scale, which leads to limits of 0.003 and 0.2 Hz.

The high frequency (short wave) wave period and wave height were calculated by using the T_p entered in XBeach and by using the H point data, which represents the H_{rms} wave height, based on the instantaneous wave energy. XBeach hydrostatic does not calculate the changes in the short wave period. The short wave period [s] is calculated as:

$$T_{m-1,0} = \frac{T_p}{1.1} \tag{5.3}$$

The short wave height [m] is calculated by:

$$H_{m0} = \sqrt{2} H_{rms} \tag{5.4}$$

From the short wave period and short wave height, a JONSWAP spectrum and a delta function spectrum were estimated, which were then added to the low frequency spectrum, see figure 5.7. From the resulting total spectra, the total spectral wave period and wave height were calculated, using the moments m_k:

$$m_k = \int_{f=0}^{\infty} f^k S(f) df \tag{5.5}$$

$$H_{m0} = 4\sqrt{m_0} \tag{5.6}$$

$$T_{m-1,0} = \frac{m_{-1}}{m_0} \tag{5.7}$$

The resulting total spectrum based on the low frequency spectrum and the added JONSWAP spectrum, and the spectrum based on the low frequency spectrum with the delta function added were compared for each calculation and showed good agreement.

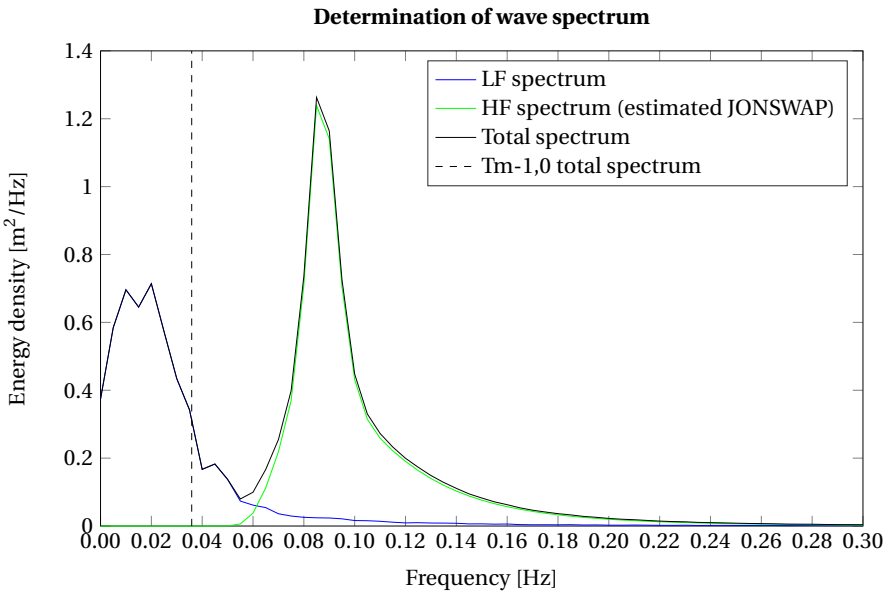

Figure 5.7: Low frequency, high frequency and total wave spectrum. The high frequency spectrum uses an estimated JONSWAP shape.

5.4. WAVE OVERTOPPING CALCULATIONS

The resulting wave parameters at the toe of the dike, for each period during which the boundary conditions were approximately constant (1 hour) were entered into the EurOtop equations, together with the freeboard, slope of the dike and roughness of the slope, with which the wave overtopping discharge ($ls^{-1}m^{-1}$) was calculated. Of the resulting overtopping discharges, one for each hour of the storm, the maximum is taken and entered into the limit state function. Because of the use of the omni-directional statistics, the angle of wave incidence is kept at an angle of 0 °to the dike normal, hence 270 °in XBeach.

5.5. ADIS SETTINGS

Within ADIS, an accuracy of 95% and a confidence level of 20% were set, which means that the true probability of failure lies with 95% certainty within 20% difference of the calculated probability of failure. These settings were chosen as a trade off between accuracy of the calculated probability of failure and duration of the calculation. For this thesis, the goal is not to calculate the probability of failure with 100% accuracy, but to gain an indication of the order of magnitude of the probability of failure and to compare different probabilities of failure for different situations. Calculating a probability of failure with a very high accuracy is also unnecessary because a schematized version of the Westkapelle sea defence is used. A seed was set for the random number generator, to be able to reproduce results. The default ADIS response surface fitting method was used, together with the default margins of the β-sphere, which means fitting a second order polynomial for the ARS and a β-sphere margin of 0.1. To be able to fit a second order polynomial, a minimum number of LSF evaluations needs to be available, $1 + n + \frac{n(n+1)}{2}$, with n the amount of stochastic variables. The standard start-up method was used, which means that ADIS tries an initial fit with a second order polynomial without cross-terms, which only needs $2n + 1$ points. Bisection can be used when no convergence is reached in a certain direction. However, when no convergence is reached with the fitting of the polynomial, it will usually also not be reached with bisection and furthermore, bisection will increase the amount of calculations. Therefore, no bisection was used. The minimum number of sampled directions was set to 50, the maximum set to 1,000. The maximum reliability index value (β) for which ADIS is able to search $Z = 0$ points in certain directions was set to 8.3, which corresponds to a probability of exceedance of approximately $4 * 10^{-16}$. The minimum number of approximated points was set to 50, such that always a reasonable amount of points are available. The first values that ADIS tries in the probability distributions of the stochastic variables are values corresponding $\beta = 4$, which corresponds to a return period that is in the same order of magnitude as the return periods that Dutch legal requirements require for dikes (1/250 - 1/10,000). The value of $\beta = 4$ was chosen to reach convergence as fast as possible, because it can be expected that the failure probability also lies in this

order of magnitude.

5.6. VALIDATION OF XBEACH WITH EXPERIMENTS OF VAN GENT (1999)

To check if the (large) wave periods ($T_{m-1,0}$) at the dike toe resulting from the calculation of the wave spectra were correct, a validation was necessary. Therefore, in order to verify the predictive capabilities of the combination of XBeach and the spectral calculations (Fourier analysis) in MATLAB, the combination of XBeach and Fourier analysis was compared to the flume experiments of Van Gent (1999) (q.v.), on which the EurOtop wave overtopping formula for $\xi_{m-1,0} > 7$ was based.

5.6.1. DESCRIPTION EXPERIMENTS VAN GENT (1999)

The experiments consist of physical model investigations in a wave flume to study wave run-up and wave overtopping for situations with shallow foreshores. The shapes of the offshore wave energy spectra, the water depth and the slope of foreshore and structure were varied. The tests were performed in the Scheldt-flume of WL | DELFT HYDRAULICS (now Deltares). The test programme consisted of tests with single and double peaked wave energy spectra, foreshores with slopes of 1:100 and 1:250, structures (dikes) with slopes of 1:2.5 and 1:4 and shallow, intermediate and deep water at the toe of the structure. The foreshores were constructed over a length of 36 m. The distance between the toe of the structure and the wave board was 40 m. Five sets of three wave gauges were placed along the foreshore, of which for this research the set at the toe of the dike was the most relevant. The set-up for the 1:100 slope foreshore and 1:4 slope structure is presented in figure 5.8.

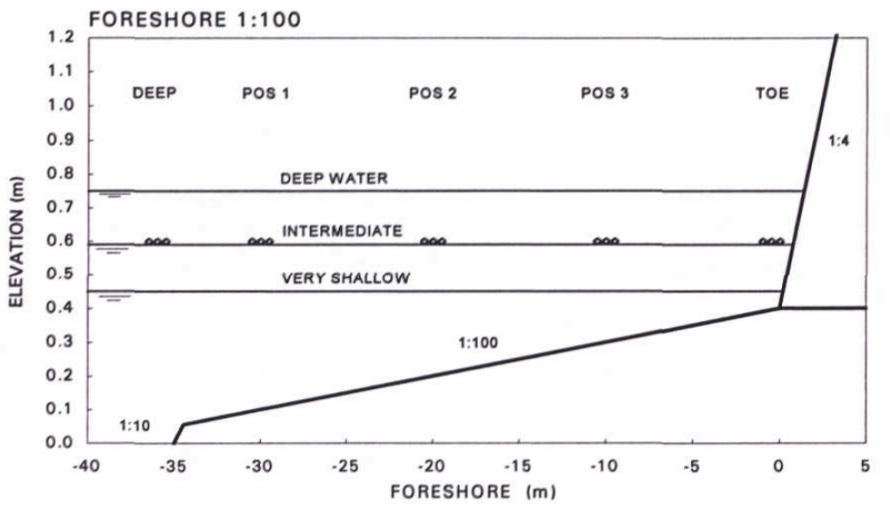

Figure 5.8: Set-up with 1:100 foreshore and 1:4 structure slope, (Van Gent, 1999).

5.6.2. DESCRIPTION XBEACH MODELS

The flume situation was entered into XBeach as a 1D model. As well as in the physical model tests, the structure was not present for the calculation of the wave parameters at the toe and only the incoming waves were considered. Also, the Scheldt-flume includes reflection compensation. Because it was not clear which frequencies could and could not be filtered out in the physical model tests, it was chosen to filter all frequencies and thus only take the incoming waves.

The A and C test series with single peaked spectra were reproduced, by using 3 different models: XBeach hydrostatic, XBeach hydrostatic with a lower value of the breaker index $gamma$ and XBeach non-hydrostatic. The results for XBeach hydrostatic will be discussed here, the results of XBeach non-hydrostatic and XBeach with a lower $gamma$-value are presented in Appendix H. Both the A and C test series use an offshore peak period of 1.6 s and an offshore wave height of 0.141 m. The difference in the series lies in the foreshore and structure slope, 1:100 and 1:4 for the A series and 1:250 and 1:2.5 for the C series.

No morphology or sediment transport was used, as the physical model tests were done in a concrete flume. Different values of the bed friction coefficient were considered to model the concrete. Finally, cf = 0.001 was chosen, but a different friction coefficient showed no real influence on the results. As offshore and

onshore boundary conditions, the 1D absorbing-generating boundary conditions were used. For the lateral boundaries, the 'wall' boundary conditions were used, to represent the flume walls. Point output (time series) of wave heights, water levels and velocities was given at the same five locations as the wave gauge arrays in the physical model tests. With these data, the wave spectra were calculated in the same way as described above in section 5.3. Again, only the incoming waves were used, as this was also done for the physical model tests. In order to calculate the wave height and wave period from the spectra, different limits to the spectra were used, because it was not clear which limits Van Gent (1999) used. The plotted spectra in Van Gent (1999) show the frequencies 0.02-1.2 Hz, however in the text it is mentioned that no cut-off was used. Therefore, for the comparison, three different spectral frequency limits were used: 0.02-1.2 Hz, 0-∞ Hz and $1/(10T_p)$-1.2 Hz. It is also unlikely that Van Gent (1999) included the very low frequency (VLF) oscillations, which range approximately from 10-150 min in prototype scale (Munk, 1950). These waves are standing waves, with a frequency equal to the resonance frequency of the basin, or in this case, flume.

5.6.3. COMPARISON OF SPECTRA, WAVE HEIGHTS AND WAVE PERIODS

The resulting wave heights and wave periods from the calculated spectra at the five locations along the slope were compared, as well as the spectra at the toe of the structure for the A test series. For the C test series, no spectra were available. The wave periods and wave heights along the slope for the A and C test series are presented in the tables in Appendix H, as well as the spectra and all the results for XBeach non-hydrostatic and XBeach with a lowered $gamma$-value. The tables in the Appendix show the water depth d, wave height H_{m0} and wave period $T_{m-1,0}$ for the five locations along the slope, with $Xtoe = 0$ being at the toe of the structure. Again, the results of the three different XBeach models are shown, as well as the different frequency limits that were used to calculate the wave parameters from the spectra. The wave spectra at the toe for test series A are presented in figure 5.9, 5.10, 5.11 and 5.12.

First off, an important point has to be noted. When the $T_{m-1,0}$ wave period is determined from the spectra as given in, cf. Van Gent (1999), different values are found than the ones that are listed in the tables in, cf. Van Gent (1999). Even though the shown spectra range from 0.02-1.2 Hz, this indicates that Van Gent (1999) included frequencies higher than 1.2 Hz in the calculation of the $T_{m-1,0}$ values. As a result, the $T_{m-1,0}$ values that Van Gent (1999) listed in the tables are lower than what would be expected from the spectra in Van Gent (1999).

The XBeach $T_{m-1,0}$ values were determined from the spectra, with the three different options for the frequency limits. The XBeach hydrostatic spectra show more energy at the peak period, due to the imposed JONSWAP spectrum, but also show less energy in the very high frequency range than the spectra from, cf. Van Gent (1999). Due to the combined effect of these two phenomena, the resulting $T_{m-1,0}$ periods for XBeach hydrostatic and frequency limits 0.02-1.2 Hz still agree quite well, even though the shape of the spectra is different.

Test A1.03 uses the largest water level, 0.753 m, with the bottom of the flume at 0 m. The spectra at the toe show quite good agreement. Test A1.06 uses the intermediate water level of 0.588 m. Here, XBeach hydrostatic shows a larger energy density in the low frequency range (0.02-0.1 Hz). Near the peak frequency, the hydrostatic model differs considerably from the measurements, because in the hydrostatic model, the spectral transformation of the high frequency wave period is not calculated. Therefore, as described above, a JONSWAP spectrum is superimposed on the low frequency spectrum, which leads to the different spectral shape. Test A1.09 uses a shallow water level of 0.494 m. The spectra agree reasonably well at the lower frequencies, but not at the higher frequencies. Again, the hydrostatic model shows a peak at the peak frequency. Due to this, the XBeach spectrum contains more energy, which leads to a larger wave height than measured in the flume experiments. The low frequency peak of the physical model lies at a somewhat lower frequency than the low frequency peak of the hydrostatic model. Test A1.12 uses a very shallow water level of 0.447 m. Again the peak at the peak frequency in the hydrostatic model is visible (with the accompanying larger wave height), as well as the difference in the location of the low frequency peaks, although they contain approximately the same energy density. Because the wave period $T_{m-1,0}$ is heavily influenced by these low frequencies a difference in the location of these peaks could lead to (large) differences in the wave period.

Table 5.2 shows the differences between the flume experiments and the XBeach hydrostatic model with frequency limits 0.02-1.2 Hz in significant wave height and wave period at the toe of the structure. In general, the wave height and wave period are represented quite well by the different models. It has to be noted that at the most offshore location, there is already a deviation in the wave height, but not in the wave period (see the tables in Appendix H). This deviation could indicate boundary problems caused by the schematization of the flume in XBeach. At the toe, in general, the frequency limits of 0.02 and 1.2 show the best results.

The wave height at the toe shows small differences with the different frequency limits, but the wave period is influenced more severely, which can be explained by considering the definition of the $T_{m-1,0}$ wave period (the first negative moment), which indicates a large influence of the energy in the low frequencies. Of the different XBeach models, in general, the non-hydrostatic model reproduces the shape of the spectra the most accurately, but the hydrostatic model produces the most accurate wave heights and periods.

The differences are largest for the tests with the lowest water depth (A1.12 and C1.12). For such small water depths and thus low amounts of wave energy, a small error in the wave spectrum already leads to a significant deviation in wave height and wave period. The absolute differences in wave height are generally small. The differences in wave period are also small, with the largest differences occurring for the A1.12 and C1.12 test. When the relative differences are considered, the errors seem larger, however, it has to be considered that a very small difference of 0.012 m in the C1.12 test, together with a wave height at the toe of only 2.4 cm, already leads to a large relative difference, due to this very small wave height.

In general, the differences between the physical model tests and XBeach hydrostatic with limits 0.02-1.2 Hz are reasonably small. The low frequency waves can be of influence on the wave overtopping, so it is recommended to study the influence of these low frequency waves on wave overtopping in more depth. Because the standard hydrostatic model and the frequency limits of 0.02-1.2 Hz perform the best, these were chosen for the remainder of this thesis.

In the figures 5.9-5.12 the XBeach $T_{m-1,0}$ periods calculated with frequency range 0.02-∞ Hz are shown together with the $T_{m-1,0}$ periods as presented in Van Gent (1999), but in the calculations with the model framework, the 0.02 - 1.2 Hz frequency limits will be used, which become 0.003-0.2 Hz when scaled to prototype scale (by scaling with the peak period). Using these limits instead of 0.02-∞ Hz gives a difference in $T_{m-1,0}$ $\leq$4% in prototype scale, due to the underestimation of the very high frequency energy in XBeach. A (maximal) difference of 4% in $T_{m-1,0}$ can result in a maximum difference of about 1% in q, so the influence of the underestimation of the very high frequency energy in XBeach is limited.

When using the limits of 0.02-1.2 Hz, for the model tests with deep water the wave period is somewhat overestimated, and for the tests with shallow water the wave period is somewhat underestimated. These differences can be explained by the definition of the $T_{m-1,0}$ wave period, in which the low frequencies have a very large influence, as well as the differences in the spectral shapes as explained before. Clear rules should be determined for calculating the $T_{m-1,0}$ wave period when infragravity waves are present, because this wave period is so sensitive to the low frequencies. The resulting wave parameters were very sensitive to changes in the frequency resolution with which the spectrum was calculated, as well as the frequency limits. As mentioned above, the frequency resolution was set at 0.005 Hz, based on expert judgement, but the determination of the frequency resolution and frequency limits for deriving the $T_{m-1,0}$ period is thus a topic for further research.

Table 5.2: Relative differences in wave height and wave period at the toe of the structure between flume experiments (cf. Van Gent (1999)) and XBeach hydrostatic, with frequency limits 0.02-1.2 Hz. Offshore significant wave height 0.141 m, offshore wave peak period 1.6 s. Mean absolute difference in wave height 15.8%, mean absolute difference in wave period 9.1%.

Test	Measured H_{m0} [m]	Modelled H_{m0} [m]	Difference in H_{m0} [%]	Measured $T_{m-1,0}$ [s]	Modelled $T_{m-1,0}$ [s]	Difference in $T_{m-1,0}$ [%]
A1.03	0.134	0.130	-4%	1.59	1.68	+6%
A1.06	0.104	0.099	-3%	1.89	2.20	+17%
A1.09	0.057	0.066	+15%	3.20	3.26	+2%
A1.12	0.036	0.045	+26%	7.33	5.58	-24%
C1.03	0.132	0.127	-4%	1.64	1.80	+10%
C1.06	0.099	0.097	-3%	2.17	2.19	+1%
C1.09	0.050	0.060	+20%	2.85	2.75	-4%
C1.12	0.024	0.036	+51%	4.27	3.87	-9%

5.6.4. CONCLUSIONS OF VALIDATION

Some general conclusions that can be drawn from the above are:

- Even though the spectra from Van Gent (1999) range from 0.02-1.2 Hz, Van Gent (1999) included frequencies higher than 1.2 Hz in the calculation of the $T_{m-1,0}$ values. As a result, the $T_{m-1,0}$ values that

Van Gent (1999) listed in the tables are lower than what would be expected from the spectra.

- Near the peak frequency the hydrostatic model differs from the measurements, because the hydrostatic model does not calculate the transformation of the high frequency wave period. The XBeach hydrostatic spectra also show less energy in the very high frequency range than the spectra from Van Gent (1999). Due to the combined effect of these two phenomena, the resulting $T_{m-1,0}$ periods for XBeach hydrostatic still agree quite well, even though the shape of the spectra is different. XBeach (hydrostatic) needs to be improved to be able to also predict the spectral shape in a correct way.
- The low frequency peaks contain approximately the same amount of energy, but are located slightly different.
- The wave period $T_{m-1,0}$ is heavily influence by the low frequencies, frequency resolution and frequency limits, which can easily lead to (large) differences in the wave period. It is recommended to determine clear guidelines on how to determine the $T_{m-1,0}$ wave period when infragravity waves are present.
- At the most offshore location (near the wave board), there is already a deviation in wave height, but not in wave period. This could indicate boundary problems or could be a model artefact from XBeach, but this needs to be investigated in more detail.
- It is recommended to study the influence of low frequency waves on wave overtopping in more depth.
- The from the wave spectra resulting wave parameters were heavily influenced by the frequency resolution with which the spectrum was determined. The determination of the frequency resolution remains a topic for further research.
- XBeach hydrostatic with frequency limits 0.02-1.2 Hz showed the best results and will be used in the remainder of the thesis. When converted to prototype scale, these limits become 0.003-0.2 Hz.

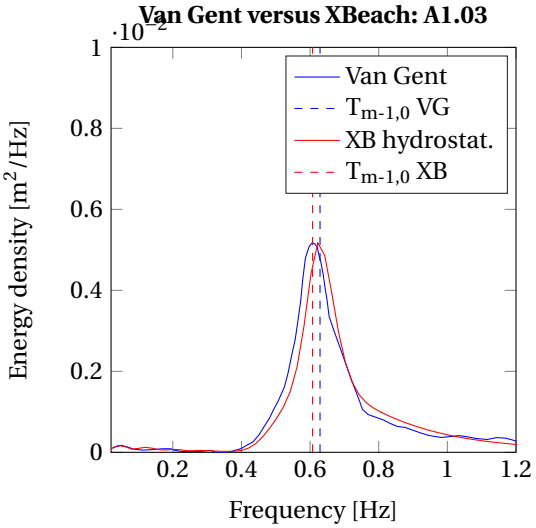

Figure 5.9: Spectra for test A1.03, cf. (Van Gent, 1999). Note that the wave periods as shown were calculated with frequency limits 0-∞ Hz. Note that the vertical axis is varying per plot.

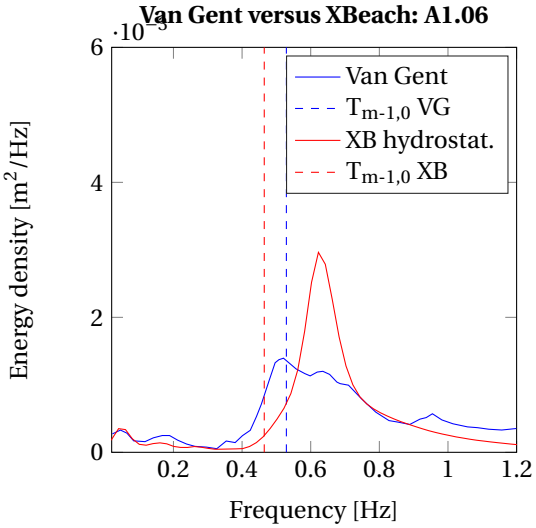

Figure 5.10: Spectra for test A1.06, cf. (Van Gent, 1999). Note that the wave periods as shown were calculated with frequency limits 0-∞ Hz. Note that the vertical axis is varying per plot.

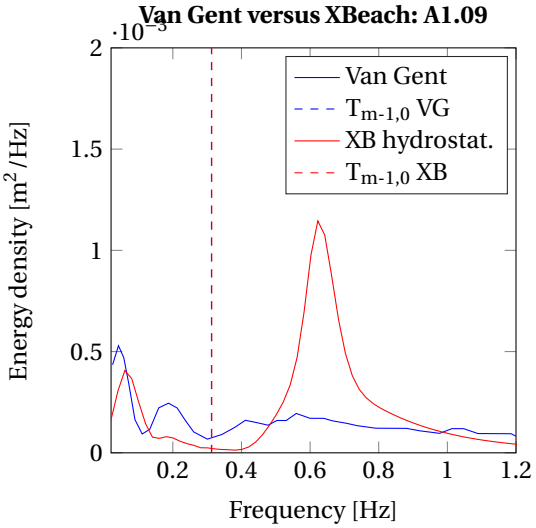

Figure 5.11: Spectra for test A1.09, cf. (Van Gent, 1999). Note that in this figure the wave periods almost coincide, which is why it seems like only one dashed line is plotted. Note that the wave periods as shown were calculated with frequency limits 0-∞ Hz. Note that the vertical axis is varying per plot.

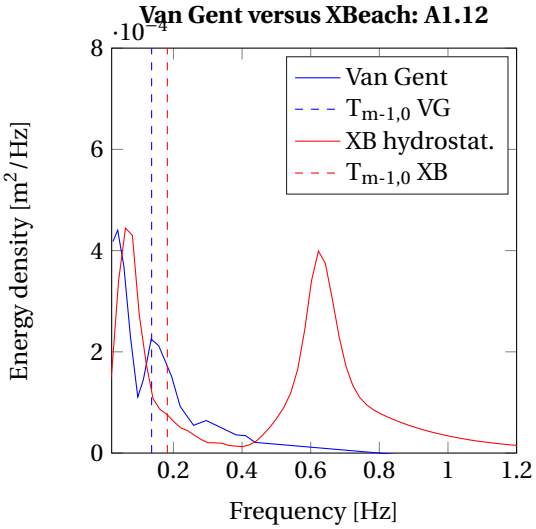

Figure 5.12: Spectra for test A1.12, cf. (Van Gent, 1999). Note that the wave periods as shown were calculated with frequency limits 0-∞ Hz. Note that the vertical axis is varying per plot.

5.7. SUMMARY & CONCLUSIONS

This chapter aimed to provide an answer to parts of the first and second sub-question: the best fit morphological, hydrodynamic, wave overtopping and probabilistic methods to determine the probability of dike failure due to wave overtopping. The models that were chosen in chapter 3 were applied in this chapter, to be able to eventually determine the probability of failure in chapter 7.

5.7.1. APPLICATION OF XBEACH

The XBeach hydrostatic models that are used for the calculations, include the long waves, the short waves on the wave group scale, flow, sediment transport and morphology. The MPI version of XBeach was used in combination with cyclic boundary conditions. A semi-2D model was used, with a rectilinear grid with variable grid cell sizes. The profiles in the cross-shore direction were based on the JARKUS profiles at Westkapelle, where the dike was schematized without the berm and in which the bathymetry was simplified to two line sections. In the alongshore direction, a section of 1 km was modelled with grid cell sizes of 50 m. No alongshore variations in the cross-shore profile were included. The wave heights and wave periods at several locations along the profile were compared to the real JARKUS bathymetries at Westkapelle and showed similar results.

5.7.2. CALCULATION OF SPECTRA

The from the XBeach calculations resulting time series at the toe of the dike were loaded into MATLAB. Only the incoming waves were used in the determination of the spectra. For each hour of data, during which the boundary conditions were regarded as being constant, two spectra were calculated, one low frequency spectrum with a high frequency JONSWAP spectrum added to it, and one low frequency spectrum with a high frequency delta function added to it. These spectra showed good agreement. For the frequency resolution 0.005 Hz was used, for the spectral limits 0.003-0.2 Hz. From these spectra the wave height (H_{m0}) and wave period ($T_{m-1,0}$) at the dike toe were determined.

5.7.3. CALCULATION OF WAVE OVERTOPPING DISCHARGE

The resulting wave parameters were entered into the EurOtop equations, together with the freeboard, main wave direction, slope of the dike and roughness of the slope, with which the wave overtopping discharge was calculated.

5.7.4. PROBABILISTIC SETTINGS

Within ADIS, an accuracy of 95% and a confidence level of 20% were set. The default ADIS response surface fitting method was used, together with the default margins of the β-sphere. The minimum number of sampled directions was set to 50, the maximum set to 1,000.

5.7.5. VALIDATION OF XBEACH

In some cases, large wave periods ($T_{m-1,0}$) at the dike toe resulted from the calculation of the wave spectra with the combination of XBeach and Fourier analysis. Therefore, this combination was compared to the flume experiments of Van Gent (1999), on which the EurOtop wave overtopping formula for $\xi_{m-1,0} > 7$ was based. From this comparison, it could be concluded that the wave height and wave period are represented reasonably well. The differences in the $T_{m-1,0}$ wave periods were caused by the very heavy weighing low frequencies in the calculation of this wave period, as well as differences in the shape of the spectra. Small differences in the low frequency energy between the flume experiments and XBeach can already lead to large differences in the $T_{m-1,0}$ wave period. Furthermore, it was determined that the resulting wave parameters at the toe are very sensitive to changes in the frequency resolution with which the wave spectrum is determined, which is a topic for further research. Finally, XBeach hydrostatic with spectral frequency limits of 0.02-1.2 Hz (in model scale) were chosen for further use in this thesis, because this combination showed the best results.

6

SENSITIVITY ANALYSIS

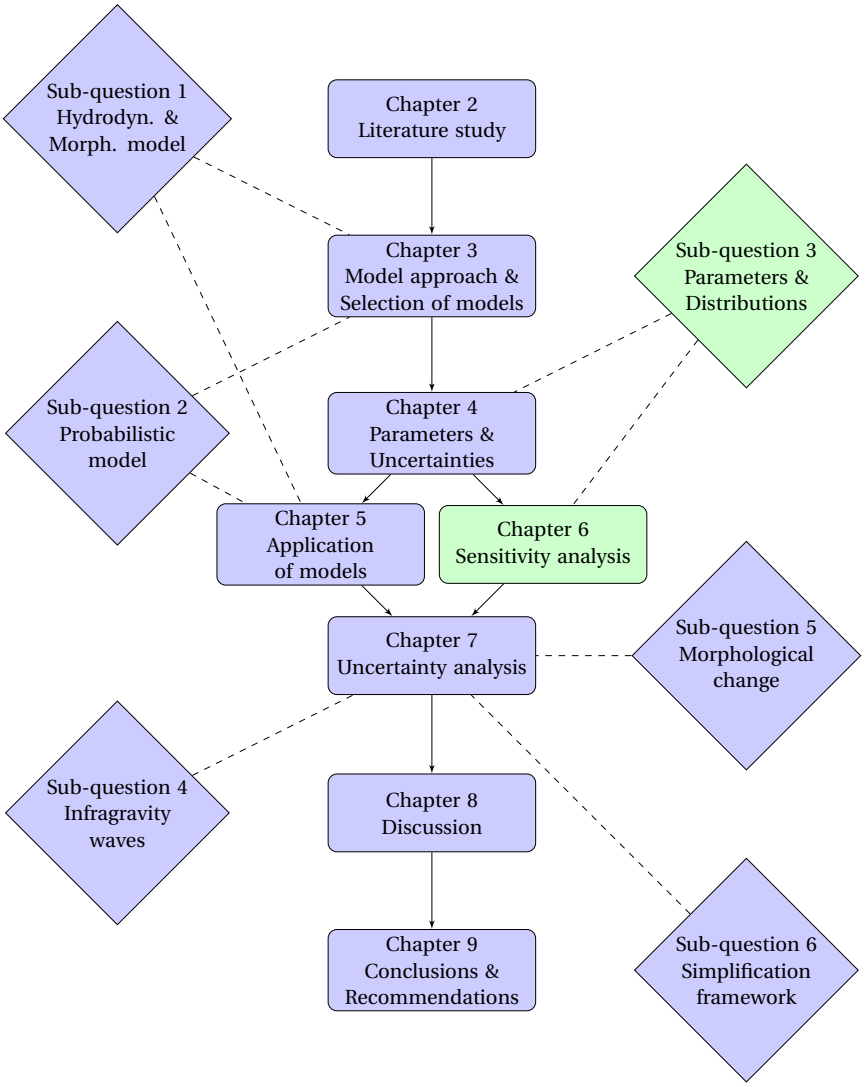

Figure 6.1: Outline of this report.

This chapter describes the sensitivity analysis, in which the influence of each parameter, that was described before in chapter 4, on the significant wave height and wave period at the dike toe, the bed level change and the wave overtopping discharge is determined. Thus, this chapter aims to provide an answer to part of the third sub-question. The third sub-question was: With which probability distribution can the important parameters be described, and which parameters have the largest influence on morphological change, wave height and wave overtopping? With the results of the sensitivity analysis, the parameters were divided into parameter sets, which were further used in the probabilistic calculations as described in chapter 7.

Section 6.1 presents an introduction to the chapter and the sensitivity analysis. The set-up of the analysis is described and the results are shown. Sections 6.2 until 6.6 describe the results of the sensitivity analysis in more detail. Finally, in section 6.7 a summary and conclusions to the chapter are presented.

6.1. INTRODUCTION

In the sensitivity analysis the influence of each parameter on the wave height, wave period, maximum bed level change and in particular the wave overtopping discharge is examined. The 17 parameters that were described in section 4.1 (q.v.) were considered for the sensitivity analysis. The uncertainty in the actual geometry of the foreshore was not considered in this thesis, hence the profile at the start of the storm was kept the same. For each parameter the mean, 5% and 95% values were taken, except for the offshore conditions (zs, H_s, T_p), for which the 1/1,000 years conditions were chosen instead of the mean, and for the location of the peak of the tide, for which 0 and π were taken, which indicates tidal high water coinciding with the peak of the surge and tidal low water coinciding with the peak of the surge. The parameters used in the sensitivity analysis are shown in figure 6.2. The different values for the parameters as used in the sensitivity analysis are shown in table 6.1. Each time, the same 2D XBeach calculation was run, as well as the EurOtop model, with only one parameter altered. These XBeach calculations contained the schematized version of the Westkapelle sea defence as described before in section 3.2 and 5.2. The results are shown in table 6.2 and Appendix I. The Appendix shows the resulting bed level changes in each of the calculations. Because the resulting wave overtopping discharges were very low, the sensitivity analysis was repeated with a lowered crest height, set at 7 m+NAP. These results are shown in table 6.3 and figure 6.3. Off course, with a change in crest height, the wave height, wave period and bed level change stay the same and only the wave overtopping discharge changes. The calculations with the lower crest level show the same trends as the calculations with the standard crest height of 12.6 m+NAP.

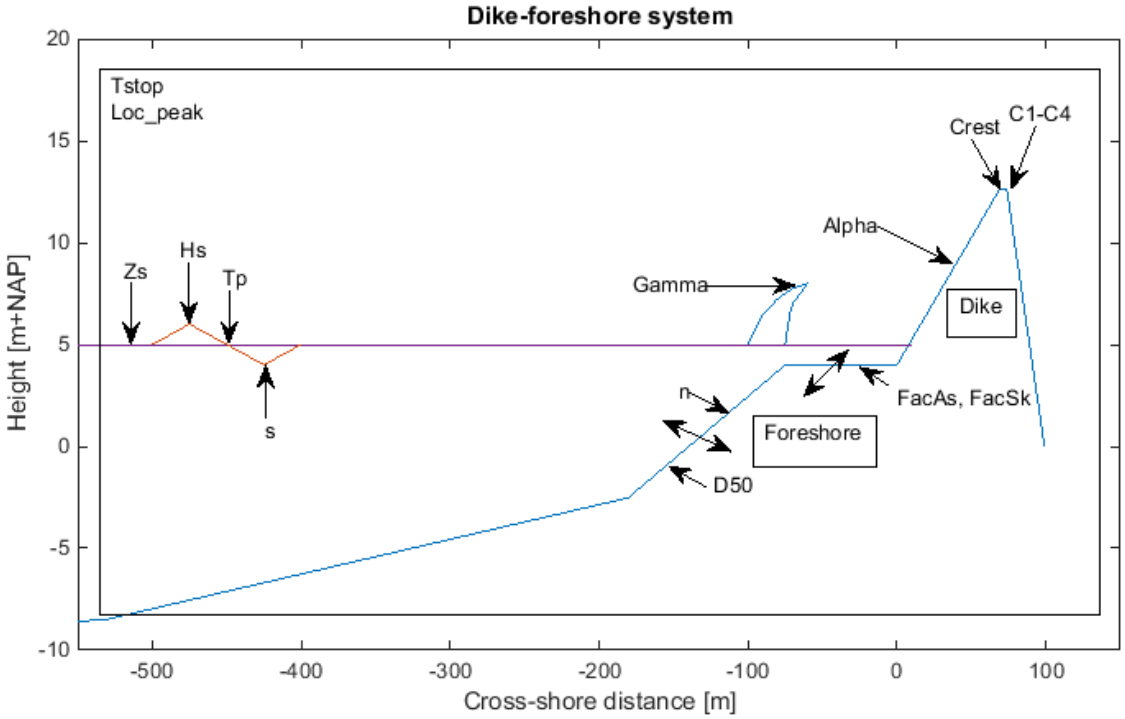

Figure 6.2: Stochastic variables as used in the sensitivity analysis.

In the last column of the tables, a division was made according to the importance of the parameters. By doing this, five sets of parameters were created:

- Set 1, Offshore conditions: 3 variables, zs, H_s, T_p.
- Set 2, Model and wave parameters: 7 variables, $C1$, $C2$, $C3$, $C4$, $gamma$, n, s.
- Set 3, Storm parameters: 2 variables, $tstop$, loc_peak.
- Set 4, Morphological parameters: 3 variables, D_{50}, $FacAs$, $FacSk$.
- Set 5, Dike parameters: 2 variables, $alpha$, $crest$.

Table 6.1: Parameter values for the sensitivity analysis. 1/1,000, 5% and 95% values for the offshore conditions, mean, 5% and 95% values for the other parameters.

Description	Parameter	Mean or 1/1,000 years value	Upper bound	Lower bound
Dike slope [-]	$alpha$	0.125	0.135	0.115
EurOtop coefficient ξ<5 [-]	$C1$	4.75	5.57	3.93
EurOtop coefficient ξ<5 [-]	$C2$	2.60	3.18	2.02
EurOtop coefficient ξ>7 [-]	$C3$	-0.92	-0.53	-1.31
EurOtop coefficient zero freeboard [-]	$C4$	1.00	1.23	0.77
Dike crest height [m]	$crest$	12.60 or 7.00	12.76 or 7.16	12.44 or 6.84
Sediment diameter [m]	D_{50}	300	380	230
Calibration factor wave asymmetry [-]	$FacAs$	0.123	0.191	0.073
Calibration factor wave skewness [-]	$FacSk$	0.375	0.582	0.222
Breaker index [-]	$gamma$	0.541	0.630	0.452
Location tidal peak [-]	loc_peak	0	0	pi
Manning friction factor [$sm^{-1/3}$]	n	0.02	0.03	0.01
Wave directional spreading [-]	s	10	20	1.5
Storm duration [hrs]	$tstop$	54.3	89.2457	29.5005
Offshore conditions [m,m,s]	zs	4.73	5.04	4.42
	H_s	5.09	6.08	4.10
	T_p	9.4	11.1	7.8

The offshore conditions had far and away the largest influence on wave conditions at the toe, bed level change and wave overtopping discharge, which was why they were chosen in set 1. The parameters in set 2 had a large influence on one or more of the test parameters. The parameters in set 3 influence the storm shape and had less influence on the test parameters than the parameters in set 2, which was why they were put together. They had a small influence on the wave height, some influence on the wave period and a large influence on the bed level change. Set 4 consists of the parameters that influence morphological change. They had almost no influence on the wave conditions and wave overtopping discharge, but do influence the bed level. The parameters in set 5 concern the dike shape, they have no influence on the wave conditions at the toe and the bed level, and only a small influence on the wave overtopping discharge. These different sets of parameters will be described in more detail below, from the most influential parameters to the parameters with the least influence.

Table 6.2: Overview results sensitivity analysis, column differences indicates the differences compared to the standard case. H_{m0} and $T_{m-1,0}$ are given for the moment when q is maximal. Difference in bed level indicates the maximum difference in bed level along the cross-shore profile at the end of the storm, where a negative value indicates a lower bed level compared to the standard case. Importance indicates the influence of the parameter on the wave height, wave period, bed level change and wave overtopping discharge. A higher value indicates more importance. Offshore conditions indicates zs, H_s and T_p.

Parameter	Value	Difference in H_{m0} [%]	Difference in $T_{m-1,0}$ [%]	Difference in q [%]	Difference in bed level [m]	Importance
Standard case	-	**1.01 m**	**25.0 s**	**$9 * 10^{-07}$ $ls^{-1}m^{-1}$**	-	-
$alpha$, 95%	0.135	-1	+0	-15	≈ 0	1
$alpha$, 5%	0.115	+0	+1	-7	≈ 0	
$C1$, 95%	5.57	+0	+0	+0	+0	4
$C1$, 5%	3.93	+0	+0	+0	+0	
$C2$, 95%	3.18	+0	+0	-99	+0	4
$C2$, 5%	2.02	+0	+0	+9265	+0	
$C3$, 95%	-0.53	+0	+0	+0	+0	4
$C3$, 5%	-1.31	+0	+0	+0	+0	
$C4$, 95%	1.23	+0	+0	+0	+0	4
$C4$, 5%	0.77	+0	+0	+0	+0	
$crest$, 95%	12.76	+0	+0	-40	≈ 0	1
$crest$, 5%	12.44	+0	+0	+36	≈ 0	
D_{50}, 95%	380	+1	-1	+14	+0.05	2
D_{50}, 5%	230	-1	+2	-16	-0.05	
$FacAs$, 95%	0.191	-1	-1	-14	+0.20	2
$FacAs$, 5%	0.073	+1	-1	+37	-0.20	
$FacSk$, 95%	0.582	-1	-1	-10	+0.30	2
$FacSk$, 5%	0.222	+2	-2	+54	-0.30	
$gamma$, 95%	0.63	+19	-1	+3070	-0.30	4
$gamma$, 5%	0.45	-18	-5	-99	+0.30	
loc_peak	π	-2	-1	-36	+0.15	3
n, 95%	0.03	-2	-8	-41	+0.30	4
n, 5%	0.01	+7	-2	+312	-0.50	
s, 95%	20	+7	+13	+309	-0.20	4
s, 5%	1.5	-8	-2	-86	+0.20	
$tstop$, 95%	89.25	-2	-12	-28	-0.30	3
$tstop$, 5%	29.5	+1	-7	+18	+0.30	
Offshore conditions, 95%	5.04, 6.08, 11.1	+48	+5	+230958	-0.4	5
Offshore conditions, 5%	4.42, 4.10, 7.8	-34	+15	-100	+0.45	

Table 6.3: Overview results sensitivity analysis for the lowered crest level of 7 m+NAP. Column differences indicates the differences compared to the standard case. H_{m0} and $T_{m-1,0}$ are given for the moment when q is maximal. Difference in bed level indicates the maximum difference in bed level along the cross-shore profile at the end of the storm, where a negative value indicates a lower bed level compared to the standard case. Importance indicates the influence of the parameter on the wave height, wave period, bed level change and wave overtopping discharge. A higher value indicates more importance. Offshore conditions indicates zs, H_s and T_p.

Parameter	Value	Difference in H_{m0} [%]	Difference in $T_{m-1,0}$ [%]	Difference in q [%]	Difference in bed level [m]	Importance
Standard case	-	**1.01 m**	**25.0 s**	**1.68 ls^{-1}m^{-1}**	-	-
$alpha$, 95%	0.135	-1	+0	-5	≈ 0	1
$alpha$, 5%	0.115	+0	+1	-2	≈ 0	
$C1$, 95%	5.57	+0	+0	+0	0	4
$C1$, 5%	3.93	+0	+0	+0	0	
$C2$, 95%	3.18	+0	+0	-73	0	4
$C2$, 5%	2.02	+0	+0	+276	0	
$C3$, 95%	-0.53	+0	+0	+0	0	4
$C3$, 5%	-1.31	+0	+0	+0	0	
$C4$, 95%	1.23	+0	+0	+0	0	4
$C4$, 5%	0.77	+0	+0	+0	0	
$crest$, 95%	7.1645	+0	+0	-37	≈ 0	1
$crest$, 5%	6.8355	+0	+0	+48	≈ 0	
D_{50}, 95%	380	+1	-1	+4	+0.05	2
D_{50}, 5%	230	-1	+2	-6	-0.05	
$FacAs$, 95%	0.191	-1	-1	-5	+0.20	2
$FacAs$, 5%	0.073	+1	-1	+11	-0.20	
$FacSk$, 95%	0.582	-1	-1	-4	+0.30	2
$FacSk$, 5%	0.222	+2	-2	+16	-0.30	
$gamma$, 95%	0.63	+19	-1	+229	-0.30	4
$gamma$, 5%	0.45	-18	-5	-80	+0.30	
loc_peak	π	-2	-1	-13	+0.15	3
n, 95%	0.03	-2	-8	-16	+0.30	4
n, 5%	0.01	+7	-2	+62	-0.50	
s, 95%	20	+7	+13	+63	-0.20	4
s, 5%	1.5	-8	-2	-48	+0.20	
$tstop$, 95%	89.25	-2	-12	-10	-0.30	3
$tstop$, 5%	29.5	+1	-7	+7	+0.30	
Offshore conditions, 95%	5.04, 6.08, 11.1	+48	+5	+2121	-0.4	5
Offshore conditions, 5%	4.42, 4.10, 7.8	-34	+15	-99	+0.45	

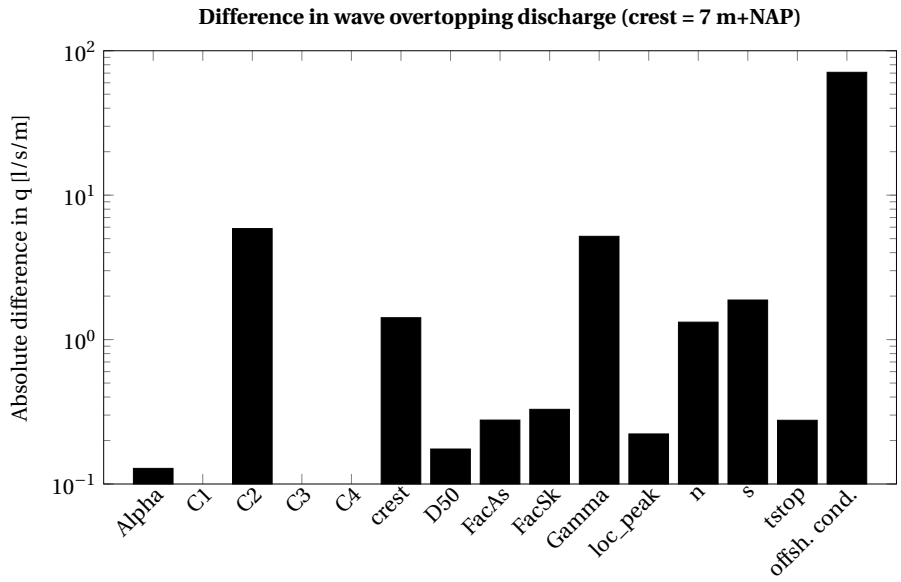

Figure 6.3: Results of the sensitivity analysis with the crest height lowered and set at 7 m+NAP. The absolute value of the difference in calculated wave overtopping discharge between higher and lower value and standard case value is shown. The larger influence of the crest level due to the lower crest height is clearly visible.

6.2. SET 1: OFFSHORE CONDITIONS

Set 1 consists of the parameters with the largest influence on wave height, wave period, bed level change and wave overtopping discharge. The offshore conditions indicate the water level zs, wave height H_s and wave period T_p, which, as mentioned in section 4.4.2 are correlated, which is why they were put together as offshore conditions. The (uncertainties in the) offshore conditions have by far the largest influence on wave height, wave period and wave overtopping discharge and also have a large influence on the bed level. Naturally, the wave height and period at the toe are directly influenced by the wave height, period and water level offshore, which explains the large influence. The wave height at the toe was larger for the more extreme conditions and smaller for the less extreme conditions, which seems logical. The wave period was larger for the more extreme conditions and the less extreme conditions, compared to the standard case. This is caused by the very shallow water depth on the foreshore with the 5% conditions, which causes severe breaking and a large shift of wave energy to the lower frequencies. With the more severe conditions, the offshore wave period is larger, which could also explain the somewhat large period at the dike toe. With the 5% conditions, the wave overtopping discharge is almost zero. With the more severe conditions, the overtopping discharge becomes much larger. For the more severe conditions, there is more erosion of the bed compared to the standard case. Because of the lower water level and wave height during the less severe conditions, the foreshore remains more intact, which explains the large bed level difference for this simulation.

6.3. SET 2: MODEL AND WAVE PARAMETERS

Set 2 consists of the parameters that have a smaller influence than the offshore conditions, but still have a large impact on wave height, period, bed level and wave overtopping discharge. These parameters are some of the parameters that were categorized under model uncertainty in chapter 4, as well as the Manning friction factor and wave directional spreading, which were placed under inherent uncertainty in space and time respectively.

6.3.1. EUROTOP COEFFICIENTS

The EurOtop coefficients appear in the wave overtopping formulae, so they have no influence on wave height, wave period or bed level. However, the influence on the wave overtopping discharge is large. This is partly caused by the rather large standard deviations of these coefficients, which results in largely different mean, 5% and 95% values. In this case only $C2$ was used, which is used for $\xi < 5$ and non-breaking waves. Which coefficient is, or coefficients are used thus depends on the type of breaking, hence on the Iribarren number.

6.3.2. BREAKER INDEX

The breaker index determines the ratio of maximum wave height over water depth. A larger value of the breaker index will therefore lead to less breaking and thus larger waves reaching the toe, which can be seen by the larger value of the wave height. The influence on the wave period was much smaller. The larger waves that reach the toe with a larger breaker index value, will also stir-up more sediment, hence increasing the sediment transport, which in turn leads to a larger change in bed level. Mainly due to the influence on the wave height, the breaker index also has a large influence on the wave overtopping discharge.

6.3.3. MANNING FRICTION FACTOR

A larger friction factor represents more friction losses and thus lower infragravity waves and velocities. The influence of the (uncertainty in the) Manning friction factor was smaller than the influence of, e.g. the breaker index, but was still considerable. The influence on the wave height and period was not that large, but especially the influence on the bed level was large. Usually, a rougher bed would lead to a larger velocity gradient near the bed, hence a larger bed shear stress and thus a larger sediment transport. With waves and possible bed forms, this is less straightforward. XBeach does not have a coupling between a larger friction factor and a larger bed shear stress in the boundary layer. The influence of the Manning friction factor on the bed level is caused by slower currents and higher water levels with a higher Manning factor. The large influence on the bed level can also partly be attributed to the probability distribution. Because not much was known about the friction factor, a uniform distribution was chosen, which leads to a large spreading in values.

6.3.4. WAVE DIRECTIONAL SPREADING

The influence of the (uncertainty in the) wave directional spreading is of the same order of magnitude as the influence of the Manning friction factor. A larger JONSWAP spreading value indicates a smaller wave directional spreading in degrees. The influence on the wave period and wave height were of the same order of magnitude. A smaller wave directional spreading in degrees leads to more bundling of the waves, hence a stronger forcing of the infragravity waves. Hence, the waves become more long crested with a lower directional spreading, which leads to more forcing of the infragravity waves. This leads to larger wave heights at the toe and a larger wave period, caused by the shift to lower frequencies by the infragravity waves. The combined influence of the wave height and period leads to a considerable influence on the wave overtopping discharge. The wave directional spreading also has quite a large influence on the bed level, which can again be explained by the bundling of the waves with smaller directional spreading and the directional dispersion of the waves with larger wave directional spreading values. The larger waves lead to larger bed shear stresses and larger sediment transports. The large influence of the wave directional spreading on the parameters at the toe can partly be explained by considering the probability distribution. A uniform distribution was chosen, which shape inherently leads to a large spreading in directional spreading values.

6.4. SET 3: STORM PARAMETERS

Set 3 consists of the storm parameters, the duration of the storm and the location of the tidal peak. These parameters were grouped together because of their influence on wave conditions, bed level and wave overtopping discharge and because they both influence the shape of the storm in time.

6.4.1. STORM DURATION

The influence of the (uncertainty in the) storm duration on the wave height is small, which seems logical, because there is no real correlation between storm duration and wave height in this model. With the storm shape used here, a larger storm duration does not lead to larger wave heights offshore and thus at the toe. The influence of the storm duration on the wave period is larger. For both the longer and shorter storm duration, the wave period becomes smaller, which is strange. It could be that by slight differences in bathymetry, different infragravity wave heights occur, which lead to different wave periods. As mentioned before, the influence of the low frequencies on the $T_{m-1,0}$ wave period is very large, so a slight difference in the low frequency energy could already lead to this difference of about 10%. To determine the exact cause of the difference in wave period, more research is necessary. Especially the influence on the wave period leads to the influence on the wave overtopping discharge. Intuitively, a larger storm duration gives a larger period during which sedimentation and/or erosion can occur, which could lead to larger bed level changes. A larger storm duration indeed leads to larger bed level changes, a shorter storm to smaller bed level changes.

6.4.2. LOCATION OF TIDAL PEAK

The hydraulic boundary conditions during a storm where the surge peak coincides with the tidal peak was shown in figure 4.5, in which it is visible that the maximum surge, wave height and wave period occur in the middle of the storm. The largest wave height and wave period occur at the moment of largest surge which, however, is not necessarily the moment with the highest water level. With the standard case, where the tidal peak coincided with the surge peak, the maximum wave overtopping discharge occurred in the middle of the storm, where water level, surge, wave height and wave period were maximum. When low tide occurred at the same moment as the maximum surge, the maximum wave overtopping discharge moved to the moment with the maximum water level, which was when the tidal level was maximal, at approximately $2/5^{th}$ of the storm duration. Therefore, the wave height, wave period and thus wave overtopping will be lower when the tidal peak does not coincide with the surge peak, because of the lower offshore wave height and wave period when the water level is maximal. Because the moment of maximum water level and maximum wave conditions do not coincide anymore, the maximum bed level change is also less.

6.5. SET 4: MORPHOLOGICAL PARAMETERS

Set 4 consists of the morphological parameters. These parameters were grouped together because of their influence on wave conditions, bed level and wave overtopping discharge and because they can all be categorized as morphological parameters.

6.5.1. GRAIN DIAMETER

The influence of the (uncertainty in the) sediment diameter on the wave height and wave period is small, which also leads to a small change in wave overtopping discharge. The influence on the bed level was much smaller than expected. However, this can be explained by the fact that the maximum bed level change was considered as diagnostic parameter, not the volume change. Furthermore, a change in grain diameter has not much influence on the bed level change in XBeach (Van Thiel de Vries, 2009). Also, the chosen standard deviation was rather small, which leads to little spreading in the 5% and 95% values.

6.5.2. WAVE SKEWNESS & ASYMMETRY PARAMETERS

The influence of the (uncertainty in the) wave asymmetry and wave skewness calibration factors in the sediment transport equations on the wave height, wave period and wave overtopping discharge was small, but the influence on the bed level was quite large. This is a result of the direct occurrence of the factors in the sediment transport formulae. Large values of the wave asymmetry and skewness calibration factors can lead to a steeper bed slope, which in this case meant less erosion compared to the standard case. Because, as described before, not much was known about these factors, a large standard deviation was chosen, which lead to largely different 5% and 95% values, which could also have had influence on the large bed level differences.

6.6. SET 5: DIKE PARAMETERS

Set 5 consists of the dike parameters. These parameters had almost no influence.

6.6.1. DIKE SLOPE

The (uncertainty in the) dike slope had virtually no influence on wave height, wave period and bed level, which is logical, because the slope is not of influence on wave transformation or bed level change. What is counter-intuitive however, is that a steeper as well as a gentler slope lead to a slightly lower wave overtopping discharge. The dike slope influences the wave overtopping through the Iribarren number, but also slightly influences the reflection of the waves, which caused the difference in wave overtopping discharge.

6.6.2. CREST HEIGHT

The (uncertainty in the) crest height also does not influence the wave height, period and bed level, which can again be explained by considering the locations were wave transformation and sediment transport takes place, on which the crest height has no influence. The influence on the wave overtopping discharge is somewhat larger, but still small. This can be explained by the definition of the stochastic crest height parameter. The difference in crest height considered here represents an error in the measurement of the crest level, which is a small error compared to the freeboard. With smaller freeboards and an equal absolute measurement error, the relative error in the measurement of the crest level becomes larger and also the influence on the wave

overtopping discharge.

6.7. SUMMARY & CONCLUSIONS

This chapter aimed to provide an answer to subquestion 3: the probability distributions that describe the important parameters, and the parameters with the largest influence on morphological change, wave height, wave period and wave overtopping. The second part was answered in this chapter, the first part was already answered in chapter 4.

6.7.1. MOST INFLUENTIAL PARAMETERS

A sensitivity analysis was performed, to determine the influence of the 17 parameters that were chosen before. For each parameter, a larger and smaller value was determined. With each of these values, a calculation with the Westkapelle 2D XBeach model was performed, of which the results were compared to a 'standard'case situation, which used the mean values of the parameters. Using the crest height of 12.6 m+NAP lead to very small wave overtopping discharges, which were approximately zero. Because it was uncertain if the sensitivity was shown correctly for such small wave overtopping discharges and because the wave overtopping discharge is the most important parameter for this research, the sensitivity analysis was performed again, but now with a crest height of 7 m+NAP. However, the two analyses showed the same trends. With the results of the sensitivity analysis, the 17 parameters were divided into subsets, where set 1 consists of the parameters with the largest influence, and set 5 of the parameters with the smallest influence.

- Set 1, Offshore conditions: 3 variables, zs, H_s, T_p.
- Set 2, Model and wave parameters: 7 variables, $C1$, $C2$, $C3$, $C4$, $gamma$, n, s.
- Set 3, Storm parameters: 2 variables, $tstop$, loc_peak.
- Set 4, Morphological parameters: 3 variables, D_{50}, $FacAs$, $FacSk$.
- Set 5, Dike parameters: 2 variables, $alpha$, $crest$.

The sets of parameters were used further in the uncertainty analysis, chapter 7.

7

UNCERTAINTY ANALYSIS

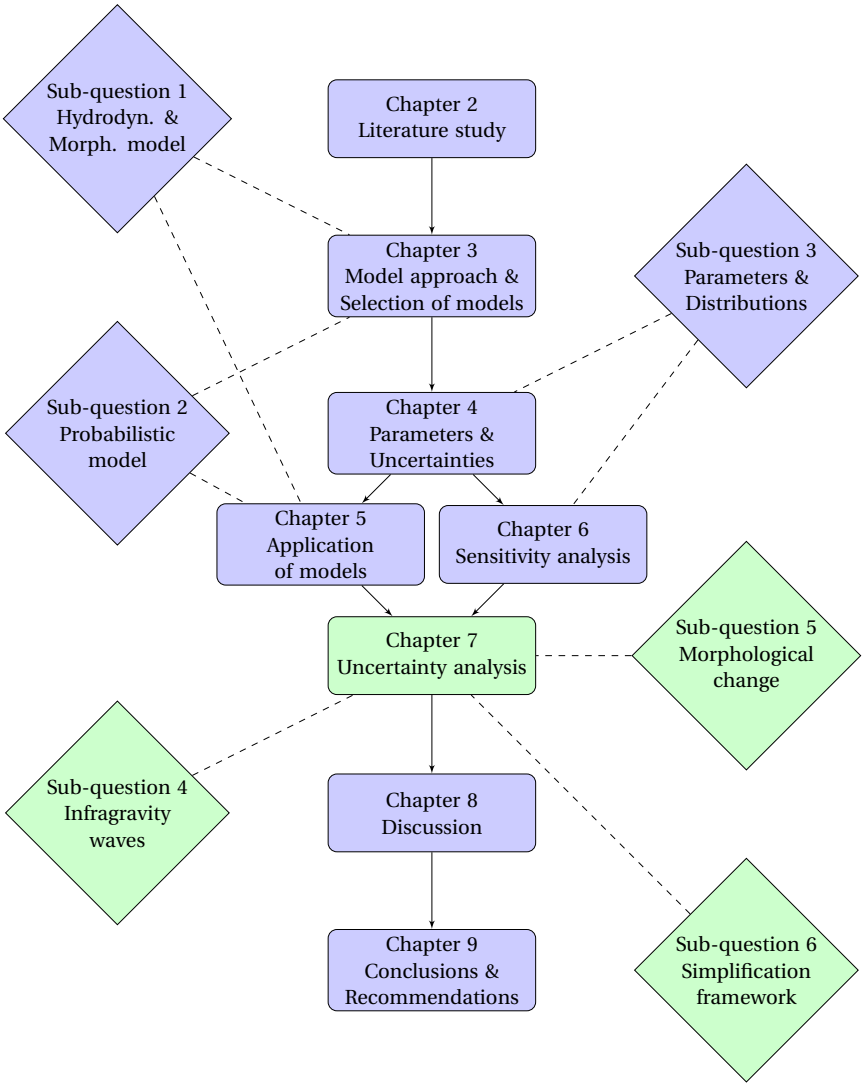

Figure 7.1: Outline of this report.

This chapter describes the uncertainty analysis. Different calculations were performed with the framework of XBeach (or the h/2-model), EurOtop and ADIS. Differences in the calculations include the use of the h/2-model, XBeach 1D and XBeach 2D, different numbers of stochastic variables, and the inclusion or exclusion of morphological changes. This chapter aims to provide answers to the fourth, fifth and sixth sub-question. These sub-questions were:

- *Subquestion 4: What is the influence of infragravity waves on the probability of dike failure due to wave overtopping?*
- *Subquestion 5: How does morphological change during severe storms influence the probability of dike failure due to wave overtopping?*
- *Subquestion 6: Which parameters dominate the failure probability and overtopping process, i.e. which parameters need to be taken into account in the probabilistic calculations?*

The influence of infragravity waves and morphological changes of the foreshore on the probability of dike failure are determined, as well as the parameters that dominate the failure probability and ways of simplifying the framework.

Section 7.1 gives an introduction and describes the set-up of the uncertainty analysis. Next, in section 7.2 the influence of the foreshore is determined. After that, in section 7.3 the influence of infragravity waves on the probability of dike failure is determined. Section 7.4 presents an analysis of the influence of morphological changes of the foreshore on the probability of dike failure. After that, in section 7.5, the influence of the stochastic variables is determined, as well as ways to simplify the framework. Finally, section 7.6 gives a summary and conclusions of the chapter.

7.1. INTRODUCTION

To be able to answer the research questions, multiple calculations were performed with the probabilistic framework of XBeach (or the $h/2$-model), EurOtop and ADIS. Table 7.1 shows which parameters are included in the calculations with different numbers of stochastic variables. Table 7.2 shows the different calculations for which the probability of failure was determined. All the results of the calculations can be found in Appendix J.

Table 7.1: Number of stochastic variables and the parameters that are included. Label indicates the name of the calculation with n parameters that will be used from now on.

Number of stochastic variables [-]	Offshore conditions	Model & wave parameters	Storm parameters	Morph. parameters	Label
3	x				Offshore conditions
10	x	x			Model parameters
12	x	x	x		Storm parameters
15	x	x	x	x	Morph. parameters

Table 7.2: The different probabilistic calculations that were performed. Calculations which were started, but not finished because of the long calculation duration, are not shown.

Type of model	Number of stochastic variables	Including morphological changes	Including tide & storm profile	Including morphological acceleration factor (morfac)	Including foreshore	Duration to run simulation
$h/2$-model	3					$\mathcal{O}$(minutes)
XBeach 1D	3					$\mathcal{O}$(day)
XBeach 2D	3					$\mathcal{O}$(day)
$h/2$-model	3				x	$\mathcal{O}$(minutes)
XBeach 1D	3				x	$\mathcal{O}$(day)
XBeach 2D	3				x	$\mathcal{O}$(day)
XBeach 1D	10				x	$\mathcal{O}$(day)
XBeach 2D	10				x	$\mathcal{O}$(day)
XBeach 1D	12		x		x	$\mathcal{O}$(month)
XBeach 1D	12	x	x	x	x	$\mathcal{O}$(week)
XBeach 1D	12	x	x		x	$\mathcal{O}$(month)
XBeach 1D	15	x	x	x	x	$\mathcal{O}$(week)
XBeach 1D	15	x	x		x	$\mathcal{O}$(month)

Calculations were performed with the schematized version of the Westkapelle sea defence, as described before in section 5.2. The $h/2$-model and XBeach 1D- and 2D-models were used to determine the wave parameters at the toe of the dike. The different sets of stochastic variables were used, as derived in the previous chapter. Inclusion of more and more different parameter sets leads to calculations with 3, 10, 12 and 15 stochastic variables. The last and least important set, set 5, with the two dike parameters, was not used, because the influence of (the uncertainty in) these parameters was very small and outside the scope of this

research (see previous chapter, chapter 6). Because neither the storm duration and location of the tidal peak, nor morphological changes were included as stochastic variables in the calculations with only the offshore conditions and the calculations with the model parameters, it was sufficient for these calculations to only use a storm duration of one hour with the maximum water level, wave height and wave period that occur during the storm, to achieve the same result as when the whole storm duration would have been used.

Systems with 4 and 8 computational cores at 2.6 Gigahertz and 16 Gigabytes of memory were used for the calculations. The 1D and 2D calculations with the offshore conditions only, and the calculation with the model parameters had approximately the same duration, caused by the acceleration when using MPI with the 2D calculations, which cannot be used with 1D calculations. When the morphological changes and the whole storm duration are calculated as well, the 2D calculations take much longer than the 1D calculations, even when using MPI. 2D XBeach calculations with the storm parameters and morphological parameters were started, but were not viable, caused by a calculation duration in the order of a month. Therefore, for these long calculations, only the 1D XBeach model was used. To accelerate the 1D calculations with the storm parameters and with the morphological parameters even more, a morphological acceleration factor of 10 was used in some calculations. The morphological acceleration factor (morfac) speeds up the morphological time scale relative to the hydrodynamic time-scale. Hence, when a simulation of 10 minutes is performed with a morfac of 6, the morphological evolution over one hour is simulated. The results of the calculations including a morfac can be found in Appendix J.

To be able to determine the influence of the foreshore on the probability of dike failure, calculations with the $h/2$-model, XBeach 1D and XBeach 2D were performed, including and excluding the foreshore and using only the three offshore condition parameters as stochastic variables.

To be able to determine the influence of the infragravity waves on the probability of dike failure, the calculations with the $h/2$-model and the 1D and 2D XBeach models with only the offshore parameters as stochastic variables were performed. The results will also be compared to ENDEC, which was used in a similar calculation framework in HKV (2014).

The morphological parameters were placed under set 4, which means that they are only included as stochastic variables in the calculations with 15 stochastic variables. To determine the influence of morphological changes of the foreshore on the failure probability, a calculation with the storm parameters but without calculating the morphological changes was performed. A calculation with the same number of stochastic parameters (12) with calculation of the morphological changes was performed as well. Furthermore, a calculation in which the morphological parameters were included as stochastic variables and in which the morphological changes were calculated was done. This leads to a calculation with 12 parameters without calculation of the morphological changes, with 12 parameters and with calculation of the morphological changes, and a calculation with 15 stochastic variables with calculation of the morphological changes. With the results of these calculations, the influence of morphological changes of the foreshore on the dike failure probability can be determined.

The modelling framework was previously described in section 5.1 (q.v.). Figure 7.2 shows the set-up of the probabilistic calculation framework, for a situation with XBeach, including the morphological parameters (15 stochastic variables) and including morphological changes.

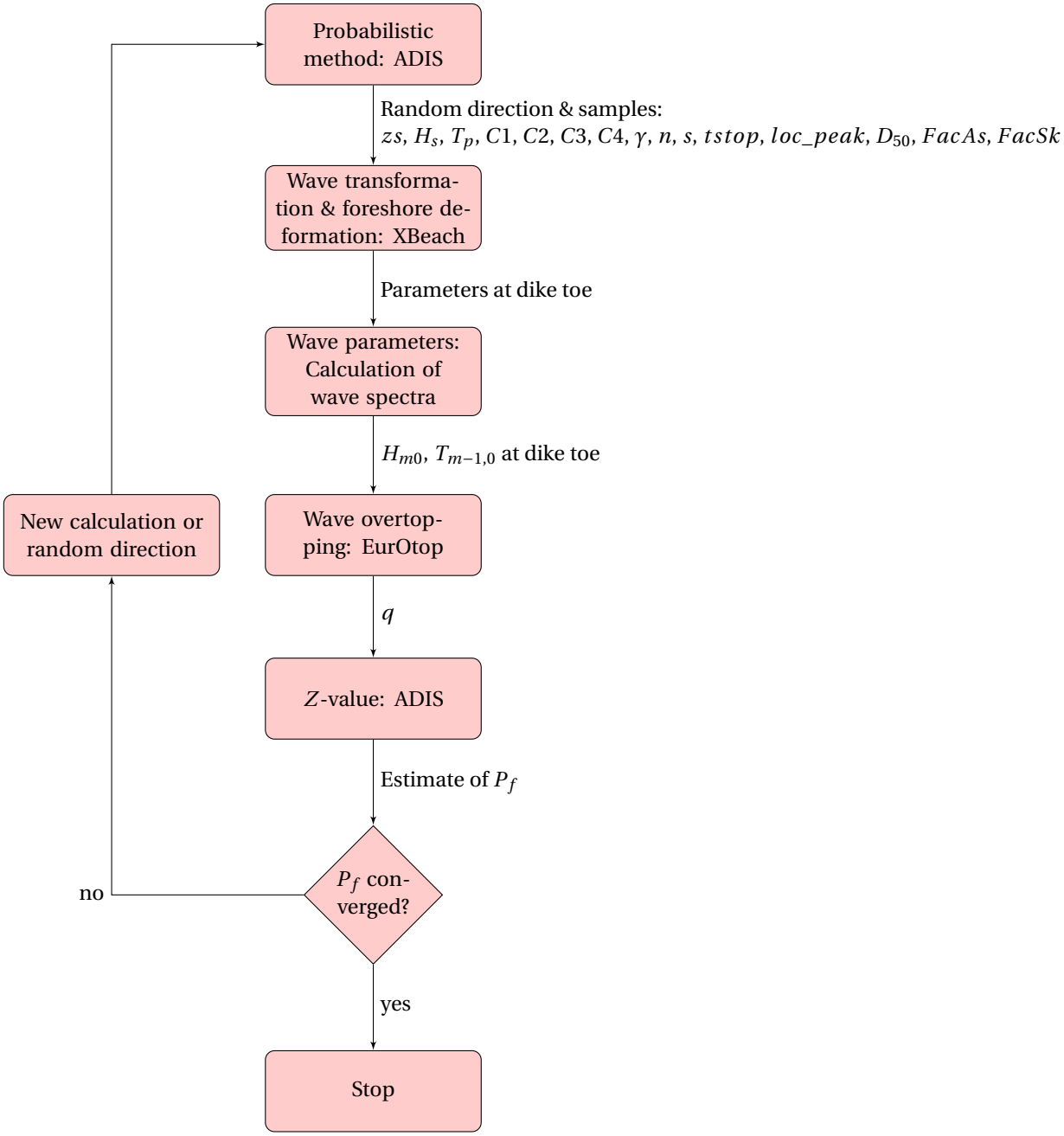

Figure 7.2: Modelling framework with 15 stochastic variables.

7.2. INFLUENCE OF THE FORESHORE

As shown in table 7.3, calculations with the probabilistic modelling framework were performed with the $h/2$-model and XBeach 1D and 2D models, with the offshore conditions as stochastic variables, including and excluding the foreshore. Comparing the results of these calculations can give an indication of the influence of the foreshore. Figure 7.3 shows the schematized bathymetry with and without foreshore.

The $h/2$-model calculations, which exclude the infragravity waves and wave set-up, lead to a difference in probability of failure of about a factor 40 between the case with and without the foreshore. The dominant parameter is the water level, which is large for the case without foreshore and even larger for the case with foreshore. The offshore wave heights are approximately the same, but due to the foreshore, the wave height at the dike toe is lower in the case with foreshore. As mentioned before, the $h/2$-model does not calculate changes in wave period. The counteractive effects of a larger water level but lower wave height at the dike toe, make that the difference in failure probability between the case with and without foreshore is not as large as what was found in HKV (2014).

The 1D XBeach calculation without foreshore lead to a probability of failure of $5.68 * 10^{-2}$, the 2D calculation to $4.78 * 10^{-5}$, showing the influence of the overestimation of the infragravity waves in the 1D model. The calculations with foreshore resulted in failure probabilities of $1.64 * 10^{-5}$ for the 1D-model and $1.56 * 10^{-6}$ for the 2D-model. This means a reduction of the failure probability of order 10^3 for the 1D-model and order 30 for the 2D-model. Compared to HKV (2014), where a (very large) reduction of 10^5 was found, these reductions are smaller. However, as mentioned before, that study used ENDEC instead of XBeach, which excludes the infragravity waves. Again, the more severe wave breaking due to the foreshore leads to lower wave heights at the dike toe when the foreshore is present, but this also leads to a transfer of wave energy to the lower frequencies, which increases the wave period.

Intuitively, the results from the calculations in this thesis seem more realistic than the results from PC-Ring and ENDEC. The results that were found are however results with a schematized version of the Westkapelle sea defence. For different dike-foreshore systems, the results could be different.

Table 7.3: Results of the probabilistic calculations, from which the influence of the foreshore on the probability of dike failure is determined. Number of calculations indicates the number of exact calculations, so without the ARS estimations (see section 5.5).

Type of model	Number of stochastic variables [-]	Including foreshore	Probability of failure [year^{-1}]	β-value [-]	Number of calculations [-]
$h/2$-model	3		$9.78 * 10^{-7}$	4.76	40
XBeach 1D	3		$5.68 * 10^{-2}$	1.58	98
XBeach 2D	3		$4.78 * 10^{-5}$	3.90	45
$h/2$-model	3	x	$2.29 * 10^{-8}$	5.47	23
XBeach 1D	3	x	$1.64 * 10^{-5}$	4.15	112
XBeach 2D	3	x	$1.56 * 10^{-6}$	4.66	43

Figures 7.4 and 7.5 show the results of a calculation with XBeach 1D and 2D with foreshore, with offshore conditions for which $Z \approx 0$ and with the smallest distance to the origin in standard normal (U) space (which is not necessarily exactly the same as the design point, which needs to be a point in the failure space $Z < 0$). Visible is that the offshore conditions for the 2D model need to be more extreme to reach approximately the same amount of wave overtopping, which explains the difference in probability of failure between the 1D and 2D model. It is also visible that the wave period at the toe is largely different. The graphs show relatively much more low frequency wave energy contributing to the total wave energy in the 1D model, whereas in the 2D model the total wave height is almost only comprised of high frequency wave energy. This leads to the much larger $T_{m-1,0}$ period at the dike toe in the 1D model, which leads to a larger wave overtopping discharge. It is visible that the infragravity wave heights at the toe of the dike are rather large, even though the water depth is not that large. These large infragravity waves can exist because they have such a large wavelength, that they do not break on the (compared to the wavelength) relatively short foreshore.

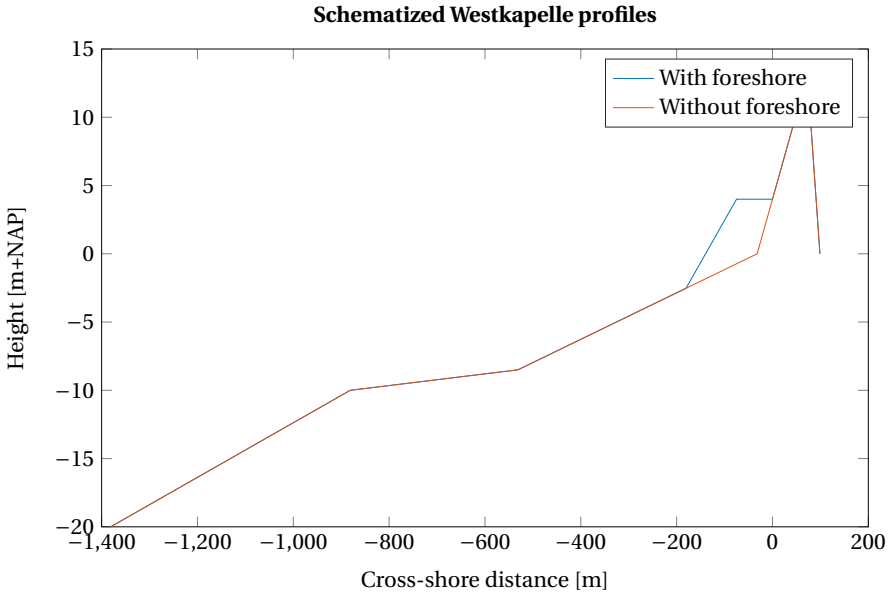

Figure 7.3: Schematized Westkapelle sea defence bathymetry with and without foreshore.

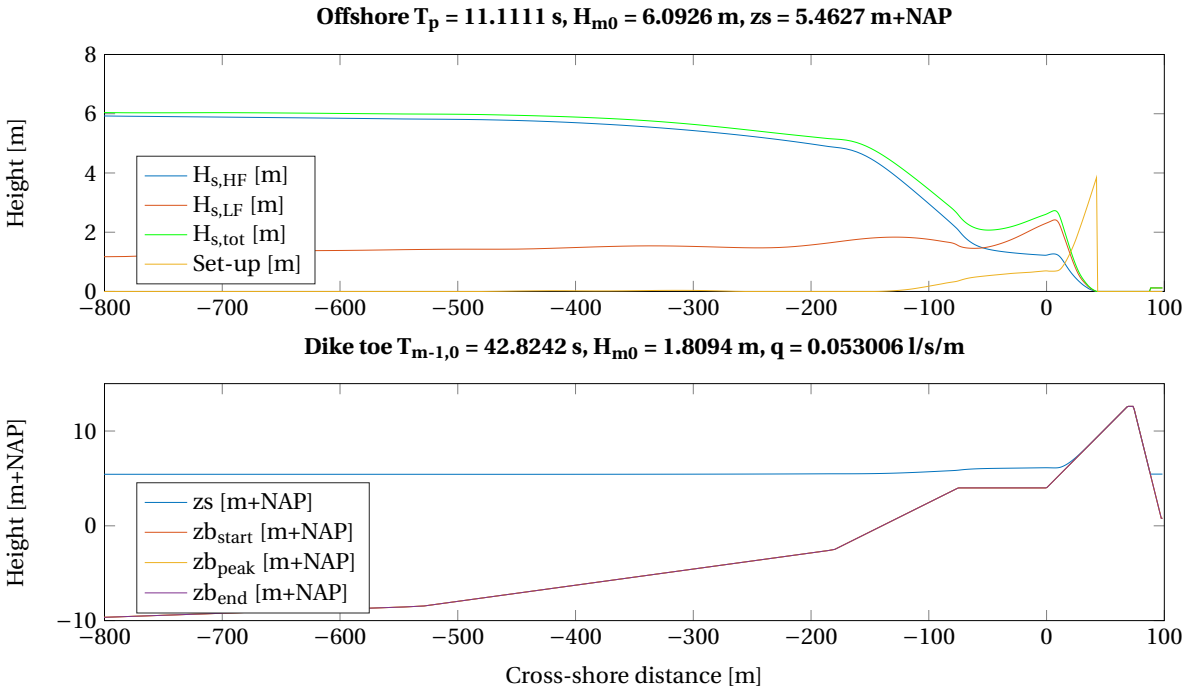

Figure 7.4: XBeach 1D with the offshore conditions as stochastic variables, such that $Z \approx 0$ and with the smallest distance to the origin in standard normal space. Note that not the whole profile is visible, but rather the part from -800 m until 100 m.

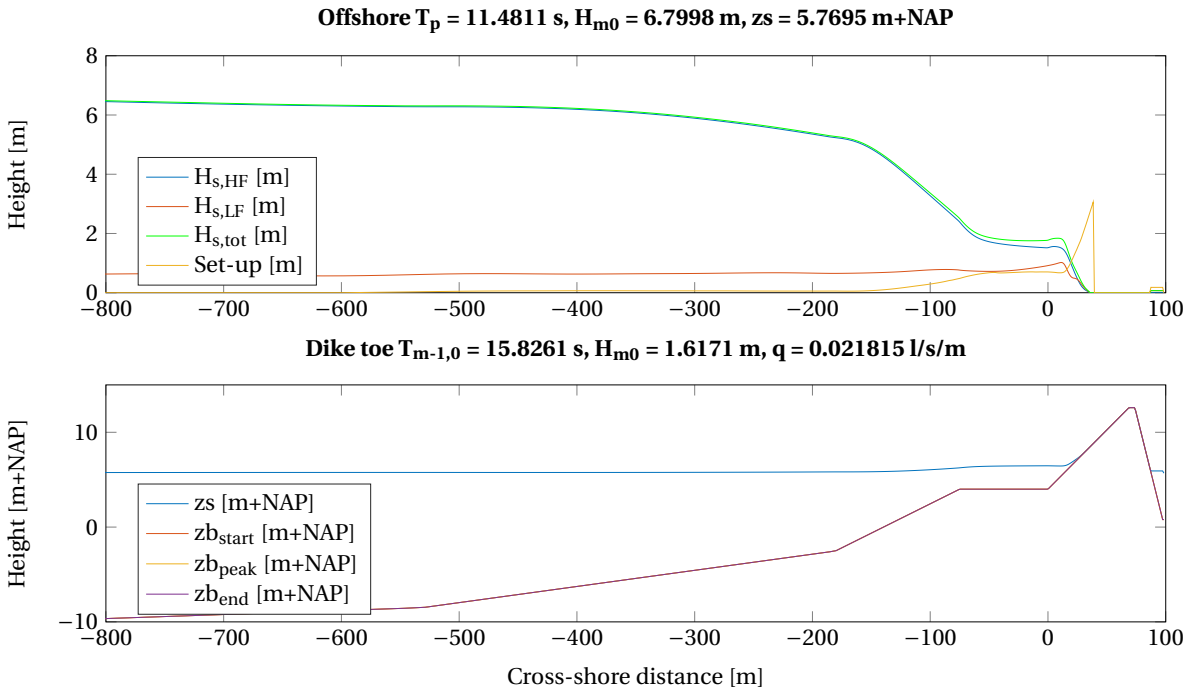

Figure 7.5: XBeach 2D with the offshore conditions as stochastic variables, such that $Z \approx 0$ and with the smallest distance to the origin in standard normal space. Note that not the whole profile is visible, but rather the part from -800 m until 100 m.

7.3. INFLUENCE OF INFRAGRAVITY WAVES

This section determines the influence of infragravity waves on the probability of dike failure due to wave overtopping. To do this, the results of several calculations are compared, the calculations with the $h/2$-model and XBeach 1D and 2D with the offshore conditions as stochastic variables, as well as the results from HKV (2014), which used a combination of ENDEC and PC-Ring, and 13 stochastic variables (different parameters with different probability distributions, as well as directional statistics). These calculations are hydrodynamic only, hence they do not yet include the morphological changes of the foreshore. The calculations also do not yet include the storm duration and phase of the tide, due to which it is sufficient to not calculate the whole storm duration, but just one hour. The duration of these calculations was a few minutes for the $h/2$-model to approximately a day for the other models. The different calculations with their results are shown in table 7.4 below. Table 7.5 shows the values of the stochastic parameters in the case where the LSF $Z \approx 0$ and with the smallest distance to the origin in standard normal space.

Table 7.4: Results of the probabilistic calculations, from which the influence of infragravity waves on the probability of dike failure is determined. Number of calculations indicates the number of exact calculations, so without the ARS estimations (see section 5.5).

Type of model	Including infragravity waves	Number of stochastic variables [-]	Probability of failure [year^{-1}]	β-value [-]	Number of calculations [-]	Reference
$h/2$-model		13	$3.00 * 10^{-8}$	5.42	-	(HKV, 2014)
ENDEC		13	$6.00 * 10^{-11}$	6.44	-	(HKV, 2014)
$h/2$-model		3	$2.29 * 10^{-8}$	5.47	23	
XBeach 1D	x	3	$1.64 * 10^{-5}$	4.15	112	
XBeach 2D	x	3	$1.56 * 10^{-6}$	4.66	43	

Table 7.5: The values of the stochastic parameters in the case where the LSF $Z \approx 0$ and with the smallest distance to the origin in standard normal space, for the $h/2$-model and XBeach 1D and 2D, with the offshore parameters as stochastic variables.

Parameter	$h/2$-model, 3	XB 1D, 3	XB 2D, 3
zs [m+NAP]	7.33	5.45	5.77
$H_{m0,offsh}$ [m]	6.25	6.09	6.8
$T_{p,offsh}$ [s]	11.55	11.11	11.48
$H_{m0,toe}$ [m]	1.66	1.8	1.61
$T_{m-1,0,toe}$ [s]	11.55	42.9	15.61
q [ls^{-1}m^{-1}]	0.01	0.05	0.02

The calculations of HKV (2014) used the actual JARKUS transect 1832 bathymetry, with the local crest height instead of the mean crest height of the Westkapelle sea defence. For the hydrodynamic calculations, the $h/2$-model and ENDEC model were used. For the probabilistic calculations, PC-Ring was used, which uses a combination of FORM and directional sampling. Furthermore, PC-Ring uses a SWAN database with local wave parameters based on directional wind/wave statistics. Different stochastic variables with different probability distributions from the ones in this thesis were used. No morphological changes were calculated.

In spite of these differences, the results with the $h/2$-model are quite similar. The calculations with the $h/2$-model show very small probabilities of failure, caused by the exclusion of wave set-up and infragravity waves. The ENDEC model does include the wave set-up, but not the infragravity waves. In the calculations of HKV (2014), using ENDEC leads to an even smaller probability of failure, even though the larger water level, due to the wave set-up is included. This is counter-intuitive, the reason for this result is not clear and should be investigated further.

Using XBeach leads to much larger probabilities of failure than ENDEC and the $h/2$-model, about a factor 50 between the $h/2$-model and XBeach 2D and 10^4 between ENDEC and XBeach 2D. This is caused by the inclusion of wave set-up and infragravity waves, compared to the $h/2$-model, and the inclusion of infragravity waves, compared to the ENDEC model. As mentioned before in section 3.3 and Appendix E, XBeach 1D overestimates the infragravity waves. Due to the exclusion of the wave directional spreading in XBeach 1D, the waves become more or less long crested (like in a flume), which leads to a larger forcing of the infra-

gravity waves. XBeach 2D includes the wave directional spreading, which gives more realistic infragravity wave height values. With the analogy of XBeach 1D as a flume, XBeach 2D is similar to a basin. Hence, the failure probability of XBeach 1D is overestimated compared to XBeach 2D, due to the overestimation of the infragravity waves in XBeach 1D. This overestimation gives approximately a factor 10 difference in the failure probability, compared to XBeach 2D. The more realistic XBeach 2D failure probability is also much larger than the ones calculated with the $h/2$-model and ENDEC. The inclusion of the infragravity waves leads to much larger failure probabilities. Hence, a lower estimation of the failure probability is made, when using ENDEC or the $h/2$-model to describe the dike-foreshore system of the Westkapelle sea defence.

Figures 7.4 and 7.6 show the results of a calculation with the $h/2$-model and XBeach 1D, again with offshore conditions for which $Z \approx 0$ and with the smallest distance to the origin in standard normal (U) space. The offshore wave conditions do not differ very much, but the offshore water level is very different. In the $h/2$-model, the water level is clearly the dominant parameter. Because the $h/2$-model does not calculate the change in wave period, the value at the dike toe is very different from XBeach. Because the wave period at the toe with the $h/2$-model is so much smaller than with XBeach, and because the wave heights do not differ largely, a much smaller freeboard (thus more extreme water level) is needed to reach the same amount of wave overtopping, which also explains the difference in the calculated probabilities of failure.

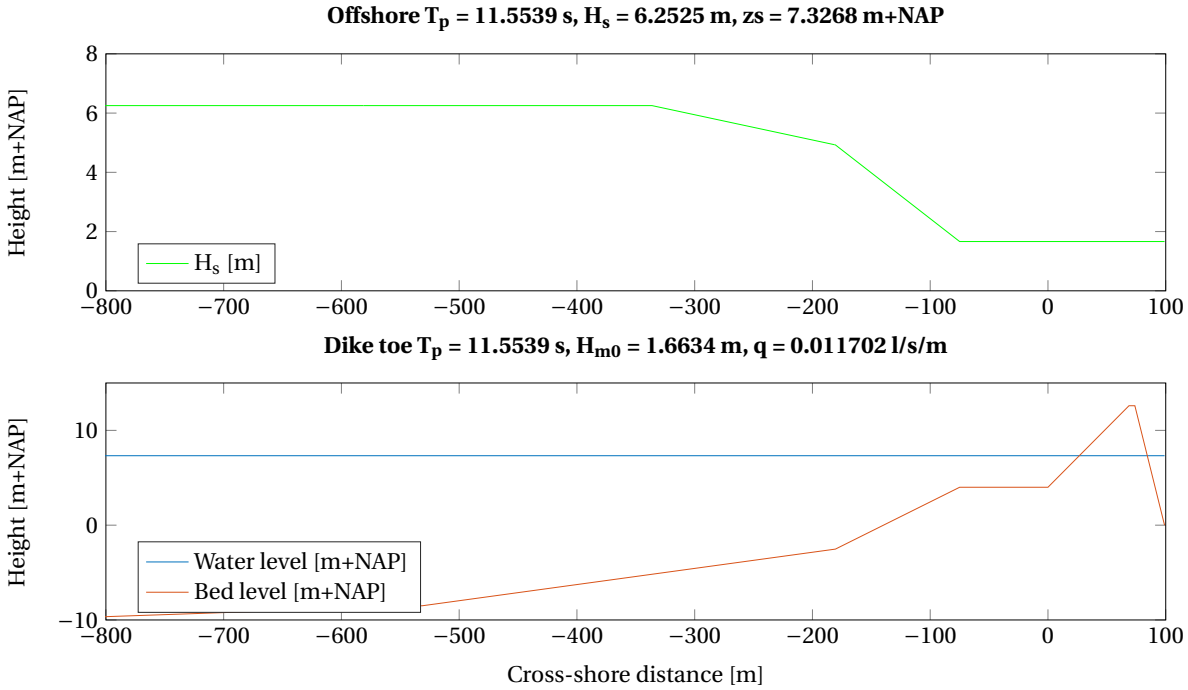

Figure 7.6: $h/2$-model with the offshore conditions as stochastic variables, such that $Z \approx 0$ and with the smallest distance to the origin in standard normal space. Note that not the whole profile is visible, but rather the part from -800 m until 100 m.

7.4. INFLUENCE OF MORPHOLOGICAL CHANGE

This section determines the influence of morphological changes of the foreshore on the dike failure probability due to wave overtopping. Therefore, the results of the calculations without morphological changes, with morphological changes, without morphological stochastic parameters and with morphological stochastic parameters (12 and 15 stochastic variables) will be compared. Because of their long calculation duration, these calculations were only performed with the XBeach 1D-model. Calculations with the 2D-model were started, but had a much too large calculation duration, so they were not finished. The calculations that were performed were:

- Calculation including storm parameters as stochastic, but without calculation of morphological changes.
- Calculation including storm parameters as stochastic and including the calculation of morphological changes.

- Calculation including morphological parameters as stochastic and including the calculation of morphological changes.

The duration of the calculations was a few weeks. As mentioned before, even though XBeach 2D gives better results, no 2D XBeach was used for these calculations, because the calculation duration was over a month. The results of the calculations are shown below in table 7.6.

Table 7.6: Results of the probabilistic calculations, from which the influence of morphological changes of the foreshore on the probability of dike failure is determined. Number of calculations indicates the number of exact calculations, so without the ARS estimations (see section 5.5).

Type of model	Number of stochastic variables [-]	Including morphological changes	Probability of failure [year^{-1}]	β-value	Number of calculations [-]
XBeach 1D	12		$1.23 * 10^{-4}$	3.67	391
XBeach 1D	12	x	$1.55 * 10^{-4}$	3.61	354
XBeach 1D	15	x	$5.30 * 10^{-4}$	3.27	484

The extra stochastic variables, compared to the calculations described in the previous section, increased the number of calculations necessary to reach a converged probability of failure. This is a direct result of the inclusion of more parameters, which enlarges the search space (more dimensions).

Figure 7.7-7.9 and table 7.7 present the results of the simulations for which $Z \approx 0$ and with the smallest distance to the origin in standard normal space. The inclusion of morphological changes leads to a larger probability of failure, albeit a very small difference, as can be seen from the difference in the two calculations with 12 stochastic variables. Due to the erosion of the foreshore, the wave dissipation becomes less, which gives larger wave heights at the toe of the dike. However, the transfer from high frequency wave energy to the lower frequencies becomes less as well, which gives a smaller wave period. In this case, these effects almost cancel one another out, which leads to the small difference in probability of failure, even though the difference in the bathymetry is quite large, due to erosion of the foreshore. Again, the large infragravity wave heights are visible. As mentioned before, these large infragravity waves can exist because they have such a large wavelength, that they do not break on the (compared to the wavelength) relatively short foreshore.

The inclusion of the extra three (morphological) stochastic variables in the calculation with 15 parameters leads to an even larger probability of failure, albeit again not that much larger (about 3 times). The inclusion of the morphological parameters as stochastic variables has thus somewhat more influence on the probability of failure than the inclusion of the morphological process itself. In this case, a somewhat different failure mode seems to be found. The values of the stochastic variables of the calculations with 12 parameters without and with morphological changes are approximately the same. However, the values for the calculation with the extra three morphological stochastic variables shows different values of the stochastic variables. The $C2$ EurOtop parameter was used in this case, albeit with a much smaller value than in the other calculations, which leads to more wave overtopping. Furthermore, the Manning friction factor and wave directional spreading values are somewhat different. The found Manning friction factor is somewhat smaller, which leads to less dissipation of wave energy. The larger JONSWAP wave directional spreading value indicates less directional spreading, hence a stronger forcing of the infragravity waves. Furthermore, the wave asymmetry and wave skewness factors are somewhat larger. which leads to a little bit less erosion. The combined effect of this is that the offshore conditions need to be less extreme to reach the same amount of wave overtopping, which leads to the somewhat larger probability of failure. Thus, the combined influence of the morphological process and the morphological stochastic parameters is about a factor 4 in the failure probability. Compared to the influence of the infragravity waves, the influence of morphological changes of the foreshore is smaller, but still has influence.

Table 7.7: The values of the stochastic parameters in the case where the LSF $Z \approx 0$ and with the smallest distance to the origin in standard normal space, for the calculations with the storm parameters and a static foreshore, storm parameters and a dynamic foreshore, and the morphological parameters and a dynamic foreshore. * indicates that the value is the mean value and that the parameter was not stochastic in that calculation.

Parameter	XB 1D, 12, static	XB 1D, 12, dynamic	XB 1D, 15, dynamic
zs [m+NAP]	5.04	4.96	4.56
$H_{m0,offsh}$ [m]	5.97	5.91	5.02
$T_{p,offsh}$ [s]	11.2	11.12	11.61
$C1$ [-]	5.04	5.03	4.26
$C2$ [-]	3	2.99	2.5
$C3$ [-]	-0.78	-0.79	-1.04
$C4$ [-]	1.01	1.01	1.11
$gamma$ [-]	0.63	0.63	0.63
n [sm$^{-1/3}$]	0.025	0.025	0.019
s [-]	6.82	6.8	8.01
$Tstop$ [hrs]	54.52	54.45	51.42
Loc_peak [-]	6.0844	6.065	5.73
D_{50} [m]	$3.00 * 10^{-4}$ *	$3.00 * 10^{-4}$ *	$2.95 * 10^{-4}$
$FacAs$ [-]	0.123 *	0.123 *	0.135
$FacSk$ [-]	0.375 *	0.375 *	0.492
$H_{m0,toe}$ [m]	1.76	2.37	2.05
$T_{m-1,0,toe}$ [m]	51.38	37.05	38.85
q [ls^{-1}m^{-1}]	0.06	0.15	0.1

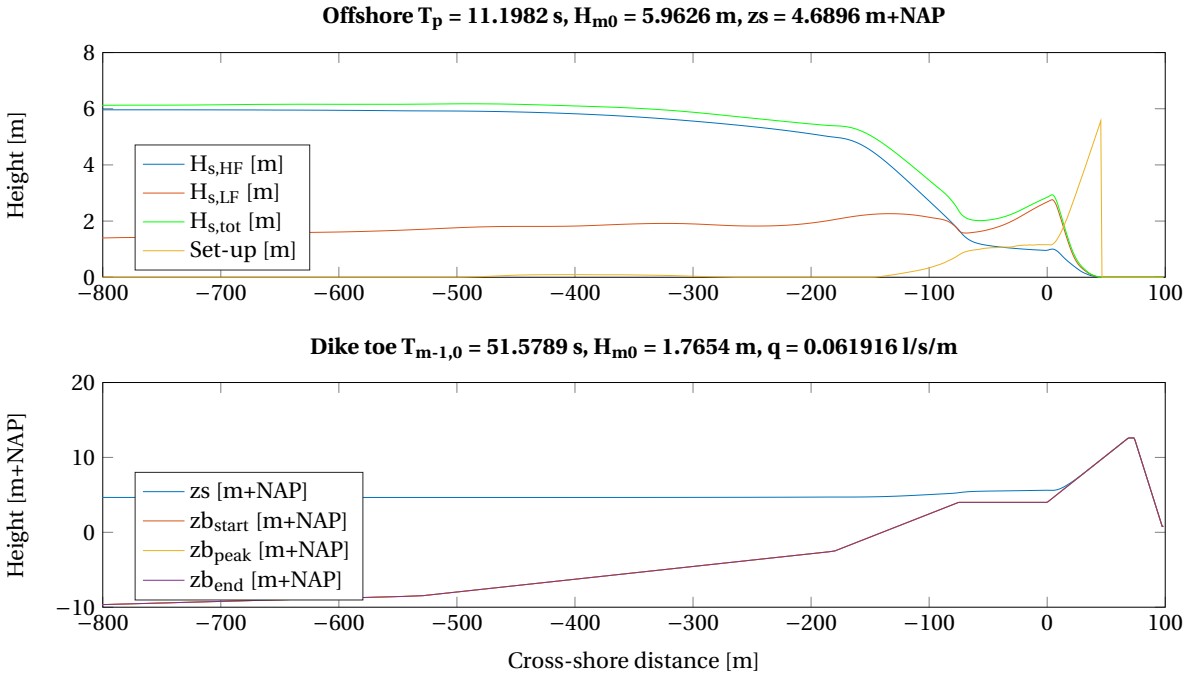

Figure 7.7: XBeach 1D with the storm parameters as stochastic variables and a static foreshore, such that $Z \approx 0$ and with the smallest distance to the origin in standard normal space. Note that not the whole profile is visible, but rather the part from -800 m until 100 m.

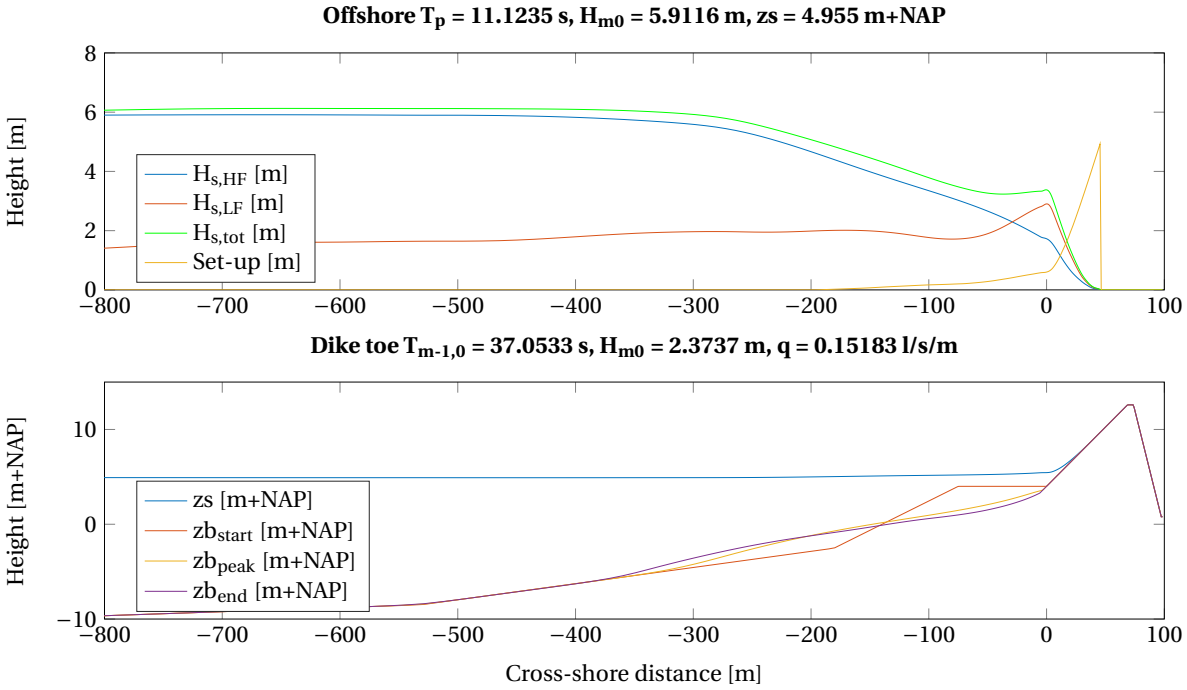

Figure 7.8: XBeach 1D with the storm parameters as stochastic variables and a dynamic foreshore, such that $Z \approx 0$ and with the smallest distance to the origin in standard normal space. Note that not the whole profile is visible, but rather the part from -800 m until 100 m.

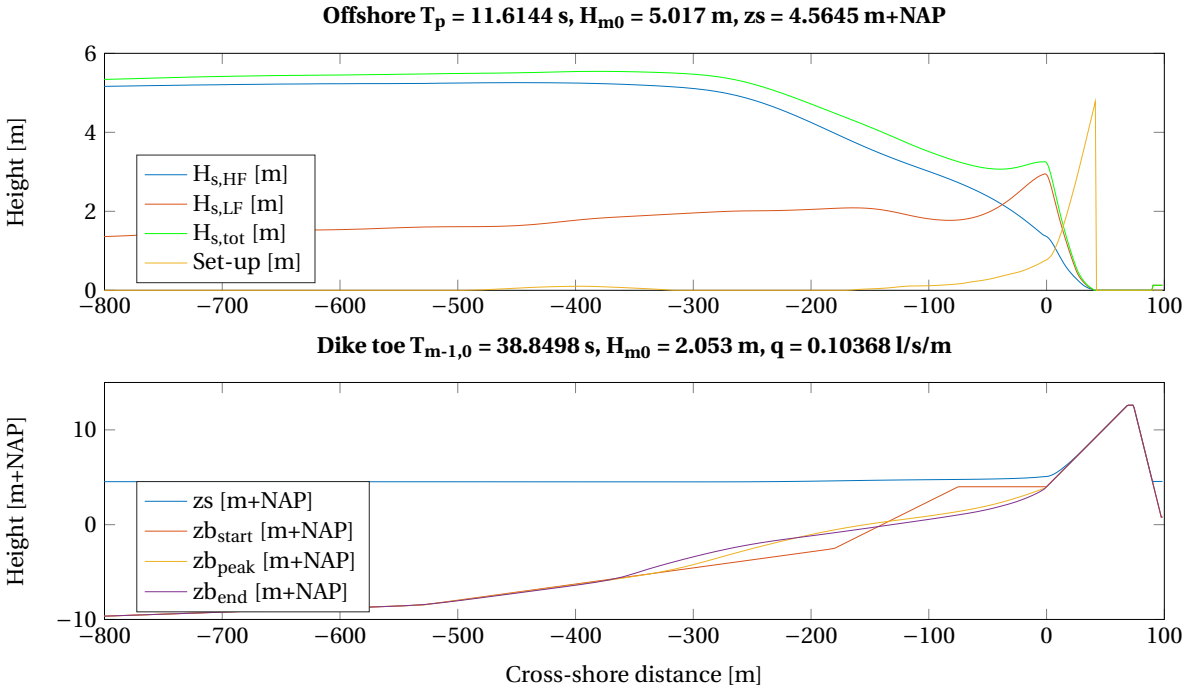

Figure 7.9: XBeach 1D with the morphological parameters as stochastic variables and a dynamic foreshore, such that $Z \approx 0$ and with the smallest distance to the origin in standard normal space. Note that not the whole profile is visible, but rather the part from -800 m until 100 m.

7.5. INFLUENCE OF PARAMETERS & SIMPLIFYING THE FRAMEWORK

The influence of the different stochastic variables can be studied in different ways, e.g. by determining the influence coefficients (α-values), by determining the design point, by considering the ADIS start-up method calculations, or by comparing the probabilistic calculations with different numbers of stochastic variables.

7.5.1. CALCULATION OF DESIGN POINT & INFLUENCE COEFFICIENTS

The influence coefficients (α-values), which determine the influence of each stochastic variables on the probability of failure, are usually calculated within a FORM calculation. The design point is defined as the point in the failure space with the largest probability density. With a level II method, a linear and 'explicit' reliability function, in which all stochastic variables occur, and with only independent random variables, the design point is usually determined by transforming the stochastic parameters and reliability function to standard normal distributions. After that, the influence coefficients are determined with (for that specific case derived) analytical formulae.

However, determining the influence coefficients in other types of probabilistic models is not as straightforward. Furthermore, with a non-linear reliability function, the distribution of the reliability function is not normal and has to be approximated, after which the design point and influence coefficients need to be determined with partial derivatives. When the random variables are not normal distributed, the parameters have to be converted to normal distributed variables, as well as the reliability function. When dependent variables are included, a transformation from dependent to independent stochastic variables is needed, such as the Rosenblatt transformation (Rosenblatt, 1952).

ADIS, a level III method, does not calculate a design point or influence coefficients. With the stochastic variables and LSF used in this thesis, all the above mentioned complicating factors occur. The main problem is deriving the influence coefficients from the design point. The analytical formulations that can be used with FORM, can certainly not be used with ADIS and the calculation framework. The reliability function $Z = \log(q_{crit}) - \log(q)$ looks linear, but because the stochastic variables are not directly represented in the reliability function, the function is actually highly non-linear, especially with the use of XBeach. Also, the random variables are not all normal distributed. Furthermore, the mean values of offshore significant wave height and wave peak period are dependent on the value of the water level. All this greatly complicates the determination of a design point and influence coefficients for the calculations in this thesis.

Vrijling and Van Gelder (2002) describes three methods to determine influence coefficients in level III methods:

- Center of gravity;
- Method of angles;
- Nearest to the mean.

The use of directional and importance sampling in ADIS are two other complicating problems with the first two methods, due to which a non-straightforward transformation is required. The third method, however, can be used with importance sampling and/or directional sampling.

In the method nearest to the mean, the distance to the origin of all the samples in the failure domain is derived:

$$|u_i| = \sqrt{\sum_{j=1}^{n} u_{ij}^2} \text{ for } i = 1...M \tag{7.1}$$

where u are standard normal values, i is the number of samples in the failure domain [-] and j is the number of stochastic variables [-]. The sample with the smallest distance to the origin is taken to be the design point.

For this thesis, this method was added to ADIS. First, the random variables are transformed to normal distributed variables. Then, the evaluated random directions are determined, after which the exact evaluations are determined. Only the exact calculations are used, because the ARS fit could sometimes give (slightly) deviating results of the LSF. Furthermore, due to the β-sphere, the calculations with a result close to $Z = 0$ are always exact XBeach evaluations. Of these exact and evaluated simulations, the standard normal values of the stochastic variables are determined for the calculations where $Z<0$. Then, for each of these simulations, the design point in U-space is determined by using equation 7.1 and choosing the sample with the smallest distance to the origin. The design point in X-space and the determination of the influence coefficients are performed by analytical formulae:

$$X_{DP,j} = U_{DP,j}\sigma_j + \mu_j \tag{7.2a}$$

$$\alpha_j = -\frac{X_{DP,j} - \mu_j}{\beta \sigma_j} \tag{7.2b}$$

where X_{DP} indicates the design point in X-space, U_{DP} the design point in U-space, μ and σ the mean and standard deviation of the to a normal distribution transformed parameter j, and β the reliability index [-].

7.5.2. RESULTS OF DESIGN POINT & INFLUENCE COEFFICIENTS CALCULATIONS

The results for the calculation including the morphological parameters as stochastic variables (15 stochastic parameters) and using a morfac of 10 can be found in figure 7.10. The figure shows that the water level is the most influential parameter, followed by the wave period, storm duration, sediment diameter, wave height, wave asymmetry factor and breaker index. A larger water level, wave height and wave period lead to more wave overtopping, which seems logical. A shorter storm duration leads to more wave overtopping, which is counter-intuitive, because including the morphological changes in the calculation led to a larger probability of failure. A larger sediment diameter leads to a larger wave overtopping discharge, which is again counter-intuitive. With larger grains, it would be expected that the morphological changes would be less, and that the dissipative foreshore would stay more intact. Furthermore, it is striking that the asymmetry factor has such a large influence, while the skewness factor has almost no influence. The same holds for the breaker index, a higher breaker index value would lead to less wave breaking, so probably higher waves reaching the dike, hence more wave overtopping. However, the design point shows a lower value than the mean value.

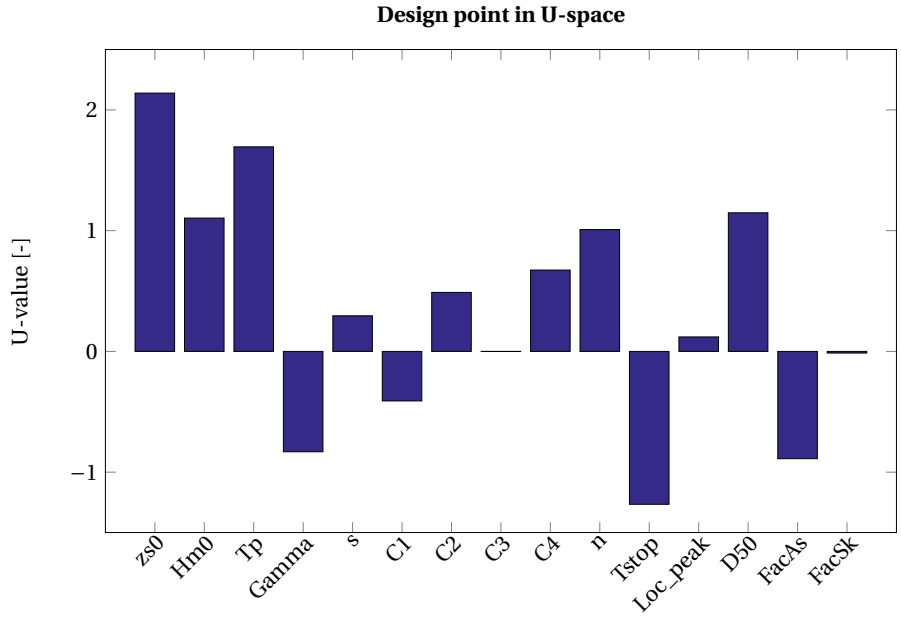

Figure 7.10: U-values in the design point for the calculation including the morphological parameters as stochastic and including a morphological calculation factor. These results are not satisfactory or indicative.

Concluding, the results are not satisfactory or indicative and the method to determine the design point should be improved. Many of the design point values that were found seem counter-intuitive. First of all, the determination of the design point with equation 7.1 gives better results with increasing numbers of samples. Therefore, in calculations with only small numbers of exact calculations, the estimate of the design point could deviate from the real design point. Furthermore, the transformation of the design point from U-space to X-space and the determination of the α-values are done with analytical formulae, which do not give the right results in a complex situation with a non-linear reliability function, non-normal distributed variables and dependent stochastic variables. As explained before, all these situations occur in this case, so other formulations should be sought to be able to better approximate the design point and influence coefficients.

7.5.3. START-UP METHOD CALCULATIONS

To still try to gain some insight in the influence of the different stochastic parameters, another method was sought. The start-up method performs, at the start of ADIS, a number of calculations equal to two times

the number of stochastic variables. This is done to get a first indication of the sensitivity and influence of each parameter. These calculations are each time performed with a β-value of -4 and +4 for one stochastic variable. For the other stochastic variables the mean value is used. The resulting Z-values of the reliability function can be used as an indication of the influence of the parameter on the failure probability. However, it has to be noted that the sensitivity of a parameter commonly depends on the point of reference. The start-up method described here is actually a mean value approach, like the sensitivity analysis. The influence of each parameter determined by comparing to its mean value, hence with a relatively low water level and small waves. When the influence of the parameters in the design point would be assessed, this could give different sensitivities of different parameters. However, to still get some indication of the influence of the parameters, the start-up method calculations were used.

The results of the calculation with the morphological parameters as stochastic variables (15 stochastic variables) and a morfac of 10 are presented in table 7.8 and figure 7.11. The trends were approximately the same for all the calculation types. The main difference is the influence of the wave directional spreading, which has almost no influence in the 1D XBeach calculations. This can, as described before, be attributed to the fact that the wave directional spreading is not included in XBeach 1D. The offshore conditions (water level, significant wave height and wave peak period) have the largest influence. The breaker index and storm duration have a large influence on the failure probability as well. The Manning friction factor, sediment size and wave skewness calibration factor have less influence. The wave directional spreading and EurOtop factor $C3$ have only a very small influence. Due to the mean value approach, the $C3$ coefficient was used here instead of $C2$ (cf. 1/1,000 year values in the sensitivity analysis). The reason for the small influence of the directional spreading was described above. The other EurOtop factors, the phase of the tide and the wave asymmetry calibration factor have almost no influence at all. The influence of the other EurOtop factors can be explained by the fact that only one of the factors is used (at a time), depending on the Iribarren number.

Table 7.8: Start-up method calculation results of the calculation with the XBeach 1D-model, 15 stochastic variables, morphodynamic calculation and a morfac of 10. Indicated in the second and third column are the resulting Z-values of the reliability function for a β-value of -4 or +4 of the indicated parameter. The last column indicates the importance of each parameter, the higher the number, the more important the parameter is.

XB 1D 15 variables morpho-dyn. morfac	Z for $\beta = -4$	Z for $\beta = +4$	Difference	Importance
$zs0$	1.505	0.007	-1.499	5
H_{m0}	1.505	0.148	-1.357	5
T_p	1.505	0.230	-1.276	5
$gamma$	1.505	0.601	-0.905	4
s	0.963	0.952	-0.011	2
$C1$	1.000	1.000	0	1
$C2$	1.000	1.000	0	1
$C3$	1.015	0.985	-0.029	2
$C4$	1.000	1.000	0	1
n	1.134	1.257	0.123	3
$tstop$	-0.105	1.021	1.126	4
loc_peak	1.190	1.189	-0.001	1
D_{50}	1.146	0.913	-0.233	3
$FacAs$	1.006	1.013	0.007	1
$FacSk$	0.982	1.125	0.143	3

It has to be mentioned that the influences of the parameters found here are based on a mean value approach and apply to the case considered in this thesis and can possibly not be applied directly at another location.

7.5.4. STRENGTH & LOAD PARAMETERS

By considering the previous subsections, the stochastic parameters can be categorized into 'resistance' and 'solicitation' parameters, i.e. the parameters that, with a larger simulated value, positively or negatively influence the Z-value, see table 7.9. Hence, with this characterization, not necessarily the actual loads on the dike

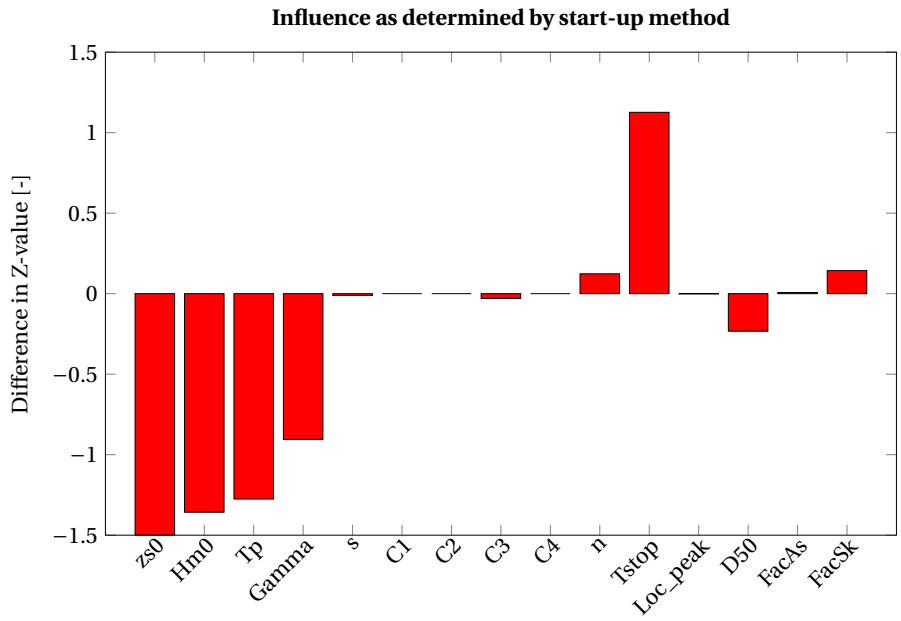

Figure 7.11: Results of the analysis of the start-up method calculations for the calculation including the morphological parameters as stochastic and including a morphological calculation factor. The resulting differences in Z-value of the LSF for an increase in a certain parameter are shown.

are considered as load parameters, or the parameters of the foreshore or dike as strength parameters.

It can be seen from the table that the results do not agree. The design point values are not indicative, as was explained above. The results from the start-up method calculations show the same trends as when the influence of the parameters on the wave overtopping discharge in the sensitivity analysis (chapter 6) would be considered. This can be explained by the fact that both are 'mean value approaches', as was explained before. It has to be noted that instead of the $C2$ EurOtop coeifficient, here $C3$ was used, which is caused by the here considered reference point (mean value versus 1/1,000 years value for the offshore conditions in the sensitivity analysis). Furthermore, the sensitivity analysis was performed with the 2D XBeach model, here the 1D-model is considered, which explains the small influence of the wave directional spreading. As mentioned before, the design point and influence coefficients did not yet show promising results. Therefore, only the results from the start-up method will be discussed here.

The offshore conditions are load parameters, which seems logical. The breaker index is a load parameter as well, allowing larger wave heights at a certain water depth with a larger breaker index value. The wave directional spreading is also a load parameter (larger JONSWAP directional spreading value, less directional spreading), but has almost no influence in the 1D-model. In a 2D-model, the influence is larger. A larger value of the Manning friction factor leads to more friction losses, hence lower infragravity waves and velocities, making it a strength parameter. The storm duration is a strength parameter as well, which is counterintuitive, because including the morphological changes led to a larger probability of failure. This could be an artifact of the mean value approach, and has to be investigated further. The location of the tidal peak could be considered as a load parameter, but its influence is small. The grain diameter is a load parameter, so a larger grain diameter apparently leads to more wave overtopping. This is strange, because intuitively, larger sediment would be less mobile, so the dissipative foreshore would remain more intact, and less overtopping would occur. This could again be an artefact of the mean value approach and again needs to be investigated further. Also, as mentioned before, the grain diameter has not much influence on the bed level in XBeach, cf. (Van Thiel de Vries, 2009). The wave asymmetry and skewness factors are both strength parameters. A larger value of these parameters leads to a steeper bed slope. It depends on the situation if this would lead to more wave overtopping or not. Hence, also when using only the start-up method results for the characterization of load and strength variables, still some counter-intuitive results occur.

Table 7.9: Categorization of the parameters into load and strength variables, for the design point values and start-up method values.

Parameter	Influence according to design point	Influence according to start-up method
$zs0$	load	load
H_{m0}	load	load
T_p	load	load
$gamma$	strength	load
s	load	load
$C1$	strength	-
$C2$	load	-
$C3$	-	load
$C4$	load	-
n	load	strength
$tstop$	strength	strength
loc_peak	load	load
D_{50}	load	load
$FacAs$	strength	strength
$FacSk$	strength	strength

7.5.5. COMPARISON OF NUMBER OF STOCHASTIC VARIABLES

Another way to determine the influence of the parameters is comparing the calculations with different numbers of stochastic variables. Then, the influence of each parameter set that was determined in chapter 6 can be determined.

Table 7.10 and figure 7.12 show the results of the calculations with different numbers of stochastic variables. From the difference between the calculations with only the offshore conditions (3 stochastic variables) and with the model parameters (10 stochastic variables), about a factor 20, it can be seen that the model parameters in set 2 still have a fairly large influence. For the 2D calculations, the probabilities of failure for the offshore conditions and offshore conditions & model parameters have almost the same value, the influence of the extra parameters in the 2D model is thus small. Even a decrease in the failure probability was found, see also table 7.11. However, this is probably caused by the accuracy of the calculated failure probabilities, which was that the actual probability of failure lies with 95% certainty within 20% of the calculated probability. Because the values of these two probabilities of failure are so close to one another, the 20% increase and decrease values partly overlap and the decrease in failure probability that was found might as well be an increase. The difference between the probabilities of failure determined by the calculations with the model parameters (10 stochastic variables) and with the storm parameters (12 stochastic variables) is about a factor 2. This difference is caused by the location of the tidal peak. In the calculation with the model parameters, the peak of the surge coincides with the peak of the tide. In the calculation with the storm parameters, the peak of the surge could also coincide with low tidal water. This leads to a slightly smaller probability of failure. Hence, the storm parameters of set 3 only have a small influence on the failure probability. The influence of the morphological changes of the foreshore was determined in the previous section, by comparing the calculations with the storm parameters, with 12 stochastic variables (morphostatic and morphodynamic). The difference was not that large, with a larger failure probability when the morphological changes were included. Including the morphological parameters as stochastic as well (15 parameters in total), leads to an increase in the failure probability with about a factor 3. Thus, the morphological parameters also have some influence. In the previous subsection on the start-up method calculations, it was derived that the sediment size and wave skewness factor had some influence, the wave asymmetry factor almost none. However, in the section on the design point values, it was determined that the sediment size and wave asymmetry calibration factor had some influence and the wave skewness factor not. This discrepancy should be investigated in more detail. As mentioned before, the influences of the parameters found here do not need to automatically also apply for a different dike-foreshore system.

7.5.6. WAYS OF SIMPLIFYING THE FRAMEWORK

In the previous sections, the influence of including the infragravity waves and morphological changes of the foreshore was determined, as well as the influence of the different stochastic variables. For the case con-

Table 7.10: Comparison of the calculations with different numbers of stochastic variables.

Type of model	Number of stochastic variables [-]	Including morpho-logical changes	Including tide, storm profile	Probability of failure [year^{-1}]	β-value	Number of calculations [-]
XBeach 1D	3			$1.64 * 10^{-5}$	4.15	112
XBeach 1D	10			$2.85 * 10^{-4}$	3.45	341
XBeach 1D	12		x	$1.23 * 10^{-4}$	3.67	391
XBeach 1D	12	x	x	$1.55 * 10^{-4}$	3.61	354
XBeach 1D	15	x	x	$5.30 * 10^{-4}$	3.27	484

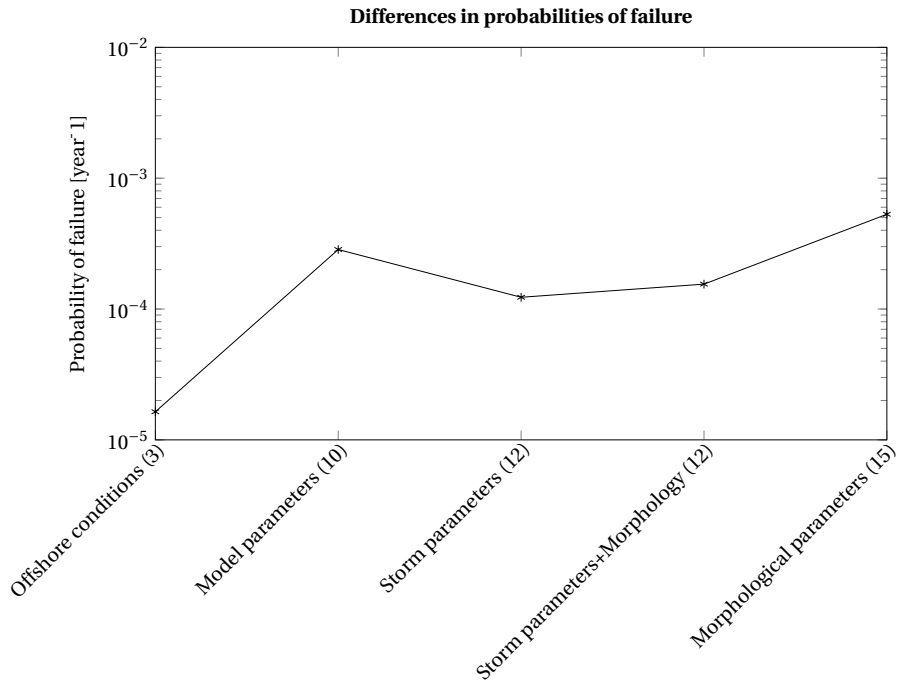

Figure 7.12: Probabilities of failure for the calculations with different numbers of stochastic variables.

sidered in this thesis, including the wave set-up and infragravity waves leads to much larger probabilities of failure (factor 10^3 for XBeach 1D and 10^2 for XBeach 2D). Hence, these processes should not be excluded from the calculations. Including the morphological changes had less influence (a factor 4 for the combined influence of the process itself and the morphological stochastic variables), however the changes in the cross-shore profile can be large. Excluding the morphological changes could thus still lead to an underestimation of the failure probability. The parameters with the largest influence were the offshore conditions and the breaker index. The storm duration only has a large influence in calculations which also determine the morphological changes of the foreshore. The offshore conditions and breaker index should certainly not be excluded, and in calculations with morphological changes, the storm duration as well. The wave directional spreading did not have much influence (especially in the 1D model). The EurOtop coefficients have some influence and the location of the tidal peak has a small influence. Possibly, the wave directional spreading could be excluded as a stochastic variable in the 1D model, the location of the tidal peak in the 1D and 2D models. The results of all the calculations can be found in Appendix J. The difference between the 1D and 2D calculations was about a factor 10-25, due to the overestimation of the infragravity waves in the 1D calculations. Hence, the simplification of 2D to 1D saves a lot of computational time, but also gives a higher probability of failure. Finally, using a morfac of 10 did not lead to largely different probabilities of failure, but it reduces the calculation duration by about a factor 10 (when the morphological changes are calculated).

7.6. SUMMARY & CONCLUSIONS

This chapter aimed to provide an answer to sub-questions 4, 5 and 6: the influence of infragravity waves and morphological changes of the foreshore on the probability of dike failure due to wave overtopping, as well as the parameters that dominate the failure probability and ways of simplifying the framework. The uncertainty analysis was done by performing multiple calculations with the probabilistic calculation framework as described before. For example, the different numbers of parameters were used (as determined in the previous chapter), the XBeach 1D- and 2D-model were used, and the morphological changes were excluded and included. For the calculations including the storm duration and/or morphological changes, only the 1D XBeach model was used, because the calculation duration when using the 2D-model was over a month. Results of calculations with different models, amounts of stochastic variables and including or excluding infragravity waves or morphological changes of the foreshore can be found in table 7.11.

Table 7.11: Results (probabilities of failure [year^{-1}]) of calculations with different models, amounts of stochastic variables and including or excluding infragravity waves or morphological changes of the foreshore.

Type of profile	Model & number of stochastic variables	Short waves	Short waves & infragravity waves
Dike	$h/2$-model, 3	$9.78 * 10^{-7}$	
	XBeach 1D, 3		$5.68 * 10^{-2}$
	XBeach 2D, 3		$4.78 * 10^{-5}$
Dike & static foreshore	$h/2$-model, 3	$2.29 * 10^{-8}$	
	XBeach 1D, 3		$1.64 * 10^{-5}$
	XBeach 2D, 3		$1.56 * 10^{-6}$
	XBeach 1D, 10		$2.85 * 10^{-4}$
	XBeach 2D, 10		$1.12 * 10^{-6}$
	XBeach 1D, 12		$1.23 * 10^{-4}$
Dike & dynamic foreshore	XBeach 1D, 12		$1.55 * 10^{-4}$
	XBeach 1D, 15		$5.30 * 10^{-4}$

7.6.1. THE FORESHORE: INFLUENCE

The $h/2$-model calculations, which exclude the infragravity waves and wave set-up, lead to a difference in probability of failure of about a factor 40 between the case with and without the foreshore. The dominant parameter is the water level, which is large for the case without foreshore and even larger for the case with foreshore. The counteractive effects of a larger water level but lower wave height at the dike toe, make that the difference in failure probability between the case with and without foreshore is not as large as what was found in HKV (2014). A reduction of the failure probability of order 10^3 was found for the 1D-model and of order 30 for the 2D-model. Compared to HKV (2014), where a (very large) reduction of 10^5 was found, these reductions are smaller. Again, the more severe wave breaking due to the foreshore leads to lower wave heights at the dike toe when the foreshore is present, but this also leads to a transfer of wave energy to the lower frequencies, which increases the wave period.

7.6.2. INFRAGRAVITY WAVES: IMPORTANCE

Results from different calculations were compared to one another and to the results of HKV (2014). Including the wave set-up and infragravity waves by using XBeach leads to much larger failure probabilities (factor 10^3 for XBeach 1D and 10^2 for XBeach 2D), than when the $h/2$-model is used. XBeach 2D includes the wave directional spreading, which XBeach 1D does not. Therefore, the results of XBeach 2D are more realistic, because XBeach 1D overestimates the infragravity waves. However, the improved performance compared to e.g. the $h/2$-model and the short calculation durations make XBeach 1D a good alternative as well. The large difference in failure probability when including the infragravity waves indicates that a lower estimation of the failure probability is made, when one of the models (ENDEC or the $h/2$-model) of the current Dutch safety assessment tools is used to describe the dike-foreshore system as considered in this thesis.

7.6.3. MORPHOLOGICAL CHANGES: IMPORTANCE

Results from other calculations were compared to determine the influence of morphological changes of the foreshore on the probability of dike failure due to wave overtopping. Because of the long calculation duration of these simulations, only the 1D XBeach model was used. For some calculations, a morfac of 10 was used, which proved to have almost no influence on the calculated failure probability. The inclusion of morphological changes leads to a failure probability that was a bit larger, but not that much. The inclusion of the three morphological parameters as stochastic variables lead to an increase in the failure probability of about a factor three. The combined influence of the morphological process and the morphological stochastic variables, about a factor four, is thus not very large when compared to the influence of the infragravity waves (and wave set-up), but is still somewhat too large to be excluded.

7.6.4. PARAMETER INFLUENCE & SIMPLIFICATIONS TO THE MODEL TRAIN

The influence of the stochastic variables was studied by considering the design point and influence coefficients, the start-up method calculations and by comparing the calculations with different numbers of stochastic variables. After that, ways to simplify the framework were discussed.

Determining the influence coefficients with other methods than FORM is not straightforward. Complicating factors are non-linear reliability functions, non-normal distributed parameters and reliability functions and dependent stochastic variables. Different methods exist to determine the design point in level III methods, however when directional and/or importance sampling is used, only the method nearest to the mean can be used. Therefore, that method was implemented into ADIS for this thesis. However, the results are not yet satisfactory. The determination of the design point with the method nearest to the mean gives better results with an increasing number of samples. Furthermore, the analytical formulae that were used to determine the design point in X-space and the influence coefficients do not work correctly with e.g. dependent stochastic variables. Other methods should be considered to determine the influence coefficients.

The start-up method calculations were used to determine the influence of the stochastic variables. The trends were approximately the same for all the calculations, with the exception of the wave directional spreading, which has almost no influence in XBeach 1D calculations. The offshore conditions have the largest influence on the failure probability, the location of the tidal peak is one of the least influential parameters. Furthermore, the parameters were categorized into strength and load parameters. This categorization lead to some strange observations for the storm duration, sediment diameter and wave calibration factors, which need to be investigated further.

A comparison of the number of stochastic variables used in the calculations was made as well, to determine the most important parameter sets. The parameters in set 1 (offshore conditions) and 2 (model parameters) had the largest influence on the failure probability in the 1D model. The parameters of set 3 (storm parameters) had a small influence. The morphological parameters in set 4 had some influence.

The framework could be simplified by possibly excluding he wave directional spreading (in 1D calculations) and the phase of the tide. A further reduction in calculation time could be achieved by using a morfac for the calculations including the morphological changes. The infragravity waves (and wave set-up), as well as the offshore conditions and breaker index should certainly not be excluded.

8

DISCUSSION

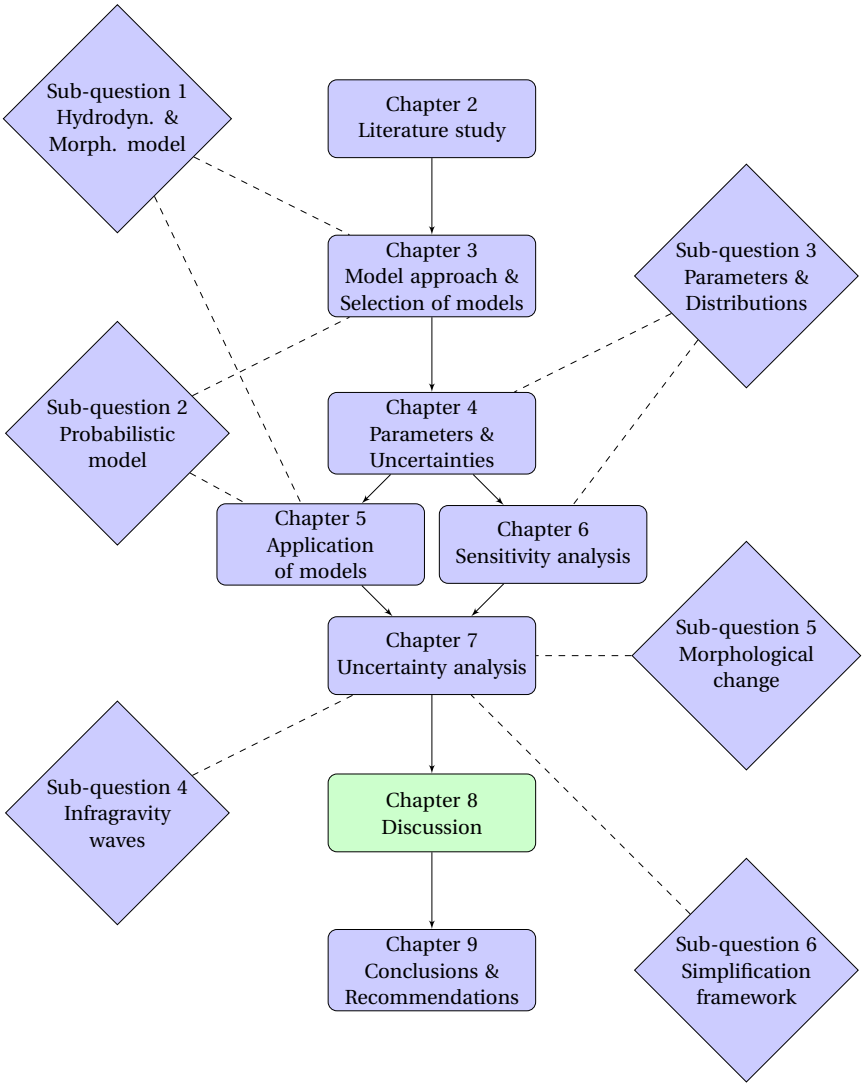

Figure 8.1: Outline of this report.

This chapter presents the discussion of the research as presented in this report. Each of the discussion points as well as the limitations are presented from section 8.1 onward. The value of the results is described, as well as the possible applications. Furthermore, the study is compared to previous research, the limitations are discussed, as well as several other important points.

8.1. VALUE OF THE RESULTS

This thesis has presented a method with which infragravity waves and morphological changes of a sandy foreshore can be included in the calculation of the probability of dike failure due to wave overtopping. Before this thesis, this was not yet possible. That the influence of the morphological changes and especially the infragravity waves can be large, was described in the previous chapter (q.v.). The morphological changes considered here, were the changes during (severe) storms. Furthermore, the parameters that dominate the failure probability were determined, i.e. the parameters that need to be taken into account in the probabilistic calculations. The focus was on the Westkapelle sea defence, a hybrid defence. The method developed in this study can, with a few changes as will be described below, also be applied at other locations. Using this method offers more insight insight into the contribution of foreshores to flood protection and can possibly increase the use of foreshores as a supplement to more conventional dike reinforcement methods.

As shown in this thesis, it is important that the infragravity waves are included in the calculation of the dike failure probability due to wave overtopping at a dike-foreshore system. The method developed in this thesis could possibly be used to assess dike-foreshore systems in light of the new Dutch assessment tools based on flood risk instead of exceedance probabilities of hydraulic loads. Using the calculation framework increases the knowledge on dike-foreshore systems and could pave the way for an increase in the implementation of Building with Nature solutions. The results of this thesis contribute to the BE-SAFE project on safety of flood defences with vegetated foreshores.

8.2. COMMENTS ON PREVIOUS RESEARCH

Chapter 2 described the previous research on the subject. The previous research stated that wave energy is dissipated on foreshores by wave breaking, and that in the wave spectrum a shift from the peak frequency to the lower frequencies occurs. All these processes were also found in this study. Severe wave breaking occurred on the foreshore and the wave periods found at the dike toe were much larger than the offshore high frequency wave peak period.

Van der Meer (1997) showed that wave energy is dissipated on foreshores by wave breaking, which leads to a reduction in wave height compared to the case in which no foreshore is present. A distinction between shallow and deep foreshore was made, where $h_{toe}/H_{s,toe} < 4$ indicates a shallow foreshore. Very shallow foreshores were defined as well, by $H_{s,toe}/H_{s,offshore} < 0.5$. For the cases considered in this thesis, the water depth at the toe was about 1-2.5 m, the wave height at the toe 1.5-3 m and the offshore wave height about 5-7 m during design conditions. This makes the foreshore always shallow and almost always very shallow. Van der Meer (1997) mentions that because of the change in the energy density spectrum by waves breaking on a shallow or very shallow foreshore, the peak period T_p is not a useful measure anymore to calculate the run-up, which was also found in this thesis for the wave overtopping. Furthermore, on foreshores where intense breaking occurs, the wave set-up becomes of large importance on the run-up and overtopping, which was found here as well.

Previous research (e.g. Holterman (1998) & Van Gent (1999)) recommended using the $T_{m-1,0}$ wave period instead of the wave peak period (T_p) in the above situations, to determine the wave run-up or wave overtopping. Indeed, the $T_{m-1,0}$ wave period performs better than the peak period, but the $T_{m-1,0}$ wave period is very sensitive to changes in the low frequency energy, frequency resolution and frequency (cut-off) limits. It is therefore recommended to derive clear guidelines on how to determine the $T_{m-1,0}$ wave period when infragravity waves are present.

It was stated that beach nourishments do not always reduce the wave overtopping discharge (Suzuki et al., 2012). Constructing a foreshore is different from constructing a beach nourishment. Also, in this thesis a reduction in the failure probability was found when the foreshore was included in the calculations. However, the reduction that was found was much smaller than what was found in HKV (2014), caused by the inclusion of infragravity waves and morphological change of the foreshore. Considering a different dike-foreshore system could also give different results.

The influence of a foreshore on the probability of dike failure due to wave overtopping was studied in HKV (2014), also considering the Westkapelle sea defence. This study did not include the influence of infragravity waves and morphological changes of the foreshore, which are both included in the method developed in this thesis.

Roeber and Bricker (2015) show that during extreme storms, infragravity waves can steepen over a fringing reef into a tsunami-like wave that causes excessive damage and casualties. The steep fringing reef face causes a very short wave-breaking zone, which releases the bound infragravity waves with little energy loss. A policy

change with the adoption of phase-resolving models was proposed for regions with fringing reefs or other types of bathymetry that favour the abrupt release of infragravity waves. A strong decrease in wave energy due to wave breaking on the slope of the foreshore was also found here, especially in the calculations without morphological change. As mentioned before, the wave breaking causes a shift to the lower wave frequencies. Furthermore, large infragravity wave heights were found at the horizontal part of the foreshore, even though the water depth on the foreshore was not that large. As mentioned before, with the current calculation method, neither infragravity waves, nor morphological changes of the foreshore can be included. Furthermore, the large influence of the infragravity waves on the probability of failure was described, which enforces the claim to adopt phase-resolving or even more detailed models.

Most of the previous research was done with flume experiments, which cannot include the wave directional spreading. As described before, XBeach 1D can be compared to a wave flume, XBeach 2D to a wave basin. Hence, XBeach 1D does also not include the wave directional spreading. As mentioned earlier, the exclusion of the wave directional spreading leads to an overestimation of the infragravity waves. This same overestimation is also present in physical flume model tests.

8.3. MODELLING DIKE-FORESHORE SYSTEMS AND APPLICATION AT OTHER LOCATION

In this thesis, a schematized version of the Westkapelle sea defence was used. The mean crest height of the whole defence was used as crest level, the dike berm was not included and the foreshore bathymetry was schematized. Furthermore, the uncertainty in the actual foreshore bathymetry at a certain moment was not yet included. Hence, the focus of this thesis was on developing a method to include the infragravity waves and morphological changes in the calculation of the probability of dike failure due to wave overtopping, not to calculate exact probabilities of failure of the actual Westkapelle sea defence.

The for this thesis chosen method consists of XBeach hydrostatic 1D or 2D, EurOtop and ADIS. In an ideal case, where computational duration is not an issue, ADIS, XBeach hydrostatic 2D and EurOtop could be used. Otherwise, XBeach 1D should be used to save computational time.

When clear insight in the importance of each stochastic variable is necessary, FORM could be used, however FORM can have difficulties with the complex LSF. When the method to determine the design point and influence coefficients in ADIS is improved, ADIS can also provide clear insight in the importance of each parameter.

As mentioned before, XBeach 2D gives better results than XBeach 1D, but the duration of the calculations becomes very large when using XBeach 2D with the calculation of morphological changes. Compared to the method currently used in the Dutch standards, the results of XBeach 1D are already much more realistic, with the inclusion of infragravity waves and morphological changes of the foreshore. XBeach non-hydrostatic was able to predict the shape of the wave spectrum at the dike toe better than XBeach hydrostatic, but XBeach hydrostatic still gave better results of the wave height and wave period.

XBeach non-hydrostatic or SWASH could in theory be used to determine the wave transformation and wave overtopping, but these models do not yet include the calculation of morphological changes, cannot predict small wave overtopping discharges accurately and have a much larger calculation duration than XBeach hydrostatic. Hence, the EurOtop formulae are still the best option to calculate the wave overtopping discharge, although the influence of infragravity waves and wave set-up should be studied in more detail. Concluding, XBeach hydrostatic 1D, EurOtop and ADIS are currently the best choice to model a dike-foreshore system with a sandy foreshore. When, in the future, the computational capacity increases and XBeach non-hydrostatic and/or SWASH are further developed, XBeach hydrostatic 2D, EurOtop and ADIS, XBeach non-hydrostatic 2D and ADIS or SWASH and ADIS could become the preferred options.

The framework derived in this thesis can be applied at other locations without many problems. Without issues, the actual JARKUS profile could be applied. The calculation framework, or 'model train', meaning ADIS, XBeach and EurOtop, could also be applied for other dike-foreshore systems. The same probability distributions could be used when considering another Dutch coastal dike-foreshore system. Just the parameters of the distributions would need to be altered. For a non-coastal dike-foreshore system or dike-foreshore system outside of The Netherlands, the probability distributions themselves need to be changed as well. The sensitivity and uncertainty analysis as performed in this thesis, resulted in the most important parameters and processes for this dike-foreshore system, the schematized version of the Westkapelle sea defence. With a different location, different parameters could have different influences. For example, when an inland dike-foreshore system would be considered, wave heights could be less extreme, as well as morphological changes.

Therefore, a new sensitivity analysis is recommended for a new location.

8.4. DURATION OF CALCULATIONS

For this thesis, a schematized version of the Westkapelle sea defence was considered. The crest height of this defence is rather large, which causes low probabilities of failure, and could also influences the amount of calculations necessary to reach a converged probability of failure. Compared to a case with a lower crest level, more calculations are necessary for the here considered defence. Furthermore, the strict criterion of 0.1 $ls^{-1}m^{-1}$ for the wave overtopping discharge, causes that many calculations are necessary to find a $Z \approx 0$ point. When this criterion would have been e.g. 10 $ls^{-1}m^{-1}$ (e.g. with a grass covered inner slope), finding a $Z \approx 0$ point would be easier, hence less calculations would have been necessary. In other words, a lower dike with a well-protected inner slope would have been an easier case, but with the case considered, here the calculation framework was immediately pushed to its boundaries, which was helpful for developing the method as well.

The main limitation of the research is the calculation duration of the calculations with many stochastic variables and including morphological changes of the foreshore. Because the calculation duration for the calculations with storm parameters and morphological parameters (12 and 15 stochastic variables) and the 2D XBeach model was much too long (over a month, without morfac), the 1D model was used for these long calculations. However, even with the 1D model, some calculations took a few weeks. Furthermore, as explained before, the 1D model overestimates the infragravity waves, due to the exclusion of the wave directional spreading in XBeach 1D. Using the 2D XBeach model would yield more realistic results. This, however, requires finding a solution for the long calculation durations.

Methods to reduce the calculation duration could be e.g. a morphological acceleration factor, cyclic boundary conditions, lower resolution or smaller size of the computational grid. Cyclic boundary conditions were already used for the 2D calculations. A lower resolution of the computational grid or less grid cells in the alongshore direction were also tested, but did not result in a strong decrease in calculation duration. A solution could be to use a morphological acceleration factor, which was used for some of the 1D calculations already and showed almost no influence on the probability of failure (see Appendix J).

Other solutions could be, for example, monitoring the morphological changes during the storm. If the morphological development becomes smaller than a certain boundary value, and the peak of the storm has already passed, the calculation could be stopped. Another possibility is stopping the calculation after the maximal wave overtopping discharge has been reached. In this thesis, the maximum wave overtopping discharge always occurred in the middle of the storm, except when the surge peak coincided with tidal low water. In that case, the maximum wave overtopping discharge occurred at about $2/5^{th}$ of the storm duration. Of course, this can change when a different dike-foreshore system is considered. Currently, ADIS tries to find the $Z = 0$ point for one random direction at a time. Implementing an algorithm with which multiple random directions are examined at the same time could potentially save a lot of calculation time.

One hour of the storm was calculated for the simulations without the storm duration and location of the tidal peak as stochastic variables, and without morphological changes. This gives the same results as calculating the whole storm duration (storm duration not stochastic, so always the mean value), and saves computation time. For the calculations including morphological changes of the foreshore, the whole storm duration was used. However, this leads to long calculation durations.

A limit of 200 hours was set on the storm duration, to limit the computational time. However, setting such a limit results in a discontinuity in the LSF, which could result in more simulations necessary to reach a converged probability of failure. The calculations could converge to long storm durations, so a limit on the storm duration could actually be not physically correct. If the calculation duration is not an issue at all, the limit of 200 hours could just be removed. For the case considered in this thesis, the calculations did not converge to very long storms. However, this should be determined for each new location at which the calculation framework is supposed to be used.

8.5. EUROTOP FORMULAE & INFLUENCE OF $T_{m-1,0}$ ON q

Figures 8.2 and 8.3 show the influence of $T_{m-1,0}$ and ξ on the wave overtopping discharge, for four different wave heights at the dike toe, a dike slope of 0.125 and a freeboard of 7 m. Visible is that the overtopping discharge is very sensitive to the wave period (or breaker parameter) in the range of about 5-20 s (or 0-2 when ξ is considered). This is in the range of the EurOtop formula for $\xi < 5$ and with breaking waves. When the waves become non-breaking, but ξ is still smaller than 5, the formula for non-breaking waves is used, which is independent of the breaker parameter, hence the constant q value. With further increasing wave period

and breaker parameter, interpolation is used between the different EurOtop formulae ($5 < \xi < 7$). Here, the wave overtopping discharge starts increasing again. For very large breaker parameters, the formula for $\xi > 7$ is used. In this range, the overtopping discharge is gradually increasing. Summarizing, for wave periods between 5-20 s (or $\xi < 2$) the influence on q is very large, for 10-70 s ($2 < \xi < 5$), depending on the wave height, the discharge is constant, and for periods larger than 30-70 s ($\xi > 5$), again depending on the wave height, the wave overtopping discharge is gradually increasing.

For the case considered in this thesis, the $T_{m-1,0}$ wave periods at the dike toe during design conditions in the different calculations were rather large (15-50 s), with significant wave heights at the dike toe of 1-3 m, however the dike slope of 0.125 keeps the breaker parameter rather low (mostly between 1-5), which causes the breaker parameter (and wave period) to be in the range where the influence on q is very large or zero. It is therefore important that the $T_{m-1,0}$ period at the dike toe is correct, because the conditions are not always in the area of zero influence or a gradually increasing q. Hence, the aforementioned points of attention on the $T_{m-1,0}$ period, being the very heavy weighing low frequencies and the large influence of the frequency limits and frequency resolution on this wave period need to be considered in more detail.

The EurOtop formulae for $\xi < 5$ were based on situations with not too shallow foreshores, such that either breaking or non-breaking waves occur. A dike slope of 1:2 leads to mostly non-breaking waves, a dike slope of 1:4 to mostly breaking waves. The dike slope as considered in this thesis of 1:8, would lead to breaking waves when the foreshore is not too shallow. However, the foreshore was shallow and almost always very shallow (see section 8.2).

As mentioned before, the experiments of Van Gent (1999) studied wave run-up and wave overtopping on shallow foreshores, and showed (very) large wave periods at the dike toe, just like in the case considered in this thesis. A formulation was derived for $\xi > 7$ in which with increasing values for the breaker parameter, the wave overtopping increases gradually. However, this formula was derived based on dike slopes of 1:2.5 and 1:4, and not on 1:8 as in this thesis.

The combination of a (very) shallow foreshore and dike slope of 1:8 make that the case considered here is (largely) outside the previously studied area. The results of Van Gent (1999) showed largely the same trends, with either a slope of 1:2.5 or 1:4, which could indicate that, when the wave period becomes very large, the wave overtopping is not dependent anymore on the dike slope, but on the wave parameters only. Therefore, it is possible that, for to the very large wave periods and the dike slope of 1:8 as found in this thesis, the wave overtopping is actually not dependent on the dike slope, but only on the wave parameters. It is therefore questionable if the EurOtop formulae calculate the right amount of wave overtopping for these types of situations, because in the formulae, the wave overtopping is dependent on the dike slope. This could possibly lead to a lower estimation of the wave overtopping when using the EurOtop formulae in these kinds of situations.

If the influence of the dike slope is negligible in situations where the infragravity wave is dominant in the physical process, hence in situations where a very large wave period occurs, needs to be investigated in more detail. Furthermore, currently, the EurOtop formulae use the $T_{m-1,0}$ wave period. As described before, this wave period is very sensitive to the low (infragravity wave) frequencies. It is currently unknown if using this wave period leads to overestimation of the wave overtopping discharge. More research is required to determine the influence of the infragravity waves on wave overtopping and to be able to determine if the $T_{m-1,0}$ wave period is a good predictor or not. The EurOtop formulae were not derived for the in this study occurring wave spectra, with large amounts of low frequency energy. Furthermore, the EurOtop equations currently use the still water level, the SWL. Large infragravity waves can give large wave set-up values, which give larger wave overtopping discharges. Further research on the influence of infragravity waves should also include the influence of the wave set-up on the wave overtopping, and determine if the wave set-up should be included in the EurOtop formulae.

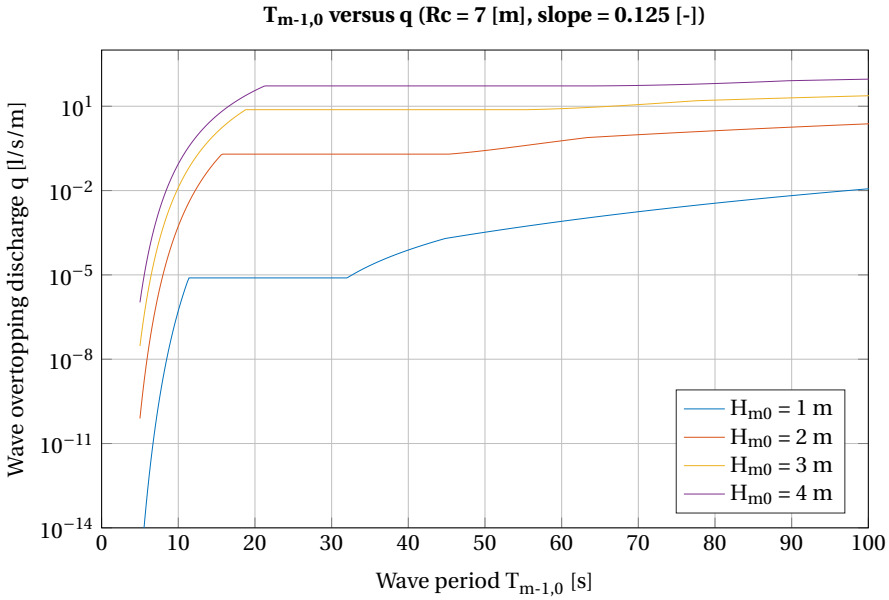

Figure 8.2: Influence of $T_{m-1,0}$ on the wave overtopping discharge, for four different wave heights at the dike toe, a dike slope of 0.125 and a freeboard of 7 m.

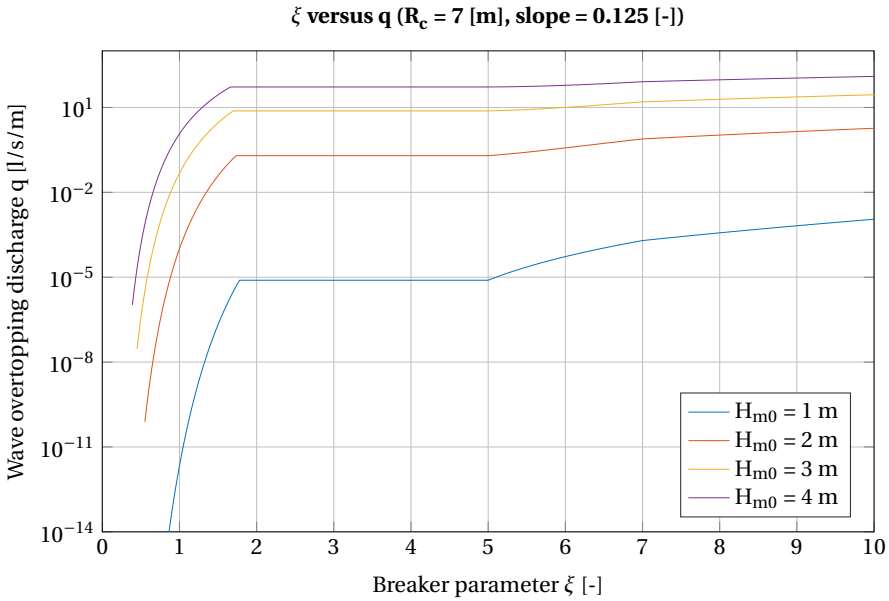

Figure 8.3: Influence of ξ on the wave overtopping discharge, for four different wave heights at the dike toe, a dike slope of 0.125 and a freeboard of 7 m.

8.6. UNCERTAINTY IN INFRAGRAVITY WAVE HEIGHTS

The infragravity waves that were found in this study were rather large, and showed to have a large influence on the probability of failure, especially with a 1D model. XBeach calculations can be performed with or without the insertion of infragravity waves (energy) at the offshore boundary. When infragravity waves are inserted at the offshore boundary, their height and period is related to the short wave groups. When no infragravity waves are inserted at the offshore boundary, all infragravity wave energy is generated within the model. For the calculations in this thesis, the option with insertion of offshore infragravity waves was chosen and also used in the validation with the experiments of Van Gent (1999). To further validate the calculated infragravity waves, a validation of XBeach could be performed by comparing with actual offshore and near-shore heights and periods of infragravity waves. The offshore infragravity wave data could be retrieved from a wave buoy, for the near-shore infragravity waves, the (old situation at the) Petten sea defence could be used, because large amounts of data are available for that location.

8.7. EXPERIMENTS OF VAN GENT (1999)

As mentioned before, it was unknown which frequencies Van Gent (1999) could filter in the physical flume experiments, and which frequencies not. Therefore, it is also unknown if the measured wave heights and wave periods in that study include reflected infragravity waves or not. For this thesis, it was estimated that all frequencies could be filtered and that thus only the incoming waves are used. Because the physical model experiments were conducted in a wave flume, the infragravity waves were possibly overestimated. This is caused by the exclusion of wave directional spreading in a wave flume.

The same issue holds for the very low frequency oscillations. As mentioned before, it was unknown if and which cut-off frequencies were used in the physical model experiments. Therefore, it is also unknown if the VLF oscillations were included in the measured wave heights and wave periods or not. Cut-off limits seem necessary, because the VLF oscillations cannot be filtered from the measured signal.

Even though the spectra from Van Gent (1999) range from 0.02-1.2 Hz, frequencies higher than 1.2 Hz were included in the calculation of the $T_{m-1,0}$ values. As a result, the $T_{m-1,0}$ values that Van Gent (1999) listed in the tables are lower than what would be expected from the spectra. Near the peak frequency the hydrostatic XBeach model differs from the measurements, because the hydrostatic model does not calculate the transformation of the high frequency wave period. The XBeach hydrostatic spectra also show less energy in the very high frequency range than the spectra from Van Gent (1999). Due to the combined effect of these two phenomena, the resulting $T_{m-1,0}$ periods for XBeach hydrostatic still agree quite well, even though the shape of the spectra is different. XBeach (hydrostatic) should be improved to be able to also predict the spectral shape in a correct way.

Finally, the cut-off limits themselves, as well as the frequency resolution with which the wave spectra are determined are points of attention. Changes in the resolution or cut-off limits showed to be heavily influencing the estimated wave heights and wave periods. More research on which cut-off limits need to be used (if cut-off limits need to be used) and with which frequency resolution the wave spectra should be calculated, could possibly improve the estimation of the wave heights and periods at the dike toe.

8.8. COMPARISON OF SHORT TERM AND LONG TERM MORPHOLOGICAL CHANGE

Figure 8.4 shows a comparison between the schematized bathymetry before and after the design storm, as well as the real JARKUS profiles at transect 1832 of the years 2008 (without the foreshore), 2009 (first year with the foreshore present), 2010 (after one year of morphological change) and 2014 (the foreshore was renourished in 2015).

As is visible, the profile after the storm shows a characteristic storm profile, where the sediment that is eroded is deposited somewhat lower in the profile. The JARKUS profile of 2010 shows that the foreshore slope has changed, but the horizontal part of the foreshore is still largely intact. In 2014, the foreshore has almost completely vanished. The profile after the storm is much more similar to the 2014 profile than to the 2010 profile. The horizontal part of the foreshore with a width of 75 m has almost completely vanished. Hence, the morphological changes during such a severe storm can be considerable. As was shown before, the foreshore leads to more intense wave breaking, but this also increases the low frequency energy, thus the $T_{m-1,0}$ wave period. With part of the foreshore eroded, the wave breaking becomes less and the wave period also becomes smaller. As explained before, the combined effect of these phenomena leads to some difference in wave overtopping discharge between the simulations where morphological change is excluded

or included, but because these phenomena have opposite influences, the difference in wave overtopping is not that extreme.

It is also visible that the 2008 profile, without the foreshore, is still largely different from the profile after the storm or the 2014 profile. There is still much more sediment present in the profiles after the storm and from 2014. Therefore it is more likely that the difference in failure probability between the 2009 and 2014 profiles is closer to a factor 1-4, like the difference in failure probability without and with morphological changes, than to a factor 30 or 10^3, which were the factors of difference that were found between the situations with and without foreshore.

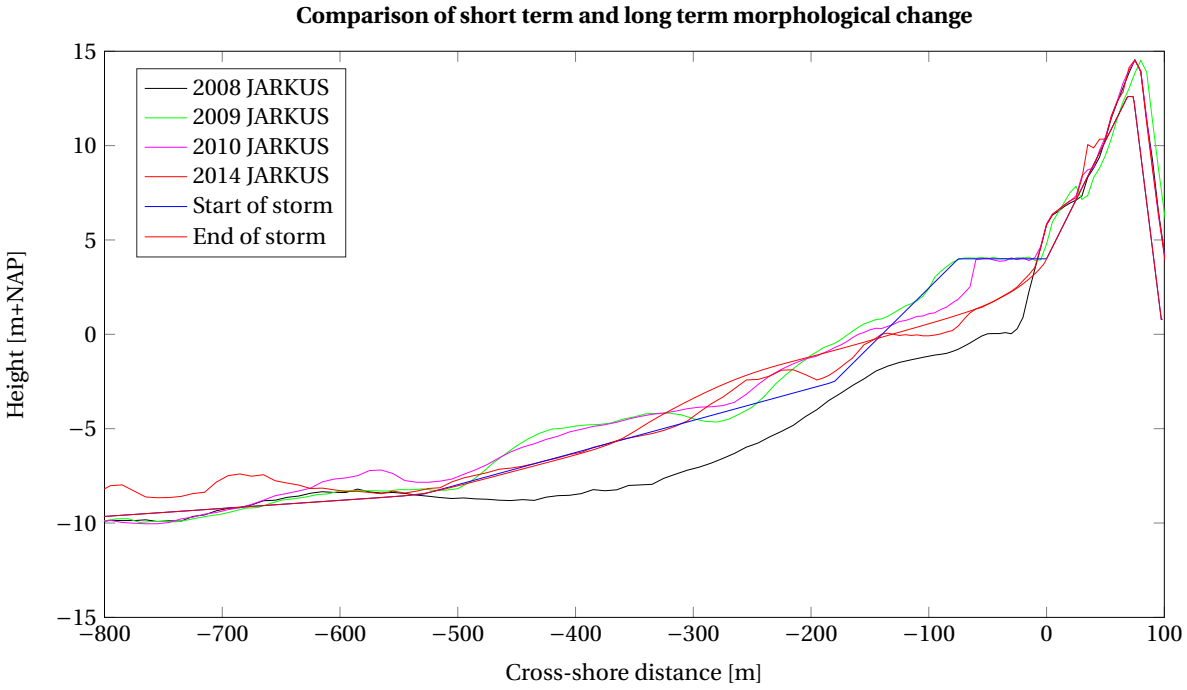

Figure 8.4: Comparison of short term and long term morphological change. Schematized Westkapelle sea defence bathymetry before and after the design storm, as well as the JARKUS transect 1832 profiles of 2008, 2009, 2010 and 2014.

8.9. PROBABILITIES & STATISTICS

Several variables were estimated as being uniform distributed, because no information on the probability distribution of these parameters was known. Furthermore, the standard deviations of some parameters were estimated. Improving the knowledge on the probability distributions of these parameters can improve the results of the framework at the current case study location. If, for another location, information is available on the probability distributions of all the parameters, this is not a problem.

For this thesis, omni-directional statistics were used. Using directional statistics (statistics defined per wind directional bin) can result in an improvement of the calculated failure probability, as well as give more insight in the correlations between parameters (e.g. water level and wave height). Using the omni-directional statistics is somewhat less exact. However, the currently available directional statistics generally include the joint probability distribution of wind speed and water level or wind speed and wave height. Because the wind speed is not used in XBeach calculations, it has no influence. To be able to use a hydraulic load model with combined wind and water level statistics, a deterministic step could be included to change this forcing into a forcing fit for XBeach (with water level and waves).

In this thesis, the correlation between the mean values of water level, wave height and wave period was considered according to the statistics in the stations ('steunpunten') from the HR 2006 for dunes (e.g. Deltares (2004)), where this correlation is 1. Spread around these mean values is introduced by the standard deviations of the parameters. The other stochastic parameters were considered as independent (or with correlation 0). Determining and including the correlations between the different parameters in more detail can possibly improve the determined value of the failure probability and can lead to shifts in the influence coefficients.

As mentioned before, determining the design point and influence coefficients in ADIS is not straightforward at all. One of the methods described in Deltares (2013) (q.v.) was implemented for this thesis, but the results were not promising enough yet. The main problem is the calculation of the influence coefficients from the design point, which cannot be done with an analytical formulation, as can be used with a simpler LSF or FORM. Inclusion of the correlations between the parameters necessitates a Rosenblatt or other transformation, to transform the dependent variables into independent variables. This transformation was not yet included in this study. Inclusion of this transformation will possibly yield better results when using this method.

However, other methods were applied as well, such as using the start-up method calculations or comparing the calculations with different amounts of parameters. These methods may give less definite answers than the influence coefficients, but still can give an indication of the influence of the different parameters on the failure probability. However, it has to be noted that when the start-up method calculations are used, the influence of each parameter relative to its mean value is determined, instead of the influence relative to the design point. This can lead to different sensitivities and influences. Indeed, counter-intuitive behaviour of the storm duration, sediment diameter and wave asymmetry calibration factor was found, which could be an artefact of the mean value approximation, but this needs to be further investigated.

To create the figures 7.4-7.9 in the previous chapter, calculations for which $Z \approx 0$ were sought and the calculation with the smallest distance to the origin in standard normal space (U-space) was chosen, which is not necessarily the same as the design point, which needs to lie in the failure space ($Z < 0$). This showed less counter-intuitive results than the design point calculations. Preferably, the design point should have been used, but because the calculation of the design point showed to cause some problems, this solution was chosen. Another (intermediate) option would be to search for $Z \approx 0$ points and, when available, choose a point for which $Z < 0$. In an ideal case with a large amount of points available, this point would be the same as the design point.

8.10. LOCATION OF DIKE TOE

In this study, the location of the dike toe was kept at a certain location, regardless of the amount of sedimentation or erosion occurring. Erosion at the initial location can somewhat shift the actual location of the dike toe. Keeping the location of the dike toe constant during the storm instead of updating the location of the toe can lead to differences in water depth, wave height and wave period, and thus wave overtopping discharge. Implementing an 'online' update of the dike toe location could possibly improve the results of the framework with a certain margin.

8.11. SCHEMATIZATION OF THE TIDE

For this thesis, the tide was schematized as an M2-tide, with an amplitude equal to the in reality occurring spring tidal level. Improvements could be made by including other tidal constituents, as well as including the spring-neap cycle. The storm would then occur at a random phase of the tide and spring-neap cycle.

9

CONCLUSIONS & RECOMMENDATIONS

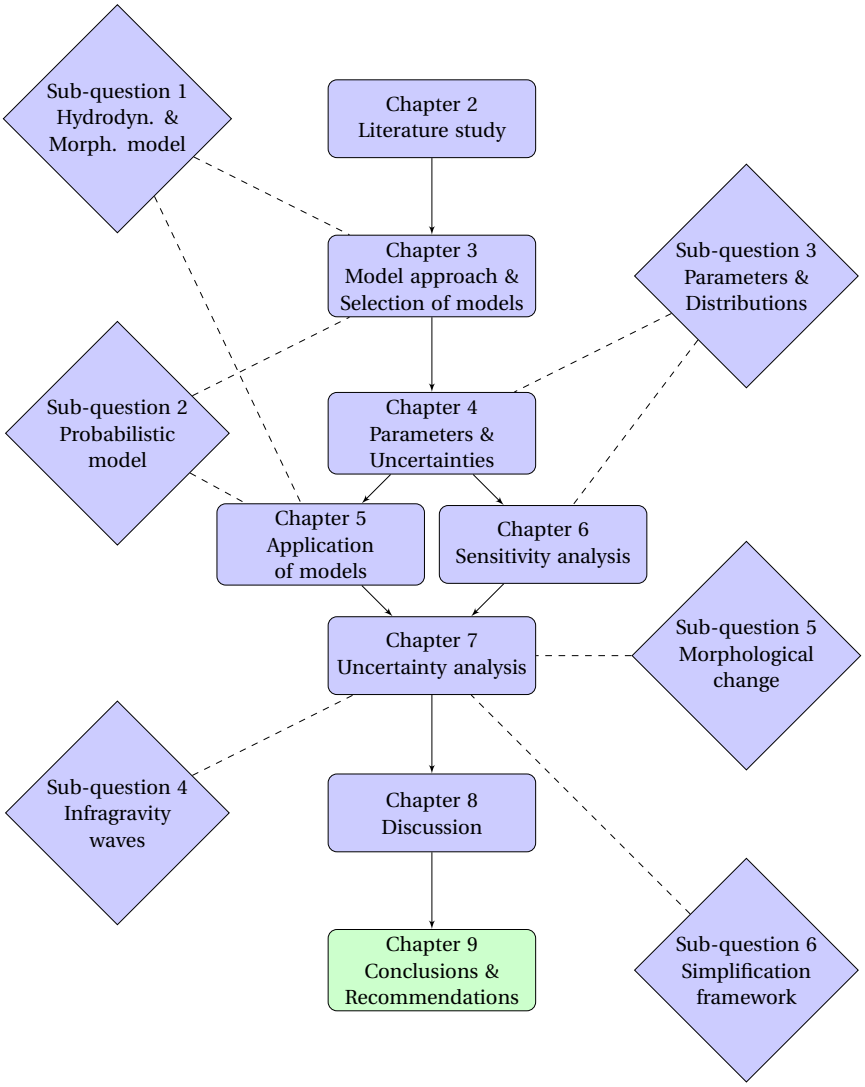

Figure 9.1: Outline of this report.

In this chapter, the conclusions resulting from the previous chapters are presented, as well as the recommendations and pointers for future research. Section 9.1 presents the conclusions and section 9.2 presents the recommendations and possible further research.

9.1. CONCLUSIONS

The conclusions are given below. Each research question is listed, after which the conclusions are presented.

9.1.1. MAIN QUESTION

The main research question was: How can infragravity waves and morphological changes of a sandy foreshore be included in the calculation of the probability of dike failure due to wave overtopping?

Because a single model that includes all this does not exist, a model framework or 'model train' was developed, in which different models are combined. The modelling framework best fit to solve the questions in this thesis has been determined as a combination of XBeach hydrostatic, EurOtop and ADIS.

First, ADIS determines a random direction and samples. Using the samples, XBeach calculates the wave transformation and morphological changes, from which several parameters at the dike toe result. With MATLAB, the wave spectrum at the toe of the dike is determined, for each hour of the storm. The wave spectra then serve as input for the EurOtop formulae, which calculate the wave overtopping discharges, again for each hour of the storm. The maximum wave overtopping discharge during the storm is taken and entered into the LSF. ADIS calculates the Z-value. When a converged probability of failure is found, the calculations are stopped. Otherwise, the process is repeated with new samples and/or a new random direction. Using this framework, the infragravity waves and morphological changes of the foreshore are included in the determination of the dike failure probability due to wave overtopping.

Hence, this is largely different from the current Dutch safety assessments, which, when a shallow foreshore is present, use the $h/2$-model or the 'foreshore module' (ENDEC). These models do not include infragravity waves or morphological changes. The $h/2$-model does also not include the wave set-up. Both these models do not calculate the change in wave period.

9.1.2. SUB-QUESTION 1: HYDRODYNAMIC AND MORPHOLOGICAL MODEL

The first sub-question was: What method is appropriate to calculate the morphological changes of the foreshore, the infragravity waves and wave overtopping during a storm?

XBeach hydrostatic was chosen to model the hydrodynamics and morphological changes of the foreshore. The hydrostatic version was chosen for its limited calculation durations, and inclusion of the calculation of infragravity waves and morphological changes. Using for example the $h/2$-model could lead to underestimations, because the wave set-up and infragravity waves are not included in these models. Furthermore, the $h/2$-model does not calculate the wave period transformation. Both 1D and 2D XBeach models were used. The 2D-models give more realistic results, because they include the wave directional spreading, which results in a more realistic representation of the infragravity wave heights. XBeach 1D overestimates the infragravity waves by excluding the wave directional spreading, but was also used for its limited calculation duration.

The EurOtop formulae were chosen to model the wave overtopping discharge, because they are the most commonly used formulae and form a set of equations that can be used for all types of wave breaking conditions and slopes. Furthermore, the EurOtop formulae are the only formulae that include the infragravity waves in any way, by using the $T_{m-1,0}$ wave period. Also, the EurOtop formulae are capable of calculating small and large discharges, and the calculation duration is negligible. Numerical models such as XBeach non-hydrostatic and SWASH were also considered, but the calculation duration of these models was too large. Furthermore, these models are able to predict large wave overtopping discharges, but have difficulties predicting small discharges, on which the focus of this thesis lies.

9.1.3. SUB-QUESTION 2: PROBABILISTIC METHOD

The second sub-question was: With what kind of probabilistic framework can the probability of dike failure due to wave overtopping, influenced by a sandy, erodible foreshore be calculated?

ADIS was chosen as the probabilistic method for this thesis, because ADIS can be used for small probabilities of failure and medium amounts of random variables. ADIS was the method with the least amount of simulations necessary to calculate the probability of failure. The method was used before in a probabilistic dune safety assessment in combination with XBeach (Den Bieman et al., 2014). ADIS, a level III method, can cope with large amounts of stochastic variables, non-normal distributed variables, non-linear reliability functions, dependent stochastic variables and multiple reliability functions, all of which but the last occur in the case considered in this thesis.

When insight in the importance of each stochastic variable is necessary, FORM could also be used instead of ADIS, however FORM can have difficulties with the complex LSF. When the method to determine the

design point and influence coefficients in ADIS is further improved, ADIS can also provide clear insight in the importance of each parameter

9.1.4. SUB-QUESTION 3: CHOICE OF PARAMETERS & PARAMETERS WITH LARGEST INFLUENCE ON OVERTOPPING

The third sub-question was: With which probability distribution can the important parameters be described, and which parameters have the largest influence on morphological change, wave height and wave overtopping?

17 stochastic variables were chosen according to expert judgement and categorized according to Van Gelder (2000). The distribution type and parameters of the distributions were determined for each of the parameters. The parameters with the largest influence on the wave overtopping discharge were determined by a sensitivity analysis. This resulted in five sets of parameters, ranked from largest influence to smallest influence:

- Set 1, Offshore conditions: 3 variables, zs, H_s, T_p.
- Set 2, Model and wave parameters: 7 variables, $C1$, $C2$, $C3$, $C4$, $gamma$, n, s.
- Set 3, Storm parameters: 2 variables, $tstop$, loc_peak.
- Set 4, Morphological parameters: 3 variables, D_{50}, $FacAs$, $FacSk$.
- Set 5, Dike parameters: 2 variables, $alpha$, $crest$.

9.1.5. SUBQUESTION 4: INFLUENCE OF INFRAGRAVITY WAVES

The fourth sub-question was: What is the influence of infragravity waves on the probability of dike failure due to wave overtopping?

The results of calculations including and excluding infragravity waves were compared to determine the influence of the infragravity waves on the failure probability. Including infragravity waves (and wave set-up) leads to much larger failure probabilities (factor 50 between the $h/2$-model and XBeach 2D and a factor 10^4 between ENDEC and XBeach 2D). The failure probabilities calculated with XBeach 1D were a factor 10-10^2 larger than the ones calculated with XBeach 2D, due to the overestimation of the infragravity waves in XBeach 1D by excluding the wave directional spreading. Hence, the influence of the infragravity waves (and wave set-up) is large. For the dike-foreshore system considered in this thesis, e.g. ENDEC or the $h/2$-model give lower estimations of the failure probability, because they exclude the infragravity waves.

For the $h/2$-model, much larger water levels are necessary to reach the same amount of wave overtopping discharge, because the model does not calculate the change in wave period. The wave periods at the dike toe in XBeach are much larger than in the $h/2$-model. Hence, the offshore conditions need to be much more extreme in the $h/2$-model to reach the same amount of wave overtopping. This explains the difference in the calculated probabilities of failure of the $h/2$-model and XBeach.

9.1.6. SUB-QUESTION 5: INFLUENCE OF MORPHOLOGICAL CHANGES OF THE FORESHORE

The fifth sub-question was: How does morphological change during severe storms influence the probability of dike failure due to wave overtopping?

Results of several calculations with and without the calculation of morphological changes, and with and without the morphological stochastic parameters were compared to determine the influence of the morphological changes of the foreshore on the dike failure probability. The inclusion of the morphological changes leads to a somewhat larger failure probability (factor 4). Hence, the influence of the morphological changes of the foreshore on the probability of dike failure is not that large in this system, when compared to the influence of the infragravity waves. The influence is however still somewhat too large to be excluded.

Due to the erosion of the foreshore, the wave dissipation becomes less, which gives larger wave heights at the toe of the dike. However, this also reduces the transfer from high frequency to low frequency energy, which gives smaller wave periods at the toe. In this case, these effects almost cancelled one another out, which lead to the small difference in probability of failure, even though the difference in the bathymetry was quite large, due to erosion of the foreshore.

9.1.7. SUB-QUESTION 6: PARAMETERS THAT DOMINATE THE FAILURE PROBABILITY

The sixth sub-question was: Which parameters dominate the failure probability and overtopping process, i.e. which parameters need to be taken into account in the probabilistic calculations?

The stochastic parameter sets were further used in an uncertainty analysis, with the exception of set 5, the dike parameters, because of the small influence (of their uncertainty). Amongst others, the influence of the parameters on the failure probability was determined by considering the start-up method calculations. The offshore conditions had the largest influence on the failure probability. The breaker index had a large influence as well. The wave directional spreading had only a very small influence (in a 1D calculation, more influence in a 2D calculation), as well as the phase of the tide.

For the dike-foreshore system considered in this thesis, the infragravity waves should certainly not be excluded, because of their large influence on the failure probability. The morphological changes had less influence, but still too much influence to be excluded. Furthermore, the stochastic variables that should certainly not be excluded are the offshore conditions and the breaker parameter. Parameters that possibly can be excluded were the location of the tidal peak and the wave directional spreading (in a 1D model).

A reduction in calculation times could be achieved by using a morphological acceleration factor, which showed to have almost no influence on the probability of failure. However, this does not result in a reduction in calculation time when the morphological changes are not calculated. Other methods to reduce the calculation duration could be stopping the calculation after the maximum wave overtopping discharge has been reached, or implementing an algorithm into ADIS that can evaluate multiple random directions at a time.

9.2. RECOMMENDATIONS & FURTHER RESEARCH

Recommendations and pointers for further research will be given in this section. The recommendations and options for further research can be derived from the conclusions and the discussion as stated in the previous chapter.

9.2.1. CALCULATION DURATION

The main issue of the in this thesis determined probabilistic calculation framework is the calculation duration, as mentioned in the previous chapter. The previous chapter also stated remedies for this problem: using a morphological acceleration factor, stopping the XBeach calculation when the maximum wave overtopping discharge during a storm has been reached, and/or modifying ADIS such that multiple random directions are examined at the same time. Another remedy that was used in this study, was applying a maximum storm duration of 200 hours, Assessing the validity of this assumption could be done by analysing real storm duration data, or checking if the calculations of the framework converge to long storm durations (which they did not do for the case considered here).

9.2.2. WAVE OVERTOPPING MODEL

The combination of a (very) shallow foreshore and dike slope of 1:8 make that the case considered here is (largely) outside the previously studied area. As mentioned before, it is possible, that when the wave period becomes very large, the wave overtopping is not dependent anymore on the dike slope, but on the wave parameters only. It is therefore questionable if the EurOtop formulae calculate the right amount of wave overtopping for these types of situations, because in the formulae, the wave overtopping is dependent on the dike slope. This could possibly lead to a lower estimation of the wave overtopping when using the EurOtop formulae in these kinds of situations. Further research is necessary to determine if this is actually the case.

Furthermore, the EurOtop formulae use the $T_{m-1,0}$ wave period. As described before, this wave period is very sensitive to the low (infragravity wave) frequencies. It is currently unknown if using this wave period leads to overestimation of the wave overtopping discharge. More research is required to determine the influence of the infragravity waves on wave overtopping and to be able to determine if the $T_{m-1,0}$ wave period is a good predictor or not. Also, the EurOtop formulae were not derived for the in this study occurring wave spectra, with large amounts of low frequency energy.

Furthermore, the EurOtop equations currently use the still water level, the SWL. Large infragravity waves can give large wave set-up values, which give larger wave overtopping discharges. Further research should also include the influence of the wave set-up on the wave overtopping.

All these problems should preferably be studied by doing field experiments. Physical model tests could be done as well. These physical model tests should preferably be done in a wave basin instead of a wave flume, because of the overestimation of the infragravity wave height in a wave flume by ignoring the wave directional spreading.

9.2.3. REFLECTED, INFRAGRAVITY & VLF WAVES

The infragravity waves that were found in this study were rather large, and showed to have a large influence on the probability of failure, especially with a 1D model. To further validate the calculated infragravity waves, a validation of XBeach could be performed by comparing with actual offshore and near-shore heights and periods of infragravity waves. The offshore infragravity wave data could be determined from a wave buoy, for the near-shore infragravity waves, the (old situation at the) Petten sea defence could be used, because large amounts of data are available for that location.

Filtering of reflected waves and filtering of infragravity waves and VLF oscillations in physical model test are important points of attention. In reality, reflected waves, infragravity waves and VLF oscillations do occur. Thus, it would be best to include reflected waves, infragravity waves and VLF oscillations in the models as well. Hence, possibly no cut-off frequencies for the wave spectra should be used. Clear guidelines on which frequency resolution and, if necessary, cut-off frequencies to use when determining wave spectra could improve results as well.

9.2.4. PROBABILITY DISTRIBUTIONS OF THE PARAMETERS

The distribution type and/or parameters of the distribution of several parameters can be improved by doing a data analysis on these parameters. Data of these parameters should be gathered, after which the data analysis should be performed. Several methods are available to determine the probability distribution type of a parameter as well as the parameters of the distribution, see e.g. Vrijling and Van Gelder (2002). Determining the correlations between parameters could be done by assembling data on these parameters at the desired location and determining e.g. the joint probability distribution of these parameters.

Developing directional statistics only including the water level or wave height, or finding an implementation for the directional statistics including wind speed and water level or wind speed and wave height is a topic for further research. Using directional instead of omni-directional statistics could lead to an improvement of the calculation framework and more insight in the correlations between the parameters. A method could be sought, with which the current statistics, based on the joint probability between wind speed and water level, wind speed and wave height or wind speed and wave period could be applied in the for this thesis derived framework.

9.2.5. INFLUENCE OF STOCHASTIC VARIABLES ON FAILURE PROBABILITY

An initial implementation of the calculation of the design point and influence coefficients with ADIS was made for this thesis, but did not show promising results yet. Improving this implementation gives more insight in the influence of certain parameters, with which possibly simplifications of the model framework could be made. This could in turn lead to a reduction of the calculation times. The main problem was the calculation of the influence coefficients from the design point. This cannot be done with an analytical formulation, because e.g. of the non-linear reliability function and dependent stochastic variables. Finding and especially implementing a good way to calculate the influence coefficients from the design point is necessary. Furthermore, improvements could be made to the nearest to the mean method, and a Rosenblatt transformation or other type of transformation from dependent to independent variables could be implemented.

Due to the unrealistic results of the determination of the design point, the start-up method calculations were also used. In this way, the influence of each parameter compared to its mean value is determined, not the influence relative to the design point. This method led to better results, but still some counter-intuitive results were produced, possibly caused by the mean value approach. The causes of these results should be investigated further.

Also, calculations for which $Z \approx 0$ were sought and the calculation with the smallest distance to the origin in standard normal space (U-space) was chosen. This is not necessarily the same as the design point, but showed less counter-intuitive results than the design point calculations. Preferably, the design point should have been used, but because the calculation of the design point showed to cause some problems, this solution was chosen. Another (intermediate) option would be to search for $Z \approx 0$ points and, when available, choose a point for which $Z < 0$. In an ideal case with a large amount of points available, this point would be the same as the design point.

ADIS also gives the ARS fit as output (second order polynomial with cross-terms). Using the derivatives of this function could help to determine the influence coefficients, but this was not yet implemented yet for this thesis.

9.2.6. DIKE TOE LOCATION

The location of the dike toe was kept at the initial location (location at the start of the storm) in this thesis, regardless of the change of the location of the toe during the storm. Implementing a changing location of the dike toe could be done by using multiple XBeach output points close to one another, and determining after the XBeach calculation which point was closest to the dike toe at which moment. However, using more output points leads to a longer calculation duration, due to the writing of more output data. Another option to implement a changing dike toe location would be to e.g. let XBeach determine the intersection of the hard structure (dike) and the erodible sand. This would then need to be implemented in XBeach, which is more difficult than the first option, but could give better results when considering the calculation duration. However, the EurOtop formulae were based on physical model tests, in concrete flumes and basins. If using a changing dike toe would thus give more realistic wave overtopping results is questionable.

9.2.7. SCHEMATIZATION OF THE TIDE

Including more tidal constituents in the framework, besides the M2, as well as including the spring-neap tidal cycle results in a better approximation of reality. This will probably give a better approximation of the failure probability.

BIBLIOGRAPHY

Battjes, J. A. (1971). Run-up distributions of waves breaking on slopes. *Journal of the waterways, harbors and coastal engineering division*, 97(1):91–114.

Battjes, J. A. (1974). Surf similarity. *Coastal Engineering Proceedings*, 1(14).

Battjes, J. A., Bakkenes, H. J., Janssen, T. T., and Van Dongeren, A. R. (2004). Shoaling of subharmonic gravity waves. *Journal of Geophysical Research: Oceans (1978–2012)*, 109(C2).

Battjes, J. a. and Janssen, J. P. F. M. (1978). Energy loss and set-up due to breaking of random waves. *Proceedings of the 16th international conference on coastal engineering*, 1(1):569–587.

Battjes, J. a. and Stive, M. J. F. (1985). Calibration and verification of a dissipation model for random breaking waves. *Coastal Engineering*, pages 649–660.

Bertotti, L. and Cavaleri, L. (1994). Accuracy of wind and wave evaluation in coastal regions. *Coastal Engineering Proceedings*, 1(24).

Bijker, E. W. (1967). Some considerations about scales for coastal models with movable bed.

Booij, N., Ris, R. C., and Holthuijsen, L. H. (1999). A third-generation wave model for coastal regions: 1. Model description and validation. *Journal of Geophysical Research*, 104:7649.

Bosboom, J. and Stive, M. J. F. (2012). *Coastal Dynamics I: Lectures Notes CIE4305*. VSSD.

Bowen, A. J. (1980). Simple models of nearshore sedimentation; beach profiles and longshore bars. *The Coastline of Canada, Geological survey Canada*, 80-10:1–11.

Bowen, A. J., Inman, D. L., and Simmons, V. P. (1968). Wave set-down and set-up. *Journal of Geophysical Research*, 73(8):2569–2577.

Brandenburg, P. (2010). Scale dependency of dune erosion models.

Bruun, P. (1954). *Coast erosion and the development of beach profiles*. Beach Erosion Board Corps of Engineers.

Buckley, M. and Lowe, R. (2013). Evalution of nearshore wave models in steep reef environments. *Coastal Dynamics*, pages 249–260.

Cavaleri, L. and Rizzoli, P. M. (1981). Wind wave prediction in shallow water: Theory and applications. *Journal of Geophysical Research: Oceans (1978–2012)*, 86(C11):10961–10973.

CIRIA (2007). *The Rock Manual: The use of rock in hydraulic engineering*, volume 683. Ciria.

Collins, J. I. (1972). Prediction of shallow water spectra. *Journal of Geophysical Research*, 77(15):2693–2707.

de Haan, L. and Resnick, S. I. (1977). Limit theory for multivariate sample extremes. *Zeitschrift für Wahrscheinlichkeitstheorie und verwandte Gebiete*, 40(4):317–337.

Dean, R. G. (1977). *Equilibrium beach profiles: US Atlantic and Gulf coasts*. Department of Civil Engineering and College of Marine Studies, University of Delaware.

Dean, R. G. (1987). Additional sediment input to the nearshore region. *Shore and beach*, 55(3-4):76–81.

Deltares (2004). Golfstatistiek op relatief diep water 1979-2002. Technical report.

Deltares (2007). Dune erosion-product 3: probabilistic dune erosion prediction method. Technical report.

Deltares (2013). Hydra Ring Scientific Documentation.

Deltares (2015a). XBeach 1D - Probabilistic model: ADIS, settings, Model uncertainty and Graphical User Interface. page 65.

Deltares (2015b). Xbeach Manual. Technical report, Deltares, Delft.

Den Bieman, J. P., Stuparu, D. E., Hoonhout, B. M., Diermanse, F. L. M., Boers, M., and Van Geer, P. F. C. (2014). Fully probabilistic dune safety assessment using an advanced probabilstic method. *Coastal Engineering*, pages 1–10.

Den Heijer, C. K., Baart, F., and van Koningsveld, M. (2012). Assessment of dune failure along the Dutch coast using a fully probabilistic approach. *Geomorphology*, 143-144:95–103.

Diermanse, F. L. M., Klis, H., Geerse, C. P. M., van Noortwijk, J. M., Gerritsen, H., and Groeneweg, J. (2007). SBW-Statistiek basisvariabelen. Technical report.

Dingemans, M. W. (1998). A review of the physical formulations in SWAN. Technical report.

Ditlevsen, O. and Madsen, H. O. (1996). *Structural reliability methods*, volume 178. Wiley New York.

DWW (2002). Inventarisatie effecten wijzigingen golfrandvoorwaarden. Technical report, Dienst Weg- en Waterbouwkunde.

EcoShape (2011). Perspectief Natuurlijke keringen: Een eerste verkenning ten behoeve van het Deltaprogramma. Technical report.

Eldeberky, Y. and Battjes, J. A. (1995). Parameterization of triad interactions in wave energy models.

EurOtop (2007). EurOtop. Wave Overtopping of Sea Defences and Related Structures: Assessment Manual. Technical Report August.

Galappatti, G. and Vreugdenhil, C. B. (1985). A depth-integrated model for suspended sediment transport. *Journal of Hydraulic Research*, 23(4):359–377.

Garrett, C. J. R. (1967). Discussion: the adiabatic invariant for wave propagation in a nonuniform moving medium. In *Proceedings of the Royal Society of London A: Mathematical, Physical and Engineering Sciences*, volume 299, pages 26–27. The Royal Society.

Genz, A. C. and Malik, A. A. (1980). Remarks on algorithm 006: An adaptive algorithm for numerical integration over an N-dimensional rectangular region. *Journal of Computational and Applied Mathematics*, 6(4):295–302.

Grooteman, F. (2011). An adaptive directional importance sampling method for structural reliability. *Probabilistic Engineering Mechanics*, 26(2):134–141.

Guza, R. T., Thornton, E. B., and Holman, R. A. (1984). Swash on steep and shallow beaches. *Coastal Engineering Proceedings*, 1(19).

Harris, F. J. (1978). On the use of windows for harmonic analysis with the discrete Fourier transform. *Proceedings of the IEEE*, 66(1):51–83.

Hasselmann, K. (1962). On the non-linear energy transfer in a gravity-wave spectrum. *J. Fluid Mech*, 12(481-500):15.

Hasselmann, K. (1974). On the spectral dissipation of ocean waves due to white capping. *Boundary-Layer Meteorology*, 6(1-2):107–127.

Hasselmann, K., Barnett, T. P., Bouws, E., Carlson, H., Cartwright, D. E., Enke, K., Ewing, J. A., Gienapp, H., Hasselmann, D. E., and Kruseman, P. (1973). Measurements of wind-wave growth and swell decay during the Joint North Sea Wave Project (JONSWAP). Technical report.

Hasselmann, S., Hasselmann, K., Allender, J. H., and Barnett, T. P. (1985). Computations and parameterizations of the nonlinear energy transfer in a gravity-wave specturm. Part II: Parameterizations of the nonlinear energy transfer for application in wave models. *Journal of Physical Oceanography*, 15(11):1378–1391.

HKV (2005). Deep water boundary conditions (ELD, EUR, YM6, SCW and SON).(Diepwater randvoorwaarden (ELD, EUR, YM6, SCW en SON)). Technical report.

HKV (2014). Effect of nourishment on failure probability of Westkapelle sea defence. Technical Report August.

Holterman, S. R. (1998). Golfoploop op dijken met ondiep voorland. Technical report, TU Delft, Delft.

Holthuijsen, L. H. (2007). *Waves in oceanic and coastal waters*. Cambridge University Press.

Hughes, S. A. (2004). Estimation of wave run-up on smooth, impermeable slopes using the wave momentum flux parameter. *Coastal Engineering*, 51(11):1085–1104.

Hunt, I. A. (1959). Design of seawalls and breakwaters. *Journal of Waterways and Harbours Division*, 85:123–152.

Janssen, P. A. E. M., Komen, G. J., and De Voogt, W. J. P. (1984). An operational coupled hybrid wave prediction model. *Journal of Geophysical Research: Oceans (1978–2012)*, 89(C3):3635–3654.

Jonkman, S. N. (2013). BE SAFE: Bio-Engineering for safety using vegetated foreshores.

Kaminsky, G. M. and Kraus, N. C. (1993). Evaluation of depth-limited wave breaking criteria. In *Ocean Wave Measurement and Analysis (1993)*, pages 180–193. ASCE.

Kolmogorov, A. N. (1933). *Sulla determinazione empirica di una legge di distribuzione*. na.

Lamb, H. (1932). *Hydrodynamics 6th ed.*.

Longuet-Higgins, M. S. and Stewart, R. (1960). Changes in the form of short gravity waves on long waves and tidal currents. *Journal of Fluid Mechanics*, 8(04):565–583.

Longuet-Higgins, M. S. and Stewart, R. W. (1962). Radiation stress and mass transport in gravity waves, with application to 'surf beats'. *Journal of Fluid Mechanics*, 13(04):481–504.

Longuet-Higgins, M. S. and Stewart, R. W. (1964). Radiation stresses in water waves; a physical discussion, with applications. In *Deep Sea Research and Oceanographic Abstracts*, volume 11, pages 529–562. Elsevier.

Mai, S. and Lieberman, N. V. (2001). Wave Load and Wave Propagation over Forelands. pages 1–9.

Mase, H. (1989). Random wave runup height on gentle slope. *Journal of Waterway, Port, Coastal, and Ocean Engineering*, 115(5):649–661.

Miche, A. (1944). Mouvements ondulatoires de la mer en profondeur croissante ou de croissante. Forme limite de la houle lors de son de ferlement. Application aux digues maritimes. Deuxieme partie. Mouvements ondulatoires periodiques en profondeur reguli. *Annales des Ponts et Chauss {é} es*.

Miles, J. W. (1957). On the generation of surface waves by shear flows. *Journal of Fluid Mechanics*, 3(02):185–204.

Munk, W. H. (1950). Origin and generation of waves. *Coastal Engineering Proceedings*, 1(1):1.

Phillips, O. M. (1957). On the generation of waves by turbulent wind. *Journal of fluid mechanics*, 2(05):417–445.

Plant, W. J. (1982). A relationship between wind stress and wave slope. *Journal of Geophysical Research: Oceans (1978–2012)*, 87(C3):1961–1967.

Putnam, J. A. and Johson, J. W. (1949). The dissipation of wave energy by bottom friction. *Eos, Transactions American Geophysical Union*, 30(1):67–74.

Reniers, A., Van Dongeren, A. R., Battjes, J. A., and Thornton, E. B. (2002). Linear modeling of infragravity waves during Delilah. *Journal of Geophysical Research: Oceans (1978–2012)*, 107(C10):1.

Reniers, A. J. H. M., Roelvink, J. A., and Thornton, E. B. (2004). Morphodynamic modeling of an embayed beach under wave group forcing. *Journal of Geophysical Research: Oceans (1978–2012)*, 109(C1).

Rijnsdorp, D. P., Smit, P. B., and Zijlema, M. (2014). Non-hydrostatic modelling of infragravity waves under laboratory conditions. *Coastal Engineering*, 85:30–42.

RIKZ (2006). De Veiligheid van de primaire waterkeringen in Nederland: Achtergrondrapport HR2006 voor de Zee en Estuaria. Technical report.

Ris, R. C., Holthuijsen, L. H., and Booij, N. (1999). A third-generation wave model for coastal regions: Verification. *Journal of Geophysical Research*, 104:7667.

Roeber, V. and Bricker, J. D. (2015). Destructive tsunami-like wave generated by surf beat over a coral reef during Typhoon Haiyan. *Nature Communications*, 6.

Roelvink, D., Reniers, A., van Dongeren, A., van Thiel de Vries, J., Lescinski, J., and McCall, R. (2010). XBeach model description and manual. Technical report.

Roelvink, D., Reniers, A., van Dongeren, A., van Thiel de Vries, J., McCall, R., and Lescinski, J. (2009). Modelling storm impacts on beaches, dunes and barrier islands. *Coastal Engineering*, 56(11-12):1133–1152.

Roelvink, J. A. (1993). Dissipation in random wave groups incident on a beach. *Coastal Engineering*, 19(1):127–150.

Rosenblatt, M. (1952). Remarks on a multivariate transformation. *The annals of mathematical statistics*, pages 470–472.

RWS/RIKZ (2000). Richtingsafhankelijke extreme waarden voor HW-standen, golfhoogte en golfperioden. Technical report.

Sheremet, A., Kaihatu, J. M., Su, S.-F., Smith, E. R., and Smith, J. M. (2011). Modeling of nonlinear wave propagation over fringing reefs. *Coastal Engineering*, 58(12):1125–1137.

Snyder, R. L., Dobson, F. W., Elliott, J. A., and Long, R. B. (1981). Array measurements of atmospheric pressure fluctuations above surface gravity waves. *Journal of Fluid mechanics*, 102:1–59.

Soulsby, R. (1997). *Dynamics of marine sands: a manual for practical applications*. Thomas Telford.

Steetzel, H. (1993). Cross-shore sediment transport during storm surges.

Stive, M. J. F. and Dingemans, M. W. (1984). Calibration and verification of a one-dimensional wave energy decay model. Technical report.

Stockdon, H. F., Holman, R. a., Howd, P. a., and Sallenger, A. H. (2006). Empirical parameterization of setup, swash, and runup. *Coastal Engineering*, 53:573–588.

Suzuki, T., Verwaest, T., Veale, W., Trouw, K., and Zijlema, M. (2012). a Numerical Study on the Effect of Beach Nourishment on Wave Overtopping in Shallow Foreshores. *Coastal Engineering Proceedings*, 1:waves.50.

TAW (1998). Grondslagen voor waterkeren. Technical report, Technische Adviescommissie voor de Waterkeringen, Rotterdam.

TNO (1999). Theoriehandleiding PC-Ring, Deel B: Statistische modellen. Technical report, TNO, Rijswijk.

Van de Graaff, J., Van Gent, M. R. A., Boers, M., Diermanse, F. L. M., Walstra, D. J., and Steetzel, H. J. (2007). Technisch rapport Duinafslag. Technical report.

Van der Meer, J. (2002). Technisch Rapport Golfoploop en Golfoverslag bij Dijken. pages 15–25.

Van der Meer, J. and Bruce, T. (2013). EurOtop revisited. Part 1 : sloping structures. *Proceedings of the ICE, Coasts, Marine Structures and Breakwaters*, 1.

Van der Meer, J. W. (1997). Golfoplooop en golfoverslag bij dijken. Technical report, Waterloopkundig laboratorium| WL, Delft.

Van der Most, H. (1979). Golfvervorming bij hoog voorland. Technical report, TU Delft, Delft.

Van Dooren, P. and de Ridder, L. (1976). An adaptive algorithm for numerical integration over an N-dimensional cube. *Journal of Computational and Applied Mathematics*, 2(3):207–217.

Van Gelder, P. H. A. J. M. (2000). *Statistical methods for the risk-based design of civil structures*. PhD thesis, Delft University of Technology.

Van Gent, M. and Giarrusso, C. (2005). Influence of foreshore mobility on wave boundary conditions. *Proc. Int. Conference on Ocean Waves . . .*, pages 1–10.

Van Gent, M. R. A. (1999). Physical model investigations on coastal structures with shallow foreshores: 2D model tests with single and double-peaked wave energy spectra. Technical report, WL| Delft Hydraulics, Delft.

Van Rijn, L. C., van Rijn, L. C., and van Rijn, L. C. (1993). *Principles of sediment transport in rivers, estuaries and coastal seas*, volume 2. Aqua publications Amsterdam.

Van Thiel de Vries, J. S. M. (2009). Dune erosion during storm surges.

Van Vledder, G., Groeneweg, J., and Jacobse, S. (2004). Reliability of SWAN at the Petten Sea Defence. *29th Coastal Engng. Conf.*, 1(June):907–919.

Vellinga, P. (1986). Beach and dune erosion during storm surges.

Verheij, H. J. (2006). IJsselmeer zoekt verdieping. Technical Report december, WL| Delft Hydraulics, Delft.

VNK2 (2015). Achtergrondrapport Dijkring 29 - Walcheren. Technical report, Veiligheid Nederland in Kaart 2, AnteaGroup.

Vrijling, J. K., Roos, A., Ale, B. J. M., Van der Brand, D., De Bruyn, L., Bueno de Mesquita, K. G., Van Gelder, P. H. A. J. M., Van Hengel, W., Janssen, J. P. F. M., and Vrouwenvelder, A. C. W. M. (2014). *Probability in Civil Engineering*.

Vrijling, J. K. and Van Gelder, P. H. A. J. M. (2002). Probabilistic Design in Hydraulic Engineering.

Vrouwenvelder, A. C. W. M. and Steenbergen, H. M. G. M. (2003). Theoriehandleiding PC-RING. Deel C: Rekentechnieken. Technical report.

Welch, P. D. (1967). The use of fast Fourier transform for the estimation of power spectra: A method based on time averaging over short, modified periodograms. *IEEE Transactions on audio and electroacoustics*, 15(2):70–73.

Zijlema, M., Stelling, G., and Smit, P. (2011). SWASH: An operational public domain code for simulating wave fields and rapidly varied flows in coastal waters. *Coastal Engineering*, 58(10):992–1012.

Zijlema, M. and Stelling, G. S. (2008). Efficient computation of surf zone waves using the nonlinear shallow water equations with non-hydrostatic pressure. *Coastal Engineering*, 55(10):780–790.

A

OVERVIEW OF GENERAL FLOW AND WAVE EQUATIONS

The equations that are commonly used to describe wave transformation processes are given below, viz. the wave action/energy balance (section A.1), the (non-hydrostatic) shallow water equations (section A.2) and the radiation stress tensor (section A.3).

A.1. ACTION BALANCE

All information about the sea surface is contained in the energy density. Wave models determine the evolution of energy density or action density in space and time. The wave action balance equation, including frequency shifting, is given by, e.g. (Garrett, 1967):

$$\frac{\partial A}{\partial t} + \frac{\partial c_x A}{\partial x} + \frac{\partial c_y A}{\partial y} + \frac{\partial c_\sigma A}{\partial \sigma} + \frac{\partial c_\theta A}{\partial \theta} = \frac{S_{tot}}{\sigma} \tag{A.1}$$

where $A = E/\sigma$ is the action density [Jm^{-2}], $E(\sigma,\theta;x,y,t)$ is the energy density [Jm^{-2}], σ is the relative radian frequency [-], c_x, c_y, c_σ and c_θ are the propagation speeds in spatial, spectral and directional space. S_{tot} can include generation and dissipation terms. Wave action is conserved in the presence of currents. If no ambient currents are present, the action balance equation can be simplified to an energy balance equation, using $A = E/\sigma$:

$$\frac{\partial E}{\partial t} + \frac{\partial c_x E}{\partial x} + \frac{\partial c_y E}{\partial y} + \frac{\partial c_\theta E}{\partial \theta} = S_{tot} \tag{A.2}$$

By integrating over all frequencies and directions in an irregular wave field, the following energy conservation equation is obtained:

$$\frac{\partial E}{\partial t} + \frac{\partial}{\partial x}\left(E c_g \cos\theta\right) + \frac{\partial}{\partial y}\left(E c_g \sin\theta\right) = S_{tot} \tag{A.3}$$

The energy balance describes the energy of an arbitrary travelling wave component. The wave action balance can be used to describe this component in the case of wave-current interactions.

A.2. SHALLOW WATER EQUATIONS

The shallow water equations described the flow below a pressure surface in a fluid. The three-dimensional shallow water equations are:

$$\frac{\mathrm{D}u}{\mathrm{D}t} = -\frac{1}{\rho}\frac{\partial p}{\partial x} \pm F_x \tag{A.4a}$$

$$\frac{\mathrm{D}v}{\mathrm{D}t} = -\frac{1}{\rho}\frac{\partial p}{\partial y} \pm F_y \tag{A.4b}$$

$$\frac{\mathrm{D}w}{\mathrm{D}t} = -\frac{1}{\rho}\frac{\partial p}{\partial z} - g \pm F_z \tag{A.4c}$$

$$\frac{\partial u}{\partial x}+\frac{\partial v}{\partial y}+\frac{\partial w}{\partial z}=0 \tag{A.4d}$$

where u, v and w are the velocities in x, y and z direction [ms^{-1}], ρ is the density of water [kgm^{-3}], g is the gravitational acceleration [ms^{-2}], p is the pressure [Nm^{-2}] and F indicates the forcing terms, e.g. the bed shear stresses or wave forces. These equations can be used to describe the flow in a fluid. The first three equations describe the conservation of momentum, the last equation describes the conservation of mass. In a model which uses the non-hydrostatic shallow water equations, the pressure p is split into two parts, a non-hydrostatic and hydrostatic part. A 2D model in which the long-shore currents are neglected uses the first, third and fourth equations. A 2D depth-averaged model uses the first, second and fourth equations.

A.3. RADIATION STRESSES

The radiation stress tensor described the additional forcing on a fluid due to the presence of waves, causing a change in horizontal momentum. The transport of wave-induced momentum is equivalent to a stress and is called radiation stress. The radiation stress tensor is defined as, e.g. (Longuet-Higgins and Stewart, 1960):

$$S_{xx}=\left(n-\frac{1}{2}+n\cos^2\theta\right)E \tag{A.5a}$$

$$S_{yy}=\left(n-\frac{1}{2}+n\sin^2\theta\right)E \tag{A.5b}$$

$$S_{xy}=n\cos\theta\sin\theta E \tag{A.5c}$$

$$S_{yx}=n\sin\theta\cos\theta E \tag{A.5d}$$

where S_{xx} and S_{yy} are normal stresses [Nm^{-1}] and S_{xy} and S_{yx} are shear stresses [Nm^{-1}]. θ is the wave direction [°] and n is the ratio group velocity over phase velocity [-]. The tensor can be used to describe the forcing due to the presence of waves, which changes the horizontal momentum. A varying radiation stress induces mean surface and mean flow variations, like wave-induced currents and wave set-up.

B

EMPIRICAL & NUMERICAL MODELS

This Appendix gives an overview of many of the available empirical and numerical models to describe wave transformation and morphological changes. First, the empirical models are described in section B.1. Next, the numerical models are given (section B.2).

B.1. EMPIRICAL MODELS

In this section, commonly used empirical models are described, first the equations that model wave transformation, then the equations that model morphological changes and sediment transport.

B.1.1. WAVE TRANSFORMATION

This section deals with near-shore hydrodynamic processes. When travelling from deep to intermediate to shallow water, wave height, length and direction change until they break and lose their energy. Bosboom and Stive (2012) and Holthuijsen (2007) give extensive overviews of these processes, this section is partly based on these two references. Several processes can be distinguished:

WIND INPUT

In general, one of two models for the generation of waves by the wind are used. E.g. Lamb (1932) states that when two substances with different speeds move over each other, they create instabilities. When the wind blows over the water, the first waves are very short and small, gradually getting longer and higher. On the other hand, e.g. Phillips (1957) and Miles (1957) suggest that waves are generated by resonance between wind-induced pressure waves and water waves. The general expression for the generation of waves by wind is written as:

$$S_{in}(\sigma,\theta) = A + BE(\sigma,\theta) \tag{B.1}$$

which consists of a linear and exponential growing part. An expression for the linear part is given in Cavaleri and Rizzoli (1981). An expression for the exponential part is given by e.g. Plant (1982) or Snyder et al. (1981).

SHOALING

The dispersion relation, derived from linear wave theory, is given by:

$$\omega = \sqrt{gk\tanh kh} \tag{B.2}$$

in which ω is the frequency [rad s^{-1}], k is the wave number [rad m^{-1}], g is the gravitational acceleration [=9.81 ms^{-2}] and h is the local water depth [m]. Considering a single long-crested harmonic propagating normally to an alongshore uniform sandy coast with parallel depth contours and using the dispersion relation, a decreasing water depth gives a decreasing wave speed and wave length. Using the energy balance, and using the fact that the dissipation outside the breaker zone is approximately zero, integration of the energy balance along a wave ray gives:

$$U = Ec_g = Enc = \text{constant} \tag{B.3}$$

where U is the energy flux per unit wave crest width [$Jm^{-1}s^{-1}$], n is the ratio wave group velocity to wave celerity [-]. Using the relation $E = 1/8\rho g H^2$, the wave heights at a deep water (n=1/2) and shallow water location can be related. This leads to:

$$\frac{H}{H_0} = \sqrt{\frac{1}{\tanh kh}\frac{1}{2n}} = K_{sh} \tag{B.4}$$

where K_{sh} is the shoaling factor [-]. It is 1 in deep water, decreases to 0.91 and then rises to infinity.

Other processes involved with shoaling are asymmetry and skewness. Asymmetry is defined as the pitched forward shape of a wave travelling in shallow water. It can be defined by considering the shallow water propagation speed $c = \sqrt{gh}$. The crest of a wave with amplitude a will propagate with a velocity $c = \sqrt{g(h+a)}$, the trough will propagate with $c = \sqrt{g(h-a)}$. Skewness is the gradual peaking of the wave crest and flattening of the trough.

REFRACTION

The rate of change of the wave direction θ along a wave ray can be written as:

$$\frac{\mathrm{d}\theta}{\mathrm{d}n} = -\frac{1}{c}\frac{\partial c}{\partial m} \tag{B.5}$$

This equation is valid along a wave ray and for a stationary situation, with a spatially variable depth and no currents. If one considers an obliquely incident wave instead of an normally incident wave, one can see that the sections of the crest in deeper parts travel faster than in the shallower parts, which leads to the crest turning to the depth contour. This effect is called refraction and can be described by Snell's law:

$$\frac{\sin\phi}{c_2} = \frac{\sin\phi}{c_1} = \text{constant} \tag{B.6}$$

with ϕ being the angle relative to the shore normal [°], c_1 and c_2 being the phase velocity [ms^{-1}]. Along a wave ray $\frac{\sin\phi}{c}$ is constant, but this is only valid for parallel depth contours. If it is assumed that no wave energy moves laterally along the wave crest, if the energy balance is again integrated and if one location is again assumed to be in deep water, the following can be derived:

$$\frac{H}{H_0} = \sqrt{\frac{1}{2n}\frac{c_0}{c}\frac{b_0}{b}} = K_{sh}K_r \tag{B.7}$$

In the case of parallel depth contours, K_r can be written as:

$$K_r = \sqrt{\frac{\cos\phi_0}{\cos\phi}} \tag{B.8}$$

Converging wave rays will lead to relatively high wave heights, diverging wave rays will lead to relatively low wave heights.

Currents can also change the direction of the waves: the wave turns to the area with lower propagation speed of the crest. The rate of change of the wave direction due to depth- and current-induced refraction is:

$$c_{\theta,ref,d+c} = -\frac{c_g}{c}\frac{\partial c}{\partial m} - \frac{\partial U_n}{\partial m} \tag{B.9}$$

U_n is the velocity of the current [ms^{-1}].

BOTTOM FRICTION

Bottom friction covers the processes in the thin wave boundary layer near the bed. The time-averaged energy dissipation rate per unit bottom surface area at the bottom can be written as:

$$\overline{D}_{bfr} = -\overline{\tau_b u_b} \tag{B.10}$$

where τ_b and u_b are the magnitudes of the time-varying shear stress [Nm^{-2}] and particle velocity at the bottom [ms^{-1}]. The particle velocity can be obtained from linear wave theory, the shear stress is mostly determined by one of two types of models, drag-law models and eddy-viscosity models. The drag-law models use a quadratic law to estimate the shear stress:

$$\tau_b = \rho c_f u_b^2 \tag{B.11}$$

where c_f is a dimensionless friction factor, related to the Chézy coefficient by $c_f = g/C^2$. The bottom friction coefficient c_f based on Manning's roughness coefficient n is:

$$c_f = \sqrt{\frac{n^2 g}{h^{1/12}}} \tag{B.12}$$

Filling in this coefficient gives the energy-dissipation rate, approximated as, e.g. Collins (1972):

$$\overline{D}_{bfr} = -\rho c_f u_{rms,b} |u_{rms,b}| \tag{B.13}$$

Where $u_{rms,b}$ is the root mean square orbital velocity at the bottom [ms^{-1}]. A commonly used model is the one of Bertotti and Cavaleri (1994):

$$D_{bfr}(\sigma,\theta) = -c_f \frac{\sigma^2}{g^2 \sinh^2(kd)} E(\sigma,\theta) \tag{B.14}$$

For eddy-viscosity models, the horizontal velocity u and the vertical velocity w are composed of a mean, a wave and a turbulent part, e.g. $u = U + \tilde{u} + u'$. The turbulent shear stress is then defined as:

$$\tau(z) = \rho \overline{u'w'} \tag{B.15}$$

WAVE SET-UP

The radiation stress tensor was defined in section A.3. An increase of momentum transport (i.e. increase in radiation stress) over a horizontal distance is equivalent to exerting an opposite force on the water body:

$$F_x = -\frac{\partial S_{xx}}{\partial x} - \frac{\partial S_{xy}}{\partial y} \text{ in the x-direction} \tag{B.16a}$$

$$F_y = -\frac{\partial S_{yy}}{\partial y} - \frac{\partial S_{yx}}{\partial x} \text{ in the y-direction} \tag{B.16b}$$

Considering a one-dimensional case of a harmonic wave at normal incidence, ignoring bottom friction and other horizontal forces, a balance can be derived between the radiation stress gradient and the pressure term due to the water level slope $\frac{d\bar{\eta}}{dx}$:

$$\frac{dS_{xx}}{dx} + \rho g \left(h + \bar{\eta}\right) \frac{d\overline{\eta}}{dx} = 0 \tag{B.17}$$

where ρ is the density of water [kgm^{-3}] and h is the water depth [m]. For a positive radiation stress gradient, the slope of the mean surface is negative, and for a negative radiation stress gradient, the slope is positive. Taking $\bar{\eta}$ in deep water and using the energy balance, the following equation for the set-down can be derived (Longuet-Higgins and Stewart, 1962):

$$\bar{\eta} = -\frac{1}{16}\frac{H_b^2}{h} \text{ set-down, in the shallow water approximation} \tag{B.18}$$

where H_b is the wave height at the point of breaking [m]. Assuming shallow water and assuming that the water depth decreases monotonically towards the beach, gives:

$$\frac{d\overline{\eta}}{dx} = -K\frac{dh}{dx} \tag{B.19}$$

with $K = \frac{\frac{3}{8}\gamma^2}{1+\frac{3}{8}\gamma^2}$. Integrating from the point of incipient breaking gives:

$$\overline{\eta} = \overline{\eta}_b + K(h_b - h) \tag{B.20}$$

where small b indicates at the point of breaking. γ is the breaker index, see the section on wave breaking for the definition. The maximum set-up relative to the mean waterline is then:

$$\overline{\eta}_{max} = \frac{5}{16}\gamma H_b \tag{B.21}$$

LONG WAVES

Considering bi-chromatic wave pairs, if one ignores the turbulent mixing, bottom friction and non-linear terms from the momentum and continuity equations, and also considers normally incident waves on an alongshore uniform beach and a horizontal bed, one ends up with:

$$\frac{\partial^2 \eta}{\partial t^2} - gd\frac{\partial^2 \eta}{\partial x^2} = \frac{1}{\rho}\frac{\partial^2 S_{xx}}{\partial x^2} \tag{B.22}$$

where η is the elevation relative to a certain level [m], d is the depth relative to a certain level [m] and ρ is the density [kgm^{-3}]. Combining this equation with the long wave elevation and expression for the radiation stress in terms of a mean and fluctuating part of the wave energy, an expression for the surface elevation is (Longuet-Higgins and Stewart, 1964):

$$\eta_{l,b}(x,t) = \frac{-\left(2n-\frac{1}{2}\right)\hat{\mathrm{E}}(x,t)}{\rho\left(gd-c_g^2\right)} \tag{B.23}$$

Summating this equation for a large number of wave components gives an estimation for the bound long wave for each bi-chromatic pair (Reniers et al., 2002). Using the dispersion relation, it can be shown that for shallow water and bound long waves, the amplitude of the fluctuating part of the wave energy $\hat{E}$ is proportional to $h^{-1/2}$ (Battjes et al., 2004). Using this gives for free long waves (Green's law):

$$\hat{\eta}_{l,f} \propto h^{-\frac{1}{4}} \tag{B.24}$$

The parameter β_b, which is analogous to the Iribarren number and indicates the shoaling of bound long waves is given by:

$$\beta_b = \frac{h_x}{\Delta\omega}\sqrt{\frac{g}{h_b}} \tag{B.25}$$

where h is the water depth [m]. For 'short' long waves this reduces to Longuet-Higgins and Stewart (1964) , for very long waves this reduces to Green's law (Battjes et al., 2004).

WAVE-WAVE INTERACTIONS

Wave-wave interactions consist of the transfer of energy amongst the waves by resonance. The exact expression for the quadruplet wave-wave interactions is (Hasselmann, 1962):

$$\begin{aligned} S_{nl} = {} & \iiint T_1(\vec{k}_1,\vec{k}_2,\vec{k}_1+\vec{k}_2-\vec{k}_4)E(\vec{k}_1,)E(\vec{k}_2)E(\vec{k}_1+\vec{k}_2-\vec{k}_4)\,\mathrm{d}\vec{k}_1\,\mathrm{d}\vec{k}_2 \\ & -E(\vec{k}_4)\iiint T_2(\vec{k}_1,\vec{k}_2,\vec{k}_4)E(\vec{k}_1)E(\vec{k}_2)\,\mathrm{d}\vec{k}_1\,\mathrm{d}\vec{k}_2 \end{aligned} \tag{B.26}$$

A widely used method is the discrete interaction approach, as described in Hasselmann et al. (1985). This approach considers the interactions of each wave component in the spectrum in only two quadruplets. This approach reduces the computational time to manageable proportions.

The triad wave-wave interactions are mostly described by the discrete triad approximation (lumped triad approximation), determined by Eldeberky and Battjes (1995).

WAVE BREAKING

Distinction can be made between deep water wave breaking (white-capping) and depth-induced (shallow water) wave breaking.

White-capping: Hasselmann

A commonly used formula for the dissipation by white-capping is the one from Hasselmann (1974), which defines the white-capping term $D_w(\omega,\theta)$:

$$D_w(\omega,\theta) = -\Gamma\bar{\omega}\frac{k}{\bar{k}}E(\omega,\theta) \tag{B.27}$$

where Γ is a steepness dependent coefficient [-], k is the wave number [m^{-1}], and $\bar{\omega}$ and $\bar{k}$ are a mean frequency [s^{-1}] and mean wave number [m^{-1}].

Battjes & Janssen
One of the most used models for wave-breaking is the one defined by Battjes and Janssen (1978). The average energy loss in a single breaking wave per unit time and per unit horizontal bottom area is given by:

$$D_{surf,wave} = -\frac{1}{4}\alpha_{BJ}\rho g f_0 H^2 \tag{B.28}$$

where $\alpha_{BJ} \approx 1$ is a tunable coefficient [-], f_0 is the inverse of the zero-crossing wave period [s^{-1}] and H is the wave height of the breaking wave [m]. Using the fraction of breaking waves Q_b, the average for all waves can be written as:

$$\overline{D}_{surf} = -\frac{1}{4}\alpha_{BJ} Q_b \overline{f}_0 H_b^2 \tag{B.29}$$

where H_b is the (maximum) wave height at breaking [m]. A wave starts breaking when the particle velocity exceeds the velocity of the wave crest, which corresponds to a crest angle of approximately 120°. Miche (1944) described the limiting wave steepness based on Stokes wave theory:

$$\left[\frac{H}{L}\right]_{max} = 0.142 \tanh kh \tag{B.30}$$

For shallow water, it can be derived that:

$$\gamma = \left[\frac{H}{L}\right]_{max} = \frac{H_b}{h_b} \approx 0.88 \tag{B.31}$$

where γ is the breaker index [-] and h_b is the water depth at breaking [m]. Using solitary wave theory, γ= 0.78 is derived. Battjes and Stive (1985) found the values between 0.6 and 0.83 with an average of 0.73. Kaminsky and Kraus (1993) found 0.6-1.59 with an average of 0.78.

Roelvink
Another formulation is the one by Roelvink (1993), for surf-beat type models:

$$\overline{D}_w = \frac{\alpha}{\pi} Q_b \sigma E_{tot} \tag{B.32a}$$

where

$$Q_b = 1 - \exp\left[-\left(\frac{H_{rms}}{H_{max}}\right)^n\right], H_{rms} = \sqrt{\frac{8E_{tot}}{\rho g}}, H_{max} = \frac{\gamma \tanh kh}{k} \tag{B.32b}$$

in which $\alpha = \mathcal{O}(1)$ and $n = \mathcal{O}(10)$.

B.1.2. FORESHORE DEFORMATION

Empirical formulations describing the processes that influence the foreshore deformation are given in this section.

SEDIMENT TRANSPORT

Many different transport relations exist. Several commonly used formulations for non-cohesive sediment are described here, using the volume transport per unit width, S [$m^3 s^{-1} m^{-1}$].

Bijker
This formula gives the bed load and suspended load transport, including the transport by waves (Bijker, 1967). It is divided into two parts:

$$S_b = bD_{50}\frac{u}{C}\sqrt{g}(1-\phi)\exp(A_r) \tag{B.33a}$$

$$S_s = 1.83 S_b \left(I_1 \ln\left(\frac{33.0h}{r_c}\right) + I_2\right) \tag{B.33b}$$

where h is the water depth [m] and ϕ is the porosity [-]. For the definitions of A_r, b, I_1 and I_2, see Bijker (1967).

Van Rijn
The formula by Van Rijn et al. (1993) gives the bed load and suspended load transport, including transport by waves. Transport below a certain reference height is treated as bed load transport, above the reference height as suspended load. The bed load transport is given by:

$$|S_b| = 0.006\rho_s w_s D_{50} M^{0.5} M_e^{0.7} \tag{B.34}$$

where S_b is the bed load, here expressed in [kgm^{-1}s^{-1}], M is a sediment mobility number due to waves and current [-] and M_e is the excess sediment mobility number [-], see for definitions Van Rijn et al. (1993). The values for S_b are then used in expressions for the bed load transport by waves and by currents. The wave related suspended load transport is given by:

$$S_{s,w} = f_{SUSW}\gamma U_A L_T \tag{B.35}$$

in which f_{SUSW} is a user defined tuning parameter [-], γ= 0.2 is the phase lag coefficient and U_A and L_T are a velocity asymmetry value [ms^{-1}] and the suspended sediment load [kgm^{-2}], given by $0.007\rho_s D_{50} M_e$, see also Van Rijn et al. (1993).

Soulsby-Van Rijn
This equation gives the bed load and suspended load transport, including the transport by waves. It is generally expressed in the equilibrium concentration C_{eq}. It is given by:

$$C_{eq} = \frac{A_{sb} + A_{ss}}{h}\left(\left(|u^E|^2 + 0.018\frac{u_{rms}^2}{C_d}\right)^{0.5} - u_{cr}\right)^{2.4}(1 - \alpha_b m) \tag{B.36}$$

where $u_{rms,b}$ is the near bed short wave orbital velocity [ms^{-1}], u_{cr} a critical velocity [ms^{-1}], C_d the drag coefficient. The bed slope is given by m and α_b is a calibration factor. The factors A_{ss} and A_{sb} are the suspended and bed load coefficients, dependent on the grain size, density of the sediment and water depth, see Soulsby (1997)

CROSS-SHORE PROFILE

Commonly used formulae to describe the long term cross-shore profile make use of the equilibrium shoreface profile, while for the shorter (storm) time-scale, the erosion profile (post-storm profile) is used. Several common expressions are given below.

Bruun
Bruun (1954) was one of the first who described the dynamic equilibrium profile. He described the profile using the local water depth h:

$$h = A\left(x'\right)^m \tag{B.37}$$

where m= 2/3 is an exponent, x' is the offshore distance, measured from the mean water line and positive in offshore direction [m] and A is a dimensional constant [m$^{1/3}$]. Typical magnitudes of A are in the order of 0.10.

Dean
Dean (1977) considered a uniform energy dissipation per unit volume of water across the surf zone, for a certain grain size: $\epsilon(D_{50}) = D/h$ (loss in wave power). Using this approach, the energy balance can be written as (for normally incident waves on an alongshore uniform coast):

$$\frac{\mathrm{d}\left(Ec_g\right)}{\mathrm{d}x} = -D = -h\epsilon\left(D_{50}\right) \tag{B.38}$$

where D_{50} is the grain size for which 50% of the sediment is finer. Using a simple dissipation model, the shallow water approximation and integrating, gives:

$$h(x') = \left(\frac{24\epsilon\left(D_{50}\right)}{5\rho g^{3/2}\gamma^2}\right)^{2/3}\left(x'\right)^{2/3} \tag{B.39a}$$

where

$$\left(\frac{24\epsilon\,(D_{50})}{5\rho g^{3/2}\gamma^2}\right)^{2/3} = A \tag{B.39b}$$

where ρ is the density of water [kgm^{-3}] and γ is the breaker index, see the section on wave breaking. Dean (1987) showed that, using the fall velocity w_s [ms^{-1}], the relation for A could be written as:

$$A = 0.5 w_s^{0.44} \tag{B.40}$$

Bowen

Bowen (1980) derived an expression for the equilibrium profile from the equation for boundary layer streaming:

$$h \simeq (7.5 w_s)^{2/3} / g^{1/3} x^{2/3} \tag{B.41a}$$

where

$$A = 0.39 w_s^{0.44} \tag{B.41b}$$

Vellinga

Vellinga (1986) used the erosion profile approach and derived a scale relation showing the effect of grain size on the erosion profile shape. Using the scale relation, it was derived that:

$$h = A(x')^{0.78} \tag{B.42a}$$

where

$$A = 0.39 w_s^{0.44} \tag{B.42b}$$

in which, here, x is the offshore distance measured from the storm surge level instead of MSL [m].

B.2. NUMERICAL MODELS

According to Sheremet et al. (2011), numerical wave models can be divided into two categories: stochastic (phase averaged) and deterministic (phase-resolving). The stochastic models simulate the wave processes in a probabilistic way, often based on empirical formulations. Deterministic models simulate wave processes based on the conservation laws. The deterministic models resolve the individual waveforms. For an overview of some of the available models, see table B.1, which was based on Buckley and Lowe (2013).

Table B.1: Overview of commonly used numerical models.

Model	Class	Breaking formulation	Reference
ENDEC	Wave action balance	Parametric	(Stive and Dingemans, 1984)
SWAN	Wave action balance	Parametric	(Booij et al., 1999)
XBeach	Wave action balance with phase resolving IG	Parametric	(Roelvink et al., 2009)
SWASH	NLSW + non-hydrostatic terms	Shock-capturing	(Zijlema et al., 2011)

B.2.1. ENDEC

Battjes and Janssen (1978) describe a model, ENDEC (ENergy DECay), for the prediction of the dissipation of energy in random waves breaking on a beach. Stive and Dingemans (1984) give the verification of the ENDEC model. Here, it was applied to an extensive set of both laboratory and field data. ENDEC is a one-dimensional wave energy decay model. In The Netherlands, it is commonly known as the 'foreshore module' (voorlandmodule), which is still often used for the safety assessment of dikes with foreshores. It uses the wave action balance. For the bottom friction, the expression derived by Putnam and Johson (1949) is used. For the wind input, the growth curves of Janssen et al. (1984) are used, which are discrete. For wave breaking, an edited version of the breaking formula of Battjes and Janssen (1978) is applied. Furthermore, refraction due to bottom variations and current variations are part of the model (Stive and Dingemans, 1984).

B.2.2. SWAN

Booij et al. (1999) presents a numerical wave model to compute random, short-crested waves in coastal regions with shallow water and ambient currents, called SWAN (Simulating WAves Nearshore). In Ris et al. (1999) the SWAN model is verified in stationary mode with measurements in five real field cases. SWAN (Simulating Waves Nearshore) is a numerical model to compute random short-crested waves in coastal regions with shallow water and ambient currents. It is a phase-averaged spectral wave model. It predicts the spectral evolution of wave action in space and time. Van Vledder et al. (2004) presents an investigation on the reliability of the SWAN wave prediction model and hydraulic boundary conditions at the Petten Sea Defence by hind-casting five storm events. Dingemans (1998) gives a review of the formulations of the physical processes applied in the SWAN model and also presents alternative formulations.

SWAN uses the wave action balance, for a description refer to Appendix A. The transfer of wind energy to the waves (wind input) is described by the resonance mechanism of Phillips (1957) and the feedback mechanism of Miles (1957), see the section on wind input. The dissipation of wave energy is given by the contributions of white-capping, bottom friction and depth-induced breaking. The white-capping formulation that is used is the one of Hasselmann (1974), see the section on wave breaking. The bottom friction dissipation is defined by Bertotti and Cavaleri (1994), refer to the section on bottom friction. SWAN uses the wave breaking formulation by Battjes and Janssen (1978), see formula B.28, in a slightly different form. For the quadruplet wave-wave interactions the formulation of Hasselmann et al. (1985) is used, for the triad interactions Eldeberky and Battjes (1995) is applied (Booij et al., 1999).

B.2.3. SWASH

Zijlema et al. (2011) presents a computational procedure to simulate non-hydrostatic, free-surface, rotational flows in one and two horizontal dimensions, called SWASH. SWASH is a phase-resolving spectral wave model, solving the non-linear shallow water equations with added non-hydrostatic terms. SWASH uses the non-hydrostatic shallow water equations, which can be derived from the Reynolds-averaged Navier-Stokes equations, refer to Appendix A. SWASH uses the bottom friction coefficient c_f based on Manning's roughness coefficient n. In SWASH, the depth-limited breaking is accounted for by a shock-capturing conservation scheme (Zijlema and Stelling, 2008). With a large number of vertical layers, when waves approach breaking, a sawtooth waveform develops. The energy at the discontinuity is dissipated through the shock-capturing scheme. Herein, it is the viscosity that determines the scale at which dissipation takes place. Therefore, the Prandtl mixing length hypothesis is used (Zijlema et al., 2011). With a single vertical layer, the sawtooth waveform develops too late, due to the lack of vertical resolution, which requires an additional formulation for the onset of breaking (Rijnsdorp et al., 2014). Rijnsdorp et al. (2014) compared the non-hydrostatic wave model SWASH to flume observations of infragravity waves propagating over a plane slope and barred beach.

C

FAST FOURIER TRANSFORM

This Appendix describes the Fast Fourier Transform, a method to derive the wave spectrum from a series of data, e.g. from a wave buoy. Furthermore, the Welch method and Hann window are described, which were used to determine the wave spectra. Section C.1 described the Fast Fourier Transform, section C.2 shows the Welch method. Finally, section C.3 gives a description of the Hann window.

C.1. FFT

The data record can be reproduced as a Fourier series:

$$\eta(t) = \sum_{i=1}^{N} a_i \cos(2\pi f_i t + \alpha_i) \tag{C.1}$$

where a_i and α_i are the amplitude and phase of each frequency f_i. The variance density spectrum is defined by :

$$E(f) = \lim_{\Delta f \to 0} \frac{1}{\Delta f} E\left(\frac{1}{2}a^2\right) \tag{C.2}$$

where $\Delta f = 1/D$, with D is the duration of the record or part of the record (The record is usually split up into 20-30 minute sections). Equation C.1 can be written as:

$$\eta(t) = \sum_{i=1}^{N} \left[A_i \cos(2\pi f_i t) + B_i \sin(2\pi f_i t)\right] \tag{C.3}$$

with amplitude and phase:

$$a_i = \sqrt{A_i^2 + B_i^2} \quad \text{and} \quad \tan\alpha_i = -\frac{B_i}{A_i} \tag{C.4}$$

The amplitudes A_i and B_i can be determined by with the Fourier integrals:

$$A_i = \frac{2}{D}\int_D \eta(t)\cos(2\pi f_i t)\,\mathrm{d}t \tag{C.5a}$$

$$B_i = \frac{2}{D}\int_D \eta(t)\sin(2\pi f_i t)\,\mathrm{d}t \tag{C.5b}$$

For a more detailed description of the Fast Fourier Transform, refer to Holthuijsen (2007).

C.2. WELCH'S METHOD

Welch's method is used to estimate the power of a signal at different frequencies and can thus be used to determine a wave spectrum. Welch'method can be described by (Welch, 1967):

- Divide the time series data into K (overlapping) segments.
- Apply a window to each segment. Most window functions give more influence to the data at the centre of the set than to data at the edges. The segments are therefore commonly overlapped.

- Calculate the finite Fourier transforms of the sections, which gives (modified) periodograms. A periodogram is a power spectral density estimate, which is used to identify the most dominant frequencies of a time series.
- The periodograms are then averaged, which gives the spectral estimate.

C.3. HANN WINDOW

A window function is a function which is zero outside some interval. When a data sequence is multiplied by a window function, the resulting data is also zero outside the window. The Hann, Von Hann or Hanning window is given by (Harris, 1978):

$$w(n) = 0.5\left(1 - \cos\left(\frac{2\pi n}{N-1}\right)\right) \tag{C.6}$$

where N is the number of points and n is a parameter with integers, which runs from 0 until $N-1$.

D

WAVE RUN-UP & WAVE OVERTOPPING

This Appendix describes the empirical formulations on wave run up (section D.1) and wave overtopping (section D.2).

D.1. WAVE RUN-UP

Wave run-up is defined as the vertical difference between the highest point of wave run-up and the still water level (SWL). The most used run-up height is the $R_{u2\%}$ [m], the wave run-up height which is exceeded by 2% of the number of incoming waves. In the past decade, the design and assessment has changed from using the run-up to using the overtopping (EurOtop, 2007). However, the run-up is still valuable, for example in determining the number of overtopping waves over a dike.

D.1.1. OLD DELFT FORMULA

The old Delft formula is a rule of thumb and can be used as a first estimate. It is defined as:

$$R_{u2\%} = 8 H_s \tan\alpha \tag{D.1}$$

where H_s is the significant wave height [m] and α is the angle of the slope with the horizontal [°]. It is only valid for high wave steepness.

D.1.2. HUNT'S EQUATION

Hunt's equation (Hunt, 1959), later edited in Battjes (1971) is given by:

$$\frac{R_{max}}{H_s} = \xi \tag{D.2}$$

in which H_s is the significant wave height [m] and ξ is the Iribarren number, surf similarity or breaker parameter [-] (see also Appendix B).

D.1.3. MASE

Mase (1989) found that:

$$\frac{R_{u2\%}}{H_{mean}} = 1.86 \xi_{mean}^{0.71} \tag{D.3}$$

in which H_{mean} is the mean wave height [m] and ξ_{mean} is the Iribarren number, based on the mean wave height and period [-]

D.1.4. HUGHES

Hughes (2004) gives a relation according to:

$$\frac{R_{u2\%}}{h} = 1.75\left(1 - e^{-[1.3\cot\alpha]}\right)\left[\sqrt{\frac{M_F}{\rho_w g h^2}}\right] \text{ for } \frac{H_{mean}}{L} < 0.0225 \text{ and } \frac{1}{4} \leq \tan\alpha \leq 1 \tag{D.4a}$$

$$\frac{R_{u2\%}}{h} = 4.4\left(\tan\beta\right)^{0.7}\left[\sqrt{\frac{M_F}{\rho_w g h^2}}\right] \text{ for } \frac{H_{mean}}{L_{mean}} > 0.0225 \text{ and } \frac{1}{5} \leq \tan\alpha \leq \frac{2}{3} \text{ and for any value of } \frac{H_{mean}}{L_{mean}} \text{ and } \frac{1}{30} \leq \tan\alpha \leq \frac{1}{5}. \tag{D.4b}$$

in which h is the water depth at breaking [m], L_{mean} is the mean wave length [m], $\left[\sqrt{\frac{M_F}{\rho_w g h^2}}\right] = A_0\left(\frac{h}{gT^2}\right)^{-A_1}$ [-], $A_0 = 0.6392\left(\frac{H}{h}\right)^{2.0256}$ [-] and $A_1 = 0.1804\left(\frac{H}{h}\right)^{-0.391}$ [-].

D.1.5. STOCKDON

Stockdon et al. (2006) derived an expression for all natural beach types, according to:

$$R_{u2\%} = 1.1\left(0.35\alpha(H_0L_0)^{1/2} + \frac{[H_0L_0(0.564\alpha^2 + 0.004)]^{1/2}}{2}\right) \tag{D.5a}$$

and for $\xi_0 > 1.25$

$$R_{u2\%} = 0.73\alpha(H_0L_0)^{1/2} \tag{D.5b}$$

where H_0 and L_0 are the deep water wave height [m] and period [s], respectively.

D.1.6. EUROTOP

The European Overtopping Manual (EurOtop) (EurOtop, 2007) is the most comprehensive source on wave run-up and wave overtopping. The general formula for the run-up, for probabilistic design is given by:

$$\frac{R_{u2\%}}{H_{m0}} = 1.65\gamma_b\gamma_f\gamma_\beta\xi_{m-1,0} \tag{D.6a}$$

with a maximum of

$$\frac{R_{u2\%}}{H_{m0}} = 1.00\gamma_b\gamma_f\gamma_\beta\left(4.0 - \frac{1.5}{\sqrt{\xi_{m-1,0}}}\right) \tag{D.6b}$$

where H_{m0} is the spectral wave height [m] and $\xi_{m-1,0}$ the Iribarren number, in this case based on the spectral wave height and period [-]. The formula is valid in the range of $0.5 < \gamma_b\xi_{m-1,0} \leq 8$ to 10. The statistical distribution around the average wave run-up height is described by a normal distribution with a coefficient of variation $V = 0.07$.

The first part of this equation can be used for $\xi_{m-1,0} \approx 1.7-1.8$. For higher values of the breaker parameter, the second part of the equation is used. Using the set of equations, the wave run-up can be described for the whole range of slopes and wave breaking conditions.

For oblique waves the angle of wave attack is defined as the angle between the direction of propagation of waves and the axis perpendicular to the structure (for perpendicular wave attack $\beta = 0^\circ$). For oblique wave attack with angles over 45°, the wave overtopping will eventually be zero, if the angle of wave attack is large enough. For run-up and short-crested waves, the influence factor γ_β is calculated, viz.

$$\gamma_\beta = 1 - 0.0022|\beta| \;\; 0^\circ \leq \beta \leq 80^\circ \tag{D.7}$$

For large angles, an estimation was made in Van der Meer (2002):

$$\gamma_\beta = 0.824 \;\; for: |\beta| \geq 80^\circ \tag{D.8}$$

For angles between 80°and 110°the wave height and wave period need to be adjusted, due to decreasing wave height and wave period when waves approach a structure:

$$H_{m0} \text{ is multiplied by } \frac{110 - |\beta|}{30} \tag{D.9}$$

$$T_{m-1,0} \text{ is multiplied by } \sqrt{\frac{110 - |\beta|}{30}} \tag{D.10}$$

For angles larger than 110°, we may assume zero run-up (EurOtop, 2007).

The influence of roughness and permeability, and the influence of a berm is accounted for by γ_f and γ_b. The definition of these parameters can be found in the next section on wave overtopping.

D.2. WAVE OVERTOPPING

Wave overtopping occurs because of waves running up the face of a flood defence. If the run-up levels are large enough, water will pass over the crest of the defence. This is called 'green water' overtopping, where a continuous sheet of water passes over the crest. Waves can also break on the face of the defence and produce splash which is carried over the crest by its own momentum or by the wind. Small volumes of water may be carried over the crest in the form of spray, by wind acting on the wave crests directly in front of the defence. Wave overtopping is characterized by the overtopping discharge q per meter width of the defence, averaged over time. The overtopping discharge depends on (EurOtop, 2007):

- the wave run-up;
- the existing freeboard.

D.2.1. VAN DER MEER AND BRUCE

According to Van der Meer and Bruce (2013) overtopping at straight slopes (gentle to very steep) can be described by the following set of formulae:

$$\frac{q}{\sqrt{gH_{m0}{}^3}} = \frac{0.023}{\sqrt{\tan\alpha}}\gamma_b\xi_{m-1,0}\exp\left(-(2.7\frac{R_c}{\xi_{m-1,0}H_{m0}\gamma_b\gamma_f\gamma_\beta\gamma_v})^{1.3}\right) \tag{D.11a}$$

with a maximum of:

$$\frac{q}{\sqrt{gH_{m0}{}^3}} = 0.09\exp\left(-(1.5\frac{R_c}{H_{m0}\gamma_f\gamma_\beta})^{1.3}\right) \tag{D.11b}$$

In probabilistic analyses, the model error is accounted for by assuming the coefficients 0.023 & 2.7 and 0.09 & 1.5 to be normal distributed with $\sigma(0.023) = 0.003$ & $\sigma(2.7) = 0.20$ and $\sigma(0.09) = 0.013$ & $\sigma(1.5) = 0.15$. These formulae give almost the same wave overtopping as the Van der Meer (2002) formulae, but will give better results for low and zero freeboards.

D.2.2. INFLUENCE FACTORS EURTOP

The formulae described in Van der Meer (2002) and EurOtop (2007) are the most commonly used to describe wave overtopping. The influence factors in these formulae are described in more detail below.

OBLIQUE WAVE ATTACK

For overtopping calculations with oblique wave attack, the parameter γ_β represents the influence of the oblique wave attack. For overtopping and short-crested waves, the influence factor γ_β is calculated, viz.

$$\gamma_\beta = 1 - 0.0033|\beta| \;\; 0^\circ \le \beta \le 80^\circ \tag{D.12}$$

For large angles, an estimation was made in Van der Meer (2002):

$$\gamma_\beta = 0.736 \;\; for : |\beta| \ge 80^\circ \tag{D.13}$$

For angles between 80°and 110°the wave height and wave period need to be adjusted in the same way as for run-up mentioned above.

ROUGHNESS AND PERMEABILITY

The influence of roughness and permeability is accounted for by γ_f (see table D.1) (EurOtop, 2007).

Reference type	γ_f
Concrete	1.0
Asphalt	1.0
Closed concrete blocks	1.0
Grass	1.0
Basalt	0.90
Small blocks over 1/25 of surface	0.85
Small blocks over 1/9 of surface	0.80
1/4 of block revetment 10 cm higher	0.90
Rip rap (optimum dimensions)	0.75

Table D.1: Roughness coefficients γ_f for different types of revetment (EurOtop, 2007).

VERTICAL WALLS

The reduction due to (relatively small) vertical walls on top of the slope can be up to 35%. The effect is accounted for by:

$$\gamma_v = 1.35 - 0.0078\alpha_{wall} \tag{D.14}$$

where α_{wall} is the slope of the wall (for vertical wails, α_{wall}= 90). The Overtopping Manual (EurOtop, 2007) restricts the equation above to the conditions below:

- the average slope of $1.5H_{m0}$ below the still water line to the foot of the wall (excluding a berm) must lie between 1:2.5 to 1:3.5;
- the width of all berms together must be no more than $3H_{m0}$;
- the foot of the wall must lie between about $1.2H_{m0}$ under and above the still water line;
- the minimum height of the wall (for a high foot) is about $0.5H_{m0}$. The maximum height (for a low foot) is about $3H_{m0}$.

BERMS

The influence of a berm is determined by γ_b, it is dependent on the length of the berm B and the water level, see figure D.1. d_b is the distance between SWL and the berm level. At both sides of the berm, the slope is intersected at a vertical distance H_{m0} from the horizontal center plane of the berm, giving a length L_{berm}, see figure D.1 (EurOtop, 2007).

$$\gamma_b = 1 - \frac{B}{L_{berm}}\left(0.5 + 0.5\cos\left(\pi\frac{d_b}{x}\right)\right) \quad for \;\; 0.6 \leq \gamma_b \leq 1.0 \tag{D.15}$$

with

$x = R_{u2\%}$ for berm above SWL
$x = 2H_{m0}$ for berm below SWL

D.2.3. TOLERABLE DISCHARGES

In chapter 2 an EurOtop table with tolerable wave overtopping discharges was presented. Below, several other tables are shown, with limits for vehicles, pedestrians and property.

Table D.2: Overtopping limits for vehicles (EurOtop, 2007).

Hazard type and reason	Mean discharge, q [ls^{-1}m^{-1}]	Max volume, V [lm^{-1}]
Driving at low speed, overtopping by pulsating flows at low flow depths, no falling jets, vehicle not immersed	10-50	100-1,000
Driving at moderate or high speed, impulsive overtopping giving falling or high velocity jets	0.01-0.05	5-50 at high level or velocity

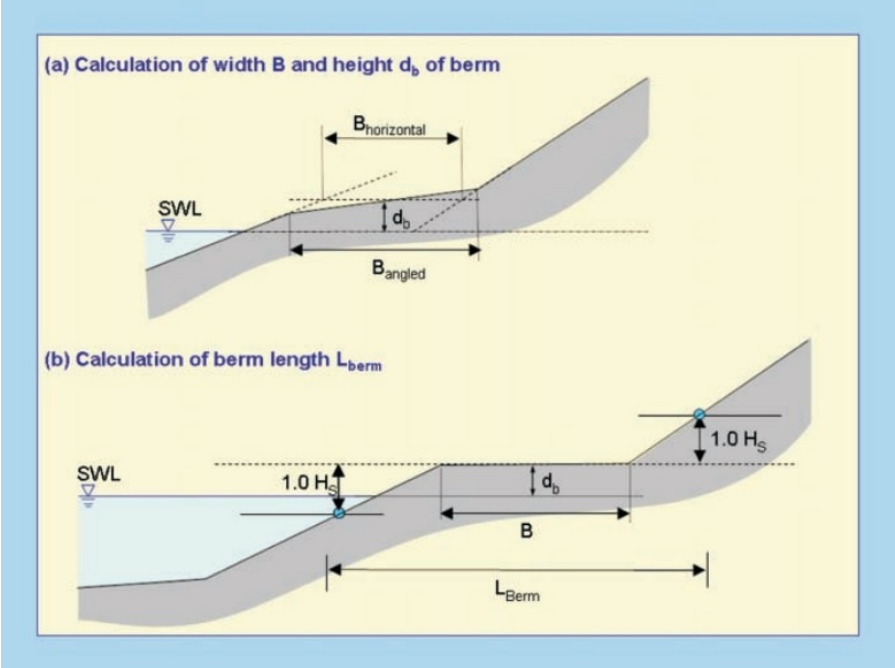

Figure D.1: Berm characteristics, (EurOtop, 2007).

Table D.3: Overtopping limits for property behind the defence (EurOtop, 2007).

Hazard type and reason	Mean discharge, q [ls^{-1}m^{-1}]	Max volume, V [lm^{-1}]
Significant damage or sinking of larger yachts	50	5,000-50,000
Sinking small boats set 5-10 m from wall, damage to larger yachts	10	1,000-10,000
Building structure elements	1	-
Damage to equipment set back 5-10 m	0.4	-

Table D.4: Overtopping limits for pedestrians (EurOtop, 2007).

Hazard type and reason	Mean discharge, q [ls^{-1}m^{-1}]	Max volume, V [lm^{-1}]
Trained staff, well shod and protected, expecting to get wet, overtopping flows at lower levels only, no falling jet, low danger of fall from walkway	1-10	500 at low level
Aware pedestrian, clear view of the sea, not easily upset or frightened, able to tolerate getting wet, wider walkway	0.1	20-50 at high level or velocity

E

COMPARISON OF XBEACH & H/2-MODEL AT THE WESTKAPELLE SEA DEFENCE

In this Appendix, the performance of XBeach is compared to the $h/2$-model and Rock Manual (CIRIA, 2007) wave height graphs for storms with return periods of 100, 1,000 and 10,000 years at the Westkapelle sea defence. The boundary conditions belonging to these return periods were determined with the probability distributions as presented in chapter 4. Section E.1 until E.3 show the results for the storms with return period of 100, 1,000 and 10,000 years. Section E.4 presents some conclusions.

E.1. 1/100 YEARS STORM

For the comparison between XBeach and the $h/2$-model, the 1D XBeach model was used, as well as the 2D-model. The models were set-up as described before, again without calculating morphological changes or sediment transport, because the h/2-model is also not capable of calculating these processes.

The 1/100 year conditions imposed on the offshore boundary of the models (-20 m+NAP) were zs= 4.13 m, H_{m0}= 4.74 m and T_p= 9.02 s. Table E.1 shows the results of the calculations with XBeach and the h/2-model for the 1/100 years storm.

Table E.1: Results of h/2-model and XBeach calculations for 1/100 years conditions. Wave height, wave period and water level at toe.

Model	H_{m0} [m]	$T_{m-1,0}$ [s]	MWL at toe [m]	q [ls^{-1}m^{-1}]
$h/2$	0.066	9.025	4.132	$3.06 * 10^{-144}$
$h/2$ set-up	0.382	9.025	4.763	$9.55 * 10^{-22}$
Graphs	0.146	9.025	4.132	$6.93 * 10^{-65}$
XBeach 1D	0.738	54.427	4.778	$1.83 * 10^{-7}$
XBeach 2D	0.520	22.006	4.763	$9.16 * 10^{-17}$

The table shows that for these conditions, because of the low water level compared to the foreshore height (4 m+NAP), there are almost no waves reaching the toe of the dike in the h/2-model. In the XBeach models however, the wave height is much higher. This can be explained by the larger water depth at the toe, caused by the wave set-up, which is not included in the h/2-model. To circumvent this problem, another calculation was performed with the h/2-model, but now with the larger mean water level at the toe according to XBeach 2D (indicated by h/2 set-up in the table). This increases the wave height a lot, but it is still lower than the wave height resulting from XBeach. Another commonly used method to calculated wave heights on uniform foreshore slopes is the one described in the Rock Manual (CIRIA, 2007) (q.v.), based on graphs, see figure E.1. Using this method with a foreshore slope < 0.01, a wave steepness between 0.03 and 0.04 and a relative water depth h/L_0 of 0.001 leads to a breaker index H_s/h of approximately 1.1, which is extremely large. These values are found by extending the graphs to the left and thus at the extreme left of the graph, which indicates that severe breaking occurs on the foreshore. This results in a wave height of approximately 0.15 m, which is again much lower than the XBeach values. This difference can again be attributed to the wave set-up, which is also not included in the method with the graphs. Even the XBeach 1D and 2D models show rather

large differences, caused by the exclusion of refraction and wave directional spreading in the 1D-model. The effect of the refraction is very small due to the fact that the waves were normally incident and the coast was straight. However, the effect of the exclusion of wave directional spreading is considerable. The bundling of waves without directional spreading leads to a larger forcing of infragravity waves and thus a larger wave height at the toe. Hence, XBeach 1D overestimates the infragravity waves. Due to the exclusion of the wave directional spreading, just as in a flume, the waves become long crested, which leads to a stronger forcing of the infragravity waves. XBeach 2D can be considered more as a basin, the inclusion of the wave directional spreading leads to more realistic infragravity wave heights.

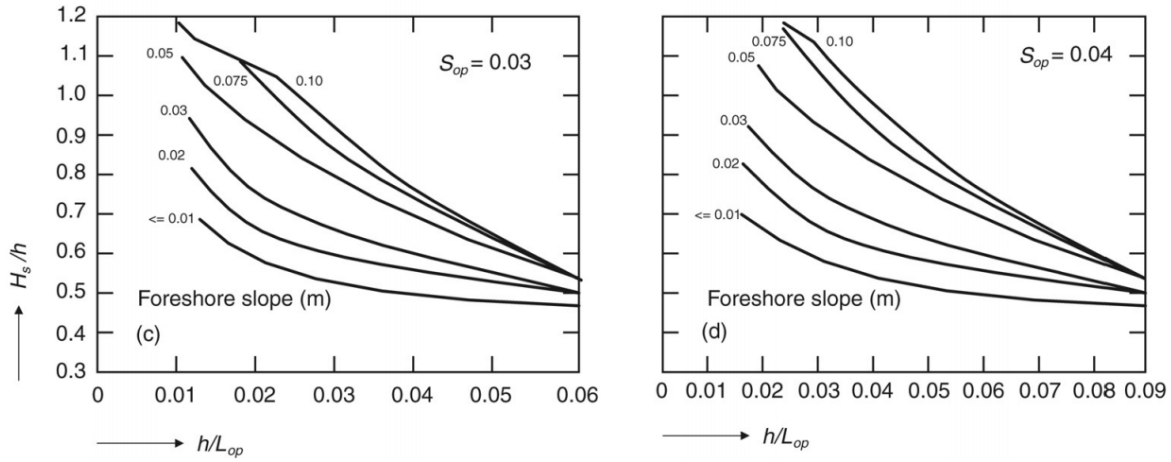

Figure E.1: Shallow water significant wave heights on uniform sloping foreshore (CIRIA, 2007). h is the water depth [m], L_{op} the offshore wave length based on the peak period [m], S_{op} the offshore wave steepness based on the peak period and [-] and H_s the significant wave height [m].

The h/2-model and the rule of thumb found in the Rock Manual both don't calculate the change in wave period. As can be seen from the XBeach calculations, the wave period actually changes a lot compared to the offshore value, which also largely influences the calculated wave overtopping discharge. It is clear that the severe breaking of the short waves on the foreshore caused a shift of the wave energy to the lower (infragravity wave) frequencies. These much larger wave periods at the toe cause much larger wave overtopping discharge value, although, for these boundary conditions the overtopping is approximately zero. The larger infragravity waves in the 1D model lead also to an even larger shift towards the lower frequencies, which is why the wave period becomes even larger than in the 2D XBeach model. The combined influence of larger wave height and wave period in the 1D model leads therefore also to a larger wave overtopping discharge.

E.2. 1/1,000 YEARS STORM

The 1/1,000 year conditions imposed on the offshore boundary of the models were zs= 4.73 m, H_{m0}= 5.09 m and T_p= 9.41 s. Table E.2 shows the results of the calculations with XBeach and the h/2-model for the 1/1,000 years storm.

Table E.2: Results of h/2-model and XBeach calculations for 1/1,000 years conditions. Wave height, wave period and water level at toe.

Model	H_{m0} [m]	$T_{m-1,0}$ [s]	MWL at toe [m]	q [ls^{-1}m^{-1}]
h/2	0.367	9.407	4.734	$8.75 * 10^{-23}$
h/2 set-up	0.658	9.407	5.315	$6.96 * 10^{-12}$
Graphs	0.734	9.407	4.734	$3.85 * 10^{-12}$
XBeach 1D	1.088	45.271	5.316	$1.06 * 10^{-4}$
XBeach 2D	0.863	18.113	5.315	$2.54 * 10^{-8}$

Even though the water level and the waves are higher the wave overtopping is still approximately zero. This is caused by the large crest height of the Westkapelle sea defence (average of 12.6 m+NAP). With these boundary conditions, the from the h/2-model resulting wave height is still less than half the wave heigth

from the XBeach models, which is again caused by the lack of inclusion of the wave set-up in the h/2-model. Therefore, again, the mean water level at the toe in the XBeach model was taken and inserted into the h/2-model, which leads to a an approximation of the wave height which is closer to XBeach, however, is still lower than the XBeach values. Using the method from the Rock Manual, with again a foreshore slope < 0.01 and a wave steepness between 0.03 and 0.04, but now with a relative water depth h/L_0 of 0.005 leads to a breaker index H_s/h of approximately 1. This is still extremely large and can only be found by extending the graphs to the left and thus at the extreme left of the graph, which again indicates severe breaking. All this results in a wave height of approximately 0.73 m, which is a lot closer to the XBeach 2D value than the h/2-model, especially considering the lack of inclusion of the wave set-up in the Rock Manual method as well as in the h/2-model. Again, due to the effect of exclusion/inclusion of the wave directional spreading, the 1D and 2D XBeach results differ, with the 1D model showing a larger wave height.

The wave period at the dike toe from the XBeach calculations is lower than the value for the 1/100 year conditions, which can be explained by the larger water depth on the foreshore, which reduces wave breaking and hence the shift to the infragravity wave frequencies. Still, the wave period is much larger than the offshore period, which one would use when using the h/2-model or the Rock Manual graphs. As explained before, the exclusion of the wave directional spreading in the 1D XBeach model leads to a much larger wave period, due to the larger infragravity waves. This much larger wave period also leads to a much larger wave overtopping discharge, which for these conditions is still approximately zero however.

E.3. 1/10,000 YEARS STORM

The 1/10,000 year conditions imposed on the offshore boundary of the models were zs= 5.35 m, H_{m0}= 5.41 m and T_p= 9.75 s. Table E.3 shows the results of the calculations with XBeach and the h/2-model for the 1/10,000 years storm.

Table E.3: Results of h/2-model and XBeach calculations for 1/10,000 years conditions. Wave height, wave period and water level at toe.

Model	H_{m0} [m]	$T_{m-1,0}$ [s]	MWL at toe [m]	q [ls^{-1}m^{-1}]
h/2	0.676	9.756	5.351	$4.08 * 10^{-11}$
h/2 set-up	0.943	9.756	5.885	$3.88 * 10^{-8}$
Graphs	1.081	9.756	5.351	$3.67 * 10^{-8}$
XBeach 1D	1.405	33.973	5.882	$1.56 * 10^{-3}$
XBeach 2D	1.206	15.565	5.885	$1.35 * 10^{-4}$

Even though the water level and the waves are again higher, the wave overtopping is still approximately zero, due to the large crest height. Now, the h/2-model wave height and XBeach wave heights at the toe are closer together, but still differ considerably. When using the mean water level at the toe from XBeach 2D in the h/2-model the resulting wave height is even closer to the XBeach 2D value, but still differs approximately with 0.20 m. Using the Rock Manual graphs, with again a foreshore slope < 0.01 and a wave steepness between 0.03 and 0.04, and now with a relative water depth h/L_0 of 0.01 leads to a breaker index H_s/h of approximately 0.8. This is a more reasonable value, but still indicates severe breaking. This breaker index results in a wave height of approximately 1.08 m, which is quite close to the XBeach 2D value, especially considering the fact that the Rock Manual graphs do not include the wave set-up. The wave heights calculated by XBeach 1D and 2D differ less than for the other boundary conditions, but still differ with approximately 0.25 m, which again is caused by the exclusion of wave directional spreading in the 1D model.

The wave periods at the dike toe from the XBeach calculations are lower than the values for the 1/100 and 1/1,000 year conditions, which can be explained by the larger water depth on the foreshore, which reduces wave breaking and hence the shift to the infragravity wave frequencies. Again, the wave period for the 2D-model is still almost twice as large as the offshore period and the period from the 1D-model is even 5 times as large. Hence, when one would use the h/2-model or the Rock Manual graphs, the wave period would be extremely underestimated. This much larger wave period also leads to a much larger wave overtopping discharge, which, even for these extreme conditions, is still approximately zero however.

E.4. CONCLUSIONS OF COMPARISON

It seems that for deeper water at the toe of the dike, thus a larger depth on the foreshore, the h/2-model and Rock Manual rule of thumb perform better than for shallower water, because the results are closer to the

results of XBeach. This can be explained by the fact that these models were not designed for use in 'special' cases as dike-foreshore systems, but for more general situations without foreshore and thus with a larger water depth at the toe. Because an increasing water depth at the toe resembles such a 'standard' situation more and more, the performance of these models increases as well.

Using the h/2-model or the Rock Manual graphs could lead to underestimation of the wave height caused by the exclusion of the wave set-up in these models, and certainly leads to an underestimation of the wave period, which is not calculated with these models. This also causes an lower estimation of the wave overtopping discharge, hence a higher estimation of the safety of the dike. It is therefore uncertain if these methods can be used for dike-foreshore systems as the Westkapelle sea defence.

The XBeach calculations, which do calculate the change in wave period, show much larger wave periods at the toe and thus much larger wave overtopping discharges. The differences between the 1D and 2D XBeach models are mainly caused by the exclusion of the wave directional spreading in the 1D-model. The results of the 2D-model are therefore more realistic. However, the 1D-model is still useful, because of its improved performance compared to the $h/2$-model and the graphs from the Rock Manual, as well as the limited calculation durations when using the 1D-model, compared to the 2D-model.

F

RELIABILITY ANALYSIS

This Appendix gives an overview of some of the available probabilistic calculation methods and of some useful procedures in reliability analysis. Section F.1 describes several common probabilistic calculation methods, section F.2 presents the transformation of a normal to a lognormal distribution. Finally, section F.3 describes the Kolmogorov-Smirnov test.

F.1. PROBABILISTIC CALCULATION METHODS

This section presents the available probabilistic calculation methods. Vrouwenvelder and Steenbergen (2003) and Vrijling et al. (2014) give extensive descriptions of the different probabilistic calculation methods. The following sections are partly based on these sources.

The Joint committee on structural safety proposed a level-classification of probabilistic calculation methods for the reliability of an element:

- Level I: Does not calculate the failure probabilities. A design method according to the standards, by using partial safety factors. The element is deemed sufficiently reliable if a certain margin is present between the representative values of the strengths and loads.
- Level II: Linearize the reliability function in the design point and approximate the probability distribution of each variable by a standard normal distribution.
- Level III: Calculate the probability of failure, by considering the probability density functions of all strength and load variables. The reliability of an element is linked directly to the probability of failure.

F.1.1. LEVEL I METHODS

With level I methods, failure probabilities are not calculated. The level I method is commonly used in standards. A single representative value of the strength is divided by a factor and a single value of the load is multiplied by a (safety) factor. The resulting strength value should be larger than the resulting load value. The representative values of strength and load can be determined by adding a certain amount of standard deviations $k_{R,S}$ to the mean value (e.g. ± 1.645 for the 95% or 5% value). The partial safety factors can be derived from the level II methods, as:

$$\gamma_R = \frac{1 + k_R V_R}{1 + \alpha_R \beta V_R} \tag{F.1a}$$

$$\gamma_S = \frac{1 + \alpha_S \beta V_S}{1 + k_S V_S} \tag{F.1b}$$

where α [-] is the influence coefficient, β is the reliability index [-] and V is the coefficient of variation [-].

F.1.2. LEVEL II METHODS

With level II methods, the reliability function is linearised in the design point.

FORM AND SORM

The First Order Reliability Method (FORM) linearizes the limit state function in the design point, the point at the failure boundary $Z = 0$ where the probability density is maximal. The distributions of the random variables are converted to the standard normal distribution. The design point is reached by iteration. A FORM calculation gives a reliability index β and influence coefficients α_i, from which the design point and probability of failure can be determined. A SORM calculation consists of a FORM calculation followed by a second order correction, which leads to an incomplete second-order function. FORM and SORM are very efficient, but fail in the case of a complex limit state function.

F.1.3. LEVEL III METHODS

Level III methods consider all the probability density functions of all variables to calculate the probability of failure.

ANALYTICAL INTEGRATION

If the joint probability density function of the strength and load is known, the probability of failure can be calculated by means of integration:

$$P_f = \iint_{Z<0} f_{R,S}(R,S)\,\mathrm{d}R\,\mathrm{d}S \tag{F.2}$$

If the strength and load are functions of one or more random variables, the reliability function can be written as $Z = g(X_1, X_2, ..., X_n)$. The probability of failure is then calculated by:

$$P_f = \iint_{Z<0} \dots \int f_{X_1,X_2,...,X_n}(X_1, X_2, ..., X_n)\,\mathrm{d}X_1\,\mathrm{d}X_2 \dots \mathrm{d}X_n \tag{F.3}$$

In most cases, the integral cannot be determined analytically.

FULL NUMERICAL INTEGRATION

It is possible to write equation F.3 as:

$$P_f = \int_0^1 \dots \int_0^1 \int_0^1 \mathbb{1}(Z)\,\mathrm{d}F_{X_1}(X_1)\,\mathrm{d}F_{X_2|X_1}(X_2|X_1) \dots \mathrm{d}F_{X_n|X_{n-1},...,X_1}(X_n|X_{n-1}, ..., X_1) \tag{F.4}$$

Several methods exist to integrate this equation, for example hypercube sampling, see the next section. A simple method is the Riemann-procedure, refer to e.g. Vrijling et al. (2014).

HYPERCUBE SAMPLING NUMERICAL INTEGRATION

Numerical integration methods for n-dimensional hypercubes can be very efficient. With hypercube sampling, the samples are more evenly distributed compared to random sampling. The range of every random variable is divided in intervals of equal probability. Random values are drawn for each of the variables, from each of the intervals. The samples are then combined. Reference is made to e.g. Genz and Malik (1980), who determined a subroutine for automatic numerical integration over an n-dimensional rectangular region. The algorithm ADAPT is presented in the paper and provides an estimation for the integral above. These methods subdivide the integration area locally where difficulty is met approaching the integral and also subdivide into the dimension in which it occurs (Van Dooren and de Ridder, 1976). Hypercube sampling is more efficient for monotonous relations, but not always for non-monotonous relations. Hypercube sampling is not specifically designed for the estimation of extremely small probabilities (Diermanse et al., 2007).

CRUDE MONTE CARLO

The Monte Carlo method consists of generating random numbers $\mathbf{u} = (u_1, ..., u_n)$ from a uniform probability density function between zero and one. Every drawing consists of a set of u-values, the failure probability can be estimated by determining the frequency with which these drawings occur in the failure space. By taking i realizations of the uniform distribution, values can be determined for every X_n.

$$\begin{aligned} X_1 &= F^{-1}_{X_1}(X_{u_1}) \\ X_2 &= F^{-1}_{X_2|X_1}(X_{u_1}|X_1) \\ &\vdots \\ X_n &= F^{-1}_{X_m|X_1,X_2,...,X_{n-1}}(X_{u_n}|X_1, X_2, ..., X_n - 1) \end{aligned} \tag{F.5}$$

If the values for the reliability functions are inserted, it is possible to check whether the obtained vector is located in the safe space. The probability of failure can be estimated by repeating this procedure many times:

$$P_f \approx \frac{j_f}{j} \tag{F.6}$$

where j is the total number of simulations [-] and j_f is the number of simulations for which failure occurs [-].

MONTE CARLO WITH IMPORTANCE SAMPLING

Importance sampling is a method to reduce the number of simulations with sufficient accuracy. Importance sampling increases the failure space relative to the total integration space. If the random numbers are drawn from the importance sampling distribution instead of the original probability distribution, more points in the failure space are found. Importance sampling can lead to a significant reduction in the amount of samples that is needed, but a wrong choice in sampling can lead to a very large variation in the estimation (Diermanse et al., 2007).

MONTE CARLO WITH DIRECTIONAL SAMPLING

Directional sampling can be considered as a special type of importance sampling, where samples are drawn as polar coordinates instead of Cartesian coordinates. For small probabilities of failure, the required sample size for a Monte Carlo simulation becomes very large. Directional sampling is an efficient method to cope with this. The probability of failure in each sample is computed conditionally on a direction in the standard normal space. With directional sampling, the random numbers $\mathbf{u}$ are divided by the length of the vector u and multiplied with λ, such that $Z(\lambda, u/|u|) = 0$, which means that λ is always larger than 0, see e.g. Ditlevsen and Madsen (1996). For small to medium amounts of random variables, directional sampling can be very effective to reduce the number of simulations, but for problems with more than 100 random variables, random drawing seems to become more efficient again (Diermanse et al., 2007).

MONTE CARLO WITH EXTREME VALUE SCALING

Extreme value scaling reduces the amount of samples needed by shifting samples from a domain with a large density to the failure domain. The failure probability is determined by calculating the probability using the shifted samples and then multiplying with a correction factor. The direction of the shift is determined by the tail of the joint probability function. A commonly used method is the method De Haan (de Haan and Resnick, 1977).

F.2. TRANSFORMATION OF NORMAL TO LOGNORMAL DISTRIBUTION

For some parameters, values smaller than zero are physically impossible to occur. When such a parameter is described by a normal distribution, there is a possibility that a negative value occurs. Therefore, for such cases, the normal distribution is transformed into a lognormal distribution by:

$$V = \frac{\sigma}{\mu} \tag{F.7a}$$

$$\zeta = \sqrt{\ln\left(1 + V^2\right)} \tag{F.7b}$$

$$\lambda = \ln \mu - \frac{1}{2}\zeta^2 \tag{F.7c}$$

where V is the coefficient of variation [-], μ is the mean of the normal distribution, σ is the standard deviation of the normal distribution, ζ is the scale parameter of the lognormal distribution and λ is the location parameter of the lognormal distribution.

F.3. KOLMOGOROV-SMIRNOV TEST

The Kolmogorov-Smirnov test (Kolmogorov, 1933) compares a chosen distribution function with statistical material. This section is based on Vrijling et al. (2014). A test quantity y is calculated for this method, described by:

$$y = max\left(\left|\frac{i}{n} - F_X\left(X_i\right)\right|\right) \tag{F.8}$$

where i is the number of the observation after ordering from small to large [-], n is the number of observations [-], F is the cumulative distribution function and X_i is the i^{th} observation after arranging. When the parameters of the distribution were not estimated from the same statistical data with which the assumed distribution is compared, then the distribution function has to be dismissed if:

$$y > \frac{\alpha}{\sqrt{n}} \tag{F.9a}$$

When the parameters of the distribution were estimated from the same statistical data with which the assumed distribution is compared, the next relation can be used:

$$y > \frac{\alpha}{\sqrt{n-r}} \tag{F.9b}$$

where α is a coefficient depending on the reliability threshold [-] and r is the amount of parameters of the distribution that have been estimated based on the statistical material [-]. α is defined as described below in table F.1.

Table F.1: Kolmogorov-Smirnov test coefficient α depending on the reliability threshold P.

P [-]	α [-]
0.10	1.23
0.05	1.36
0.01	1.63

G

XBeach input files

This Appendix presents examples of the files that were used as input for the calculations with XBeach. Section G.1 presents a parameter file, section G.2 a JONSWAP file and section G.3 a tide file. These files and other files can be found at `p:\xbeach\msc_studies\Patrick_Oosterlo` (only on the Deltares network).

G.1. Params

The params file sets all the XBeach model parameters, as shown below. For a definition of all the different parameters, refer to Deltares (2015b). This file and other files can be found at `p:\xbeach\msc_studies\Patrick_Oosterlo` (only on the Deltares network).

```
%%%%%%%%%%%%%%%%%%%%%%%%%%%%%%%%%%%%%%%%%%%%%%%%%%%%%%%%%%%%%%%%%%%%%%%%%%%%%%%%
%%% XBeach parameter settings input file                                     %%%
%%%                                                                          %%%
%%% date:     10-Aug-2015 13:14:54                                           %%%
%%% function: xb_write_params                                                %%%
%%%%%%%%%%%%%%%%%%%%%%%%%%%%%%%%%%%%%%%%%%%%%%%%%%%%%%%%%%%%%%%%%%%%%%%%%%%%%%%%

%%% Bed composition parameters %%%%%%%%%%%%%%%%%%%%%%%%%%%%%%%%%%%%%%%%%%%%%%%%%

D50          = 0.000297
D90          = 0.000445

%%% Flow boundary condition parameters %%%%%%%%%%%%%%%%%%%%%%%%%%%%%%%%%%%%%%%%%

front        = abs_2d
back         = abs_2d

%%% Flow parameters %%%%%%%%%%%%%%%%%%%%%%%%%%%%%%%%%%%%%%%%%%%%%%%%%%%%%%%%%%%%

bedfriction  = manning

%%% General %%%%%%%%%%%%%%%%%%%%%%%%%%%%%%%%%%%%%%%%%%%%%%%%%%%%%%%%%%%%%%%%%%%%

bedfriccoef  = 0.020000
cyclic       = 1
dtheta_s     = 10
gridform     = xbeach
single_dir   = 1

%%% Grid parameters %%%%%%%%%%%%%%%%%%%%%%%%%%%%%%%%%%%%%%%%%%%%%%%%%%%%%%%%%%%%

depfile      = bathy.dep
posdwn       = 0
nx           = 301
ny           = 20
alfa         = 0
vardx        = 1
```

```
dx           = -1
dy           = -1
xfile        = x.grd
yfile        = y.grd
thetamin     = -55
thetamax     = 55
dtheta       = 110
thetanaut    = 0

%%% MPI parameters %%%%%%%%%%%%%%%%%%%%%%%%%%%%%%%%%%%%%%%%%%%%%%%%%%%%%%%%%%%%%%%%

mpiboundary  = auto

%%% Model time %%%%%%%%%%%%%%%%%%%%%%%%%%%%%%%%%%%%%%%%%%%%%%%%%%%%%%%%%%%%%%%%%%

tstop        = 184718.647931
CFL          = 0.700000

%%% Morphology parameters %%%%%%%%%%%%%%%%%%%%%%%%%%%%%%%%%%%%%%%%%%%%%%%%%%%%%%%

wetslp       = 0.260000
struct       = 1
ne_layer     = nebed.dep

%%% Physical constants %%%%%%%%%%%%%%%%%%%%%%%%%%%%%%%%%%%%%%%%%%%%%%%%%%%%%%%%%%

g            = 9.810000
rho          = 1025
depthscale   = 1

%%% Physical processes %%%%%%%%%%%%%%%%%%%%%%%%%%%%%%%%%%%%%%%%%%%%%%%%%%%%%%%%%%

swave        = 1
lwave        = 1
flow         = 1
sedtrans     = 1
morphology   = 1

%%% Roller parameters %%%%%%%%%%%%%%%%%%%%%%%%%%%%%%%%%%%%%%%%%%%%%%%%%%%%%%%%%%%

beta         = 0.138000

%%% Sediment transport parameters %%%%%%%%%%%%%%%%%%%%%%%%%%%%%%%%%%%%%%%%%%%%%%%%

facSk        = 0.359191
facAs        = 0.117808

%%% Tide boundary conditions %%%%%%%%%%%%%%%%%%%%%%%%%%%%%%%%%%%%%%%%%%%%%%%%%%%%

zs0file      = tide.txt
tideloc      = 2
paulrevere   = 0

%%% Wave boundary condition parameters %%%%%%%%%%%%%%%%%%%%%%%%%%%%%%%%%%%%%%%%%%%

instat       = jons
taper        = 100

%%% Wave breaking parameters %%%%%%%%%%%%%%%%%%%%%%%%%%%%%%%%%%%%%%%%%%%%%%%%%%%%

gamma        = 0.541000
alpha        = 1.262000
gammax       = 2.364000

%%% Wave numerics parameters %%%%%%%%%%%%%%%%%%%%%%%%%%%%%%%%%%%%%%%%%%%%%%%%%%%%

wavint       = 120

%%% Wave-spectrum boundary condition parameters %%%%%%%%%%%%%%%%%%%%%%%%%%%%%%%%%%

bcfile       = filelist.txt
```

```
random       = 0

%%% Output variables %%%%%%%%%%%%%%%%%%%%%%%%%%%%%%%%%%%%%%%%%%%%%%%%%%%%%%%%

outputformat = netcdf
tintp        = 1
tintg        = 1800
tstart       = 0

nglobalvar   = 1
zb

npointvar    = 4
H
zs
zb
uu

npoints      = 1
0.0 500.0
```

G.2. FILELIST, JONSWAP

A JONSWAP file defines the wave boundary conditions. With changing wave boundary conditions, multiple JONSWAP files are defined and called by a file-list file. The JONSWAP file defines the significant wave height [m], wave peak period [s^{-1}], main wave direction [°], JONSWAP peak enhancement factor [-], wave directional spreading [-] and the highest frequency used to create the JONSWAP spectrum [s^{-1}]. This file and other files can be found at `p:\xbeach\msc_studies\Patrick_Oosterlo` (only on the Deltares network).

```
Hm0        =     3.8631
fp         =     0.1239
mainang    =   270.0000
gammajsp   =     3.3000
s          =     5.7500
fnyq       =     1.0000
```

G.3. TIDE

The tide file defines the water level boundary conditions. The first column represents the time in seconds, the second and third column the water level in metres. This file and other files can be found at `p:\xbeach\msc_studies\Patrick_Oosterlo` (only on the Deltares network).

```
    0.0000000e+00  -1.9696710e+00  -1.9696710e+00
    1.8000000e+03  -2.1216953e+00  -2.1216953e+00
    3.6000000e+03  -2.1366320e+00  -2.1366320e+00
    5.4000000e+03  -2.0133511e+00  -2.0133511e+00
    7.2000000e+03  -1.7594001e+00  -1.7594001e+00
    9.0000000e+03  -1.3905246e+00  -1.3905246e+00
    1.0800000e+04  -9.2966806e-01  -9.2966806e-01
    1.2600000e+04  -4.0551350e-01  -4.0551350e-01
    1.4400000e+04   1.4933951e-01   1.4933951e-01
    1.6200000e+04   7.0044661e-01   7.0044661e-01
    1.8000000e+04   1.2137076e+00   1.2137076e+00
    1.9800000e+04   1.6575328e+00   1.6575328e+00
    2.1600000e+04   2.0048497e+00   2.0048497e+00
    2.3400000e+04   2.2348213e+00   2.2348213e+00
    2.5200000e+04   2.3341674e+00   2.3341674e+00
    2.7000000e+04   2.2980048e+00   2.2980048e+00
    2.8800000e+04   2.1301529e+00   2.1301529e+00
    3.0600000e+04   1.8428845e+00   1.8428845e+00
    3.2400000e+04   1.4561390e+00   1.4561390e+00
    3.4200000e+04   9.9624724e-01   9.9624724e-01
    3.6000000e+04   4.9424937e-01   4.9424937e-01
    3.7800000e+04  -1.6087356e-02  -1.6087356e-02
```

```
23     3.9600000e+04  -5.0042433e-01  -5.0042433e-01
24     4.1400000e+04  -9.2604392e-01  -9.2604392e-01
25     4.3200000e+04  -1.2639388e+00  -1.2639388e+00
26     4.5000000e+04  -1.4906650e+00  -1.4906650e+00
27     4.6800000e+04  -1.5898417e+00  -1.5898417e+00
28     4.8600000e+04  -1.5532004e+00  -1.5532004e+00
29     5.0400000e+04  -1.3811188e+00  -1.3811188e+00
30     5.2200000e+04  -1.0826043e+00  -1.0826043e+00
31     5.4000000e+04  -6.7472760e-01  -6.7472760e-01
32     5.5800000e+04  -1.8154371e-01  -1.8154371e-01
33     5.7600000e+04   3.6743170e-01   3.6743170e-01
34     5.9400000e+04   9.3909386e-01   9.3909386e-01
35     6.1200000e+04   1.4988488e+00   1.4988488e+00
36     6.3000000e+04   2.0128083e+00   2.0128083e+00
37     6.4800000e+04   2.4499400e+00   2.4499400e+00
38     6.6600000e+04   2.7840361e+00   2.7840361e+00
39     6.8400000e+04   2.9953754e+00   2.9953754e+00
40     7.0200000e+04   3.0719722e+00   3.0719722e+00
41     7.2000000e+04   3.0103340e+00   3.0103340e+00
42     7.3800000e+04   2.8156783e+00   2.8156783e+00
43     7.5600000e+04   2.5015961e+00   2.5015961e+00
44     7.7400000e+04   2.0891819e+00   2.0891819e+00
45     7.9200000e+04   1.6056874e+00   1.6056874e+00
46     8.1000000e+04   1.0827834e+00   1.0827834e+00
47     8.2800000e+04   5.5454074e-01   5.5454074e-01
48     8.4600000e+04   5.5259097e-02   5.5259097e-02
49     8.6400000e+04  -3.8271850e-01  -3.8271850e-01
50     8.8200000e+04  -7.3106612e-01  -7.3106612e-01
51     9.0000000e+04  -9.6727935e-01  -9.6727935e-01
52     9.1800000e+04  -1.0761088e+00  -1.0761088e+00
53     9.3600000e+04  -1.0505312e+00  -1.0505312e+00
54     9.5400000e+04  -8.9219718e-01  -8.9219718e-01
55     9.7200000e+04  -6.1132559e-01  -6.1132559e-01
56     9.9000000e+04  -2.2605302e-01  -2.2605302e-01
57     1.0080000e+05   2.3872158e-01   2.3872158e-01
58     1.0260000e+05   7.5292290e-01   7.5292290e-01
59     1.0440000e+05   1.2832151e+00   1.2832151e+00
60     1.0620000e+05   1.7951259e+00   1.7951259e+00
61     1.0800000e+05   2.2552427e+00   2.2552427e+00
62     1.0980000e+05   2.6333425e+00   2.6333425e+00
63     1.1160000e+05   2.9043187e+00   2.9043187e+00
64     1.1340000e+05   3.0497831e+00   3.0497831e+00
65     1.1520000e+05   3.0592399e+00   3.0592399e+00
66     1.1700000e+05   2.9307588e+00   2.9307588e+00
67     1.1880000e+05   2.6711027e+00   2.6711027e+00
68     1.2060000e+05   2.2953022e+00   2.2953022e+00
69     1.2240000e+05   1.8257055e+00   1.8257055e+00
70     1.2420000e+05   1.2905610e+00   1.2905610e+00
71     1.2600000e+05   7.2222648e-01   7.2222648e-01
72     1.2780000e+05   1.5511564e-01   1.5511564e-01
73     1.2960000e+05  -3.7648515e-01  -3.7648515e-01
74     1.3140000e+05  -8.4059226e-01  -8.4059226e-01
75     1.3320000e+05  -1.2095533e+00  -1.2095533e+00
76     1.3500000e+05  -1.4617999e+00  -1.4617999e+00
77     1.3680000e+05  -1.5832132e+00  -1.5832132e+00
78     1.3860000e+05  -1.5680151e+00  -1.5680151e+00
79     1.4040000e+05  -1.4191289e+00  -1.4191289e+00
80     1.4220000e+05  -1.1479856e+00  -1.1479856e+00
81     1.4400000e+05  -7.7378913e-01  -7.7378913e-01
82     1.4580000e+05  -3.2228722e-01  -3.2228722e-01
83     1.4760000e+05   1.7587483e-01   1.7587483e-01
84     1.4940000e+05   6.8711146e-01   6.8711146e-01
85     1.5120000e+05   1.1770414e+00   1.1770414e+00
86     1.5300000e+05   1.6126825e+00   1.6126825e+00
87     1.5480000e+05   1.9645577e+00   1.9645577e+00
88     1.5660000e+05   2.2085777e+00   2.2085777e+00
89     1.5840000e+05   2.3275798e+00   2.3275798e+00
90     1.6020000e+05   2.3124269e+00   2.3124269e+00
91     1.6200000e+05   2.1625947e+00   2.1625947e+00
92     1.6380000e+05   1.8862103e+00   1.8862103e+00
93     1.6560000e+05   1.4995407e+00   1.4995407e+00
```

```
94    1.6740000e+05   1.0259624e+00   1.0259624e+00
95    1.6920000e+05   4.9447797e-01   4.9447797e-01
96    1.7100000e+05  -6.2124954e-02  -6.2124954e-02
97    1.7280000e+05  -6.0935679e-01  -6.0935679e-01
98    1.7460000e+05  -1.1132174e+00  -1.1132174e+00
99    1.7640000e+05  -1.5423566e+00  -1.5423566e+00
100   1.7820000e+05  -1.8700670e+00  -1.8700670e+00
101   1.8000000e+05  -2.0759812e+00  -2.0759812e+00
102   1.8180000e+05  -2.1473663e+00  -2.1473663e+00
103   1.8360000e+05  -2.0799326e+00  -2.0799326e+00
104   1.8540000e+05  -1.8781060e+00  -1.8781060e+00
105   1.8720000e+05  -1.5547455e+00  -1.5547455e+00
```

H

VALIDATION OF XBEACH WITH VAN GENT (1999)

This Appendix presents the results of the validation of wave heights and wave periods of the numerical model XBeach, with the physical model tests as described in Van Gent (1999) (q.v.). Section H.1 describes the results of the A test series, section H.2 describes the results of the C test series. Next, section H.3 presents the results of XBeach non-hydrostatic and XBeach hydrostatic with a lowered breaker index value.

H.1. RESULTS A TEST SERIES

Figures H.1, H.2, H.3 and H.4 show the wave spectra at the toe of the structure for the A test series. The tables below show the results for the A test series, with the results from, cf. Van Gent (1999), XBeach non-hydrostatic with spectral frequency limits 0.02-1.2 Hz, XBeach hydrostatic with a lowered breaker index value and limits 0.02-1.2 Hz, XBeach hydrostatic with limits 0-∞ Hz, XBeach hydrostatic with limits 0.02-1.2 Hz and XBeach hydrostatic with limits $1/(10T_p)$ (T_p at the offshore boundary) until 1.2 Hz.

H.1.1. WAVE SPECTRA A TEST SERIES

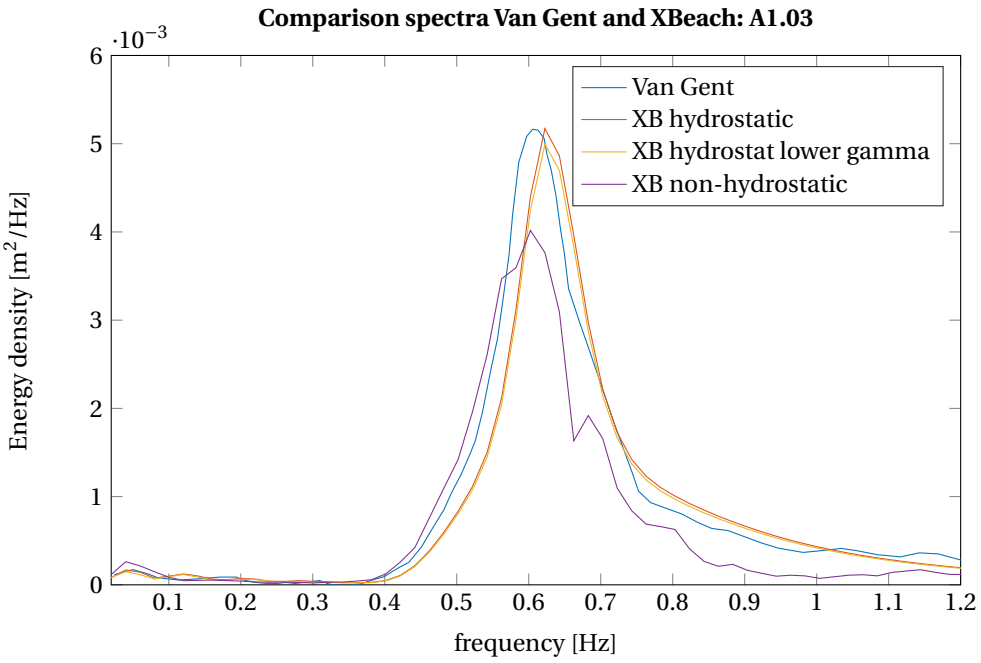

Figure H.1: Spectra for test A1.03, cf. (Van Gent, 1999).

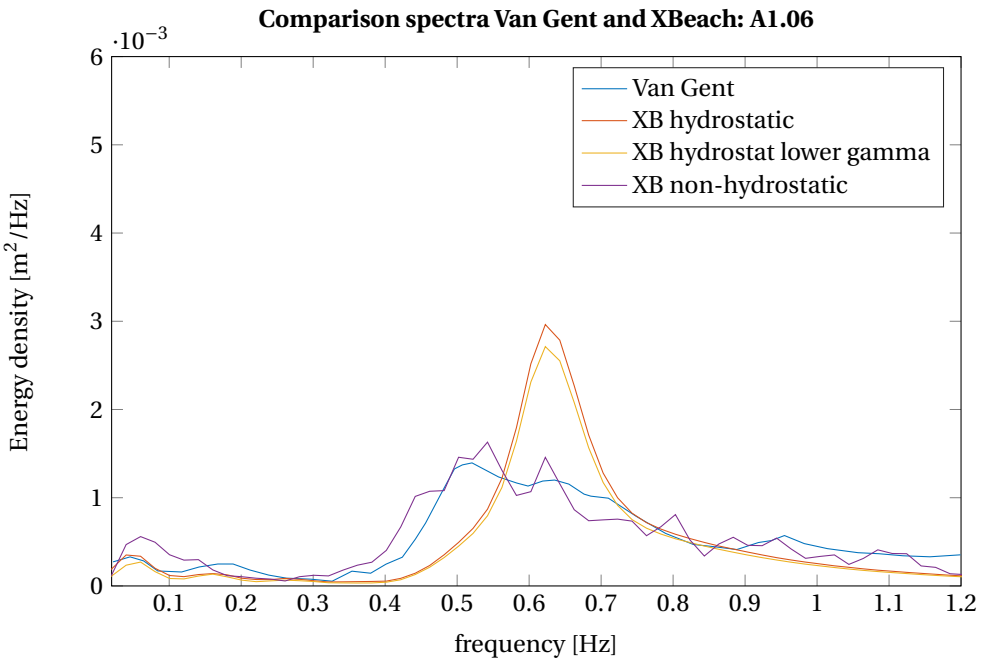

Figure H.2: Spectra for test A1.06, cf. (Van Gent, 1999).

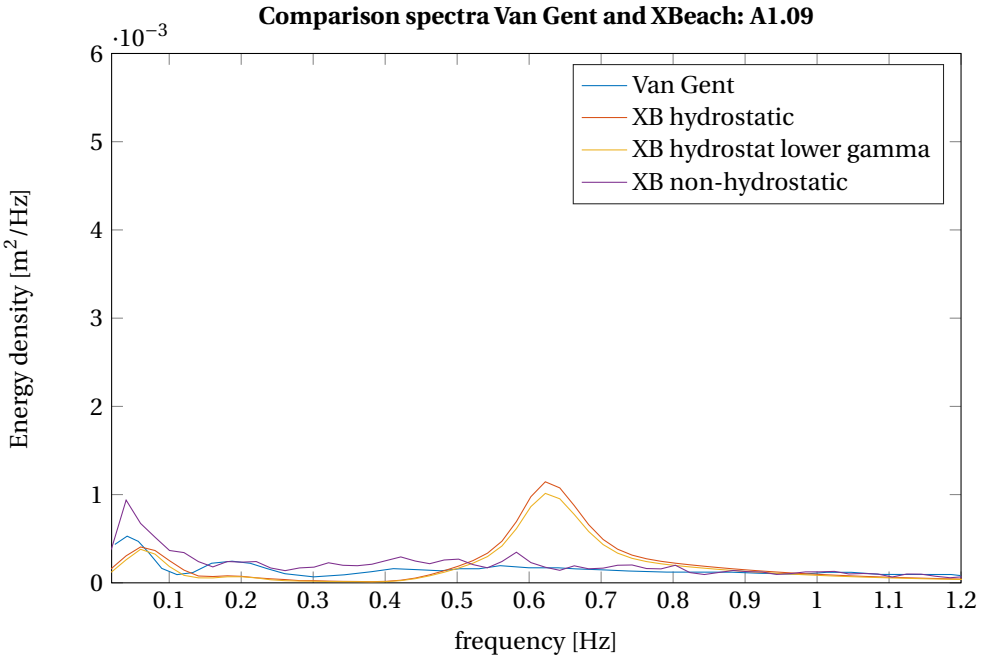

Figure H.3: Spectra for test A1.09, cf. (Van Gent, 1999).

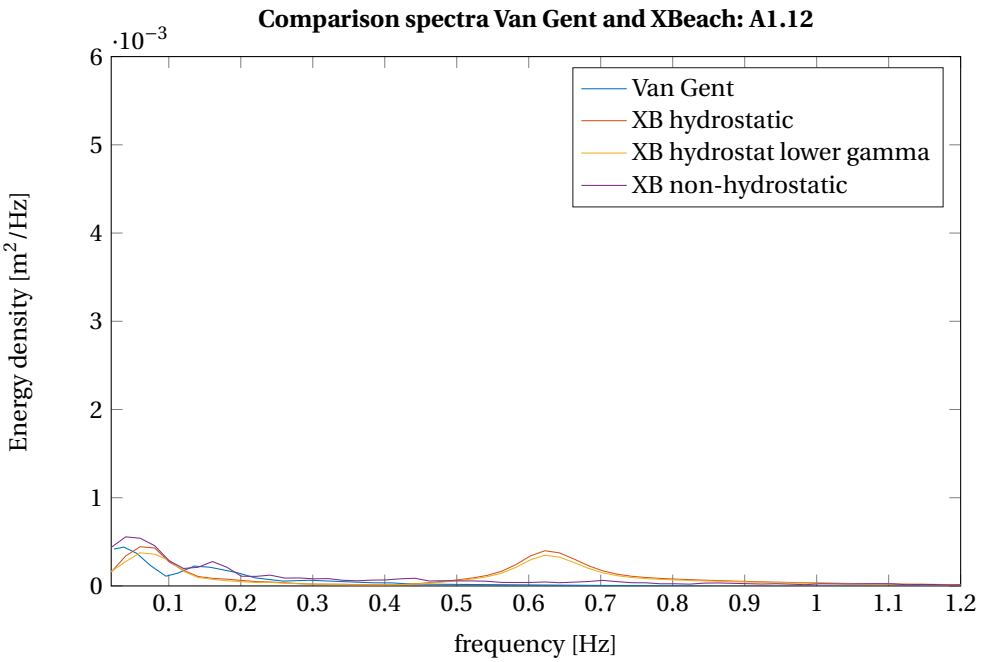

Figure H.4: Spectra for test A1.12, cf. (Van Gent, 1999).

H.1.2. TABLES A TEST SERIES

Table H.1: Results for test A1.03, offshore H_{m0} 0.141 m, offshore T_p 1.6 s.

A1.03, foreshore 1:100, structure slope 1:4	Distance from toe [m]	d [m]	H_{m0} [m]	$T_{m-1,0}$ [s]
Van Gent (1999)	-36	0.753	0.152	1.47
	-30	0.653	0.149	1.55
	-20	0.553	0.143	1.59
	-10	0.453	0.137	1.65
	0	0.353	0.134	1.59
XB non-hydrostat., freq. limits 0.02-1.2 Hz	-36	0.753	0.1348	1.5708
	-30	0.653	0.1287	1.6194
	-20	0.553	0.1229	1.7066
	-10	0.453	0.1181	1.806
	0	0.353	0.1132	1.9739
XB hydrostat. + lowered $gamma$, freq. limits 0.02-1.2 Hz	-36	0.753	0.1396	1.4658
	-30	0.653	0.1385	1.4887
	-20	0.553	0.137	1.5287
	-10	0.453	0.1342	1.5817
	0	0.353	0.1268	1.6697
XB hydrostat., freq. limits 0-∞ Hz	-36	0.753	0.141	1.4481
	-30	0.653	0.1398	1.4734
	-20	0.553	0.1386	1.5213
	-10	0.453	0.1365	1.5938
	0	0.353	0.1311	1.7195
XB hydrostat., freq. limits 0.02-1.2 Hz	-36	0.753	0.139	1.466
	-30	0.653	0.1379	1.4908
	-20	0.553	0.1366	1.5342
	-10	0.453	0.1346	1.5924
	0	0.353	0.1292	1.6829
XB hydrostat., freq. limits $1/(10T_p)$-1.2 Hz	-36	0.753	0.139	1.4634
	-30	0.653	0.1378	1.4783
	-20	0.553	0.1364	1.4877
	-10	0.453	0.1343	1.4991
	0	0.353	0.1287	1.5389

Table H.2: Results for test A1.06, offshore H_{m0} 0.141 m, offshore T_p 1.6 s.

A1.06, foreshore 1:100, structure slope 1:4	Distance from toe [m]	d [m]	H_{m0} [m]	$T_{m-1,0}$ [s]
Van Gent (1999)	-36	0.588	0.146	1.47
	-30	0.488	0.143	1.54
	-20	0.388	0.137	1.63
	-10	0.288	0.128	1.73
	0	0.188	0.104	1.89
XB non-hydrostat., freq. limits 0.02-1.2 Hz	-36	0.588	0.1375	1.5593
	-30	0.488	0.1314	1.6409
	-20	0.388	0.1248	1.8401
	-10	0.288	0.1177	2.1282
	0	0.188	0.1013	2.6001
XB hydrostat. + lowered $gamma$, freq. limits 0.02-1.2 Hz	-36	0.588	0.1382	1.4728
	-30	0.488	0.1372	1.5237
	-20	0.388	0.133	1.6296
	-10	0.288	0.121	1.7694
	0	0.188	0.0958	2.0428
XB hydrostat., freq. limits 0-∞ Hz	-36	0.588	0.1405	1.4623
	-30	0.488	0.1396	1.5192
	-20	0.388	0.1361	1.6607
	-10	0.288	0.126	1.8929
	0	0.188	0.1024	2.3844
XB hydrostat., freq. limits 0.02-1.2 Hz	-36	0.588	0.1385	1.474
	-30	0.488	0.1377	1.529
	-20	0.388	0.1342	1.6558
	-10	0.288	0.1241	1.8469
	0	0.188	0.1008	2.2023
XB hydrostat., freq. limits $1/(10T_p)$-1.2 Hz	-36	0.588	0.1385	1.4688
	-30	0.488	0.1376	1.5028
	-20	0.388	0.1338	1.544
	-10	0.288	0.1232	1.5863
	0	0.188	0.0994	1.6738

Table H.3: Results for test A1.09, offshore H_{m0} 0.141 m, offshore T_p 1.6 s.

A1.09, foreshore 1:100, structure slope 1:4	Distance from toe [m]	d [m]	H_{m0} [m]	$T_{m-1,0}$ [s]
Van Gent (1999)	-36	0.494	0.143	1.51
	-30	0.394	0.139	1.6
	-20	0.294	0.131	1.76
	-10	0.194	0.107	1.97
	0	0.094	0.057	3.2
XB non-hydrostat., freq. limits 0.02-1.2 Hz	-36	0.494	0.1363	1.574
	-30	0.394	0.1299	1.7155
	-20	0.294	0.1216	2.1004
	-10	0.194	0.1045	2.8939
	0	0.094	0.063	5.9623
XB hydrostat. + lowered $gamma$, freq. limits 0.02-1.2 Hz	-36	0.494	0.1377	1.4839
	-30	0.394	0.1346	1.5741
	-20	0.294	0.1238	1.7647
	-10	0.194	0.0997	2.0755
	0	0.094	0.0615	3.1721
XB hydrostat., freq. limits 0-∞ Hz	-36	0.494	0.1404	1.4723
	-30	0.394	0.1388	1.5725
	-20	0.294	0.13	1.8051
	-10	0.194	0.1068	2.2033
	0	0.094	0.0667	3.7616
XB hydrostat., freq. limits 0.02-1.2 Hz	-36	0.494	0.1384	1.4851
	-30	0.394	0.1368	1.5814
	-20	0.294	0.1282	1.7915
	-10	0.194	0.1052	2.125
	0	0.094	0.0657	3.2583
XB hydrostat., freq. limits $1/(10T_p)$-1.2 Hz	-36	0.494	0.1384	1.4767
	-30	0.394	0.1367	1.5441
	-20	0.294	0.1277	1.647
	-10	0.194	0.1041	1.7563
	0	0.094	0.0636	2.1057

Table H.4: Results for test A1.12, offshore H_{m0} 0.141 m, offshore T_p 1.6 s.

A1.12, foreshore 1:100, structure slope 1:4	Distance from toe [m]	d [m]	H_{m0} [m]	$T_{m-1,0}$ [s]
Van Gent (1999)	-36	0.447	0.141	1.51
	-30	0.347	0.134	1.64
	-20	0.247	0.121	1.9
	-10	0.147	0.086	2.32
	0	0.047	0.036	7.33
XB non-hydrostat., freq. limits 0.02-1.2 Hz	-36	0.447	0.1349	1.5758
	-30	0.347	0.1278	1.7305
	-20	0.247	0.1167	2.1961
	-10	0.147	0.0881	3.2548
	0	0.047	0.0421	9.4251
XB hydrostat. + lowered $gamma$, freq. limits 0.02-1.2 Hz	-36	0.447	0.1356	1.497
	-30	0.347	0.1311	1.6181
	-20	0.247	0.1152	1.886
	-10	0.147	0.0846	2.4311
	0	0.047	0.0423	5.6664
XB hydrostat., freq. limits 0-∞ Hz	-36	0.447	0.1391	1.4804
	-30	0.347	0.1363	1.6054
	-20	0.247	0.1226	1.9184
	-10	0.147	0.0914	2.6112
	0	0.047	0.046	6.7849
XB hydrostat., freq. limits 0.02-1.2 Hz	-36	0.447	0.1371	1.4913
	-30	0.347	0.1344	1.6134
	-20	0.247	0.1209	1.901
	-10	0.147	0.0901	2.43
	0	0.047	0.0452	5.5846
XB hydrostat., freq. limits $1/(10T_p)$-1.2 Hz	-36	0.447	0.1371	1.4814
	-30	0.347	0.1342	1.5701
	-20	0.247	0.1202	1.7175
	-10	0.147	0.0888	1.9284
	0	0.047	0.0418	3.17

H.2. RESULTS C TEST SERIES

The tables below show the results for the C test series, with the results from Van Gent (1999), XBeach non-hydrostatic with spectral frequency limits 0.02-1.2 Hz, XBeach hydrostatic with a lowered breaker index value and limits 0.02-1.2 Hz, XBeach hydrostatic with limits 0-∞ Hz, XBeach hydrostatic with limits 0.02-1.2 Hz and XBeach hydrostatic with limits $1/(10T_p)$ (T_p at the offshore boundary) until 1.2 Hz.

H.2.1. TABLES C TEST SERIES

Table H.5: Results for test C1.03, offshore H_{m0} 0.141 m, offshore T_p 1.6 s.

C1.03, foreshore 1:250, structure slope 1:2.5	Distance from toe [m]	d [m]	H_{m0} [m]	$T_{m-1,0}$ [s]
Van Gent (1999)	-36	0.753	0.151	1.46
	-30	0.653	0.141	1.53
	-20	0.553	0.137	1.61
	-10	0.453	0.134	1.61
	0	0.353	0.132	1.64
XB non-hydrostat., freq. limits 0.02-1.2 Hz	-36	0.753	0.1358	1.5632
	-30	0.653	0.1235	1.6436
	-20	0.553	0.1194	1.8608
	-10	0.453	0.1158	2.0711
	0	0.353	0.1115	2.2777
XB hydrostat. + lowered $gamma$, freq. limits 0.02-1.2 Hz	-36	0.753	0.1392	1.4659
	-30	0.653	0.1356	1.5087
	-20	0.553	0.1318	1.6332
	-10	0.453	0.1279	1.7116
	0	0.353	0.1232	1.7696
XB hydrostat., freq. limits 0-∞ Hz	-36	0.753	0.1412	1.4502
	-30	0.653	0.1382	1.4976
	-20	0.553	0.1356	1.644
	-10	0.453	0.1326	1.7448
	0	0.353	0.1283	1.8417
XB hydrostat., freq. limits 0.02-1.2 Hz	-36	0.753	0.1392	1.4664
	-30	0.653	0.1363	1.5122
	-20	0.553	0.1337	1.6473
	-10	0.453	0.1307	1.7333
	0	0.353	0.1265	1.7963
XB hydrostat., freq. limits $1/(10T_p)$-1.2 Hz	-36	0.753	0.1392	1.4634
	-30	0.653	0.1362	1.4936
	-20	0.553	0.1334	1.5617
	-10	0.453	0.1301	1.5595
	0	0.353	0.1256	1.5411

Table H.6: Results for test C1.06, offshore H_{m0} 0.141 m, offshore T_p 1.6 s.

C1.06, foreshore 1:250, structure slope 1:2.5	Distance from toe [m]	d [m]	H_{m0} [m]	$T_{m-1,0}$ [s]
Van Gent (1999)	-36	0.588	0.146	1.5
	-30	0.488	0.126	1.62
	-20	0.388	0.119	1.84
	-10	0.288	0.114	2.01
	0	0.188	0.099	2.17
XB non-hydrostat., freq. limits 0.02-1.2 Hz	-36	0.588	0.1366	1.5608
	-30	0.488	0.1216	1.6903
	-20	0.388	0.1116	2.2236
	-10	0.288	0.0999	2.7924
	0	0.188	0.0861	3.539
XB hydrostat. + lowered $gamma$, freq. limits 0.02-1.2 Hz	-36	0.588	0.1386	1.4759
	-30	0.488	0.1238	1.5869
	-20	0.388	0.1115	1.8651
	-10	0.288	0.1012	2.0533
	0	0.188	0.0906	2.2376
XB hydrostat., freq. limits 0-∞ Hz	-36	0.588	0.1415	1.4635
	-30	0.488	0.1309	1.5892
	-20	0.388	0.1196	1.9194
	-10	0.288	0.1092	2.1453
	0	0.188	0.0979	2.3847
XB hydrostat., freq. limits 0.02-1.2 Hz	-36	0.588	0.1395	1.4749
	-30	0.488	0.1291	1.5793
	-20	0.388	0.118	1.8677
	-10	0.288	0.1077	2.0325
	0	0.188	0.0965	2.192
XB hydrostat., freq. limits $1/(10T_p)$-1.2 Hz	-36	0.588	0.1395	1.4688
	-30	0.488	0.129	1.5435
	-20	0.388	0.1174	1.7164
	-10	0.288	0.1067	1.7397
	0	0.188	0.0952	1.736

Table H.7: Results for test C1.09, offshore H_{m0} 0.141 m, offshore T_p 1.6 s.

C1.09, foreshore 1:250, structure slope 1:2.5	Distance from toe [m]	d [m]	H_{m0} [m]	$T_{m-1,0}$ [s]
Van Gent (1999)	-36	0.494	0.14	1.49
	-30	0.394	0.099	1.68
	-20	0.294	0.084	1.95
	-10	0.194	0.075	2.34
	0	0.094	0.05	2.85
XB non-hydrostat., freq. limits 0.02-1.2 Hz	-36	0.494	0.1364	1.5664
	-30	0.394	0.1049	1.831
	-20	0.294	0.0782	3.0032
	-10	0.194	0.0576	4.6432
	0	0.094	0.0416	6.8712
XB hydrostat. + lowered $gamma$, freq. limits 0.02-1.2 Hz	-36	0.494	0.1371	1.4868
	-30	0.394	0.1011	1.719
	-20	0.294	0.0835	2.0215
	-10	0.194	0.07	2.2779
	0	0.094	0.0561	2.6596
XB hydrostat., freq. limits 0-∞ Hz	-36	0.494	0.1399	1.4877
	-30	0.394	0.1071	1.8914
	-20	0.294	0.0899	2.4158
	-10	0.194	0.0757	2.9488
	0	0.094	0.061	3.7028
XB hydrostat., freq. limits 0.02-1.2 Hz	-36	0.494	0.1379	1.4903
	-30	0.394	0.1055	1.7319
	-20	0.294	0.0885	2.0937
	-10	0.194	0.0745	2.3697
	0	0.094	0.0599	2.7496
XB hydrostat., freq. limits $1/(10T_p)$-1.2 Hz	-36	0.494	0.1379	1.4752
	-30	0.394	0.1052	1.6156
	-20	0.294	0.0878	1.8078
	-10	0.194	0.0735	1.8586
	0	0.094	0.0586	1.931

Table H.8: Results for test C1.12, offshore H_{m0} 0.141 m, offshore T_p 1.6 s.

C1.12, foreshore 1:250, structure slope 1:2.5	Distance from toe [m]	d [m]	H_{m0} [m]	$T_{m-1,0}$ [s]
Van Gent (1999)	-36	0.447	0.139	1.52
	-30	0.347	0.079	2.05
	-20	0.247	0.06	2.2
	-10	0.147	0.049	2.52
	0	0.047	0.024	4.27
XB non-hydrostat., freq. limits 0.02-1.2 Hz	-36	0.447	0.1351	1.5793
	-30	0.347	0.0835	2.3237
	-20	0.247	0.0528	4.5557
	-10	0.147	0.0348	7.8885
	0	0.047	0.0242	12.7332
XB hydrostat. + lowered $gamma$, freq. limits 0.02-1.2 Hz	-36	0.447	0.1363	1.4931
	-30	0.347	0.0831	1.8861
	-20	0.247	0.0643	2.2532
	-10	0.147	0.0495	2.6921
	0	0.047	0.0338	3.8667
XB hydrostat., freq. limits 0-∞ Hz	-36	0.447	0.1384	1.4999
	-30	0.347	0.0888	2.2254
	-20	0.247	0.0696	2.9301
	-10	0.147	0.0538	3.9982
	0	0.047	0.0373	6.7358
XB hydrostat., freq. limits 0.02-1.2 Hz	-36	0.447	0.1364	1.4986
	-30	0.347	0.0875	1.8973
	-20	0.247	0.0685	2.2922
	-10	0.147	0.0528	2.7577
	0	0.047	0.0363	3.8696
XB hydrostat., freq. limits $1/(10T_p)$-1.2 Hz	-36	0.447	0.1363	1.4803
	-30	0.347	0.087	1.6957
	-20	0.247	0.0677	1.8759
	-10	0.147	0.0517	1.9884
	0	0.047	0.0347	2.2418

H.3. RESULTS AND CONCLUSIONS FOR XBEACH NON-HYDROSTATIC AND LOWERED GAMMA

The resulting wave heights and wave periods from the calculated spectra at the five locations along the slope were compared, as well as the spectra at the toe of the structure for the A test series. For the C test series, no spectra were available. The wave periods and wave heights along the slope for the A and C test series were presented in the tables. The tables show the water depth d, wave height H_{m0} and wave period $T_{m-1,0}$ for the five locations along the slope, with $Xtoe = 0$ being at the toe of the structure.

H.3.1. CONCLUSIONS OF VALIDATION

Test A1.03 uses the largest water level, 0.753 m, with the bottom of the flume at 0 m. The spectra at the toe all show quite good agreement . The non-hydrostatic version of XBeach shows the largest difference compared to the physical model test. Test A1.06 uses the intermediate water level of 0.588 m. Here, the physical test and non-hydrostatic version of XBeach show good agreement. Here, XBeach hydrostatic shows a larger energy density in the low frequency range (0.02-0.1 Hz). Near the peak frequency, the hydrostatic model differs considerably from the measurements, because in the hydrostatic model, the spectral transformation of the high frequency wave period is not calculated. Furthermore, the hydrostatic model shows less energy in the very high frequencies. However, the resulting wave parameters from the hydrostatic model agree quite well. Test A1.09 uses a shallow water level of 0.494 m. The spectra agree reasonably. Again, the non-hydrostatic model shows a larger energy density in the low frequencies, but the general shape of the spectrum is represented well. The hydrostatic model shows a peak at the peak frequency. Even though the peak in the low frequencies is larger for the non-hydrostatic model, it is in the same place as the physical model. The low frequency peak of the physical model lies at a somewhat lower frequency than the low frequency peak of the hydrostatic model. Test A1.12 uses a very shallow water level of 0.447 m. Again the peak at the peak frequency in the hydrostatic model is visible, as well as the difference in the location of the low frequency peaks, although they contain approximately the same energy density. Because the wave period $T_{m-1,0}$ is heavily influenced by these low frequencies a difference in the location of these peaks could lead to (large) differences in the wave period.

In general, the wave height is presented quite well by the different models, the wave period shows larger differences, but is still represented reasonably well. At the toe, in general, the frequency limits of 0.02 and 1.2 show the best results. The wave height at the toe shows small differences with the different frequency limits, but the wave period is influenced more severely, which is already clear from the definition of the $T_{m-1,0}$ wave period (the first negative moment), which indicates a large influence of the energy in the low frequencies. Of the different XBeach models, the standard hydrostatic model performs the best in most cases. The non-hydrostatic model describes the shape of the spectrum quite well, but the calculated wave parameters do not agree as well as with the hydrostatic model. The difference is caused by the fact that Van Gent (1999) used frequencies larger than 1.2 Hz to calculate the wave parameters, which were not included in the figures of the spectra. Furthermore, XBeach underestimates these very high frequencies.

In general, the differences between the physical model tests and XBeach hydrostatic with limits 0.02-1.2 Hz are reasonably small. The model with the lowered breaker index value overestimates the wave period somewhat. As mentioned above, in some situations the non-hydrostatic model shows more energy in the low frequencies, which, as shown in the tables, leads to an overestimation of the wave period at the toe compared to the physical model tests. The low frequency waves can be of influence on the wave overtopping, so it is recommended to study the influence of these low frequency waves on wave overtopping in more depth. Because the standard hydrostatic model and the frequency limits of 0.02-1.2 Hz perform the best, these were chosen for the thesis.

I

SENSITIVITY ANALYSIS: BED LEVEL CHANGES

This Appendix presents the bed level changes for each parameter in the sensitivity analysis. The figures in each of the sections show the bed level at the start of the simulations, the bed level at the end of the standard case and the bed level at the end of each of the simulations with one parameter changed.

I.1. OFFSHORE CONDITIONS

The figure below shows the resulting bed levels for the higher and lower offshore conditions.

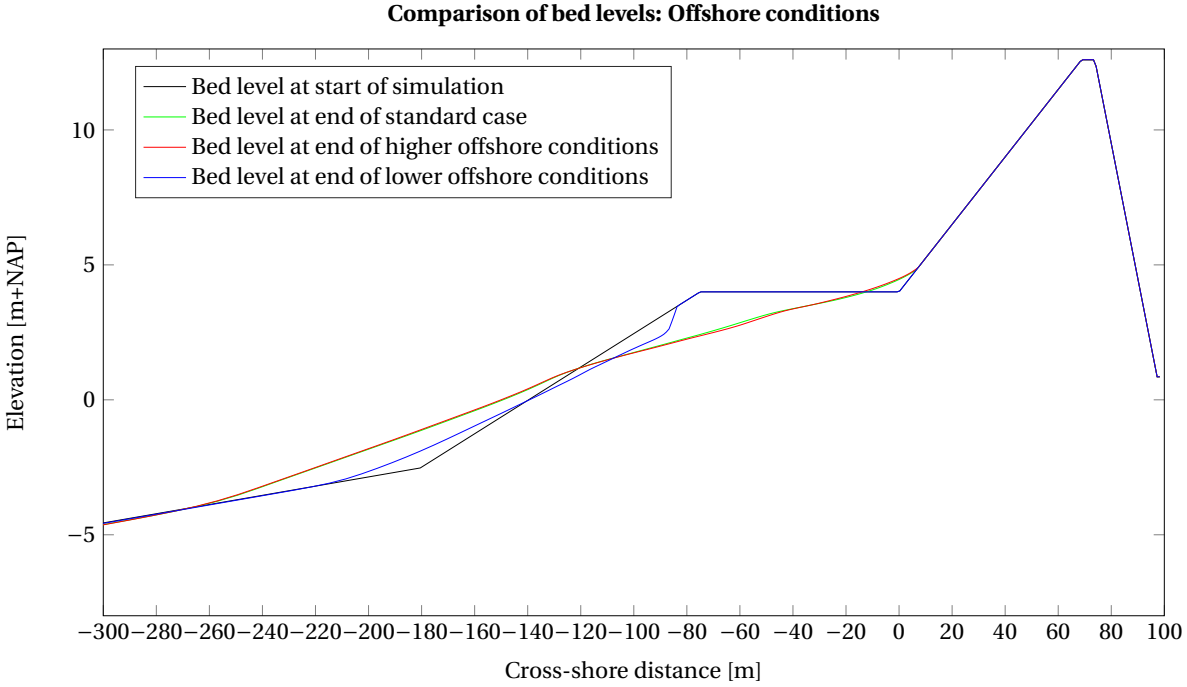

Figure I.1: Bed levels resulting from the sensitivity analysis. Upper part of the cross-shore profile, showing the foreshore and the dike.

I.2. EUROTOP COEFFICIENTS

The EurOtop coefficients do not influence the bed level, which is therefore the same as with the standard case.

I.3. BREAKER INDEX

The figure below shows the resulting bed levels for the higher and lower breaker index.

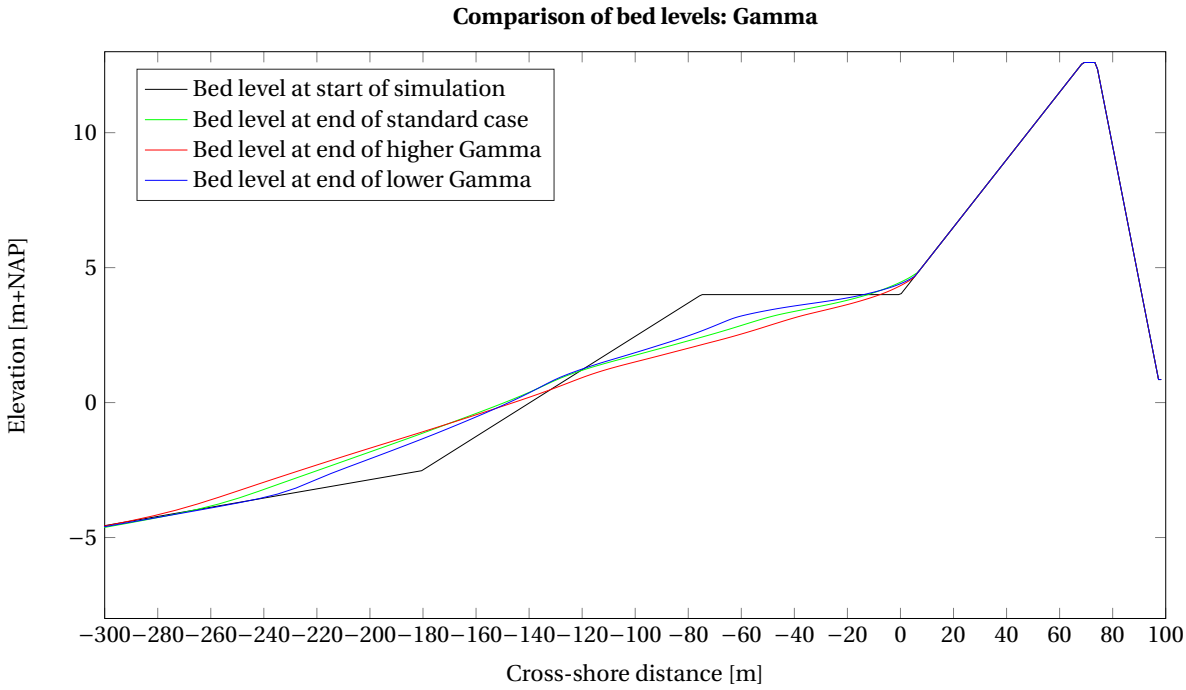

Figure I.2: Bed levels resulting from the sensitivity analysis. Upper part of the cross-shore profile, showing the foreshore and the dike.

I.4. MANNING FRICTION COEFFICIENT

The figure below shows the resulting bed levels for the higher and lower Manning friction coefficient.

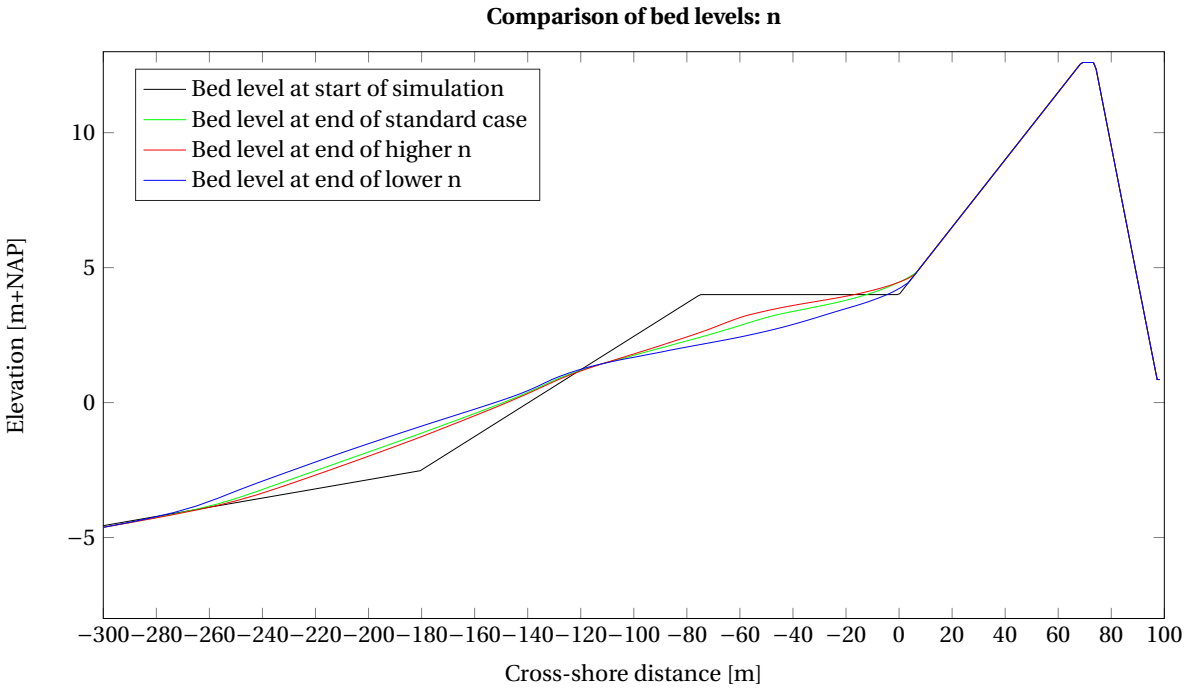

Figure I.3: Bed levels resulting from the sensitivity analysis. Upper part of the cross-shore profile, showing the foreshore and the dike.

I.5. WAVE DIRECTIONAL SPREADING

The figure below shows the resulting bed levels for the higher and lower JONSWAP wave directional spreading values.

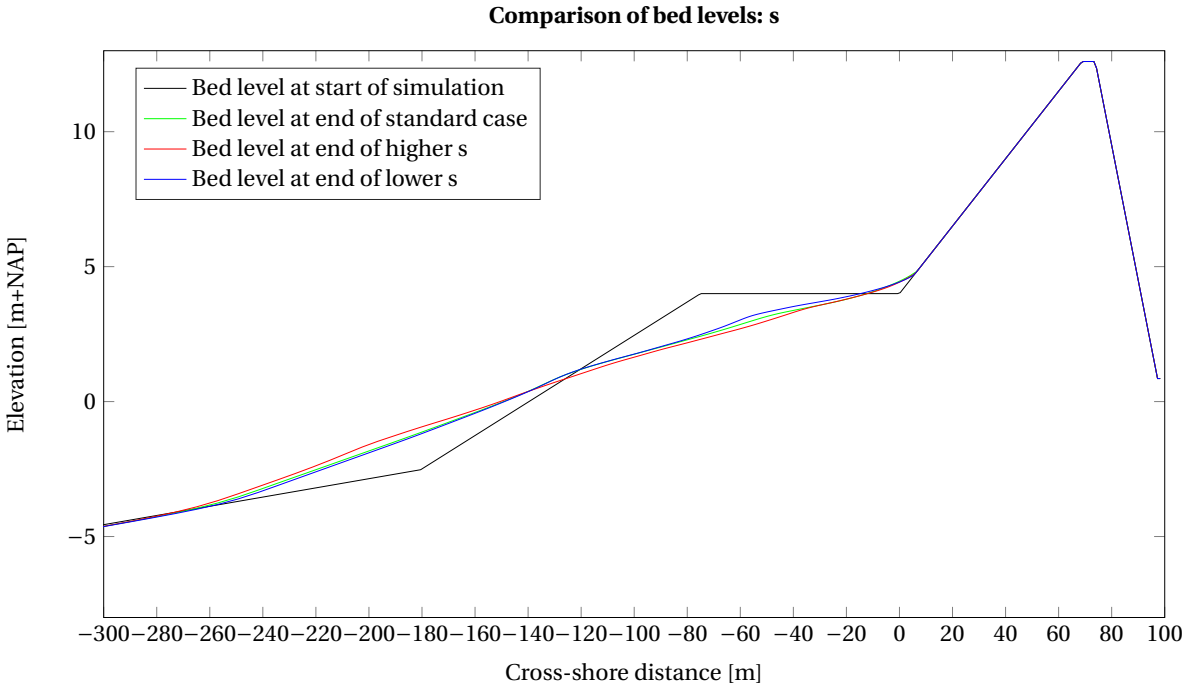

Figure I.4: Bed levels resulting from the sensitivity analysis. Upper part of the cross-shore profile, showing the foreshore and the dike.

I.6. STORM DURATION

The figure below shows the resulting bed levels for the higher and lower storm duration.

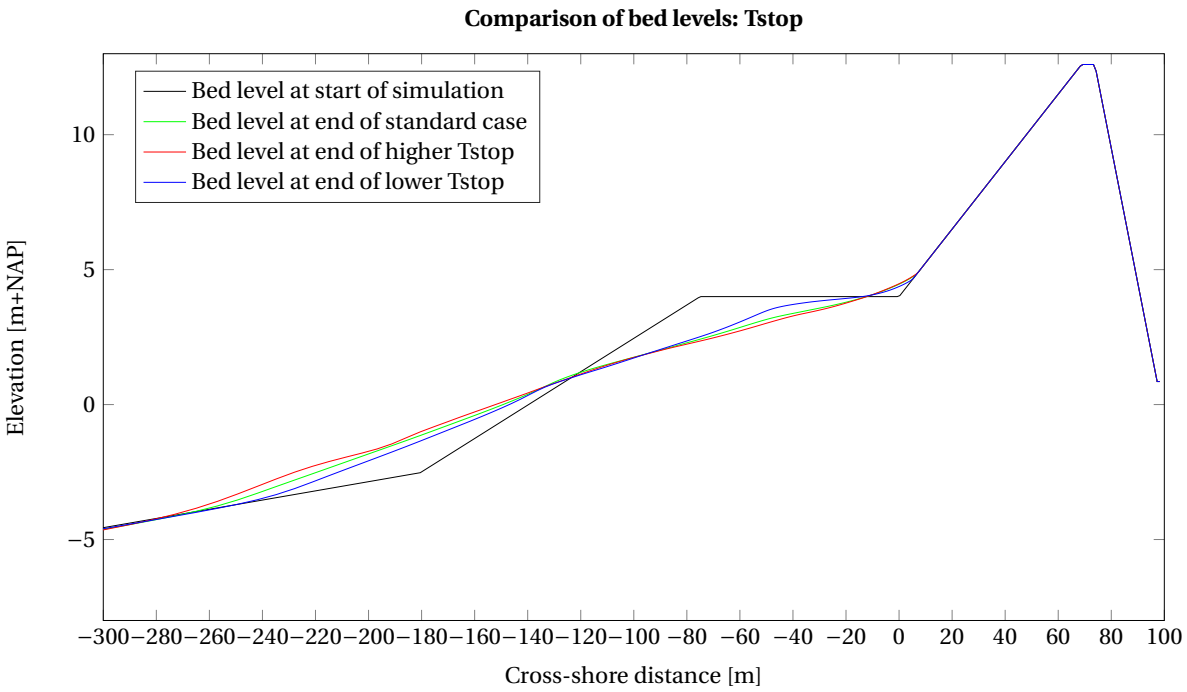

Figure I.5: Bed levels resulting from the sensitivity analysis. Upper part of the cross-shore profile, showing the foreshore and the dike.

I.7. LOCATION OF TIDAL PEAK

The figure below shows the resulting bed levels for the situation in which the peak of the tide does not coincide with the peak of the surge.

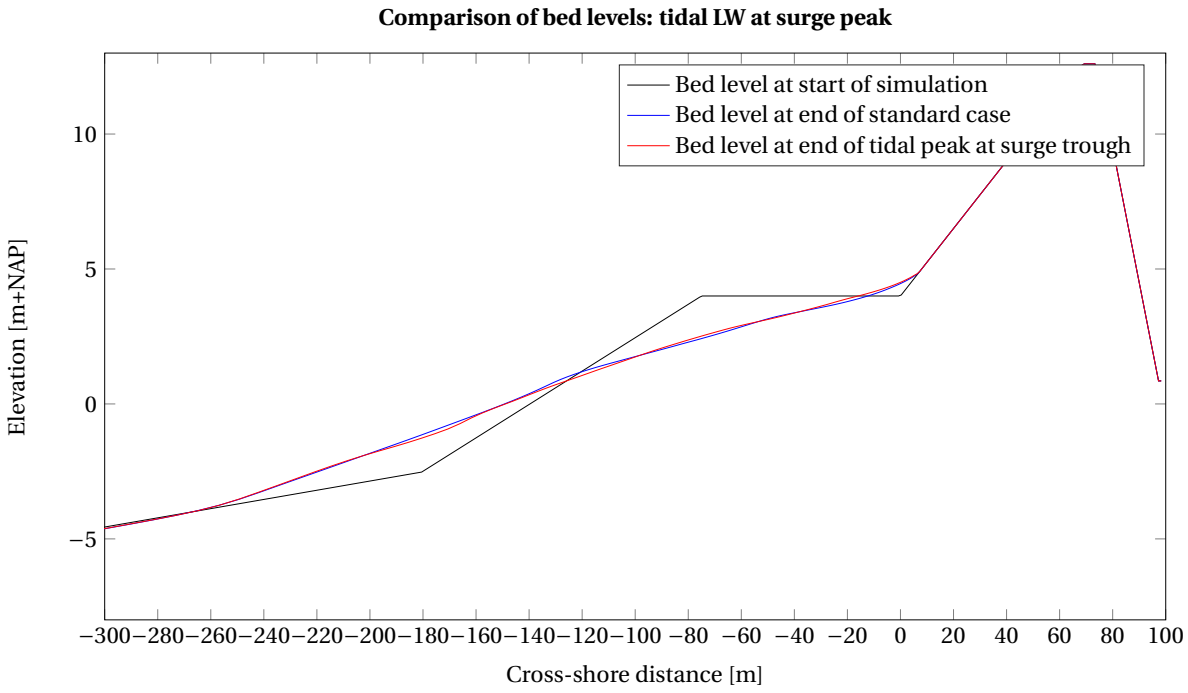

Figure I.6: Bed levels resulting from the sensitivity analysis. Upper part of the cross-shore profile, showing the foreshore and the dike.

I.8. GRAIN DIAMETER

The figure below shows the resulting bed levels for the higher and lower grain diameter.

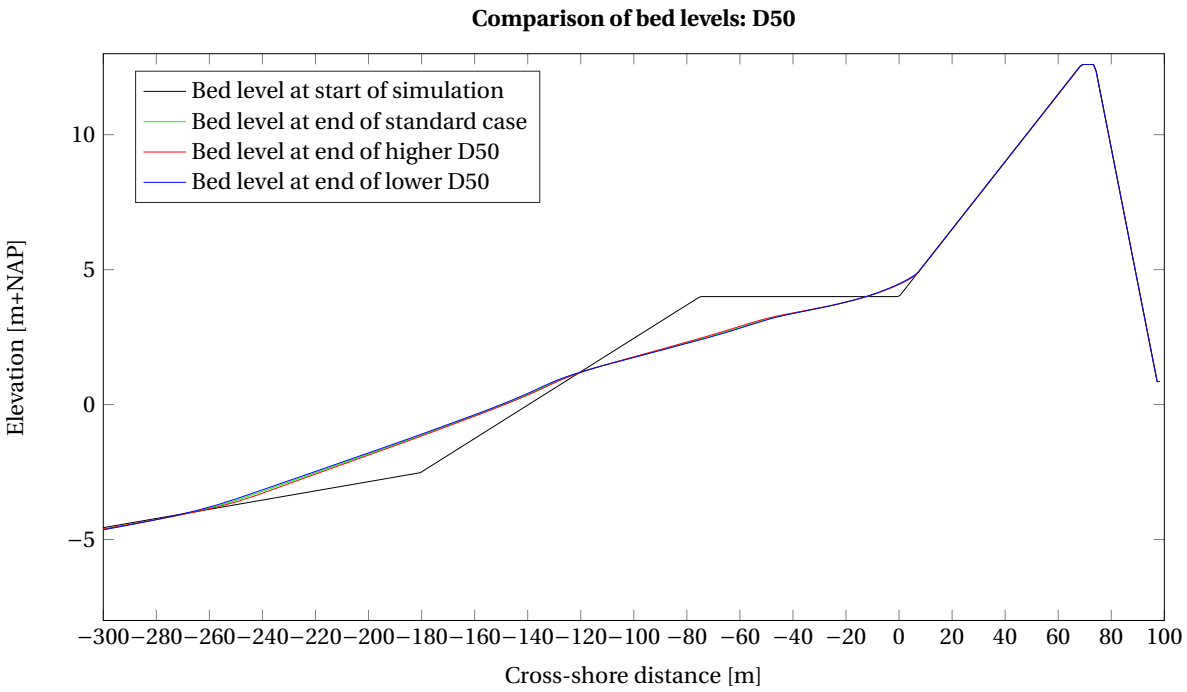

Figure I.7: Bed levels resulting from the sensitivity analysis. Upper part of the cross-shore profile, showing the foreshore and the dike.

I.9. WAVE ASYMMETRY FACTOR

The figure below shows the resulting bed levels for the higher and lower calibration factor for the wave asymmetry.

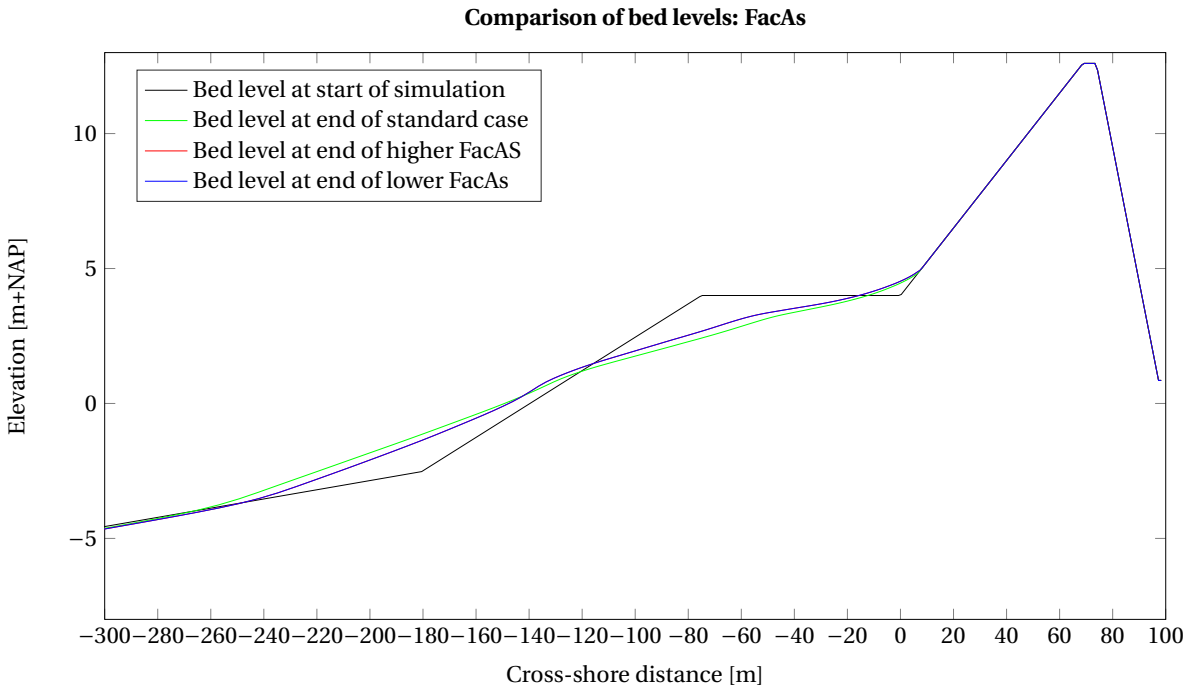

Figure I.8: Bed levels resulting from the sensitivity analysis. Upper part of the cross-shore profile, showing the foreshore and the dike.

I.10. WAVE SKEWNESS FACTOR

The figure below shows the resulting bed levels for the higher and lower calibration factor for the wave skewness.

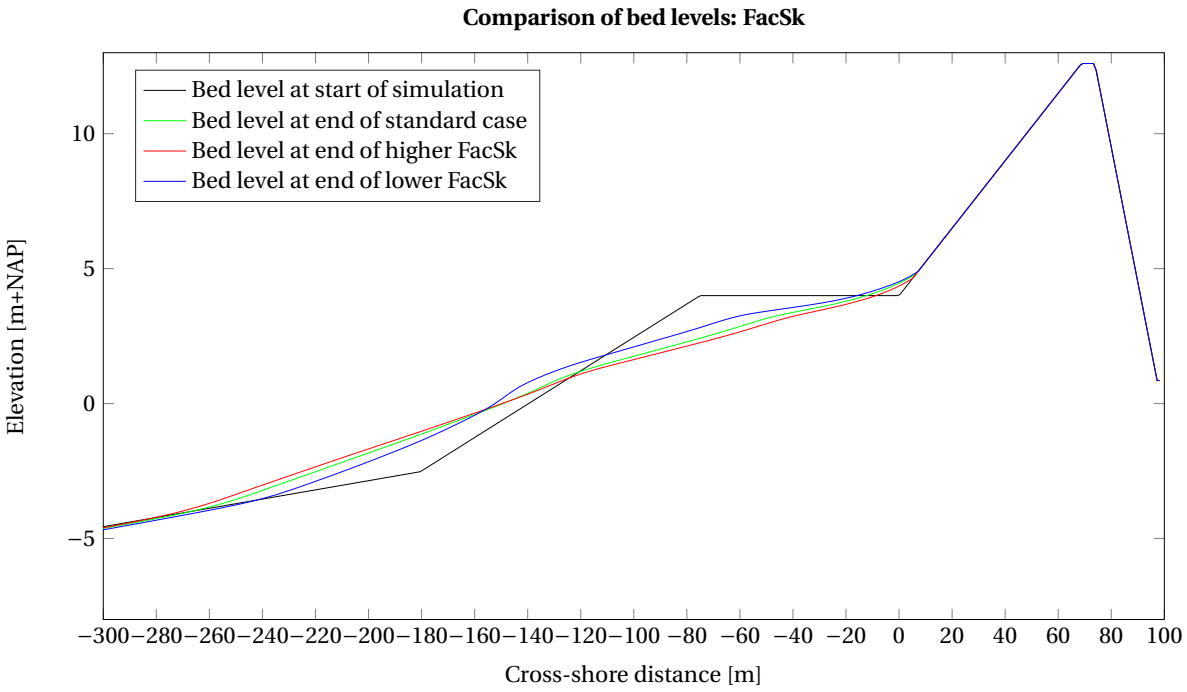

Figure I.9: Bed levels resulting from the sensitivity analysis. Upper part of the cross-shore profile, showing the foreshore and the dike.

I.11. DIKE SLOPE

The figure below shows the resulting bed levels for the higher and lower dike slope value.

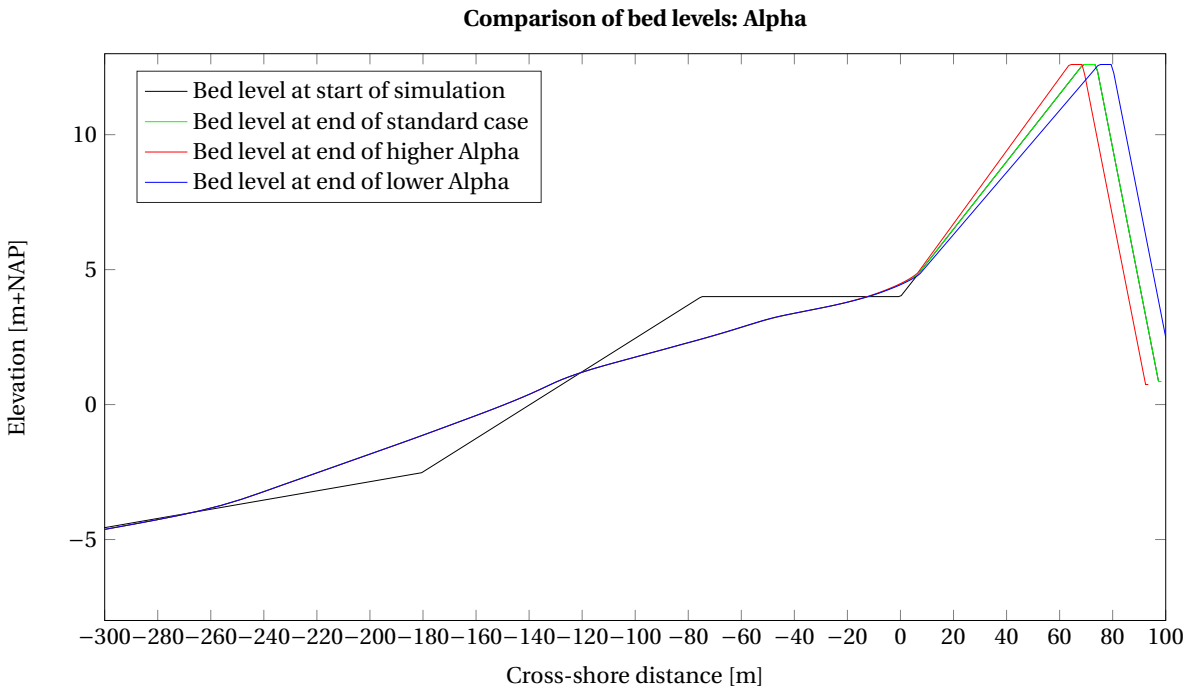

Figure I.10: Bed levels resulting from the sensitivity analysis. Upper part of the cross-shore profile, showing the foreshore and the dike.

I.12. CREST HEIGHT

The figure below shows the resulting bed levels for the higher and lower crest height.

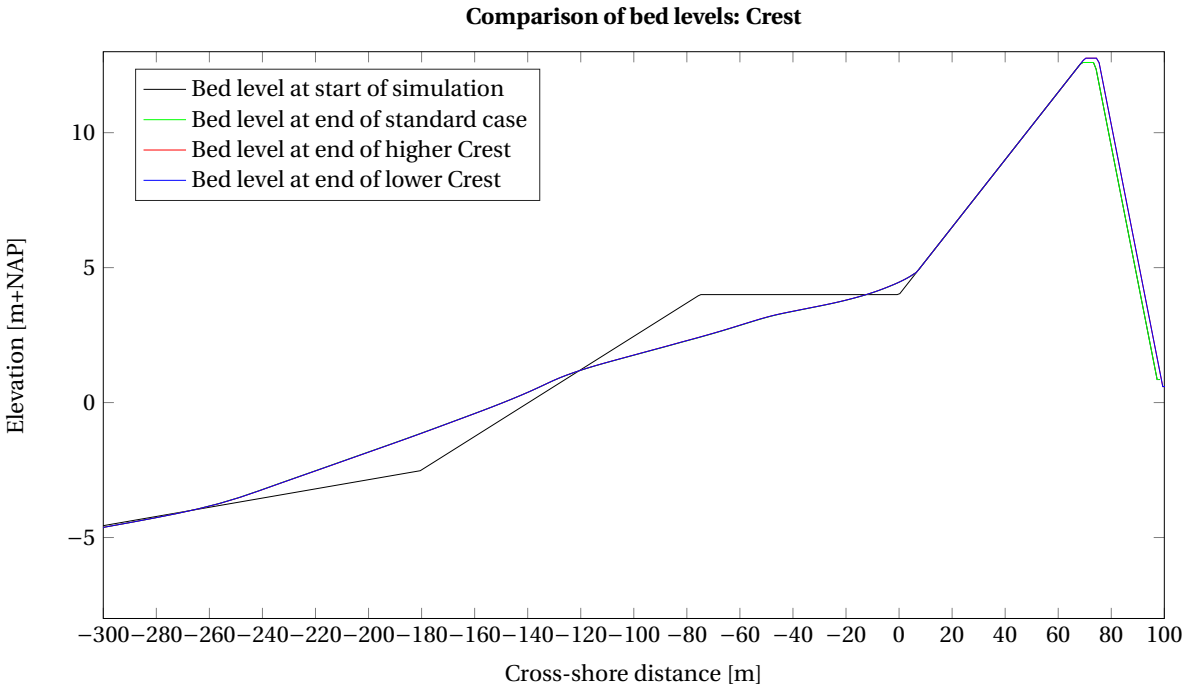

Figure I.11: Bed levels resulting from the sensitivity analysis. Upper part of the cross-shore profile, showing the foreshore and the dike.

J

UNCERTAINTY ANALYSIS RESULTS

This Appendix presents the results of the uncertainty analysis calculations. The results of the different types of calculations can be found in section J.1.

J.1. RESULTS OF THE PROBABILISTIC FRAMEWORK CALCULATIONS

The results of the different calculations performed for the uncertainty analysis are shown in tables J.1 and J.2.

Table J.1: Characteristics of the uncertainty analysis. The last three calculations, with the XBeach 2D-model, were not finished because of their extremely long calculation duration.

Calc. number [-]	Type of model	Amount of stochastic variables [-]	Including morphological changes	Including tide, storm profile	Including $morfac$	Including foreshore
1	ENDEC	13		storm duration only		
2	h/2-model	13		storm duration only		x
3	ENDEC	13		storm duration only		x
4	h/2-model	3				
5	XBeach 1D	3				
6	XBeach 2D	3				
7	h/2-model	3				x
8	XBeach 1D	3				x
9	XBeach 2D	3				x
10	XBeach 1D	10				x
11	XBeach 2D	10				x
12	XBeach 1D	12		x		x
13	XBeach 1D	12	x	x	x	x
14	XBeach 1D	12	x	x		x
15	XBeach 1D	15	x	x	x	x
16	XBeach 1D	15	x	x		x
17	XBeach 2D	12		x		x
18	XBeach 2D	12	x	x		x
19	XBeach 2D	15	x	x		x

Table J.2: Results of the uncertainty analysis. The last three calculations, with the XBeach 2D-model, were not finished because of their extremely long calculation duration.

Calc. number [-]	Type of model	Duration	Probability of failure [year^{-1}]	β-value [-]	Number of calculations	Reference
1	ENDEC		$7.20 * 10^{-6}$	4.34	-	HKV (2014)
2	h/2-model		$3.00 * 10^{-8}$	5.42	-	HKV (2014)
3	ENDEC		$6.00 * 10^{-11}$	6.44	-	HKV (2014)
4	h/2-model	$\mathcal{O}$(minutes)	$9.78 * 10^{-7}$	4.76	40	
5	XBeach 1D	$\mathcal{O}$(day)	$5.68 * 10^{-2}$	1.58	98	
6	XBeach 2D	$\mathcal{O}$(day)	$4.78 * 10^{-5}$	3.90	45	
7	h/2-model	$\mathcal{O}$(minutes)	$2.29 * 10^{-8}$	5.47	23	
8	XBeach 1D	$\mathcal{O}$(day)	$1.64 * 10^{-5}$	4.15	112	
9	XBeach 2D	$\mathcal{O}$(day)	$1.56 * 10^{-6}$	4.66	43	
10	XBeach 1D	$\mathcal{O}$(day)	$2.85 * 10^{-4}$	3.45	341	
11	XBeach 2D	$\mathcal{O}$(day)	$1.12 * 10^{-6}$	4.73	277	
12	XBeach 1D	$\mathcal{O}$(month)	$1.23 * 10^{-4}$	3.67	391	
13	XBeach 1D	$\mathcal{O}$(week)	$1.14 * 10^{-4}$	3.69	368	
14	XBeach 1D	$\mathcal{O}$(month)	$1.55 * 10^{-4}$	3.61	354	
15	XBeach 1D	$\mathcal{O}$(week)	$4.82 * 10^{-4}$	3.30	484	
16	XBeach 1D	$\mathcal{O}$(month)	$5.30 * 10^{-4}$	3.27	484	
17	XBeach 2D	>month	-	-	-	
18	XBeach 2D	>month	-	-	-	
19	XBeach 2D	>month	-	-	-	

J.2. INFLUENCE OF A MORPHOLOGICAL ACCELERATION FACTOR

Table J.3 shows the results of the calculations with and without a morphological acceleration factor of 10. Visible is that the influence of the morfac is small.

Table J.3: Results of calculations with and without $morfac$.

Type of model	Number of stochastic variables [-]	Including morphological changes	Including morfac	Probability of failure [year^{-1}]	β-value [-]	Number of calculations
XBeach 1D	12	x	x	$1.14 * 10^{-4}$	3.69	368
XBeach 1D	12	x		$1.55 * 10^{-4}$	3.61	354
XBeach 1D	15	x	x	$4.82 * 10^{-4}$	3.30	484
XBeach 1D	15	x		$5.30 * 10^{-4}$	3.27	484

J.3. START-UP METHOD CALCULATION RESULTS

This section describes the results of the start-up method calculations. The start-up method performs the first $2n$ calculations in an ADIS calculation, where n is the amount of stochastic variables. Each time, one parameter is simulated with a β-value of -4 or +4, the other parameters are kept at the mean value.

J.3.1. XBEACH 1D, 3 STOCHASTIC VARIABLES

Table J.4 presents the start-up method calculation results of the calculation with the XBeach 1D-model and 3 stochastic variables.

Table J.4: Start-up method calculation results of the calculation with the XBeach 1D-model and 3 stochastic variables. Indicated in the second and third column are the resulting Z-values of the reliability function for a β-value of -4 or +4 of the indicated parameter. The last column indicates the importance of each parameter, the higher the number, the more important the parameter is.

XB 1D 3 variables	Z for $\beta = -4$	Z for $\beta = +4$	Absolute difference	Importance
$zs0$	2.809	0.025	2.783	1
H_{m0}	2.809	0.185	2.624	1
T_p	2.809	0.242	2.567	1

J.3.2. XBEACH 2D, 3 STOCHASTIC VARIABLES

Table J.5 presents the start-up method calculation results of the calculation with the XBeach 2D-model and 3 stochastic variables.

Table J.5: Start-up method calculation results of the calculation with the XBeach 2D-model and 3 stochastic variables. Indicated in the second and third column are the resulting Z-values of the reliability function for a β-value of -4 or +4 of the indicated parameter. The last column indicates the importance of each parameter, the higher the number, the more important the parameter is.

XB 2D 3 variables	Z for $\beta = -4$	Z for $\beta = +4$	Absolute difference	Importance
$zs0$	1	0.022	0.978	1
H_{m0}	1	0.219	0.781	1
T_p	1	0.246	0.754	1

J.3.3. XBEACH 1D, 10 STOCHASTIC VARIABLES

Table J.6 presents the start-up method calculation results of the calculation with the XBeach 1D-model and 10 stochastic variables.

Table J.6: Start-up method calculation results of the calculation with the XBeach 1D-model and 10 stochastic variables. Indicated in the second and third column are the resulting Z-values of the reliability function for a β-value of -4 or +4 of the indicated parameter. The last column indicates the importance of each parameter, the higher the number, the more important the parameter is.

XB 1D 10 variables	Z for $\beta = -4$	Z for $\beta = +4$	Absolute difference	Importance
$zs0$	2.703	0.026	2.677	5
H_{m0}	2.703	0.177	2.523	5
T_p	2.703	0.235	2.468	5
$gamma$	2.703	0.573	2.129	4
s	1.329	0.962	0.367	3
$C1$	1	1	0	1
$C2$	1	1	0	1
$C3$	1.026	0.974	0.053	2
$C4$	1	1	0	1
n	0.764	1.369	0.605	3

J.3.4. XBEACH 2D, 10 STOCHASTIC VARIABLES

Table J.7 presents the start-up method calculation results of the calculation with the XBeach 2D-model and 10 stochastic variables.

Table J.7: Start-up method calculation results of the calculation with the XBeach 2D-model and 10 stochastic variables. Indicated in the second and third column are the resulting Z-values of the reliability function for a β-value of -4 or +4 of the indicated parameter. The last column indicates the importance of each parameter, the higher the number, the more important the parameter is.

XB 2D 10 variables	Z for β= −4	Z for β= +4	Absolute difference	Importance
$zs0$	1	0.023	0.978	3
H_{m0}	1	0.231	0.770	3
T_p	1	0.249	0.751	3
$gamma$	1	0.594	0.406	2
s	1	1	0	1
$C1$	1	1	0	1
$C2$	1	1	0	1
$C3$	1	1	0	1
$C4$	1	1	0	1
n	1.615	1	0.615	2

J.3.5. XBEACH 1D, 12 STOCHASTIC VARIABLES, MORPHOSTATIC & $morfac$

Table J.8 presents the start-up method calculation results of the calculation with the XBeach 1D-model, 12 stochastic variables, morphostatic calculation and a morfac of 10.

Table J.8: Start-up method calculation results of the calculation with the XBeach 1D-model, 12 stochastic variables, morphostatic calculation and a morfac of 10. Indicated in the second and third column are the resulting Z-values of the reliability function for a β-value of -4 or +4 of the indicated parameter. The last column indicates the importance of each parameter, the higher the number, the more important the parameter is.

XB 1D 12 variables morphostat. morfac	Z for β= −4	Z for β= +4	Absolute difference	Importance
$zs0$	1.711	0.025	1.686	5
H_{m0}	1.711	0.157	1.554	5
T_p	1.711	0.206	1.505	5
$gamma$	1.711	0.519	1.192	4
s	0.847	1.091	0.244	3
$C1$	1	1	$4 * 10^{-15}$	1
$C2$	1	1	0	1
$C3$	1.017	0.983	0.034	2
$C4$	1	1	0	1
n	0.696	1.711	1.015	4
$Tstop$	-0.120	0.881	1.001	4
Loc_peak	1.020	1.022	0.002	1

J.3.6. XBEACH 1D, 12 STOCHASTIC VARIABLES, MORPHODYNAMIC & $morfac$

Table J.9 presents the start-up method calculation results of the calculation with the XBeach 1D-model, 12 stochastic variables, morphodynamic calculation and a morfac of 10.

J.3.7. XBEACH 1D, 15 STOCHASTIC VARIABLES, MORPHODYNAMIC & $morfac$

Table J.10 presents the start-up method calculation results of the calculation with the XBeach 1D-model, 15 stochastic variables, morphodynamic calculation and a morfac of 10.

Table J.9: Start-up method calculation results of the calculation with the XBeach 1D-model, 12 stochastic variables, morphodynamic calculation and a morfac of 10. Indicated in the second and third column are the resulting Z-values of the reliability function for a β-value of -4 or +4 of the indicated parameter. The last column indicates the importance of each parameter, the higher the number, the more important the parameter is.

XB 1D 12 variables morphodyn. morfac	Z for $\beta = -4$	Z for $\beta = +4$	Absolute difference	Importance
$zs0$	1.506	0.008	1.498	5
H_{m0}	1.506	0.149	1.357	5
T_p	1.506	0.233	1.272	5
$gamma$	1.506	0.589	0.916	4
s	0.962	0.953	0.009	2
$C1$	1	1	0	1
$C2$	1	1	0	1
$C3$	1.015	0.985	0.030	2
$C4$	1	1	0	1
n	1.139	1.255	0.116	3
$Tstop$	-0.105	1.016	1.122	4
Loc_peak	1.186	1.186	$9.18 * 10^{-5}$	1

Table J.10: Start-up method calculation results of the calculation with the XBeach 1D-model, 15 stochastic variables, morphodynamic calculation and a morfac of 10. Indicated in the second and third column are the resulting Z-values of the reliability function for a β-value of -4 or +4 of the indicated parameter. The last column indicates the importance of each parameter, the higher the number, the more important the parameter is.

XB 1D 15 variables morphodyn. morfac	Z for $\beta = -4$	Z for $\beta = +4$	Absolute difference	Importance
$zs0$	1.505	0.007	1.499	5
H_{m0}	1.505	0.148	1.357	5
T_p	1.505	0.230	1.276	5
$gamma$	1.505	0.601	0.905	4
s	0.963	0.952	0.011	2
$C1$	1	1	0	1
$C2$	1	1	$9.99 * 10^{-15}$	1
$C3$	1.015	0.985	0.029	2
$C4$	1	1	$3.3 * 10^{-14}$	1
n	1.134	1.257	0.123	3
$Tstop$	-0.105	1.021	1.126	4
Loc_peak	1.190	1.189	0.001	1
D_{50}	1.146	0.913	0.233	3
$FacAs$	1.006	1.013	0.007	1
$FacSk$	0.982	1.125	0.143	3

K

FRAMEWORK MATLAB FILES

This Appendix presents examples of the Matlab m-files of the calculation framework, which were used for the calculations. Section K.1 gives the framework_run file, section K.2 shows the framework_LSF file and section K.3 presents the framework_XB file. These files and other files can be found at `p:\xbeach\msc_studies\Patrick_Oosterlo` (only on the Deltares network).

K.1. FRAMEWORK_RUN

The file framework_run was used to start the calculations. The file sets all the parameters, probability distributions and calculation methods for ADIS. This file and other files can be found at `p:\xbeach\msc_studies\Patrick_Oosterlo` (only on the Deltares network).

```
% FRAMEWORK_RUN.M - Run the probabilistic framework (XBeach+EurOtop+ADIS)
% to calculate the probability of dike failure due to wave overtopping
% in situations with sandy foreshores (Omni-directional probability
% distributions)
%
% Input     =   see below
% Output    =   AdaptiveDirectionImportanceSampling object
% Uses      =   framework_LSF.m, framework_XB.m, Open Earth Tools
% Used by   =   -
%
% Based on work from Joost den Bieman

%% Copyright notice
%   --------------------------------------------------------------------
%   Copyright (C) 2015 Delft University of Technology, Deltares
%       Patrick Oosterlo
%
%       p.oosterloo1@gmail.com
%
%   This library is free software: you can redistribute it and/or modify
%   it under the terms of the GNU General Public License as published by
%   the Free Software Foundation, either version 3 of the License, or
%   (at your option) any later version.
%
%   This library is distributed in the hope that it will be useful,
%   but WITHOUT ANY WARRANTY; without even the implied warranty of
%   MERCHANTABILITY or FITNESS FOR A PARTICULAR PURPOSE.  See the
%   GNU General Public License for more details.
%
%   You should have received a copy of the GNU General Public License
%   along with this library.  If not, see <http://www.gnu.org/licenses/>.
%   --------------------------------------------------------------------

% This tool is part of <a href="http://www.OpenEarth.eu">OpenEarthTools</a>.
% OpenEarthTools is an online collaboration to share and manage data and
% programming tools in an open source, version controlled environment.
```

```
% Sign up to recieve regular updates of this function, and to contribute
% your own tools.

%% Version <http://svnbook.red-bean.com/en/1.5/svn.advanced.props.special.keywords.html>
% Created: 25 Sep 2015
% Created with Matlab version: 8.4.0.150421 (R2014b)

% $Id: 4009711 $
% $Date: October 2015 $
% $Author: Patrick Oosterlo $
% $Revision: $
% $HeadURL: $
% $Keywords: framework_run $

%% Input for AdaptiveDirectionalImportanceSampling.m
SaveDir=        'c:\ADIS_Morphodynamic_15stochasts'; % Folder to save output to
MyAccuracy=     0.95;   % Accuracy of Pf within confidence interval
MyConfidence=   0.2;    % Confidence interval of Pf
ChosenSeed=     67;     % Seed for random number generator

%% 1. Create random variables needed for LimitStateFunction
NrOfRandomVariables = 15;   % Number of random variables
MyVariables(NrOfRandomVariables,1) = RandomVariable;
% Create structure with names, probability distributions and parameters

name= {...
    'zs0',       ...
    'Hm0',       ...
    'Tp',        ...
    'gamma',     ...
    's',         ...
    'C1',        ...
    'C2',        ...
    'C3',        ...
    'C4',        ...
    'n',         ...
    'tstop',     ...
    'loc_peak', ...
    'D50',       ...
    'facAs',     ...
    'facSk'      ...
    };
dist= {...
    @norm_inv,   ...
    @norm_inv,   ...
    @norm_inv,   ...
    @norm_inv,   ...
    @unif_inv,   ...
    @norm_inv,   ...
    @norm_inv,   ...
    @norm_inv,   ...
    @norm_inv,   ...
    @unif_inv    ...
    @logn_inv,   ...
    @unif_inv,   ...
    @logn_inv,   ...
    @logn_inv,   ...
    @logn_inv    ...
    };
params = {...
    {0 1},              ...
    {0 0.6},            ...
    {0 1},              ...
    {0.541 0.0541},     ...
    {1.5 10},           ...
    {4.75 0.5},         ...
    {2.6 0.35},         ...
    {-0.92 0.24},       ...
    {1 0.14},           ...
    {0.01 0.03}         ...
    {3.9379 0.3365},    ...
```

```
    {0 2*pi},           ...
    {-8.1229 0.1492},   ...
    {-2.1387 0.2936},   ...
    {-1.0239 0.2936}    ...
    };

for i=1:NrOfRandomVariables                    % Random variables structure
    MyVariables(i,1).Name                     = name{1,i};
    MyVariables(i,1).Distribution             = dist{1,i};
    MyVariables(i,1).DistributionParameters   = params{1,i};
end

%% 2. Create a LimitState object describing the problem
MyLimitState                    = LimitState;   % Call LSF calculation file
MyLimitState.Name               = 'Z';  % Name LSF
MyLimitState.LimitStateFunction = @framework_LSF;   % Call LSF definition file
MyLimitState.RandomVariables    = MyVariables;
% Call random variables structure defined above
MyLimitState.ResponseSurface    = AdaptiveResponseSurface;
% Call ARS calculation file
MyLimitState.LimitStateFunctionAdditionalVariables = {...
    % Define additional variables
    'alpha',            0.125,      ... % Dike slope
    'crest',            12.6,       ... % Crest height
    'mainang',          270,        ... % Main wave direction
    'q_crit',           0.1,        ... % Critical wave overtopping discharge
    'MinHm0',           0.5,        ... % Minimal Hm0 possible, prevent negative
    'MinTp',            2.5,        ... % Minimal Tp possible, prevent negative
    'point',            1,          ... % XB output point
    'Ttide',            12.42,      ... % Duration of tidal period
    'amp_tide',         2.15,       ... % Tidal amplitude
    'gammajsp',         3.3,        ... % Peak enhancement factor JONSWAP
    'xgrid',            [-1381.2; -881.2; -531.2; -180.485; -75; 0],... % x grid
    'zgrid',            [-20; -10; -8.5; -2.52425; 4; 4],... % z grid
    'xtoe',             0.0,        ... % x dike toe point
    'ytoe',             500.0,      ... % y dike toe point
    'ztoe',             4,          ... % z dike toe point
    'spinup',           1200,       ... % Model spin-up duration
    'reflectedwaves',   0,          ... % Don't include reflected waves
    'freqres',          0.005,      ... % Frequency resolution in spectra calculation
    'freqminlim',       0.003,      ... % Min frequency in spectra calculation
    'freqmaxlim',       0.2,        ... % Max frequency in spectra calculation
    'RSPX',             20534,      ... % RSP X location of dike
    'RSPY',             398652,     ... % RSP Y location of dike
    'Angle',            326.7,      ... % RSP Angle location of dike
    't_interv',         1,          ... % XB model output interval
    'filelist',         1,          ... % Varying offshore conditions in time
    'morfac',           [],         ... % Set morphological factor
    'RunRemote',        false,      ... % Run remote calculation
    'RunMPI',           true,       ... % Run MPI calculation
    'ModelSetupDir',    'c:\ADIS_Morphodynamic_15stochasts', ... % Model Setup folder
    'ModelRunDir',      'c:\ADIS_Morphodynamic_15stochasts', ... % Model Run folder
    'ExecutablePath',   'c:\XBeachMPI', ... % XB executable path
    'NrNodes',          8,          ... % Number of calculation nodes
    'QueueType',        'normal',   ... % XB calculation queue type
    'LSFChecker',       XBeachLimitStateFunctionChecker ... % XB calculation checker file
    };

%% (OPTIONAL) 3.a Use a weighted fit for the response surface (this is still WIP!)
MyLimitState.ResponseSurface.DefaultFit     = true;
% Use the default fitting method
MyLimitState.ResponseSurface.WeightedARS    = false;
% Weighted ARS is still work in progress
MyLimitState.ResponseSurface.FitFunction    = @polyfitn;
% Unweighed polynomial fit. Choice polyfitn/wpolyfitn follows from line above
% MyLimitState.BetaSphere.BetaSphereMargin    = 0.5;
% Set alternative beta-sphere margins
% MyLimitState.ResponseSurface.AvailableEvaluationFunction =
% @ARS_Overtopping_AvailableEvaluations;
% Uses only part of the calculations to fit an ARS

```

```
%% 4. Create a LineSearch object (currently only 1 type available)
MyLineSearcher  = LineSearch;   % Call linesearch function
MyLineSearcher.EnableBisection = false;  % Turn on/off bisection

%% 5. Create a AdaptiveDirectionalImportanceSampling object
MyADISObject    = AdaptiveDirectionalImportanceSampling(...
    MyLimitState, MyLineSearcher, MyAccuracy, MyConfidence, ChosenSeed);

%% (OPTIONAL) 5.a Use a StartUpMethod (for increased efficiency)
MyADISObject.StartUpMethods  = StartUpAxialPoints;  % Use the standard start-up method
% MyADISObject.MinNrApproximatedPoints = 10;  % set Min number of approximated points
MyADISObject.MaxNrDirections = 1000;    % set Max number of random directions

%% 6. Calculate the probability of failure
MyADISObject.CalculatePf;

%% 7. Save the results
result.ADIS.Object = MyADISObject;  % Save ADIS object
result.ADIS.P_f   = MyADISObject.Pf;    % Save Pf
result.ADIS.Beta  = norm_inv(1-MyADISObject.Pf, 0, 1);  % Save beta
result.ADIS.Calc  = MyADISObject.LimitState.NumberExactEvaluations;
% Number of exact (XB) calculations
save(fullfile(SaveDir,['results_ADIS']),'result');  % Save file

% MyADISObject.plot
% AdisPlot3D(MyADISObject);
%AdisPlotDuneErosion
%setting_figure_to_be_updated_in_the_plot
```

K.2. FRAMEWORK_LSF

The file framework_LSF was used to set-up the LSF. The wave spectra, wave overtopping discharge and z-value of the LSF are determined by this file. The file is called by framework_run.m. This file and other files can be found at `p:\xbeach\msc_studies\Patrick_Oosterlo` (only on the Deltares network).

```
function z = framework_LSF(varargin)
% FRAMEWORK_LSF.M - Set-up of the limit state function for
% the probabilistic framework (XBeach+EurOtop+ADIS)
% to calculate the probability of dike failure due to wave overtopping
% in situations with sandy foreshores
%
% Input     =   structure, see below
% Output    =   Spectral wave parameters, overtoping discharge, current z-value
% Uses      =   framework_XB.m, xb_spectra.m, overtopping.m, Open Earth Tools
% Used by   =   framework_run.m
%
% Based on work from Joost den Bieman

%% Copyright notice
%   --------------------------------------------------------------------
%   Copyright (C) 2015 Delft University of Technology, Deltares
%       Patrick Oosterlo
%
%       p.oosterloo1@gmail.com
%
%   This library is free software: you can redistribute it and/or modify
%   it under the terms of the GNU General Public License as published by
%   the Free Software Foundation, either version 3 of the License, or
%   (at your option) any later version.
%
%   This library is distributed in the hope that it will be useful,
%   but WITHOUT ANY WARRANTY; without even the implied warranty of
%   MERCHANTABILITY or FITNESS FOR A PARTICULAR PURPOSE.  See the
%   GNU General Public License for more details.
%
%   You should have received a copy of the GNU General Public License
%   along with this library.  If not, see <http://www.gnu.org/licenses/>.
%   --------------------------------------------------------------------
```

```
34
35  % This tool is part of <a href="http://www.OpenEarth.eu">OpenEarthTools</a>.
36  % OpenEarthTools is an online collaboration to share and manage data and
37  % programming tools in an open source, version controlled environment.
38  % Sign up to recieve regular updates of this function, and to contribute
39  % your own tools.
40
41  %% Version <http://svnbook.red-bean.com/en/1.5/svn.advanced.props.special.keywords.html>
42  % Created: 25 Sep 2015
43  % Created with Matlab version: 8.4.0.150421 (R2014b)
44
45  % $Id: 4009711 $
46  % $Date: October 2015 $
47  % $Author: Patrick Oosterlo $
48  % $Revision: $
49  % $HeadURL: $
50  % $Keywords: framework_LSF $
51
52  %% Settings
53  OPT = struct(...
54      'gamma',            [], ...
55      'facSk',            [], ...
56      'facAs',            [], ...
57      'tstop',            [], ...
58      'zs0',              [], ...
59      'Hm0',              [], ...
60      'Tp',               [], ...
61      'alpha',            [], ...
62      'crest',            [], ...
63      'D50',              [], ...
64      's',                [], ...
65      'loc_peak',         [], ...
66      'C1',               [], ...
67      'C2',               [], ...
68      'C3',               [], ...
69      'C4',               [], ...
70      'n',                [], ...
71      'mainang',          [], ...
72      'q_crit',           [], ...
73      'MinHm0',           [], ...
74      'MinTp',            [], ...
75      'point',            [], ...
76      'Ttide',            [], ...
77      'amp_tide',         [], ...
78      'gammajsp',         [], ...
79      'xgrid',            [], ...
80      'zgrid',            [], ...
81      'xtoe',             [], ...
82      'ytoe',             [], ...
83      'ztoe',             [], ...
84      'spinup',           [], ...
85      'reflectedwaves',   [], ...
86      'freqres',          [], ...
87      'freqminlim',       [], ...
88      'freqmaxlim',       [], ...
89      'RSPX',             [], ...
90      'RSPY',             [], ...
91      'Angle',            [], ...
92      't_interv',         [], ...
93      'filelist',         [], ...
94      'morfac',           [], ...
95      'RunRemote',        [], ...
96      'RunMPI',           [], ...
97      'ModelSetupDir',    '', ...
98      'ModelRunDir',      '', ...
99      'ExecutablePath',   '', ...
100     'NrNodes',          [], ...
101     'QueueType',        '', ...
102     'LSFChecker',       []  ...
103     );
104
```

```
105 OPT = setproperty(OPT, varargin{:});
106
107 %% Check whether run already exists
108 FolderName          = ['Run_H_' num2str(OPT.Hm0) '_T_' num2str(OPT.Tp)...
109     '_zs_' num2str(OPT.zs0) '_D50_' num2str(OPT.D50) '_locp_' num2str(OPT.loc_peak)...
110     '_gamm_' num2str(OPT.gamma) '_facsk_' num2str(OPT.facSk) ...
111     '_facas_' num2str(OPT.facAs) '_s_' num2str(OPT.s) '_C1_' num2str(OPT.C1) ...
112     '_C2_' num2str(OPT.C2) '_C3_' num2str(OPT.C3) '_C4_' num2str(OPT.C4) ...
113     '_n_' num2str(OPT.n) '_tstop_' num2str(OPT.tstop)];
114 ModelOutputDir      = fullfile(OPT.ModelRunDir, FolderName);
115 %Create output folder for calculation
116
117 if ~isdir(ModelOutputDir)
118     % Setup & run model
119     framework_XB(ModelOutputDir, OPT(:));   % Call function to set-up model
120     OPT.LSFChecker.CheckProgress(ModelOutputDir);   % Call calculation checker function
121 else
122     OPT.LSFChecker.CheckProgress(ModelOutputDir);
123 end
124
125 %% Calculate spectra, wave parameters and overtopping
126 xbo = xb_read_output(fullfile(ModelOutputDir, 'xboutput.nc'),'vars',{...
127     'point_zs','point_H','point_zb','point_uu'});   % Read XB output
128 xbi = xb_read_input(fullfile(ModelOutputDir, 'params.txt'));    % Read XB input settings
129 fp_in = xs_get(xbi, 'bcfile.fp');   % Get relevant XB output data, offshore peak frequency
130 fp_section = xs_get(xbi, 'bcfile.duration'); % Different offshore conditions in time
131 zs0_in = xs_get(xbi, 'zs0file.tide');   % Different water levels in time (tide)
132 zs0_section = xs_get(xbi, 'zs0file.time'); % (1800 s)
133 H = xs_get(xbo,'point_H');  % Get XB H output at dike toe (incl short waves)
134 zs = xs_get(xbo,'point_zs');    % Get XB water level output at dike toe (incl long waves)
135 u = xs_get(xbo,'point_uu'); % Get velocities at toe
136 zb = xs_get(xbo,'point_zb');    % Get bed level at toe
137
138 for i=1:1:length(fp_in) % Run for each set of different offshore wave conditions in time
139     Tp_in = 1/fp_in(1,i);   % Get short wave peak period
140      idssmaller = find(zs0_section<(i)*fp_section);
141     if i==length(fp_in)
142         id(i) = idssmaller(end);
143     else
144         id(i) = idssmaller(end)+1;
145     end
146     if i==1
147         max_wl = max(zs0_in(1:id(i),1));
148     else
149         max_wl = max(zs0_in(id(i-1):id(i),1));  % get water level to calculate freeboard
150     end
151
152      section(i) = ceil((i)*fp_section/(OPT.t_interv*OPT.morfac));
153     % split data into sections during which bc's are constant
154     if i==1
155         stop = section(i);
156         H_section = H(1:stop);
157         zs_section = zs(1:stop);
158         u_section = u(1:stop);
159         zb_section = zb(1:stop);
160     elseif i==length(fp_in)
161         start = section(i-1);
162         H_section = H(start:end);
163         zs_section = zs(start:end);
164         u_section = u(start:end);
165         zb_section = zb(start:end);
166     else
167         start = section(i-1);
168         stop = section(i);
169         H_section = H(start:stop);  % Get H data in section
170         zs_section = zs(start:stop);    % Get water level data in section
171         u_section = u(start:stop);  % Get velocity data in section
172         zb_section = zb(start:stop);    % Get bed level data in section
173     end
174
175    if i==1
```

```
176         [Tm10_lf, Hm0_lf, Tm10_hf, Hm0_hf, Tm10_tot(i), Hm0_tot(i)] = xb_spectra(...
177         'point',OPT.point,'Tp_hf',Tp_in,'H',H_section,'zs',zs_section,'u',u_section,...
178         'zb',zb_section,'t_interv',OPT.t_interv,'gamma',OPT.gamma,'spinup',OPT.spinup,...
179         'varying',0,'reflected',OPT.reflectedwaves,'freqres',OPT.freqres,...
180         'minlim',OPT.freqminlim,'maxlim',OPT.freqmaxlim,'path',ModelOutputDir,'figures',0);
181         %calculate spectra and wave parameters
182     else
183         [Tm10_lf, Hm0_lf, Tm10_hf, Hm0_hf, Tm10_tot(i), Hm0_tot(i)] = xb_spectra(...
184         'point',OPT.point,'Tp_hf',Tp_in,'H',H_section,'zs',zs_section,'u',u_section,...
185         'zb',zb_section,'t_interv',OPT.t_interv,'gamma',OPT.gamma,...
186         'varying',0,'reflected',OPT.reflectedwaves,'freqres',OPT.freqres,...
187         'minlim',OPT.freqminlim,'maxlim',OPT.freqmaxlim,'path',ModelOutputDir,'figures',0);
188         %calculate spectra and wave parameters
189     end
190
191     Rc = OPT.crest - max_wl;     % calculate freeboard
192     betaw = abs(OPT.mainang-270); % change from nautical to EurOtop convention
193
194     if isnan(Hm0_tot(i))==1 | Hm0_tot(i)==0 | isnan(Tm10_tot(i))==1 | Tm10_tot(i)==0
195         q_tot(i)=0; % Set q=0 for Hm0 or Tm10 is 0 or NaN
196     else
197         q_tot(i) = overtopping('Hm0',Hm0_tot(i),'Tm',Tm10_tot(i),'slope',OPT.alpha,...
198         'Rc',Rc,'betaw',betaw,'C1',OPT.C1,'C2',OPT.C2,'C3',OPT.C3,'C4',OPT.C4,...
199         'path',ModelOutputDir)*1000; % calculate overtopping, in l/s/m!
200     end
201     if q_tot(i)==0  % LSF becomes Inf if q=0 or q=NaN, so set q=1e-99
202         q_tot(i)=1e-99;
203     end
204 end
205
206 results = [Hm0_tot',Tm10_tot',q_tot'];  % Get results of Hm0, Tm-1,0 and q
207 fileID = fopen(fullfile(ModelOutputDir,'Storm_params.txt'),'w'); %Write results to file
208 fprintf(fileID,'%6s %6s %6s\n','Hm0','Tm10','q');
209 fprintf(fileID,'%6.4e %6.4e %6.4e\n',results');
210 fclose(fileID);
211
212 %% Limit State Function
213 q_final = max(q_tot);   % Calculate largest q during storm
214
215 z = log10(OPT.q_crit)-log10(q_final);   % Calculate LSF Z-value
216
217 display(['The current exact Z-value is ' num2str(z) '(Hm0 = ' num2str(OPT.Hm0)...
218     ', Tp = ' num2str(OPT.Tp) ', zs0 = ' num2str(OPT.zs0) ...
219     ', D50 = ' num2str(OPT.D50) ', locpeak = ' num2str(OPT.loc_peak)]);
220     %Display current z-value
221 display('------------------------------------------------------------------------');
```

K.3. FRAMEWORK_XB

The file framework_XB was used to set-up and run the XBeach models. The file calculates the boundary conditions and sets all XBeach parameters, after which the XBeach calculation is started. The file is called by framework_LSF.m. This file and other files can be found at `p:\xbeach\msc_studies\Patrick_Oosterlo` (only on the Deltares network).

```
1  function framework_XB(ModelOutputDir, varargin)
2  % FRAMEWORK_XB.M - Set-up and running of the XB model for
3  % the probabilistic framework (XBeach+EurOtop+ADIS)
4  % to calculate the probability of dike failure due to wave overtopping
5  % in situations with sandy foreshores
6  %
7  % Input     =   Model output directory, structure, see below
8  % Output    =   -
9  % Uses      =   Open Earth Tools
10 % Used by   =   framework_LSF.m
11 %
12 % Based on work from Joost den Bieman
13
```

```
%% Copyright notice
%   --------------------------------------------------------------------
%   Copyright (C) 2015 Delft University of Technology, Deltares
%       Patrick Oosterlo
%
%       p.oosterloo1@gmail.com
%
%   This library is free software: you can redistribute it and/or modify
%   it under the terms of the GNU General Public License as published by
%   the Free Software Foundation, either version 3 of the License, or
%   (at your option) any later version.
%
%   This library is distributed in the hope that it will be useful,
%   but WITHOUT ANY WARRANTY; without even the implied warranty of
%   MERCHANTABILITY or FITNESS FOR A PARTICULAR PURPOSE.  See the
%   GNU General Public License for more details.
%
%   You should have received a copy of the GNU General Public License
%   along with this library.  If not, see <http://www.gnu.org/licenses/>.
%   --------------------------------------------------------------------

% This tool is part of <a href="http://www.OpenEarth.eu">OpenEarthTools</a>.
% OpenEarthTools is an online collaboration to share and manage data and
% programming tools in an open source, version controlled environment.
% Sign up to recieve regular updates of this function, and to contribute
% your own tools.

%% Version <http://svnbook.red-bean.com/en/1.5/svn.advanced.props.special.keywords.html>
% Created: 25 Sep 2015
% Created with Matlab version: 8.4.0.150421 (R2014b)

% $Id: 4009711 $
% $Date: October 2015 $
% $Author: Patrick Oosterlo $
% $Revision: $
% $HeadURL: $
% $Keywords: framework_XB $

%% Settings
OPT = struct(...
    'gamma',            [], ...
    'facSk',            [], ...
    'facAs',            [], ...
    'tstop',            [], ...
    'zs0',              [], ...
    'Hm0',              [], ...
    'Tp',               [], ...
    'alpha',            [], ...
    'crest',            [], ...
    'D50',              [], ...
    's',                [], ...
    'loc_peak',         [], ...
    'C1',               [], ...
    'C2',               [], ...
    'C3',               [], ...
    'C4',               [], ...
    'n',                [], ...
    'mainang',          [], ...
    'q_crit',           [], ...
    'MinHm0',           [], ...
    'MinTp',            [], ...
    'point',            [], ...
    'Ttide',            [], ...
    'amp_tide',         [], ...
    'gammajsp',         [], ...
    'xgrid',            [], ...
    'zgrid',            [], ...
    'xtoe',             [], ...
    'ytoe',             [], ...
    'ztoe',             [], ...
    'spinup',           [], ...
```

```
    'reflectedwaves',    [], ...
    'freqres',           [], ...
    'freqminlim',        [], ...
    'freqmaxlim',        [], ...
    'RSPX',              [], ...
    'RSPY',              [], ...
    'Angle',             [], ...
    't_interv',          [], ...
    'morfac',            [], ...
    'filelist',          [], ...
    'RunRemote',         [], ...
    'RunMPI',            [], ...
    'ModelSetupDir',     '', ...
    'ModelRunDir',       '', ...
    'ExecutablePath',    '', ...
    'NrNodes',           [], ...
    'QueueType',         '', ...
    'LSFChecker',        []  ...
    );

OPT = setproperty(OPT, varargin{:});

%%
mkdir(ModelOutputDir)   % Create model output folder

%% Load initial model setup
xbModel = xb_read_input(fullfile(OPT.ModelSetupDir, 'params.txt'));

%% Set stochastic variables in XB model
xbModel = xs_set(xbModel, 'gamma', OPT.gamma);  % Peak enhancement factor JONSWAP
xbModel = xs_set(xbModel, 'facSk', OPT.facSk);  % Calibration factor wave skewness
xbModel = xs_set(xbModel, 'facAs', OPT.facAs);  % Calibration factor wave asymmetry
if OPT.tstop>200
    OPT.tstop = 200;    % Set maximum storm duration (hrs)
end
xbModel = xs_set(xbModel, 'tstop', OPT.tstop*3600); % Set storm duration
xbModel = xs_set(xbModel, 'D50', OPT.D50);  % Set D50 sediment diameter
xbModel = xs_set(xbModel, 'D90', OPT.D50*1.5);  % Set D90 sediment diameter
xbModel = xs_set(xbModel, 'bedfriccoef', OPT.n);    % Set Manning friction factor

if ~isempty(OPT.morfac)
    xbModel = xs_set(xbModel, 'morfac', OPT.morfac);
    xbModel = xs_set(xbModel, 'tintp', OPT.t_interv*OPT.morfac);
    xbModel = xs_set(xbModel, 'tintg', OPT.morfac*1800);
end

[Lambda1, Lambda2, Station1, Station2, XIntersection, YIntersection] = ...
getLambda_2Stations('RSPX',OPT.RSPX,'RSPY',OPT.RSPY,'Angle',OPT.Angle);
    % Calculate lambda for location, based on steunpunten/stations
[Wl, Wl1, Wl2, Station1, Station2, lambda] = getWl_2Stations(norm_cdf(OPT.zs0,0,1),...
Lambda1,Station1,Station2); % Calculate water level (from steunpunten/stations)
[Hs, Hs1, Hs2, Station1, Station2] = getHs_2Stations(OPT.Hm0,lambda,Wl1,Wl2,...
Station1,Station2); % Calculate wave height (from steunpunten/stations)
[Tp, Tp1, Tp2, Station1, Station2] = getTp_2Stations(OPT.Tp,lambda,Hs1,Hs2,...
Station1,Station2); % Calculate peak period (from steunpunten/stations)

if Hs<OPT.MinHm0 % Correct for small/negative Hs values
    Hs = OPT.MinHm0;
end
if Tp<OPT.MinTp % Correct for small/negative Tp values
    Tp = OPT.MinTp;
end

if ~isempty(OPT.morfac) % Create storm profile
    [to h dtwo Ho To] = bc_stormsurge('Tsurge',OPT.tstop,...
'Ttide',OPT.Ttide,'Tsim',ceil(OPT.tstop),'Tpeak',OPT.tstop/2,...
'h0',0,'ha',OPT.amp_tide,'hs',Wl-OPT.amp_tide,'Hm0_max',Hs,...
'Tp_max',Tp,'nwaves',ceil(OPT.tstop/2.5),'plot',1,...
'h_max',Wl,'phi',OPT.loc_peak)
    saveplot(gcf,ModelOutputDir,'stormshape');
    close gcf;
```

```
156 else
157     [to h dtwo Ho To] = bc_stormsurge('Tsurge',OPT.tstop,'Ttide',...
158 OPT.Ttide,'Tsim',ceil(OPT.tstop),'Tpeak',OPT.tstop/2,...
159 'h0',0,'ha',OPT.amp_tide,'hs',Wl-OPT.amp_tide,'Hm0_max',...
160 Hs,'Tp_max',Tp,'nwaves',ceil(OPT.tstop),'plot',1,...
161 'h_max',Wl,'phi',OPT.loc_peak)
162     saveplot(gcf,ModelOutputDir,'stormshape');
163     close gcf;
164 end
165
166 T1 = dtwo;
167 if ~isempty(OPT.morfac) && OPT.morfac>0 % with/without morfac
168     if mod(T1,OPT.morfac)~=0 % make dividable by morfac
169         T2 = T1+(OPT.morfac-mod(T1,OPT.morfac));
170     else
171         T2 = T1;
172     end
173 end
174 xbtide = xb_generate_tide('time',to,'front',h,'back',h) % Write tide file
175 xb_write_tide(xbtide.data(1).value,'path',ModelOutputDir)
176 xbwaves = xb_generate_waves('type','jonswap','duration',T2,...
177 'Hm0',Ho,'Tp',To,'mainang',OPT.mainang,...
178 'gammajsp',OPT.gammajsp,'s',OPT.s) % Write wave file
179 xb_write_waves(xbwaves.data(2).value,'path',ModelOutputDir,'maxduration',T2(1,1))
180 if OPT.filelist==1 %Set bcfile type
181     xbModel = xs_set(xbModel, 'bcfile', 'filelist.txt');
182 else
183     xbModel = xs_set(xbModel, 'bcfile', 'jonswap.txt');
184 end
185
186 %% Generate and set grid in XB model
187 [nx, ny] = xb_make_bathy_grid(OPT.xgrid,OPT.zgrid,OPT.xtoe,OPT.ztoe,OPT.alpha,OPT.crest,...
188 Tp,1,ModelOutputDir);   % Generate grid and bathymetry, including hard structure
189
190 xbModel = xs_set(xbModel, 'nx', nx);    % Set number of x grid points
191 xbModel = xs_set(xbModel, 'ny', ny);    % Set number of y grid points
192 fid=fopen(fullfile(ModelOutputDir, 'params.txt'),'a');
193 fprintf(fid,'\n%6s %6.0f\n %6.1f %6.1f','npoints = ',OPT.point,OPT.xtoe,OPT.ytoe);
194 % Write to model set-up file
195
196 %% Run model
197 % LINUX (add paths to Matlab)
198 ModelOutputDirLinux = path2os(ModelOutputDir);
199 ModelOutputDirLinux = ['/' strrep(ModelOutputDirLinux,':','')];
200 % WINDOWS (add paths to Matlab)
201 addpath(genpath(OPT.ExecutablePath));
202 addpath(genpath(OPT.ModelSetupDir));
203
204 if OPT.RunRemote    % Run calculation remotely
205     [~, FolderName, ~]  = fileparts(ModelOutputDir);
206     xb_run_remote(xbModel, 'nodes', OPT.NrNodes, 'queuetype', OPT.QueueType, ...
207         'netcdf', true, 'ssh_user', OPT.sshUser, 'ssh_pass', OPT.sshPassword, ...
208         'path_local', ModelOutputDir, 'path_remote', ModelOutputDirLinux, ...
209         'mpitype', 'OPENMPI', 'name', FolderName)
210 elseif OPT.RunMPI
211 % Run calculation with MPI (watch out: set XB MPI path correctly below, here c:\XBeachMPI!)
212     xb_write_input(fullfile(ModelOutputDir,'params.txt'),xbModel);
213     system(['chcp 1252 && cd c:\XBeachMPI && mpiexec -n ' num2str(OPT.NrNodes+1)...
214     ' -wdir ' ModelOutputDir ' -mapall ' OPT.ExecutablePath '\xbeach.exe']);
215 %     clc; %MPI
216 else    % Run calculation local and without MPI
217     xb_run(xbModel, 'binary', OPT.ExecutablePath, 'netcdf', true, ...
218         'path', ModelOutputDir, 'name', '', 'copy', false);
219 end
```

A method to calculate the probability of dike failure due to wave overtopping, including the infragravity waves and morphological changes

P. Oosterlo